Design and Synthesis of Fluorescein Based Molecular Probes for Hg (II) Recognition

THESIS SUBMITTED FOR THE

DEGREE OF DOCTOR OF PHILOSOPHY (SCIENCE)

OF

JADAVPUR UNIVERSITY

DECEMBER, 2022

By

HASAN MOHAMMAD

DEPARTMENT OF CHEMISTRY

JADAVPUR UNIVERSITY

JADAVPUR

K0LKATA-700032

INDIA

Prof. Mahammad Ali,

Professor,

Department of Chemistry

JADAVPUR UNIVERSITY
KOLKATA - 7 0 0 0 3 2, I N D I A
E-mail: m_ali2062@yahoo.com
Mobile: +91-9433249716

CERTIFICATE FROM THE SUPERVISOR

This is to certify that the thesis entitled **"Design and Synthesis of Fluorescein Based Molecular Probes for Hg(II) Recognition"** submitted by **Hasan Mohammad** who got his name registered on 27th February, 2015 (Index No. 25/15/Chem/23) for the award of **Ph.D. (Science) degree** of **Jadavpur University**, is absolutely based upon his own work under my direct supervision and that neither this thesis nor any part of it has been submitted for either any degree / diploma or any other academic award anywhere before.

Date: 22/12/22

Mahammad Ali

(Prof. Mahammad Ali)

Signature of the Supervisor & date with seal

Dr. Mahammad Ali
Professor
Department of Chemistry
Jadavpur University
Kolkata-700 032

Department of Chemistry
Jadavpur University
Kolkata 700 032

DEDICATED TO MY

PARENTS

Acknowledgements

I would like to express my sincere gratitude to my supervisor Prof. Mahammad Ali for the continuous support towards my Ph.D. study and related research works, for his kind patience, motivation and immense knowledge. His guidance helped me in all the time of research and writing of this thesis, which cannot be acknowledged with few words. I could not have imagined having a better advisor and mentor for my Ph.D. study.

No thanks can be enough to acknowledge my mother Mrs. Beauty begum, father Mr. Sukur Alam, my beloved wife Mrs. Umme Habiba, elder brother Mr. Hasan Sarwardi and elder sister Mrs. Ayesha Sultana. They provide me always both the moral as well as emotional support in my life. They made so many sacrifices and prayers on my behalf.

It is my pleasant duty to express my sincere gratitude to present Head, Department of Chemistry Prof. S. Bhattacharya, Dean of Science Prof. S. Chakraborty and Prof. Saurabh Das, Sectional in-charge, Inorganic Chemistry, Jadavpur University, Kolkata-700032 for their kind cooperation and encouragement. I am also grateful to Prof. S. Baitalik, Dr. P. Roy and Dr. B. B. Show, Department of Chemistry, Jadavpur University, for providing me their laboratory facilities whenever required. I also sincerely appreciate the constant encouragement of all the faculty members and non-teaching staffs, especially Mr. Baidyanath Paul, Mr. Atikur Rahaman for their helpful attitude. I am also grateful to the authorities of The Jadavpur University for allowing me to use the necessary infrastructure.

I would like to thank my lab mates, Arindam Giri, Mr. Habib Ali Molla, Mr. Rahul Bhowmick, Mr. Rabiul Alam, Mr. Abu Saleh Musha

Islam, Mrs. Kaberi Pal, Miss. Debjani Maiti, Mr. Mihir Sasmal, Miss. Ananya Dutta, Miss. Rousonara Khatun and Miss. Dolanmoni for the stimulating discussions and for all the fun we have had in the last seven years.

My thanks also go to my Collaborators Prof. Keya Chowdhuri, CSIR-Indian Institute of Chemical Biology, Kolkata-700032, India, for her kind cooperation.

I would like to thank to my entire friends of Jadavpur University and also from other institutions, especially, Dr. Prosenjit Saha, Dr. Sujan Biswas, Anal Krishna Sarkar, Subhankar Halder, Sanjukta Ghosh, Bulti Khatun and Doyel Biswas without their support this journey would not be smooth and pleasant.

I would like to thank everybody who was important to the successful insight of the thesis, as well as expressing my apology that I could not mention personally one by one.

I gratefully acknowledge UGC, New Delhi for UGC-MANF Fellowship (2012-13-MANF-MUS-WES-13502) for financial support to carry out the research work.

Last but not the least, I would gratefully acknowledge, Jadavpur University for infrastructural facilities.

Hasan Mohammad
22.12.22
Hasan Mohammad

Department of Chemistry
Jadavpur University
Kolkata– 700 032, India.

Preface

The work presented in this thesis entitled **"Design and Synthesis of Fluorescein Based Molecular Probes for Hg (II) Recognition"** was initiated in February, 2015 and have been carried out in the Department of Chemistry, Jadavpur University.

Fluorescein based fluorescent molecular probes for the present thesis works have been designed, synthesized and used for detection of selective cations along with their potential applications in biological area. Different spectroscopic techniques like ^{1}H NMR, ^{13}C NMR, Mass, UV−Vis, FTIR have been utilized to characterize the probes and their complexes. Computational studies using density functional theory have been carried out. To check bioapplicability we have also performed live Cell imaging studies.

The thesis consists of five chapters which are summarized below.

Chapter 1 contains a short introduction of fluorescent molecular sensors design and fluorescent mechanism and pathways for selective determination of Hg (II). Literature survey on Hg (II) sensors based on Fluorescein based ligands is discussed. Additionally, a very brief overview of the present work is highlighted.

Chapter 2 describes the synthesis and characterization of fluorescein-based sensor $\mathbf{L^{28}}$ with potential N_2O_2 donor atoms which was found to act as fluorogenic sensor for selective recognition of Hg^{2+} emitting at 520 nm in semi aqueous medium at pH 7.2 (10 mM HEPES buffer), temperature 25 ^{0}C.The fluorescence enhancement was explored due to the configuration transformation of the fluorescein from a spirolactam ring form to the ring-opened amide form on binding with Hg^{2+} in a 1:1 mole ratio which was established by Job's method and ESI-MS^{+} (m/z) studies. The corresponding LOD was evaluated by the 3σ method and found to be 1.24 μM. The tentative coordination environment in the $\mathbf{L^{28}}$**-Hg^{2+}** complex was established by DFT studies. The sensor demonstrates a reversible change in fluorescence upon the successive addition of Hg^{2+} and S^{2-} in $\mathbf{L^{28}}$ solution with negligible interference with other anions. The fluorescence "OFF–ON–OFF" mode of $\mathbf{L^{28}}$ was examined in the presence of Hg^{2+} and S^{2-} and finds applications in devices with logic gate functions. The $\mathbf{L^{28}}$ also exhibits bio-compatibility and negligible cytotoxicity and is suitable for fluorescence cell imaging of Hg^{2+} ions in live HepG2 cells.

Chapter 3 introduces a simple fluorescein-based reversible chemosensor $\mathbf{L^{29}}$ has been developed which selectively and sensitively recognises Hg^{2+} over other competing metal ions in 100% aqueous medium at pH 7.2 (10 mM HEPES buffer), temperature 25^0C with 44 fold fluorescence enhancement due to spirolactam ring opening upon coordination with Hg^{2+} in a 1:1 mole ratio as evidenced from Job's method and ESI-MS^+ (m/z) studies. The interaction and formation of $\mathbf{L^{29}}$ **–** $\mathbf{Hg^{2+}}$ species was supported by the observations gained from fluorescence titrations, Job's plot, ^{1}H NMR and HRMS, and other spectroscopic studies. For the Hg^{2+} interaction towards $\mathbf{L^{29}}$ the binding constant was calculated to be (3.21 ± 0.05) x 10^4 M^{-1} with detection limit 92.7 nM. On addition of S^{2-} to the $\mathbf{L^{29}}$ **–**$\mathbf{Hg^{2+}}$ complex, the fluorescence intensity was totally quenched due to removal of Hg^{2+} from the complex by S^{2-}ion arising out of stronger affinity of Hg^{2+} towards S^{2-} resulting concomitant formation of ring closed form, $\mathbf{L^{29}}$. The tentative coordination environment in the $\mathbf{L^{29}}$ **–**$\mathbf{Hg^{2+}}$ complex was established by DFT studies. $\mathbf{L^{29}}$ exhibits low cytotoxicity and cell permeability, which makes it capable for bioimaging applications in living HepG2 cells.

Chapter 4 describes a novel fluorescein derivative ($\mathbf{HL^{30}}$) was synthesized successfully by a simple two-step methods and characterized. The probe displayed excellent sensitivity and selectivity towards Hg^{2+} over other tested metal ions in CH_3OH : H_2O 7:3 medium (pH 7.2, 10 mM HEPES), which could be ascribed to the Hg^{2+} induced ring opening of the spirolactam of the flourescein moiety. The 1:1 binding of $\mathbf{HL^{30}}$ to Hg^{2+} was recognized by Job's method and confirmed by ESI-MS^- (m/z) studies and the Lod value was calculated and found to be 0.46 µM. The MTT assay revealed that $\mathbf{HL^{30}}$ exhibits low cytotoxicity toward living HepG2 cells.

Chapter 5 represents the highlights of the thesis.

List of Abbreviations

FAAS	Flame Furnance Atomic Absorption Spectroscopy
ICP-ES	Inductively Coupled Plasma Emission
ICP-MS	Inductively Coupled Mass Spectrometry
TXRF	Total Reflection X-Ray Fluorimetry
τ	Fluorescence Lifetime
$\Delta\bar{\nu}$	Stokes shift
Φ	Quantum yield
CHEQ	Chelation Enhancement of Quenching
CHEF	Chelation Enhancement of Fluorescence
HSAB	Hard–Soft Acid–Base
MLCT	Metal–Ligand Charge Transfer
ILCT	Intra–Ligand Charge Transfer
PET	Photo-induced Electron Transfer
ICT	Intramolecular Charge Transfer
PCT	Photo-induced Charge Transfer
TICT	Twisted Intramolecular Charge Transfer
FRET	Fluorescence Resonance Energy Transfer
ESIPT	Excited-State Intramolecular Proton Transfer
HOMO	Highest Occupied Molecular Orbital
LUMO	Lowest Unoccupied Molecular Orbital
HaCaT	Aneuploid immortal keratinocyte
HEPES	4-(2-Hydroxyethyl)piperazine-1-ethanesulfonic acid
DFT	Density functional theory
TDDFT	Time-dependent density functional theory
CPCM	Conductor-like Polarizable Continuum Model
ECP	Effective core potential
MeCN	Acetonitrile
MeOH	Methanol
NaOH	Sodium hydroxide
NaCl	Sodium chloride

DCM	Dichloromethane
DMF/dmf	Dimethyl formamide
H_2O	Water
DMSO/dmso	Di-methyl sulfoxide
mL	Milliliter
μM	Micro molar
μL	Micro liter
nM	Nano molar
mM	Mili Molar
fM	Femto molar
K_a	Binding constant/Association constant
K_{ass}	Association constant
K_d	Dissociation constant
K_f /K_f'	Formations constant
ex	Excitation
em	Emission
λ	Wavelength
HeLa	Human epithelial carcinoma cell
HepG2	Human hepatocellular liver carcinoma cells
HCT116	Human colon cancer
PBS	Phosphate-buffered saline
DMEM	Dulbecco's Modified Eagle's Medium
MTT	3-(4,5-di methylthiazol-2-yl)-2,5 diphenyltetrazolium bromide
%T	Percentage of Transmittance
FBS	Fetal Bovine Serum
EDTA	Ethylenediaminetetraacetic acid
Na_2H_2EDTA	Disodium EDTAdihydrate
TPEN	Tetrakis-(2-pyridylmethyl) ethylenediamine
LOD	Limit of detection
MS	Mass spectroscopy
NMR	Nuclear magnetic resonance
FT-IR	Fourier transform Infrared
Fig.	Figure
AIE	Aggregation-induced emission
SMMC-7721	Hepatocellular carcinoma cell
FI /F.I	Fluorescence Intensity
GSH	Glutathione
Cys	Cysteine
Raw 264.7	Abelson leukemia virus transformed cell
hMSCs	Human mesenchymal stem cells
BINOL	1,1'-Bi-2-naphthol
NIR	Near-infrared

MCF7	Acronym of Michigan Cancer Foundation-7 cell
FE	Fluorescence Enhancement
EJ	Lung cancer cell
Tris–HCl	Tris (hydroxymethyl) aminomethane hydrochloride
UV	Ultraviolet
Vis	Visible
h	Hours
HPLC	High-performance liquid chromatography
TMS	Tetramethylsilane
KBr	Potassium bromide
K_2CO_3	Potassium carbonate
$ESI\text{-}MS^+$	Electrospray ionization mass spectrometry
HRMS	High-resolution mass spectrometry
CH_2Cl_2	dichloromethane
$SOCl_2$	Thionyl chloride
$CDCl_3$	Chloroform-d
DMSO-d_6	Deuterated Dimethyl sulfoxide
LiCl	Lithium chloride
ATP	Adenosine triphosphate
Pi	Phosphate - Wikipedia
PPi	Pyrophosphate
CD_3OD	Methanol-d4
Et_3N	Triethylamine
MHz	Megahertz
f	Oscillator strength
°	degree
Å	Angstrom
eV	Electron volt

Contents

Introduction

Title

“Design and Synthesis of Fluorescein Based Molecular Probes for Hg(II) Recognition”

Chapter 1

1. Introduction

Now-a-days fluorescence technique is a very essential tool for the detection of metal ions at a very low concentration (from nano - to pico-molar) within a very short period of time. Several chemists, biologists and environmental scientists frequently use this tool for chemical sensing. Cations such as biologically abundant metal ions: Na^{+}, K^{+}, Ca^{2+} and Mg^{2+}, transition-metal ions: Cr^{3+}, Mn^{2+}, Fe^{2+}, Fe^{3+}, Co^{2+}, Ni^{2+} Cu^{2+}, and Zn^{2+}, and heavy-metal ions: Cd^{2+}, Hg^{2+} and Pb^{2+}, anions: CN^{-}, SO_4^{2-}, $S_2O_4^{2-}$, $P_2O_7^{4-}$, HCO_3^{-}, NO_3^{-}, NO_2^{-} Cl^{-}, F^{-}, PO_4^{3-}, S^{2-}, Br^{-}, $H_2AsO_4^{-}$,N_3^{-} ,OAc^{-},ClO_4^{-}, SCN^{-}, CO_3^{2-}, etc., gases and neutral molecules are smoothly detected by suitable fluorescent probes using this technique. Some of the cations are biologically relevant and some of very toxic and harmful. Among all of those cations, transition metal ions and toxic heavy metal ions, like mercury, are the utmost important to detect at very low concentration in the environmental and biological samples and fluorescence technique claimed to be the best for this purpose.

1.1 General aspects of mercury(II)

Among the most hazardous and ubiquitous pollutants, mercury is the most toxic element.[1] Mercury pollution spreads over the globe and remains as a danger to living body and the environment because both elemental and ionic forms can be converted to methyl mercury by bacteria in the environment, which is subsequently bio accumulated through the food chain. The mercury contamination is widespread and arises from various natural sources,[2] causing various environmental and health problems. In the living body it can easily pass through skin, respiratory and gastrointestinal tissues, where it can damage the central nervous and endocrine systems.[3] Moreover, mercury and its derivatives have a high affinity for thiol groups in enzymes and proteins resulting dysfunction of cells and consequently causing health problems.[4] In the human body the presence of Hg^{2+}causes DNA damage, prenatal brain damage, different cognitive and motion disorders, myocardial infarction, Minamata disease, some kinds of autism and damage of the brain, central nervous system, kidneys, immune system and endocrine system.[5-9] The maximum permissible level of inorganic Hg^{2+} in drinking water is 2 ppb according to the US

Environmental Protection Agency (EPA), the selective and sensitive determination of mercury ion is of typical interest, especially in on-site or in situ analyses for rapid screening applications.[10]

1.2 Conventional methods for the determination of iron and mercury ions

It is a very challenging task to develop very precise and sensitive instruments for the estimation of metal ions in the concentration ranges set by the standards and guidelines for the reasons of toxicity towards human health. There are various analytical techniques that have been developed for detection of metal ions. The most recommended common methods in watery samples include photometric methods, flame or graphite furnace atomic absorption spectroscopy (FAAS /GFAAS),[11,12] inductively coupled plasma emission or mass spectrometry (ICP-ES, ICP-MS),[13] total reflection X-Ray fluorometric (TXRF)] etc.[14] These methods are sensitive to metal ions which have a wide linear range and low detection limits, but most of them require complicated pre-treatment procedures which are very cost-effective and time-consuming and not suitable for performing assays in the common laboratories. Thus, a simple and comparatively less expensive method is needed which detects and quantifies the metal ions for real-time monitoring of environmental, biological, and industrial samples. Optical detections via colorimetric or fluorescence changes are the most convenient method among various detection techniques, due to the low time consuming, simplicity and low detection limit.[15,16] Colorimetric sensors enable on-line and field monitoring but the methods based on fluorescent molecular sensors offer distinct advantages in terms of sensitivity, selectivity, response time and local observation by fluorescence imaging spectroscopy. Not only that, fluorescent sensors are useful tool to sense *in-vitro* and *in-vivo* biologically important metal ions because of the simplicity and high sensitivity of fluorescence assays. Therefore, considerable efforts are being paid to develop selective fluorescent chemical sensors for metal ions detection.[17-18]

1.3 Introduction to spectroscopy:

God given us eyes that are the best detector for the different colour in the nature with absolute resolution. This detectability of band width through eyes restricted to visible region from the entire range of electromagnetic radiation. Spectroscopes are developed to study the interaction between electromagnetic radiations with the matter (**Figure 1.1**).

In the second half of the 19th century, the field of spectroscopy elevated to its highest level being successfully applied to the analysis of substances. Gustav Robert Kirchhoff – physicist , Robert Wilhelm Bunsen – a chemist and Carl August von Steinheil an optician, jointly manufactured a spectroscope setting the groundwork for the wide application of spectroscopy in science and technology through their works "*Chemical Analysis through Spectral Observations.*" While experimental results of spectroscopic studies are important inputs for the development of theoretical models of the structure of matter, likewise the theoretical models are necessary for the interpretation of experimental results obtained from modern spectroscopy. Spectroscopy involves the interaction between electromagnetic radiation and matter, with the objective to determine the nature of the light and matter in question. [19] A plot of intensity (power) of this radiation as a function of wavelength, frequency, or energy is called the "spectrum".

Basic idea involves: i) Excitation ii) Detection.

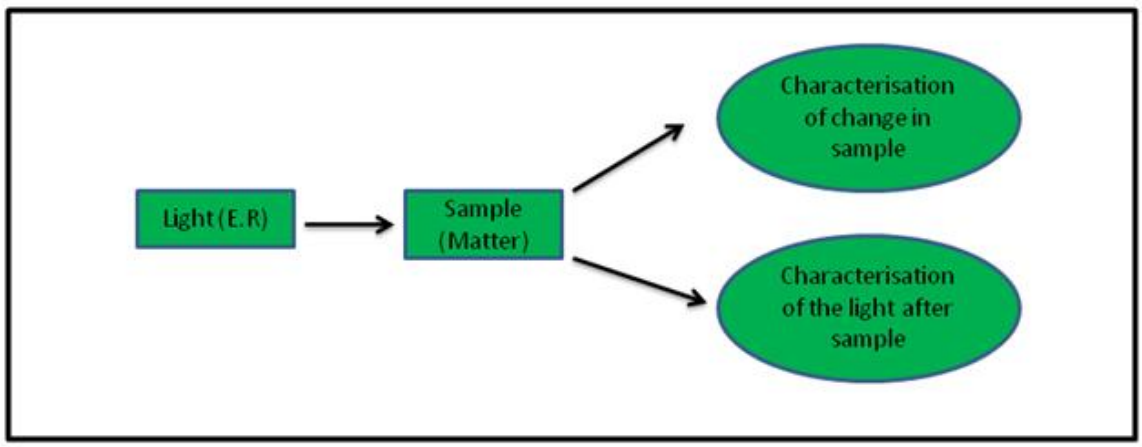

Figure 1.1: Schematic presentation of light and matter interaction.

There are two types of spectra such as continuous spectrum and line spectrum.[20,21] With the help of an absorption and emission spectra of a species a lot of information can be gathered about them. The basic difference between continuous and line spectrum is that first one contains all the wavelengths of a certain range and other one only the selective wavelengths. So the presence and absence of the lines in the spectrum makes the difference between them. When both the absorption and emission spectra of a species are put together, they form continuous spectra whereas either absorption or emission spectrum is a line spectrum. The terms absorption and

emission signifies how much light absorbed and emitted by a matter after interaction with the light. The emitted light is usually different from the incident light-which is measured by spectroscopy.

1.3.1 Absorption Spectroscopy

Absorption spectroscopy involves the absorption of photons by a sample during interaction with light and a plot of absorption of radiation as a function of frequency or wavelength of radiation is called absorption spectrum. The type of transition that an analyte may undergo changes with the change of photons' energy. In the case of IR spectroscopy, there occurs absorption of relatively low energy in the infrared region in the vibrational energy levels of a chemical bond within that molecule. Whereas, higher energy photons, will excite the valence electrons to promote to an excited state. There are a number of absorption spectroscopies namely, Infrared (IR), Atomic absorption, Raman, UV-VIS, ESR, NMR), X-ray absorption etc. [22-26]

1.3.1.1 Electronic Spectroscopy

Every moment we can see many colorful things around us from morning to night. The cause of various colours of different things is due to an electronic spectroscopy in the visible region. The UV spectroscopy is nothing but electronic spectroscopy as it is associated with promotion of an electron from lower to higher energy levels. UV spectroscopy is a type of absorption spectroscopy where a molecule absorbs electromagnetic radiation in the range of 200-400 nm and the amount of energy absorbed counts the energy difference between the ground and excited states, usually, from HOMO, the highest occupied molecular orbital to LUMO, the lowest unoccupied molecular orbital. For most of the molecules, **s** orbitals containing lone pair of electrons are involved in sigma bond formation and are low energy orbitals, whereas p orbitals and anti-bonding orbitals are higher energy orbitals. Some important transitions with increasing energies are:

$$\mathbf{n \rightarrow \pi^*,\ \pi \rightarrow \pi^*,\ n \rightarrow \sigma^* \text{ and } \sigma \rightarrow \sigma^*.}$$

UV spectroscopy obeys the Beer-Lambert law, which states that when a beam of monochromatic light is passed through a solution of an absorbing substance, the rate of decrease of intensity of radiation is proportional to the thickness of the absorbing solution, the intensity of incident radiation and the concentration of the solution and mathematically expressed as:

$$A = \log (I_0/I) = \varepsilon cl$$

with, A = absorbance or optical density, I_0 = intensity of incident radiation, I = intensity of emitted radiation from the sample cell, C = molar concentration of solute, L = path length of sample cell (cm.), ε = molar absorptivity. Transmittance (*T*) - another form of describing the absorption of light and it is simply the ratio of the intensity of the radiation transmitted through the sample to that of the incident radiation as given below.

$$\%T = [I/Io] \times 100.$$

1.3.1.2 Infrared Spectroscopy

Infrared spectroscopy uses electromagnetic radiation in the region 4000-400 cm^{-1} with total spans 12820 to 33 cm^{-1} and useful to gather the information about the molecular structure, The presence of functional groups, C=C, C=O, C≡N, OH, NH_2, $CO-CH_3$ etc and bonds C-H, C-D etc can easily be assigned through their characteristic frequencies exhibited in IR spectra. Here, vibrational transitions occur in the presence of IR light and the energies of the IR absorptions are related to the bond strength in molecules and the masses of the connected atoms. Historically, infrared spectra have been represented as percent of transmittance (%T) versus either the wavenumber(ν) or the wavelength (λ). The use of wavenumbers (in cm^{-1}) is standard. By convention, the wavenumbers are plotted in decreasing order from left to right.

1.3.1.3 Magnetic Resonance Spectroscopy

Magnetic resonance is of two types **i)** Nuclear Magnetic Resonance (NMR) and ii) Nuclear Quadrupole Resonance) (NQR) (a zero field NMR). Magnetic Resonance is associated with nucleus having non-zero spin (I ≠0) resulting to be resonance active. NMR & NQR refer to resonance from nuclei having I = ½ & I > ½ (I, is the spin of the nucleus). In the absence of external magnetic field these spins a randomly oriented (see figure below left). However, in an external magnetic field, the nuclear spins will align themselves in two possible orientations:

parallel to direction of external field or (2) antiparallel to the external field). (**Figure 1.2**)

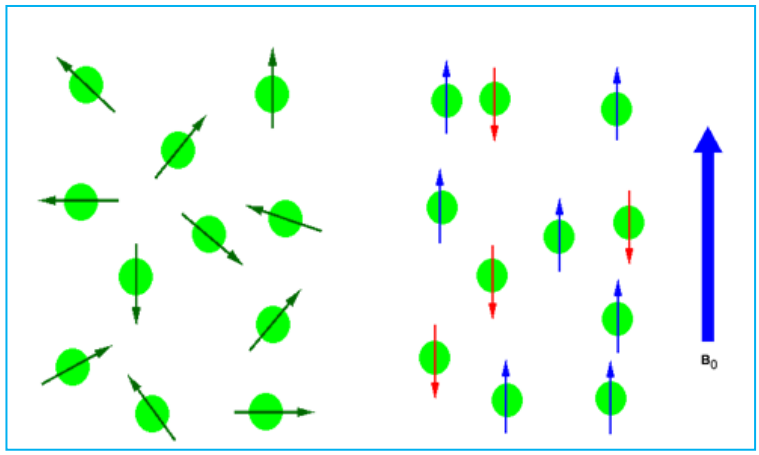

Figure 1.2. (Left) Random orientation of nuclear spins in the absence of an external magnetic field. (Right) Ordered orientation of nuclear spin in an external magnetic field.

The amount of energy, and hence the exact frequency of EM radiation required for resonance to occur is dependent on both the strength of the magnetic field applied and the type of the nuclei being studied. As the strength of the magnetic field increases the energy difference between the two spin states increases and a higher frequency (more energy) EM radiation needs to be applied to achieve a spin-flip(**Figure 1.3**).

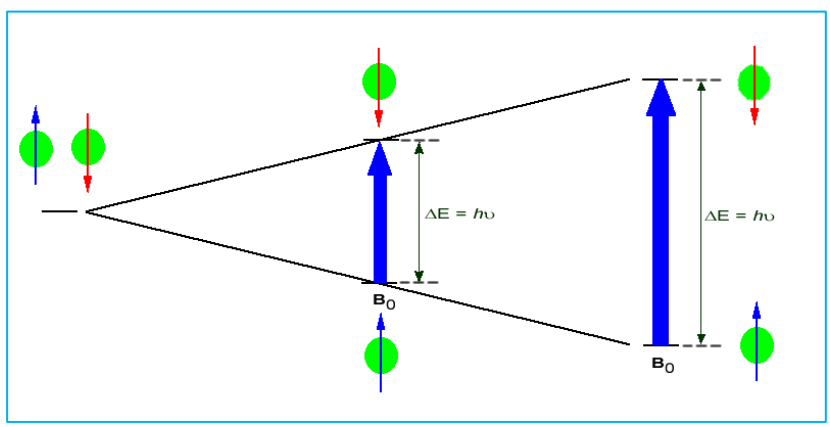

Figure 1.3. Distribution of nuclear spin populations in the two possible energy levels in nuclei with $I = ½$.

NMR spectroscopy is a powerful tool for structure elucidation of a compound by knowing number of signals, position of the signals (chemical shift), intensity of the signals and the

splitting pattern of the signals (number of peaks within a signal). Besides ^{1}H and ^{13}C many other nuclei (e.g. ^{11}B, ^{19}F, ^{31}P, and ^{195}Pt) give important information about concerned compound and its structure. NMR is an indispensable tool in chemistry extensively used for structure elucidation and also to monitor the progress of a reaction. Organic chemistry cannot be imagined without this powerful analytical tool. Proton NMR is also important because the light hydrogen nucleus is not easily detected by X-ray crystallography.

1.3.1.4 Electron Paramagnetic Resonance (EPR)

Electron paramagnetic resonance (EPR) or electron spin resonance (ESR) spectroscopy is used to study a chemical species containing one or more unpaired electron(s) such as organic and inorganic free radicals or inorganic complexes possessing a paramagnetic transition metal ion.

EPR is actually similar to NMR but it deals with electronic spin is factor in EPR whereas in case of NMR it is the nuclear spin is the main cause of spectrum. EPR is only applicable for molecules or ions with unpaired spins and for this reason it has specificity.

1.4.1 Background and introduction to fluorescence spectroscopy

The fluorescence was first reported by Nicolás Monardesin, a Spanish physician and botanist, in 1565 when he observed a blue tinge in a liquid solution of the infusion of a wood from Mexico used to treat kidney and urinary diseases, known as *Lignum nephriticum* (Latin for “kidney wood”).[27-30] In the following centuries, the unusual optical properties of the wood attracted the attention of a number of scientists like Kircher, Grimaldi, Boyle, Newton, Herschel, and many others.[27,28]

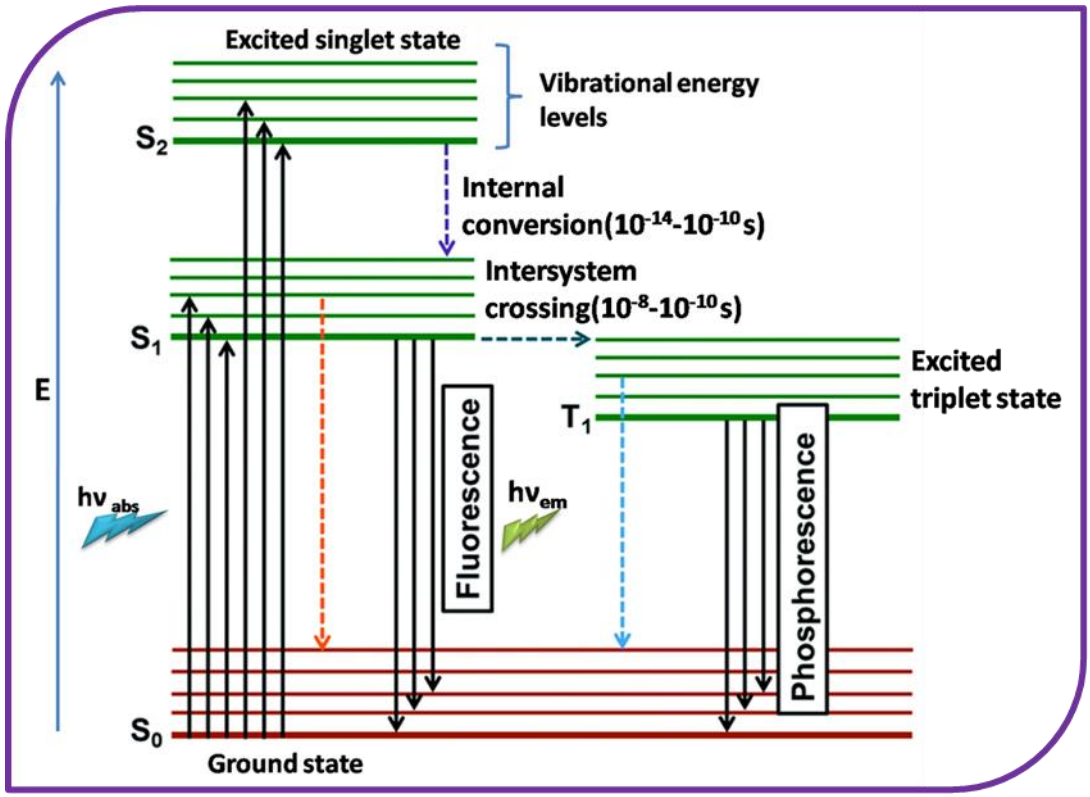

Figure 1.4. The Perrin-Jablonski diagram for different photophysical transitions.

The fluorescence was observed in fluorites by Edward D. Clarke (1819) and René Just Haüy (1822) observed while the presence of same phenomenon in chlorophyll was described by David Brewster in 1833. In 1845 John Frederick William Herschel reported the first observation of fluorescence from a quinine solution in sunlight.[31,32] Above all, George Gabriel Stokes first introduced the term "fluorescence" in his report and identified fluorescence correctly as an emission process in 1852[33] and thus it was marked as a milestone in fluorescence research. In the first line of his paper, Stokes mentioned that his research was motivated by Herschel's previous report about the quinine solution.

Alexander Jablonski in 1935 illustrated the processes that occur between the absorption and emission of light using a diagram, known as a Jablonski diagram[34] (**Figure 1.4**) which provides a theoretical basis for the development of fluorescence spectroscopy.

1.4.2 Fluorescence lifetime and Quantum yield:

The utmost significant features of a fluorophore are described by fluorescence lifetime (τ) and fluorescence quantum yield (Φ_F). The average time a molecule spends in the excited state prior to return to the ground state is known as the life time of the excited state. In the absence of any deactivating perturbations the rate constant for fluorescence emission, k_f, is inversely related to the natural radiative lifetime, τ_N, of the molecule, i.e.,

$$k_f = \frac{1}{\tau_N} = \frac{1}{\tau_f^0} \qquad (1.0)$$

In the presence of other competitive deactivation processes, the average lifetime of the molecule is much reduced and the actual lifetime, τ_f, becomes

$$\tau_f = \frac{1}{k_f + \sum k_i} \qquad (2.0)$$

Where k_i is the rate constant for the ith competitive process, assumed to be unimolecular.[35]

1.4.2.1 Excited state lifetimes:

The life time of an excited state (τ) is defined by the average time the molecule spends in the excited state prior to return to the ground state. Always triplet state life time is greater than the singlet state one. If τ_S is the lifetime in the excited state S_1, it is given by-

$$\tau_S = \frac{1}{Kr^S + K_{nr}^S} \qquad (3.0)$$

Where K_r^S and K^S_{nr} are the rate constants for radiative deactivation for the transition from S_1 to S_0 with emission of fluorescence and for non-radiative deactivation, respectively. K^S_{nr} is the sum of rate constant for internal conversion and rate constant for inter system crossing. If the only

way of de-excitation from S_1 to S_0 was fluorescence emission then lifetime is given by $\tau_S = 1/k^s_r$ and called as the radiative life time .

1.4.2.2 Fluorescence quantum yields:

The quantum efficiency (Φ_F) indicates the efficiency of a fluorescence process and is defined as the number of emitted photons relative to the number of absorbed photon. A quantum efficiency of ~ 0.9 indicates a highly efficient process whereas $\Phi_F = 0$ indicates that the molecule does not fluoresce. The fluorescence quantum yield Φ_F is the fraction of excited molecules that return to the ground state S_0 with emission of fluorescence photons is given by:

$$\phi_F = \frac{K_r^{\ S}}{K_r^S + K_{nr}^S} = K_r^s . \tau_S \qquad (4.0)$$

The much smaller radiation less decay rate (K^S_{nr}) maximizes the rate of radiative decay (k_r^S) making fluorescence quantum yield close to unity .[36,37]

1.4.3 Fluorescence Quenching:

In the fluorescence quenching process there is a decrease in fluorescence intensity of a sample. A variety of molecular interactions can be responsible for the quenching in fluorescence intensity like (a) excited-state reactions, (b) energy transfer, (c) ground-state complex formation, (d) molecular rearrangements and (e) collisional quenching included in it. To facilitate the quenching process the fluorophore (F) and quencher (Q) should come into molecular contact at the van der Waals radii distance, allowing the electron clouds of both molecules to interact (**Figure 1.5**). As in (**Figure 1.4**), the quencher remains in the ground state. Depending on the mechanism, the quenchers interact with the fluorophore in the ground state or in the excited state, which then returns to the ground state. The important point is that quenching is due to short-range interactions between F and Q.

Fluorescence quenching process that occurs shortens the lifetime of the emitting molecule in the excited state.[38] These quenching reactions may occur through energy or electron transfer processes. The fluorescence quenchers cover a wide variety of substances. The molecular oxygen

is one of the well-known collisional quencher. Paramagnetic molecular oxygen has a role on fluorophore to experience intersystem crossing to the triplet state and due to other deactivation process fluorophore is quenched.

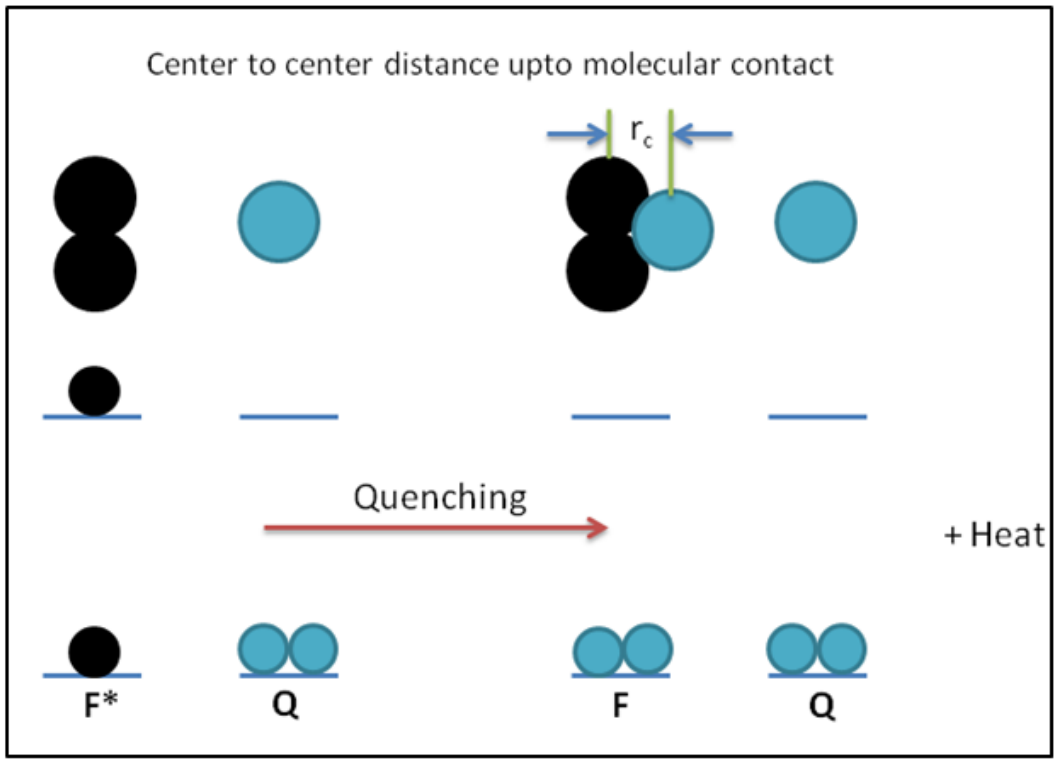

Figure 1.5. General representation Fluorescence quenching pathway.

To achieve reliable measurements of the fluorescence quantum yields or lifetime sometimes it is essential to remove dissolved oxygen from the fluorophore solution. Aliphatic amines and substituted aromatic hydrocarbons are efficient quenchers. Another common quenches include heavy atoms like iodide, bromide, pseudo halide etc as well as heavy metal ions like Hg^{2+}, Cd^{2+} etc.. Quenching by heavy atoms may be the outcome of intersystem crossing to an excited triplet state, promoted by spin-orbit coupling of the excited singlet fluorophore and the heavy atom. Quenching of fluorescence take place also by the paramagnetic substances like Mn^{2+}, Fe^{3+}, Cu^{2+} etc. either through electron transfer or energy transfer from fluorophore to the quencher.[38-40]

1.4.4.1Fluorescent sensors and Concepts of Chemosensor and Chemo dosimeter:

Based on fluorescence signaling mechanism fluorescent sensors can be categorized into four different groups:

(i)Turn-On (ii) Turn-Off, (iii) Ratiometric (**Figure 1.6**) and (iv) Chemo dosimeters.

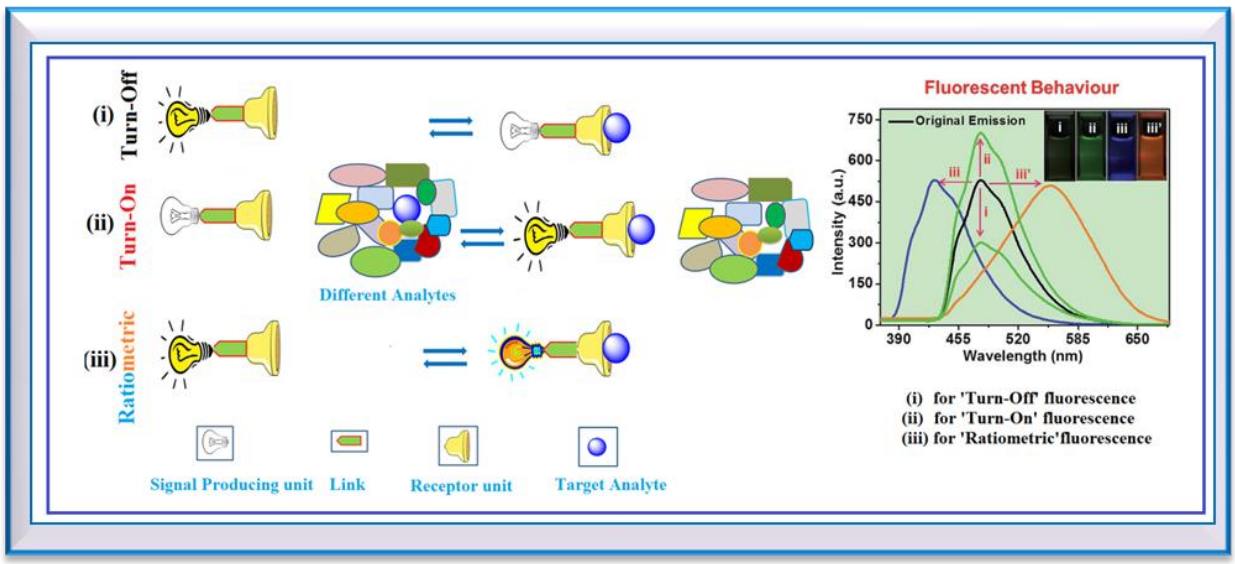

Figure 1.6. Schematic representation of various types of fluorescent molecular sensors**.**

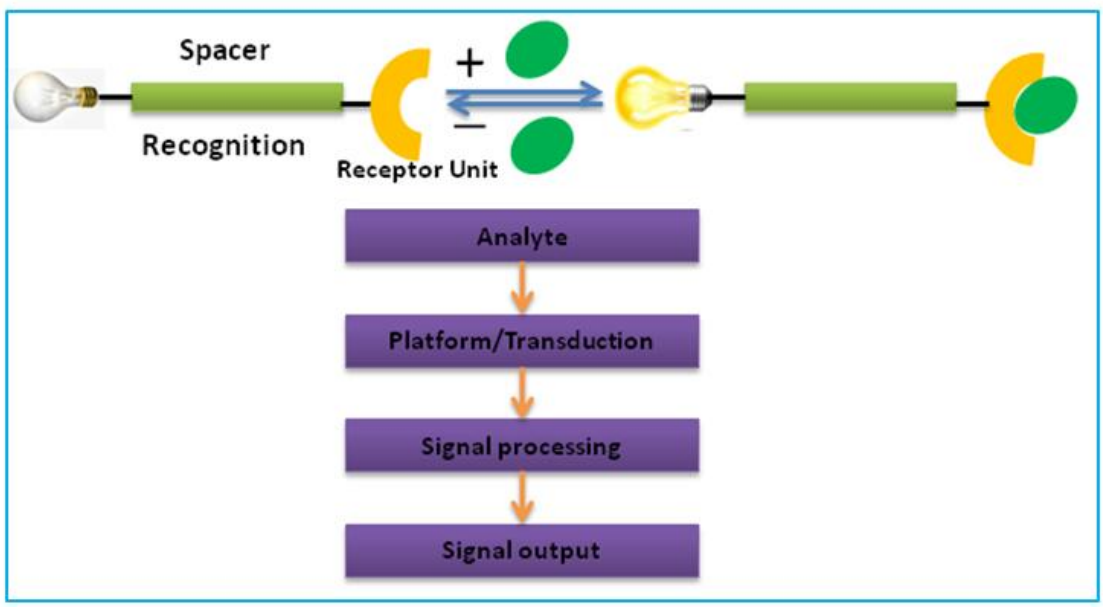

Figure 1.7. Schematic diagram showing binding of a metal ion/analyte (guest) by a molecular sensor (host), producing a complex accompanying with change in optical properties.

Hence in a broad sense, concepts of **chemosensor** arise from the **reversibility**. '***Chemosensors**' are defined by molecules of an abiotic origin that interact with the analyte to yield measurable signals with a real-time response'*. The general principle of a **chemosensor** is the enhanced and shifted emission upon recognition of the target analyte and the processes are, most of the cases, generally reversible[41,42] while the chemo dosimeter approach is irreversible one. Example of various types of fluorescence chemosensors and chemodosimeter[43-48] are given in the (**Figure 1.7** and **Figure 1.8**)

A chemosensor based on the coordination event between the receptor unit of the molecule and the analyte results with the concomitant reversible change in signal.[41,49] By the addition of a strong chelating agent (normally EDTA) or by suitable anion based on HSAB principle the reversal of optical response of the metal bound receptor of the chemosensors are generally achieved.

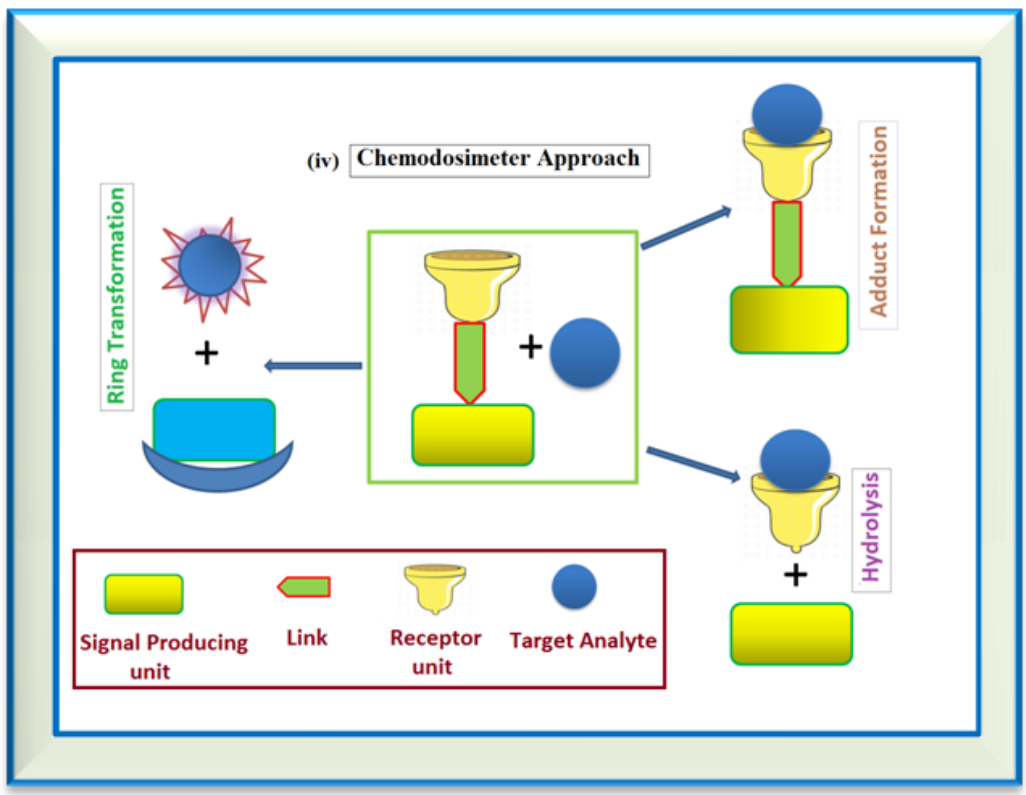

Figure 1.8. Schematic representation of various types of fluorescent Chemo dosimeter.

On the other hand, **chemo dosimeter** concept appears with respect to the **irreversible** binding. So, fluorescent chemodosimeters are the molecular systems with abiotic receptors to achieve analyte recognition in a **irreversible** transduction of a fluorescent (optical) signal and usually designed for a specific reaction induced by the analyte of interest. Here the breaking and formation of covalent bonds are associated with significant chemical transformation. This process results in the formation of products differing from the starting chemodosimeter with different optical properties.[42,50]

1.4.4.2 Applications of fluorescent chemosensors:

The applications of fluorescent chemosensors can be mainly categorized into the following important fields:

1. Detection of not only environmentally relevant metal ions but also important pollutants such as heavy metal ions.
2. Monitoring of biologically important species via fluorescence imaging in *in-vivo* or *in-vitro* systems.

Due to the distinct advantage in terms of the reusability fluorescent **chemosensors** are found to be superior to **chemodosimeters**. Hence, design of fluorescent chemosensor is an active as well as interesting field of research that provides the potential practical benefits in cell physiology and analytical and environmental chemistry providing a proving ground for manipulation and/or engineering of various photophysical processes that ultimately helps to achieve a goal of selective and sensitive signaling of targeted molecular or ionic species.[51]

1.4.5 Some conventional mechanisms for construction of fluorescent probes

The conventional mechanisms for construction of fluorescent probes have been developed such as photoinduced electron transfer (PET),[52-58] photoinduced charge transfer (PCT),[46] Intramolecular charge transfer (ICT),[53,55-58] twisted intramolecular charge transfer (TICT),[59] metal-ligand charge transfer (MLCT),[56,60] electronic energy transfer (EET),[55,56] Förster resonance energy transfer (FRET),[61] through bond energy transfer,[62] excited state intramolecular proton

transfer (ESIPT),[63] aggregation-induced enhancement of emission (AIEE) and excimer/exciplex formation.[64,55-57,65]

1.4.5.1 Photoinduced Electron Transfer (PET)

In the fluorescence spectroscopy, PET is the most important and very common process where only long range electronic interactions are possible between the fluorophore and receptor through the intervening spacer in **fluorophore—spacer—receptor** systems **(Figure 1.9)**. Here electron transfer occurs from donor to acceptor in the excited state (redox type reaction) resulting a charge separation).

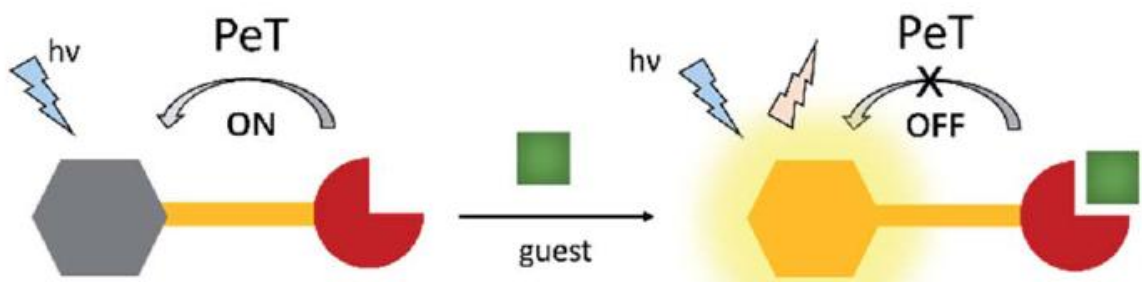

Figure 1.9. Fluorophore (A)-Spacer-Ionophore (D)

It occurs when certain photoactive materials interact with light resulting emission enhancement or quenching. It is widely used in photosynthesis and in artificial systems for the conversion of solar energy based on photoinduced charge separation. Thus, it has a great application for fluorescence sensing of cations, anions or neutral molecules.

PET based fluorescent probes are mainly consisting of an electronically independent receptor and a fluorophore that are covalently connected by a spacer thereby minimizing the ground state interactions. A PET based sensor changes its quantum yield as well as fluorescence intensity upon recognition of analyte(s).[66] In chemosensing of analytes de Silva *et. al*.[67] and Czarnik *et al*. proposed this design principle where receptors (ionophores) act as electron donors (D) and fluorophores are electron acceptors (A).

By absorbing a photon of matching energy an electron is promoted from the highest occupied molecular orbital (HOMO) to its lowest unoccupied molecular orbital (LUMO). As shown in

Figure 1.10, if the HOMO of the fluorophore lies just above the HOMO of the inophore but below of its LUMO, the electron in the HOMO of ionophore will be transferred to the HOMO of the fluorophore through space on excitation by light of an appropriate wavelength (λ_{ex}), which blocks the emission of fluorophore by blocking the LUMO→ HOMO transition of the ionophores, instead, favours the ionophore LUMO to fluorophore HOMO transition resulting a fluorescence quenching. However, when the receptor binds to its target, the PET process is blocked resulting restoration of fluorescence. According to this principle, a large number of fluoroionophores have been developed by changing the fluorophore and/or changing the binding motif.[68-71]

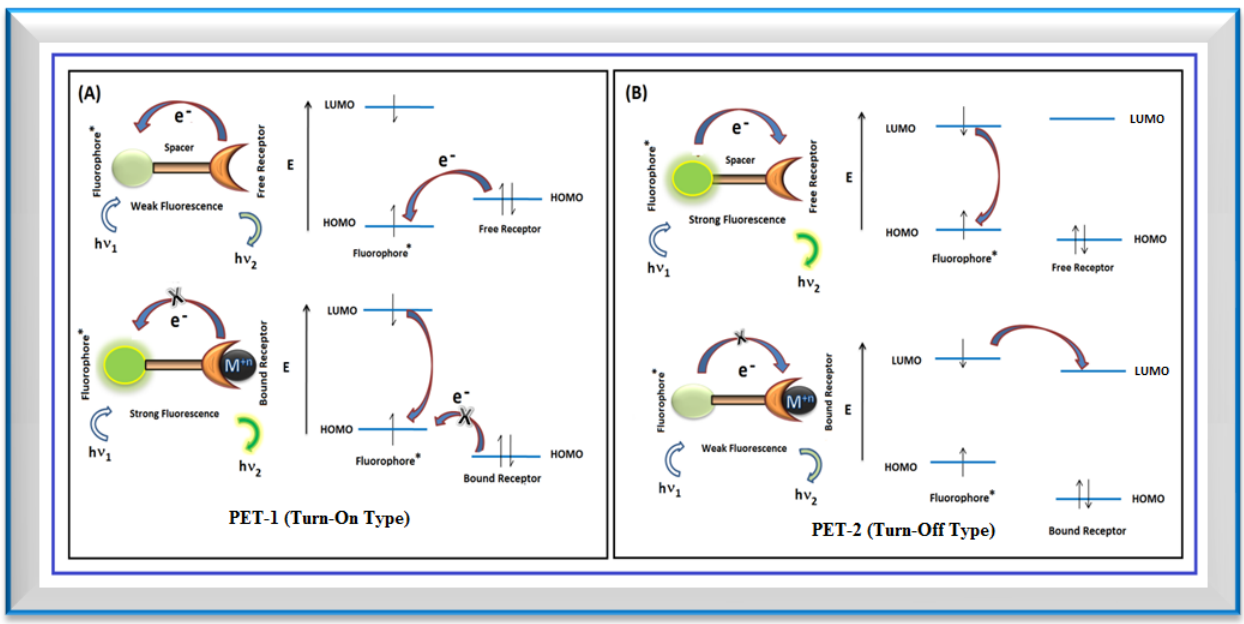

Figure 1.10. Cation recognition mechanism based on fluorescent PET sensors [(A) reductive electron transfer and (B) Oxidative electron transfer]

1.4.5.2 Photo-induced charge transfer (PCT):

When an electron-donating group (-NH_2, -NMe_2, -CH_3O) attached with a donor (D) is conjugated with an electron-withdrawing group (>C=O, -CN) on the acceptor(A), an electron will move from an orbital of D to an orbital of A, accompanied with an instantaneous change in the dipole moment of the fluorophore which is known as *photo-induced charge transfer*. PCT is a key step in the light-harvesting (LH) process for energy conversion. A positive

solvatochromism is resulted with the higher polarity of the solvent and lower energy of the relaxed state causing a red shift of the emission spectrum (**Figure 1.11**). A close relationship between the microenvironment and spectral properties anticipates a change in the photophysical properties of fluorophore through interaction of cation(s) with the donor or acceptor moiety thereby affecting the intramolecular charge transfer (ICT) efficiency. There are two different ways for the utilization of the PCT type fluorophores in cation sensing[72](**Figure 1.11**).

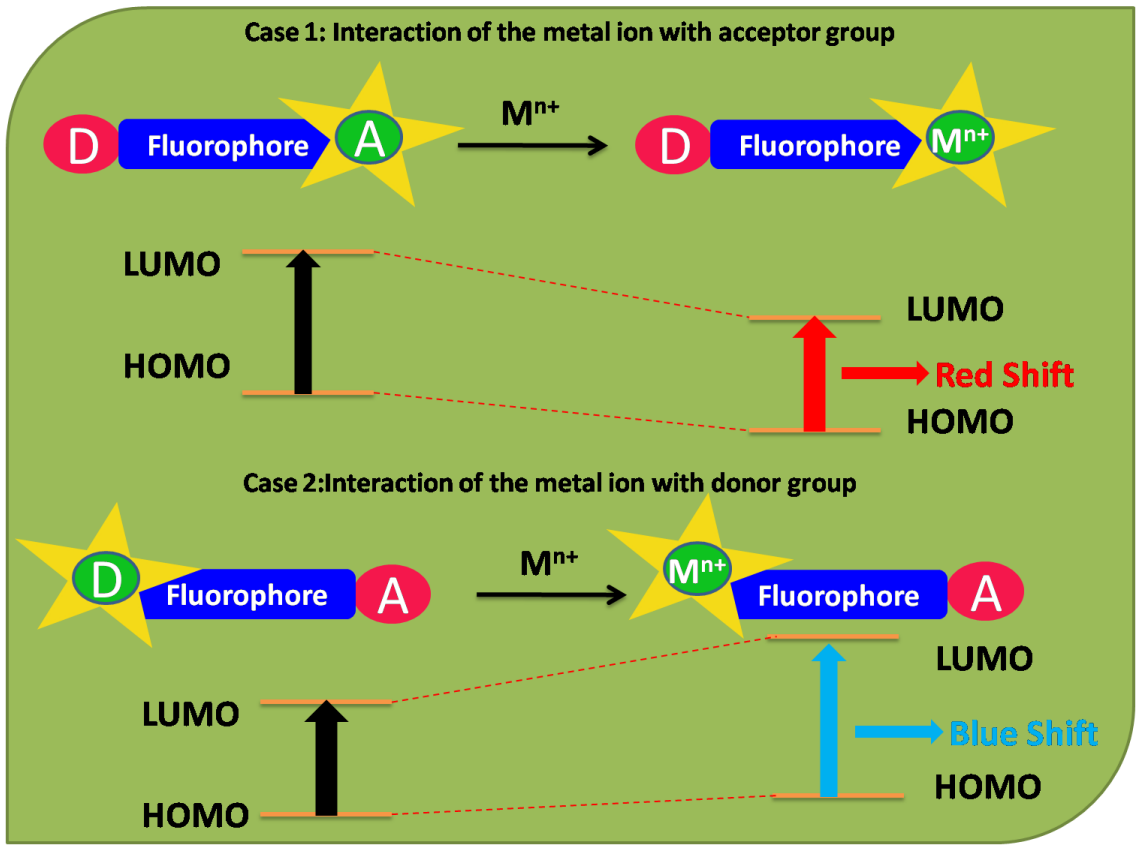

Figure 1.11. Sensing mechanisms of PCT fluorescent probes for metal cations.

The red shift occurs when cation binds to accepter; complexation enhances the electron withdrawing character of the acceptor and increases molar absorption coefficient and is explained by the cation-stabilized excited state of the fluorophore.[73] On the contrary, the blue shift in the fluorescence spectra arises when the cation binds to the donor (D) thereby reducing its electron-donating behaviour due to loss in conjugation of the system. As a consequence there

is a decrease in absorption coefficient. Compared with the absorption spectrum fluorescence spectrum often undergoes with a much smaller blue shift (**Figure 1.11**). This phenomenon arises due to photo disruption between cation and donor group.[72] Upon excitation, charge transfer from D to A produces a partial positive character on D thereby reducing its binding ability with cations. Such kind of PCT chemosensors are suitable for selective detection of metal ions.[74,75]

1.4.5.3 Chelation Enhanced Fluorescence (CHEF)

The fluorophore-receptor interaction is modified in the presence of a guest molecule leading to fluorescence turned OFF or ON due to the binding of the guest at the receptor site. Such type of interaction of a guest molecule may lead to chelation enhanced fluorescent quenching (CHEQ) or chelation enhanced fluorescence (CHEF) (**Figure 1.12**).

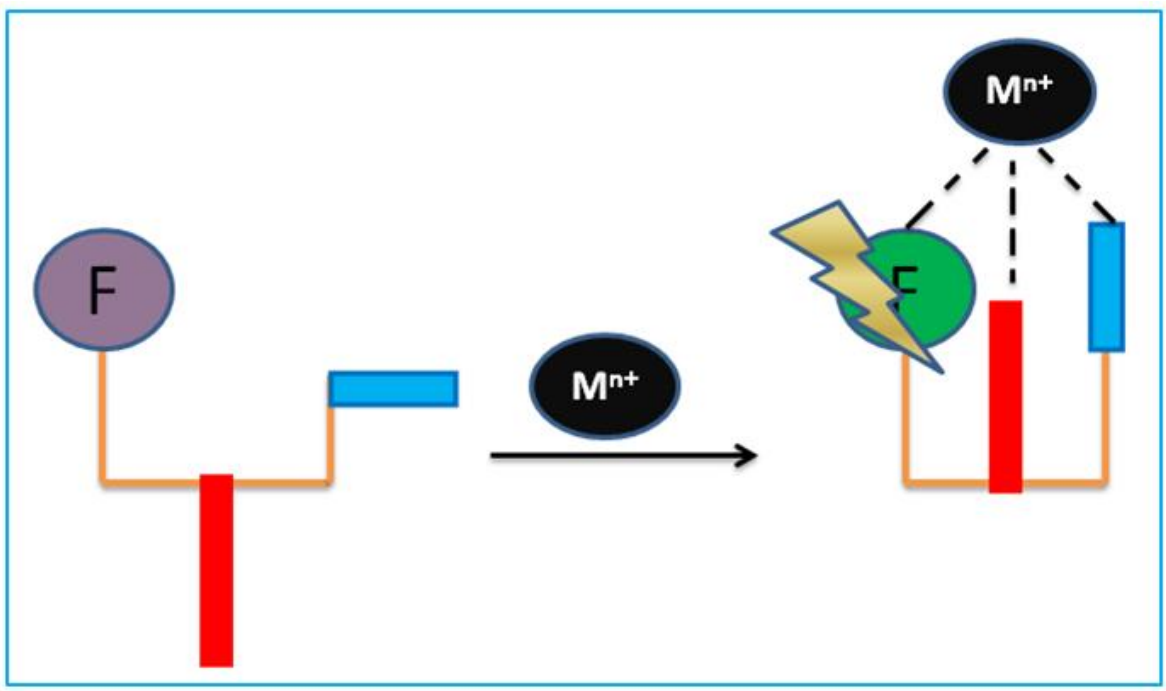

Figure 1.12. Pictorial representation of chelation enhanced fluorescence.

Here the guest molecules are in general the metal ions showing the CHEF effect. For the CHEF based fluorosensor consisting of 'fluorophore—spacer—receptor', one needs to suppress the

interaction between the fluorophore and the quenching metal ions so as to observe fluorescence changes on the metal ion binding.[53]

1.4.5.4 Excited state proton transfer (ESIPT):

The excited state proton transfer (ESPT) is prevailing in the fluorophores that contain intramolecular hydrogen bonds. A large Stokes shift, compared to the normal fluorophores is the striking photophysical property of the ESIPT chromophores.

There is intramolecular hydrogen bonding in the ESIPT chromophores where the *cis*-enol form exists at the ground state which upon photoexcitation, the singlet excited state of the enol form is populated which favours the ultrafast ESIPT process (sub picosecond time scale) leading the *cis*-keto form at the singlet excited state, which is again stabilized by intramolecular hydrogen bonding. It is to be mentioned here that no geometry relaxation occurs during this excitation process as per the mandate of the Franck–Codon principle. As the ESIPT is much faster than the fluorescence process the observed fluorescence mainly due to the keto tautomer, with few exceptions. [76]

In the ESIPT chromophores there exists six- or five-membered ring of hydrogen bonding configuration both in ground state and excited state. The transfer of a proton from hydroxyl or amino group to a neighbouring hydrogen-bonded atom of carbonyl oxygen, or imine nitrogen results in the lowering of energy level of the excited state. As the enol-form is energetically favourable reversed proton transfer may occur on relaxation of the keto-form to the ground state (**Figure 1.13**).[77]

The coordination to a metal ion results in removal of the proton involved in H-bonding which disrupts the ESIPT process. As a consequence, there may arise a significant blue shift in the emission spectra, if the hydroxyl (or amino) proton is sufficiently acidic. Therefore a strong influence of the pH of the medium as well as polarity of the solvent may be prevailing on the overall fluorescence emission spectra of ESIPT fluorophores. The excitation wavelengths of the most reported ESIPT fluorophores fall in the visible range. Therefore, the approach of ESIPT inhibition through metal coordination could be promising for the development of ratiometric probes for metal ions.[77]

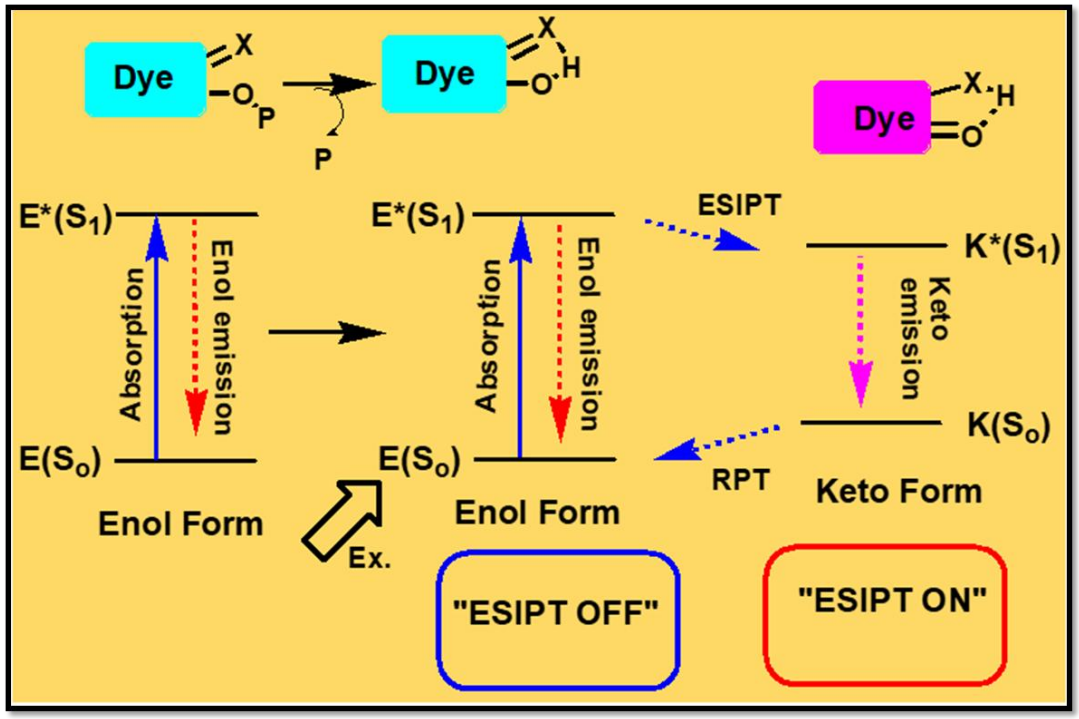

Figure 1.13. Schematic representation of hydrogen bonding interactions in the ground state and electronically excited state and ESIPT concept with respect to cation sensing.

1.4.5.5 Aggregation-based fluorescent sensing:

Recently, fluorescent probe displaying aggregation-induced enhanced emission (AIEE) which is an uncommon phenomenon displaying by organic luminophores. Most of such organic molecules have

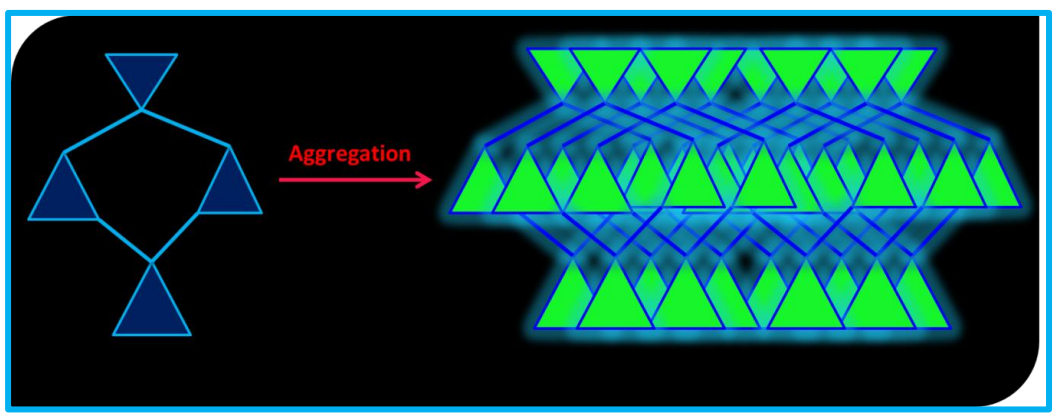

Figure 1.14. Representation of aggregation concept.

planar structure and higher photoemission efficiency in solution than in solid states. Due to free rotation of groups of organic luminophores they consume energy after they have been excited in solution.

In solid state the photoemission efficiency becomes higher than in solution when these luminophores crystallize and the free rotation of groups is restricted. This phenomenon is known as aggregation-induced emission enhancement (**AIEE**) (**Figure 1.14**). In dilute solutions these probes display no or weak emission, however in concentrated solution it is enhanced to a large manifold as a consequence of aggregation of the fluorophore species.

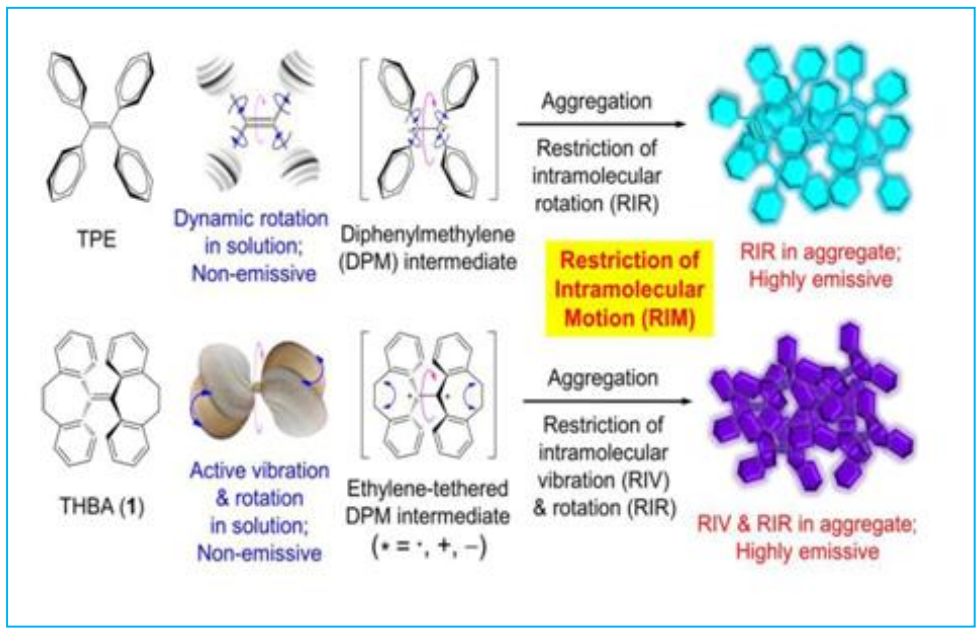

Figure 1.15. Representation Aggregation based example of AIE process (Adapted with permission from ref 78. Copyright 2015 ACS Publications).

To design novel luminogens for practical applications and technological innovations it is essential to decipher the underlying mechanisms for the AIE phenomena. Though a number of mechanisms like conformational planarization, J-aggregate formation, *E*/*Z* isomerization, (TICT), and ESIPT have been hypothesized, none of them are adequate to support all the experimental findings. Based on experimental and theoretical works three main hypotheses like Restriction of Intramolecular Rotations (RIR), Restriction of Intramolecular Vibrations (RIV), and Restriction of Intramolecular Motions (RIM) have been proposed[78] (**Figure 1.15 and** (**Figure 1.16**).

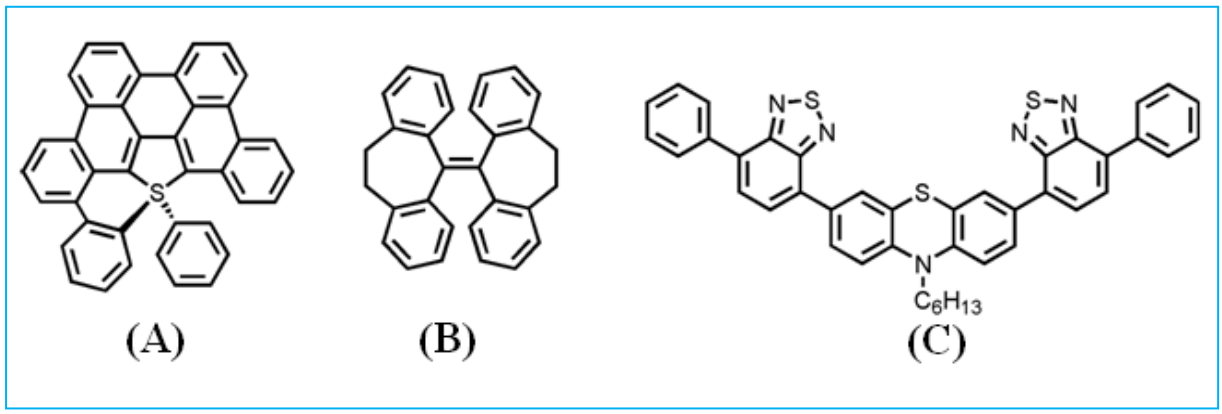

Figure 1.16. (A) Molecule displaying RIR; (B) Molecule displaying RIV and (C) Molecule displaying RIM.

Owing to the facile probe–target interaction in solution or in the solid state the AIEgens are perceived to be attractive probes for selective and quantitative sensing of various target analytes.[79,80] It is also well understood that the emission of an AIE-based system seems to be responsive to an additional competing species modulating the probe–target interaction which enables the probe to render dual sensing property. This sensor array may offer a new platform for the design of sensors for cation detection.[80,81]

1.4.5.6 Excimer / Exciplex Formation

An excimer or exciplex is a species consisting of two monomers (same or, different, respectively) which are not bound in the ground state but are bound in an excited electronic state. The difference between the equilibrium geometry of the excited state relative to the ground state produces a broad, red-shifted emission which has been taken as the experimental manifestation of excimer/exciplex[82-84] formation (**Figure 1.17**). This process can be described by:

$$A + B^* \rightarrow (AB)^*;$$

where, A and B are monomers; * denotes an excited state. In the case of an excimer, A=B, whereas for an exciplex, A≠B.

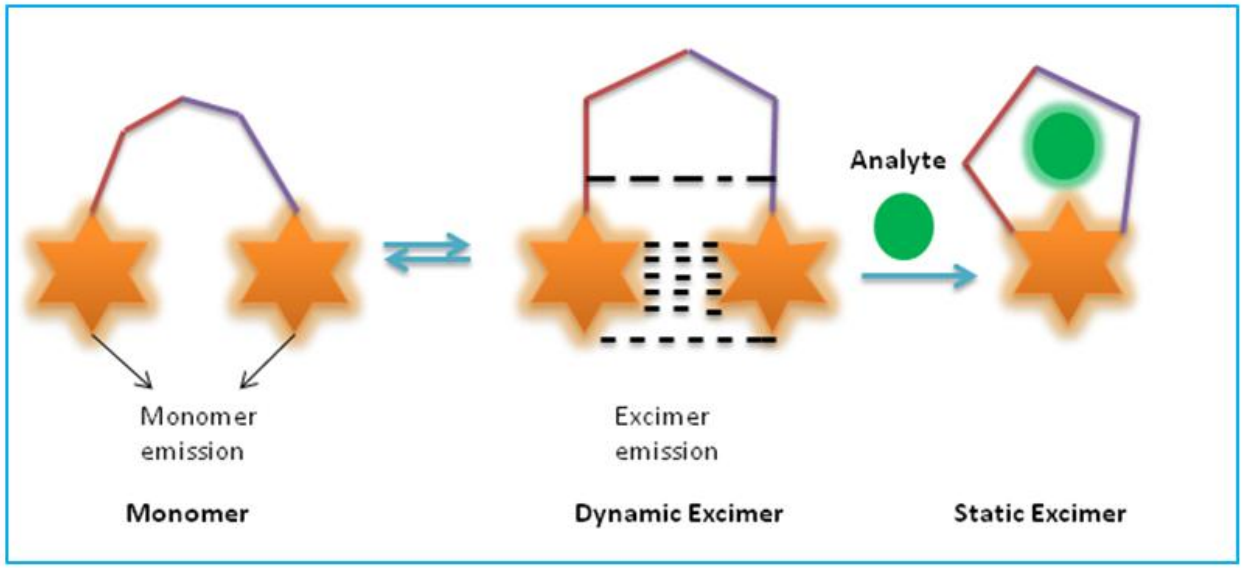

Figure 1.17. Excimer formation-based fluorescent sensing mechanism

The pyrene excimer was first reported by Förster. Since then intermolecular excited-state interactions play a key role in photochemistry and photophysics. The stabilizing interaction between a molecule in the ground state and a molecule in the excited state can be described by the ***configurational interaction model*** if the two chromophores are identical and is called excimer. If the two chromophores are different, an exciplex or a hetero excimer can be formed. The extent of overlap between the two chromophores manifests the stabilization of an excimer. Calculations suggest a picture of the excited-state complex in which the two chromophores, if they are planar, are at an optimum distance of 3.5 A in a plane in parallel orientation.

1.4.5.7.1 Förster resonance energy transfer (FRET)

The mechanism where an excited '**dye donor**' transfers energy to a '**dye acceptor**' in the ground state through a long-range dipole-dipole interaction in a nonradiative process to promote it to the excited state is known as Förster resonance energy transfer (FRET) or fluorescence resonance energy transfer or resonance energy transfer (RET) or electronic energy transfer (EET). Here a donor dye which absorbs energy of relatively shorter wavelength is attached to a receptor dye which absorbs energy of relatively longer wavelength in a single unit. The energy transfer from the excited donor to the ground state acceptor occurs by three mechanism (i)

Dexter type (short range, collisional) (ii) through-space (Förster type) mechanism (long range) or (iii) through bond mechanism. For the FRET process to be operative there should have efficient spectral overlap between the donor emission and acceptor absorption spectra in the FRET systems[85-87] (**Figure 1.18**).

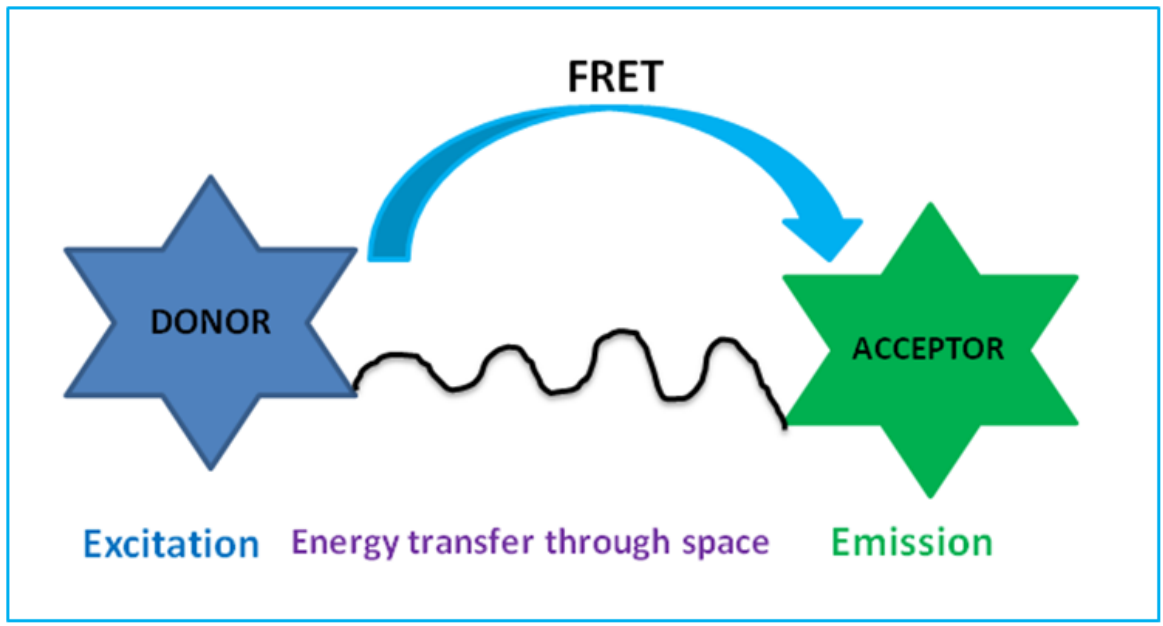

Figure 1.18. Schematic representation of through-space energy transfer.

Dexter energy transfer is a short-range, collisional or exchange energy transfer in a **non-radiative** way and differs from **Förster energy transfer** only in the **length scale**. **Förster energy transfer** is also a non-radiative energy transfer from D to A through space without involving collision between D and A but with long-range columbic dipole-dipole interaction. FRET is effective in the range 10-100 Å.

1.5.1 Chemistry of Fluorescein

Fluorescein ($C_{20}H_{12}O_5$), is a fluorophore dye of xanthene family. It has been widely used in various research fields which was first synthesized by Adolf von Baeyer in June 1871 via Friedel Craft acylation/cycLODegradation reaction using resorcinol and phthalic anhydride[88]. Fluorescein exhibits excellent spectroscopic properties with longer absorption (494 nm) and emission (512 nm) wavelengths in water, good water solubility, high fluorescence intensity,

high quantum yield, well biocompatibility and negligible toxicity at physiological pH[89] making it useful as a sensitive fluorescent label and is broadly used as a fluorescent tracer. Fluorescein-based Confocal laser scanning microscopy (CLSM) has been mentioned as a promising technology for *in vivo* histopathology during a gastro intestinal (GI) endoscopy. It is used in microscopy as a gain medium in a dye laser and also used in forensics and serology laboratories to detect bloodstains. It is also used as chemosensors for *in vitro* or *in vivo* detection of metal ions and thiols among other analytes and also for anions recognition. Fluorescein derivatives are non-fluorescent and colourless in its ring closed (spirocyclic lactone) form but gives a strong green fluorescence in the ring open carboxylic acid form in presence of a metal ion showing bright signals with high quantum yield and molar absorptivity[90-91] .The close-open equilibrium form of fluorescein is very much dependent on the pH of the medium[92-93].

The commercially available various fluorescein moieties are shown in **Figure 1.19**.

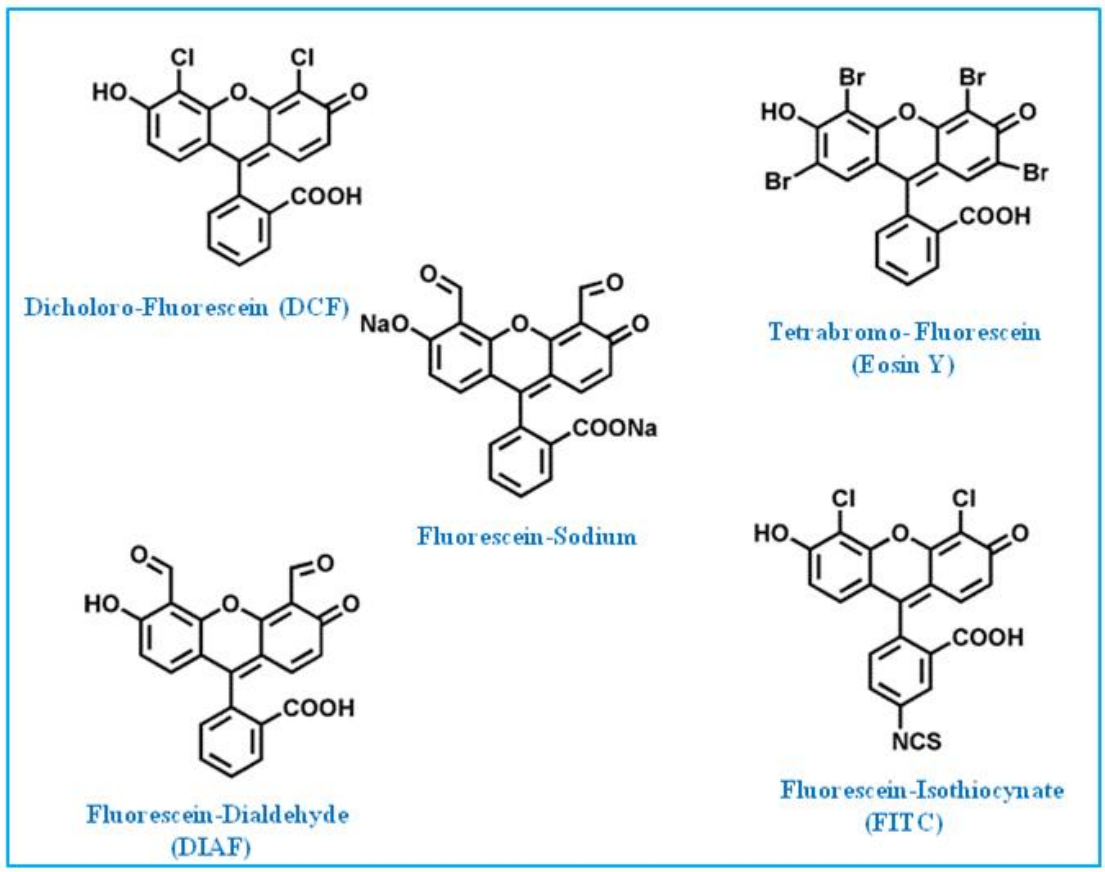

Figure 1.19. Different Fluorescein dye commercially available.

1.5.2 Mechanistic pathway:

Mechanistic path-way of the derivatives of Fluorescein moiety for cation sensing purpose is quite different. It is looking quite interesting that the spirolactam ring bearing the receptor unit is almost colorless, after metal induced breaking of this spirolactam ring leading to a change in hybridization of C atom from sp^3 (spirolactam-*C atom) to sp^2 (non-spirolactam -*C atom) is associated with a distinct green colour change giving '**turn-on**' (**Figure 1.20**) fluorescence response.[94]

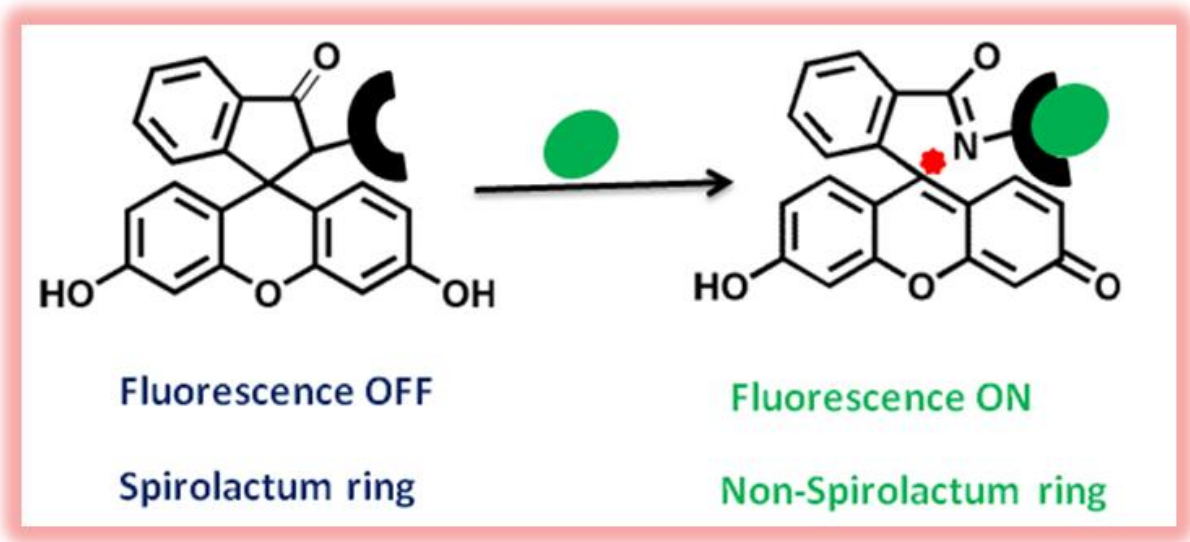

Figure 1.20. Schematic presentation of the change from *cyclic lactam* form to an *acyclic xanthene* form of the Fluorescein derivatives on binding to a metal ion.

Therefore due to OFF-ON fluorescent property, fluorescein derivatives have been designed for the recognition of iron and mercury metal ions, so that both reversible as well as irreversible reactions take place, though reversible chemosensor of Fluorescein derivative is desirable because of the advantage of re-usability of the probes.

1.6 Brief literature survey on Fluorescein based fluorescent sensor for Hg(II) :

Hg^{2+} is a most toxic heavy metal which harm to the living organism. Zhihui Xie and co workers[95] developed a new colorimetric and fluorogenic fluorescein-hydrazide based probe **L**^{1} (**Figure 1.21**) for the detection of Hg^{2+} ion in EtOH-HEPES buffer medium (v/v=1:1, pH 8.0). The probe **L**^{1} displayed high selectivity and sensitivity towards Hg^{2+} ion in the presence of other metal ions in living organism. It is found that **L**^{1} does not absorb in the range of 400 - 800 nm in a mixed solution of ethanol/HEPES (v/v = 1:1). However, on gradual addition of Hg^{2+} ion there appears three absorption peaks at 397, 504 and 641 nm out of which the peak at 641 nm is most prominent one. Fluorescence titration was carried out by gradual addition of Hg^{2+} ion with excitation wavelength 460 nm giving maximum emission at around 522 nm. The appearance of strong fluorescence at 522 nm is due to the opening of spirolactum ring mechanism via Hg^{2+} -promoted hydrolysis of fluorescein-hydrazide. Fluorescence intensity of the ligand showed a linear correlation in range of 0-3 μM of Hg^{2+} concentration with correlation coefficient of 0.9985.

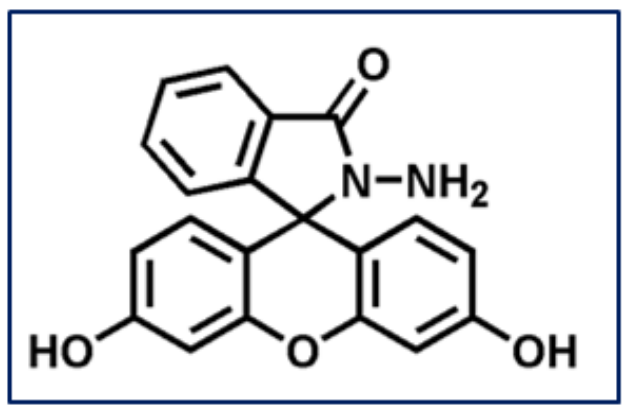

Figure 1.21. Chemical structure of **L**^{1}.

Yang et.al[96]. reported a thiosemicarbazide embedded fluorescein-based molecular probe **L**^{2} (**Figure 1.22**) displaying a highly sensitive and selective colorimetric and fluorogenic recognition of Hg^{2+} with a detection limit of 8.5 x 10^{-10} M in MeOH–H_2O (30:70, v:v) solution. The strong fluorescence emission occurs in the range of 500–600 nm.This fluorescence enhancement is due to the opening of spirolactum ring via Hg^{2+}-promoted desulfurization of **L**^{2},

producing the corresponding oxadiazole, a highly fluorescent and colorful Product. The experiment was done in phosphate buffer at pH 7.

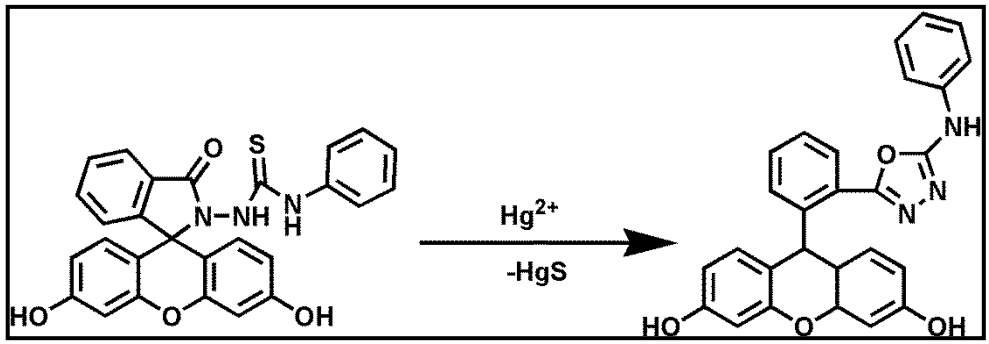

Figure 1.22. Chemical structure of $\mathbf{L^2}$ and oxadiazole.

Wanichacheva and co workers[97] reported dithia-cyclic fluorescein based highly sensitive colorimetric and fluorogenic ON-OFF fluorescent molecular $\mathbf{L^3}$ for Hg^{2+} (**Figure 1.23**) showing association constant 6.04 x 10^{10} M^{-1} in 95:5 Tris–HCl buffer/MeOH solution at pH 7.2. The probe $\mathbf{L^3}$ showed remarkable fluorescence at 514 nm when excited at 493 nm wavelength. The fluorescence was quenched with the addition of Hg^{2+}. The fluorescence quenching clearly established the ON-OFF switching mechanism. The probe showed excellent sensitivity towards Hg^{2+} and the detection limit was calculated to be 7.38 nM. The stoichiometry of binding between $\mathbf{L^3}$ and Hg^{2+} was estimated to be 1:1 from Job's plot. The fluorescence quantum yield with Hg^{2+} was found be 0.56. Sensor $\mathbf{L^3}$ exhibited observable colour change from yellow to orange in presence of Hg^{2+}, which served as a "naked-eye" indicator.

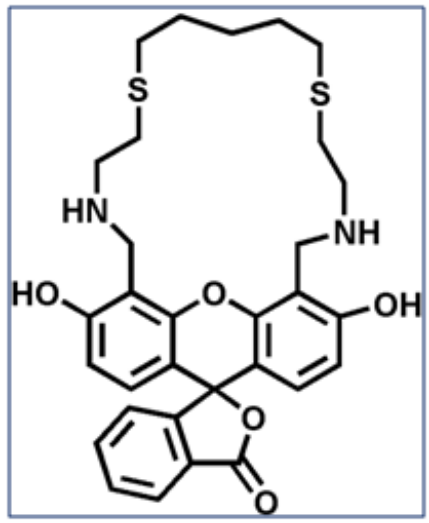

Figure 1.23. Chemical structure of $\mathbf{L^3}$.

Xu and his co-workers[98] reported a modified fluorescein-based fluorescent molecular probe, acryloyl fluorescein hydrazine (ACFH) $\mathbf{L^4}$ (**Figure 1.24**) for the detection of Hg^{2+} showing live cell imaging application. This sensor exhibited high sensitivity towards Hg^{2+} in the presence of other competing cations in terms of fluorescence enhancement and naked eye colour change. This group reported that the probe $\mathbf{L^4}$ exhibited an emission band at 512 nm upon excitation at 445nm in aqueous medium at pH 7. The detection limit was estimated as 0.86 x 10^{-9} M for $\mathbf{L^4}$. The binding ratio was found to be 1:1 for the probe and the formation constant was evaluated as 3.36 x 10^{9} M^{-1} for $\mathbf{L^4}$.

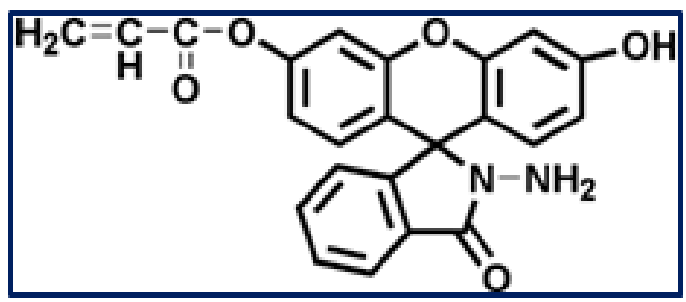

Figure 1.24. Chemical structure of $\mathbf{L^4}$.

Yang et. al.[99] developed a colorimetric fluorescent chemosensor $\mathbf{L^5}$ (**Figure 1.25**) containing thiospirolactam moiety for the recognition of Hg^{2+} in aqueous medium. Photophysical studies

were performed to investigate the signal change upon binding with Hg^{2+} in EtOH/HEPES (1/1, v/v, pH 7.4) buffer solution. This probe **L**^{5} showed 37-fold enhanced emission peak at 529 nm. Binding stoichiometry **L**^{5} and Hg^{2+} was determined as 2:1 and binding constant calculated to be 9.20×10^{4} M^{-2} from fluorescence titration data. The detection limit was calculated to be 39 nM The probe **L**^{5} was applied to image of Hg^{2+} ion in living cells and has capacity to detect mercury (II) *in vivo*.

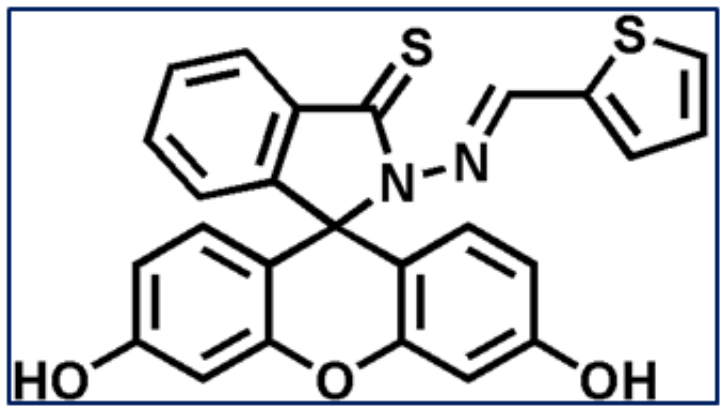

Figure 1.25. Chemical structure of **L**^{5}.

Chang and co-worker[100] developed a di-chlorofluorescein–coumarin based fluorescent chemosensor **L**^{6} **(Figure 1.26)** for the detection of Hg^{2+} with excellent selectivity and sensitivity over other cations. The probe **L**^{6} exhibited an absorption band and emission band at 505 nm and 523 nm respectively in 1% DMSO water ((DMSO:H_2O = 1:99, v/v, buffered at pH 4.8 with acetate buffer). The detection limit was found as 4.3×10^{-6} M. The binding ratio was found to be 1:1 for the probe and the association constant was evaluated as 4.5×10^{4} M^{-1} for **L**^{6}. The turn-off type behaviours in fluorescence of the dichlorofluorescein unit can be suitably studied by a ratiometric approach using the coumarin emission as an internal reference.

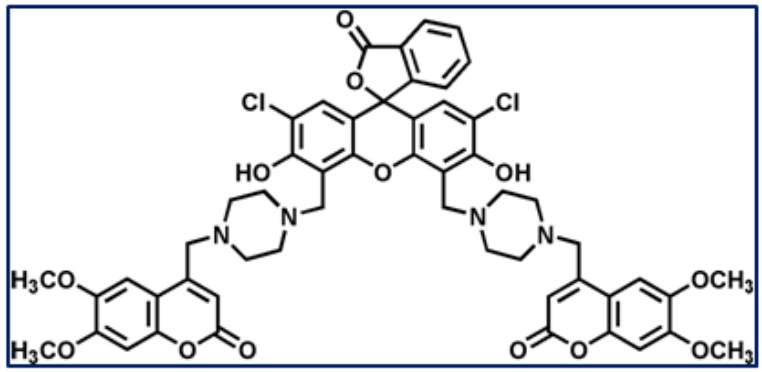

Figure 1.26. Chemical structure of **L**^{6}.

Mondal et.al.[101] developed a fluorescein-phenylalaninol (FPA) chemosensor **L7** (**Figure 1.27**) through environmentally benign mechanochemistry. The probe **L**^{7} shows simultaneous detection and removal of Hg^{2+} in aqueous medium. It shows enhancement of absorption intensity at the wavelength 460 nm and fluorescence intensity is quenched 8 fold with a red shift of 3.0 nm at 524 nm upon excitation at 495 nm while Cu^{2+} exhibited a quenching signal with a blue shift of 4.0 nm at 517 nm in aqueous medium. Observable colour change occurs in protic polar solvents due to H bonding and colourless or light pink in non-polar solvents in the presence of Hg^{2+}. The binding ratio was found to be 1:1 for the probe and the binding constant was evaluated as 1.7×10^{4} M^{-1} from absorption study and quenching constant is calculated from Stern−Volmer equation and evaluated as $K_{sv} = 2.0 \times 10^{5}$ M^{-1}. This group reported LOD as 1.65 μM from absorption study and 0.34 μM from fluorescence spectroscopic. This sensor can be used as paper strip for detection of Hg^{2+} ion.

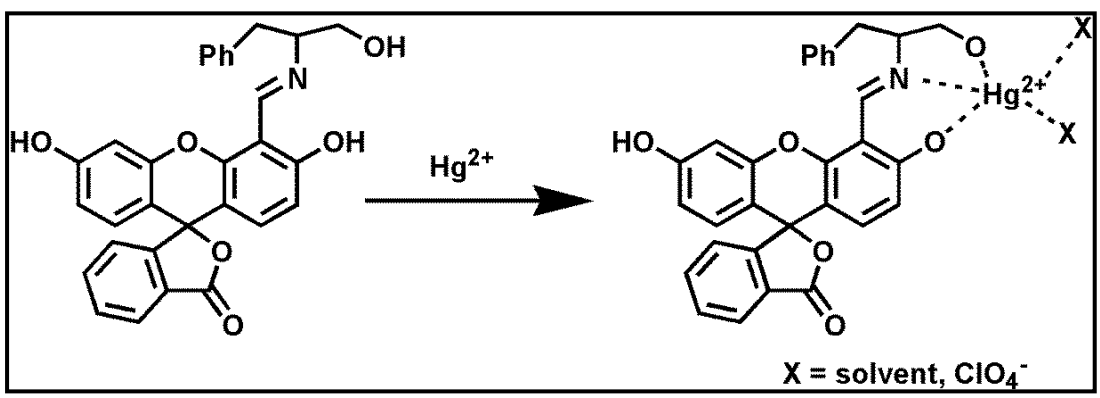

Figure 1.27. Chemical structure of **L**^{7} and **L**^{7}**-Hg**$^{2+}$ Complex.

Duan et.al.[102] developed fluorescein- carbazole based chemosensor **L**^{8} (**Figure 1.28**) for the selective detection of Hg^{2+} ion. They recorded the absorption and emission spectra of this ligand in 10 mM at pH=7 H_2O/MeOH (1:1, v/v). An absorption peak appeared at 500 nm and emission peak at 525nm along with the naked eye observation achromatic into brown, after the addition of Hg^{2+} to the solution containing **L**^{8}. The Hg^{2+} induced fluorescence enhancement occurred at 525 nm due to the "PET-OFF" (Photoinduced Electron Transfer-off) and CHEF (Chelation Enhanced Fluorescence) effect. The formation of 1:1 complex was confirmed from Job's plot. Increase in fluorescence intensity at 525 nm shows a good linearity (0.9971) with respect to the Hg^{2+} concentration in the range 0-100 μM. They reported LOD of Hg^{2+} as 40 nM. It is also applied to bioimaging and in environmental water analysis for Hg^{2+}. In addition, a paper based sensor strip containing fluorescein- carbazole could detect Hg^{2+} over other metal ions.

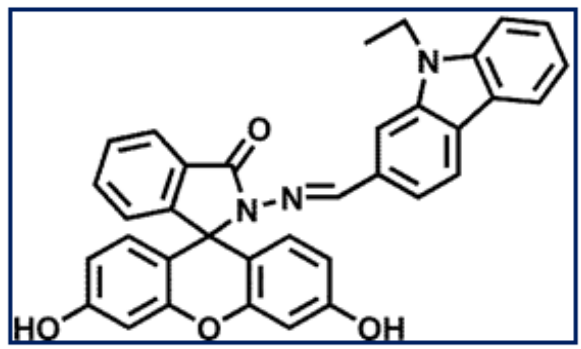

Figure 1.28. Chemical structure of **L**^{8}.

Bao *et.al*.,[103] developed a fluorescein derivative a novel chemosensor **L**^{9} (**Figure 1.29**) for the detection of Hg^{2+}.Chemosensor **L**^{9} exhibited a very strong sensitivity and high selectivity towards Hg^{2+} in an EtOH-H_2O (3:2, v/v, HEPES buffer, 0.5 mM, pH 7.15) solution. Additionally, the **L**^{9}**-Hg**$^{2+}$ ensemble displayed high selectivity towards Ag^{+}. Metal ligand binding induced spirolactam ring opening was confirmed from emission studies. The probe displayed a remarkable enhancement in fluorescence intensity at 524 nm upon excitation at 490 nm on the incremental addition of Hg^{2+} (0 to 300 μM) to **L**^{9} in EtOH/H_2O (3:2,v/v, pH=7.15). LODs for Hg^{2+} estimated to be 0.21μM. Detection limit for Ag^{+} was calculated to be 0.009 μM.The binding ratio between **L**^{9} and Hg^{2+} was determined to be 1:1 with binding constant $2.2078 \times 10^{4} M^{-1}$ from emission data using Benesi-Hildebrand plot. This probe was applied as chemosensor in monitoring the intracellular Hg^{2+} and Ag^{+} in human liver cell (L-02).

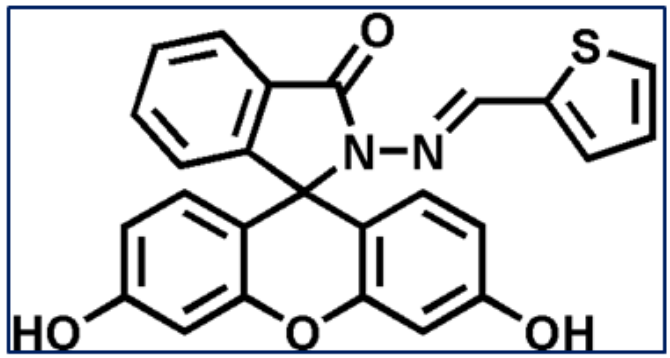

Figure 1.29. Chemical structure of $\mathbf{L^9}$.

Thakur and his coworkers[104] synthesised a ferrocene unit containing fluorescein-based ratiometric and "OFF-ON" naked eye chemosensor $\mathbf{L^{10}}$ **(Figure 1.30)** for the selective detection of Hg^{2+} and Fe^{3+} in $CH_3CN:H_2O$ (3/7, v/v) at physiological pH 7.2. The $\mathbf{L^{10}}$ displayed a new absorption band at 430 nm upon addition of 1 eq of Hg^{2+} and Fe^{3+}. Two isosbestic points were found $^{+}$ at 422 nm and 447 nm for Fe^{3} and at 404 and 451 nm for Hg^{2+}. Absence of any analyte the chemosensor showed emission band at 521 and 545 nm upon excitation at 430 nm. This is due to fluorescein moiety. With the gradual addition of Hg^{2+} and Fe^{3+} there appears a new peak observes at 473 nm with decrease in fluorescence intensity at 521 and 545 nm. The peak at 545 nm and 473 nm were chosen to explain ratiometric phenomenon.The binding constant and binding ratio with Hg^{2+} was estimated to be $3.35x10^5$ M^{-1} and 1:1 similarly for Fe^{3+} and 2.67 x 10^5 M^{-1} and 1:1 for Hg^{2+}. Jobs plot and NMR studies confirm a 1:1 binding during complexation. Detection limit was calculated to be 39 nM for Hg^{2+} and 98 nM for Fe^{3+}. Reversibility studies were performed by I^- for $\mathbf{L^{10}}$- Hg^{2+}complex and EDTA for $\mathbf{L^{10}}$-Fe^{3+} complex to explore its reusability. The electrochemical studies of $\mathbf{L^{10}}$ were performed by differential pulse voltammetry (DPV) cyclic and voltammetry (CV) in CH_3CN/H_2O (3/7). The probe $\mathbf{L^{10}}$ displays $\Delta E_{1/2}$=33 mV and 31 mV anodic shift due to binding with Hg^{2+} and Fe^{3+} ions, respectively.

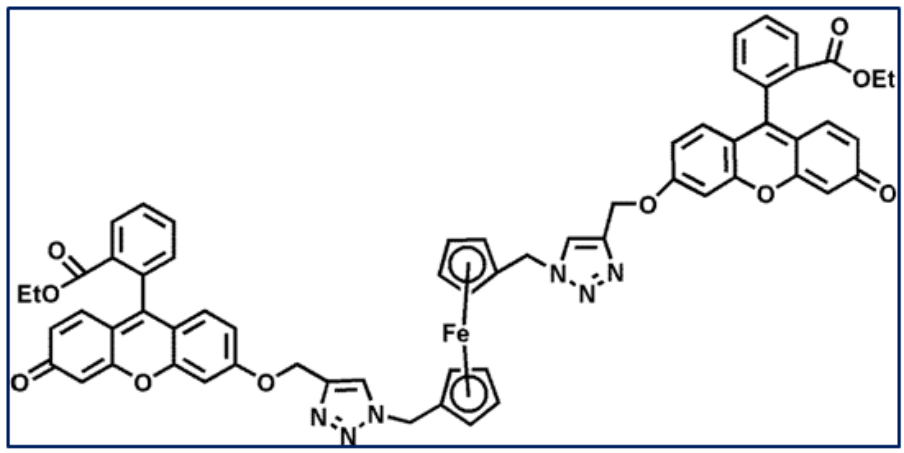

Figure 1.30. Chemical structure of $\mathbf{L^{10}}$.

Erdemir et.al.,[105] reported phenolphthalein-fluorescein based colorimetric and fluorometric chemosensor, $\mathbf{L^{11}}$ **(Figure 1.31)** for the detection of Hg^{2+} and Zn^{2+} in EtOH:H_2O (v/v = 8/2, 5 mM, HEPES, pH 7.0). This probe $\mathbf{L^{11}}$ showed enhanced emission peak centered at 520 and 500 nm in the presence of Hg^{2+} and Zn^{2+}, respectively. These phenomena further establish the ring-opening reaction of the Fluorescein spirolactam upon addition of Hg^{2+}. It works by FRET mechanism where energy transferred from the conjugated phenolphthalein donor to the fluorescein acceptor. Stoichiometry in the complex between $\mathbf{L^{11}}$- Hg^{2+} and $\mathbf{L^{11}}$- Zn^{2+} were found to be 1:2 from Jobs plots. The binding constant determined using Benesi-Hildebrand plots were found to be 2.11×10^{10} M^{-2} for Hg^{2+} and 6.45×10^{10} M^{-2} for Zn^{2+} from. The detections limits were also found to be 1.16 µM for Hg^{2+} and 0.56 µM for Zn^{2+}.The the quantum yields were determined to be 0.258 for Hg^{2+} , 0.323 µM for Zn^{2+} and 0.013 for $\mathbf{L^{11}}$. The reversible nature of this probe $\mathbf{L^{11}}$ was tested with tetrabutyalmmonium iodide (TBAI) for Hg^{2+} and EDTA for Zn^{2+}. According to this group fluorescence intensity of the complex at 500 and 520 nm were quenched after the addition of EDTA and TBAI due the exchange of Zn^{2+} and Hg^{2+} ions from complex to EDTA and TBAI, respectively. In addition, the determination of $Hg^{2+}$and Zn^{2+} in water samples were also evaluated for the practical use of the probe.

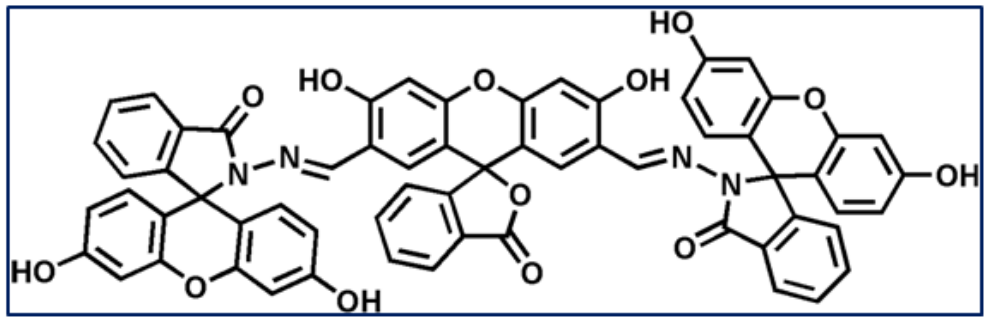

Figure 1.31. Chemical structure of $\mathbf{L^{11}}$.

He and coworkers[106] developed $\mathbf{L^{12}}$ **(Figure 1.32)**, a cell compatible novel fluorescein-based fluorescent chemosensor containing N-Ethylthioethyl-N-[N′,N′-(2′-Diethylthioethylamino)-5′-methyl-Phenoxyethyl]-2-Methoxy Aniline (EDPMA) as receptor for the detection of Hg^{2+} ion. The incorporation of multiple sulfur-based functional groups greatly enhanced the affinity of the probe for Hg^{2+}.This probe exhibited a very strong sensitivity and high selectivity towards Hg^{2+} in H_2O:MeOH (v/v = 95/5, 20 mM HEPES buffer, pH = 7.4). The probe $\mathbf{L^{12}}$ (25 μM) shows 51-fold enhancement of the fluorescence intensity at 539 nm upon excitation at 460 nm with a greenish colour through "OFF-ON" manner upon addition of Hg^{2+} (0-80 μM) over other metal ions. Fluorescence intensity of the ligand showed a linear dependence on Hg^{2+} concentration in range of 1.0–4.0 × 10^{-5} mol·L^{-1} having correlation coefficient of 0.9990 and from the slope of the plot LOD was calculated as 0.11 μM. The binding ratio was found to be 1:1 from the Job's plot. It is also applied to bioimaging for Hg^{2+}. Fluorescence image was taken successfully from HeLa cells indicating non-toxicity of $\mathbf{L^{12}}$ towards cell confirming the applicability of this sensor for biological samples.

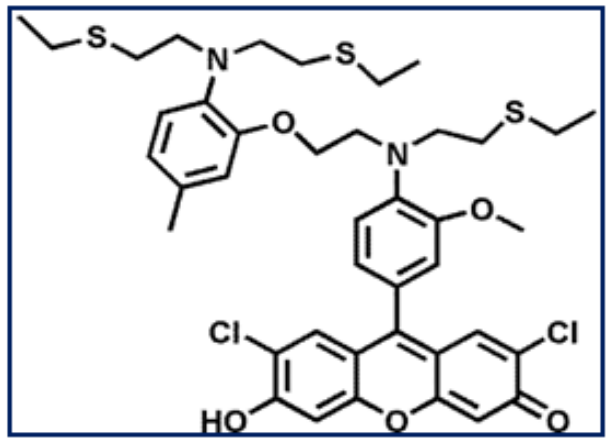

Figure 1.32. Chemical structure of **L**[12].

Boudreau *et.al.*,[107] synthesized a thionocarbonate-appended fluorescein-based "OFF-ON" chemosensor **L**[13]**(Figure 1.33.)** for the selective detection of Hg^{2+} in HEPES buffer (20 mM, 1% EtOH) at physiological pH 7.4.This **L**[13] shows very fast, affordable, sensitive and selective Hg^{2+} responsive fluorescent sensor. The probe was developed to investigate the hydrolysis reactions involved in the sensing process. The auto and Hg^{2+} assisted hydrolysis were followed by mass spectrometry and kinetics of change in fluorescence intensity upon addition of Hg^{2+}, new absorption band appears at 490 along with a peak at 455 nm which is a characteristic peak of quinoid form of fluorescein. The fluorescence intensity is enhanced 80 fold at 516 nm upon excitation at 490 nm after 90 minute. The LOD was determined to be 0.8 nM (3σ/slope).

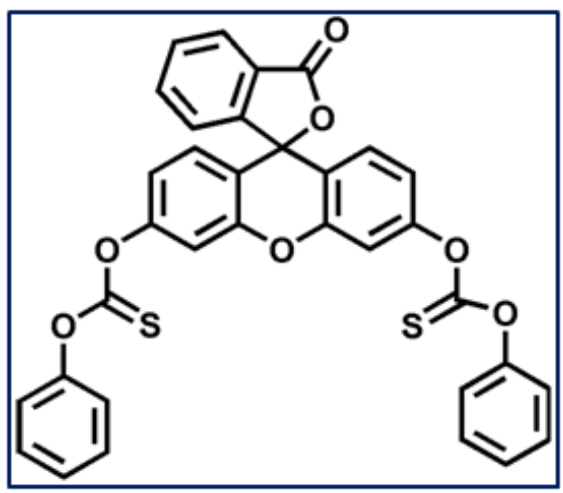

Figure 1.33. Chemical structure of **L**[13].

Wang et. al[108] synthesised a turn-on colorimetric and fluorometric AND logic gate based chemosensor **L[14] (FPSi)** **(Figure 1.34)** for the fast rapid and simultaneous detection of Hg^{2+} and F^{-} in mixed solvent DMSO : H_2O (7:3, v/v). it has been prepared by modifying fluorescein through the attachment of thiosemicarbazide and *tert*-butyldiphenylsilyl groups. They introduced a thiosemicarbazide unit due to the thiophilic character of Hg^{2+}. The **L[14]** probe exhibited a very strong sensitivity and high selectivity towards Hg^{2+} and F^{-} over others cations and anions. This was verified by fluorescence and UV–VIS absorption spectra.

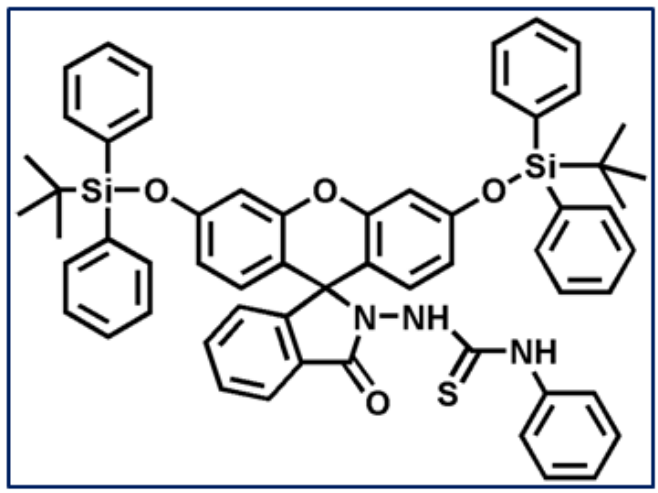

Figure 1.34. Chemical structure of **L[14]**.

Mishra et.al[109] reported CHEF induced fluorescein hydrazone based turn-on colorimetric and fluorogenic chemosensor **L[15]** **(Figure 1.35)**. for the detection of Hg^{2+}.This group reported the crystal structure of **L[15]**. The sensor showed Hg^{2+} induced fluorescence enhancement as a result of spirolactam ring-opening at 517 nm upon excitation at 465 nm in in H_2O:MeOH (v/v = 8:2, HEPES buffer (1 mM), pH = 7.4) The probe **L[15]** also detects Cu^{2+} colorimetrically in H_2O:MeOH (v/v = 8:2, HEPES buffer (1 mM), pH = 7.4) solution. An enhanced absorption intensity at 495 nm appeared due to chelation ofCu^{2+} with **L[15]**. It exhibits a visual colour change from from a yellow to light brown. the binding ratio was found to be 1:1 from the Job's plot for both Hg^{2+} and Cu^{2+}. The detection limit was given as 2.50 $x10^{-7}$ M and 4.13$x10^{-7}$ M for Hg^{2+} and Cu^{2+}respectively. B-H plot results a linear relationship with R^2 = 0.99 and binding constant was calculated to be 4.79$x10^4$ M^{-1} and 2.55$x10^5$ M^{-1} respectively for Hg^{2+} and Cu^{2+}. The reversibility of the chemosensor was demonstrated with L15 by F^- and EDTA for Hg^{2+} and Cu^{2+}. Quantum

yield of **L**[15](0.035) for Hg^{2+} found to be 0.095 in ethanol. Cytotoxicity studies revealed that probe had negligible cytotoxicity, cell permeable and suitable for the detection of Hg^{2+} in biological system in ME-180 cervical cancer cells. This sensor can be used as as memory Device and paper strip for detection of Hg^{2+} and Cu^{2+}ion as a potential application.

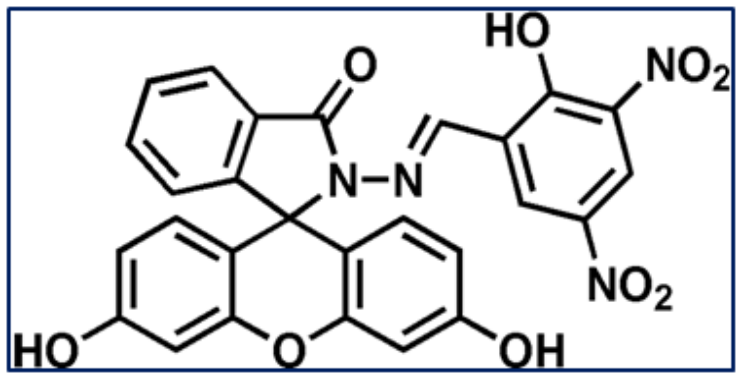

Figure 1.35. Chemical structure of **L**[15].

Pandurangappa et.al.[110] reported a fluorescein hydrazide based chemosensor, **L**[16] **(Figure 1.36)** for the detection of Hg^{2+} in a mixed water-acetonitrile (1:10, v/v,) in alkaline medium at pH = 12. In the presence of Hg^{2+} probe shows a visual colour change from colourless to green. Probe **L**[16] exhibited a colorimetric as well as fluorogenic "OFF-ON" type recognition in the absence and presence of Hg^{2+}. The probe showed high selectivity and sensitivity towards Hg^{2+} over other cations except Cu^{2+}. This interference of Cu^{2+} ion was eliminated by maintaining the pH between 9 and 12. The equilibrium between siprolactam ring open and closed forms correspond to "On and Off" state of the probe. In acetonitrile-aqueous, this probe showed an emission band at 520 nm upon excitation at 502 nm due to the opening of spirolactum ring in the presence of Hg^{2+}only. Increase in fluorescence intensity at 525 nm shows a good linearity (0.9989) with respect to the Hg^{2+} concentration and the LOD of Hg^{2+} calculated as 0.08µg/mL from spectrophotometrically and 1.5 ng/mL as calculated from fluorometrically. The limit of detection was also given as 21.9×10^{-8} M. This probe was applied successfully in lead acid battery samples for Hg^{2+} speciation.

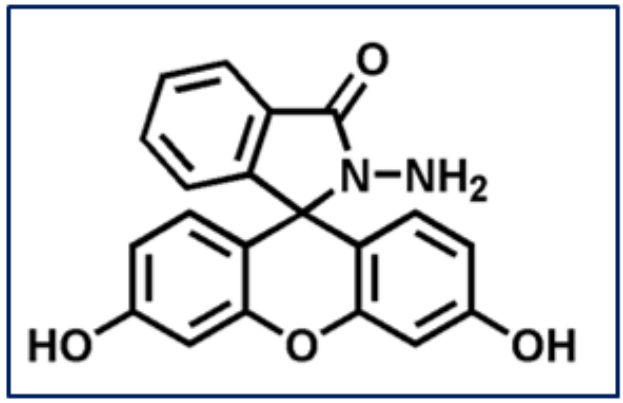

Figure 1.36. Chemical structure of **L**[16].

Pu et.al.[111] developed a new symmetric fluorescein-linked diarylethene based chemosensor **L**[17] (**Figure 1.35**) for the detection of Hg^{2+} in acetonitrile (2.0×10^{-5} mol L^{-1}) . Probe **L**[17] exhibited colorimetric as well as fluorogenic "OFF-ON" type sensing of Hg^{2+}. It displayed very selective and sensitive recognition of Hg^{2+} in the presence of other competing cations. The probe **L**[17] shows enhancement of absorption intensity at the 625 nm and fluorescence intensity at 504 nm with 64 fold enhancement upon addition of Hg^{2+} from 0 to 10 equivalent upon excitation at 420 nm. Jobs plot and ESI-MS^{+} studies confirm the 1:1 binding **L**[17] with Hg^{2+} during complexation. Fluorescence intensity of the ligand showed linearity with the Hg^{2+} concentration having correlation coefficient of 0.995 and from the slope of that plot LOD calculated as 0.33µM/L and quantum yields of **L**[17] were determined to be 0.459-0.11. The binding constant for the complex between probe and Al^{3+} was found to be $3.5x10^{5}M^{-1}$ from Benesi-Hildebrand plot. It was used to fabricate a key-pad-logic function based on the fluorescence response.

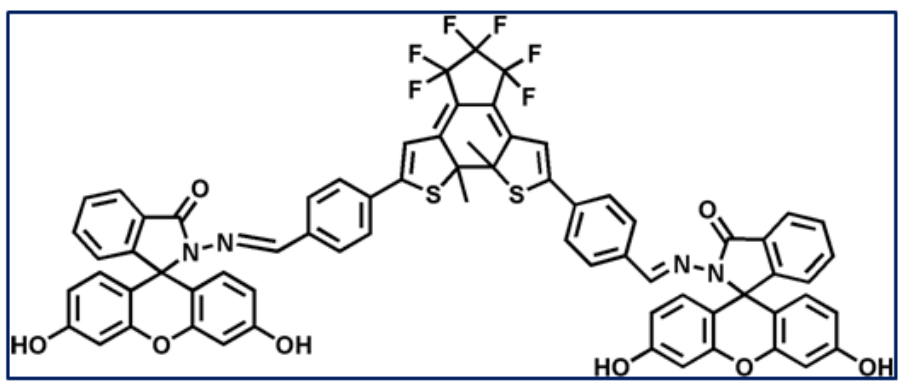

Figure 1.37. Chemical structure of **L**[17].

Lippard et.al[112] synthesised a fluorescein based water soluble chemosensor **L**^{18} **(Figure 1.38)** for the specific detection of Hg^{2+} . They introduced a 3,9-dithia-6-azaundecane unit. Due to the thiophilic character of mercury ions, the receptor bearing S atom provided a suitable binding pocket for Hg^{2+}. This probe showed high selectivity and sensitivity towards Hg^{2+} in presence of other metal ions with the appearance of an emission band at 524 nm in aqueous 50 mM HEPES buffer medium, containing 100 mM KCl at pH 7. This probe shows 5-fold enhancement of the fluorescence intensity upon excitation at 500 nm through "OFF-ON" manner upon addition of Hg^{2+} over other metal ions. The 1:1 stoichiometric ratio was confirmed from Job's plot. Reversibility and reusability of **L**^{18} studied with TPEN fluorometrically.

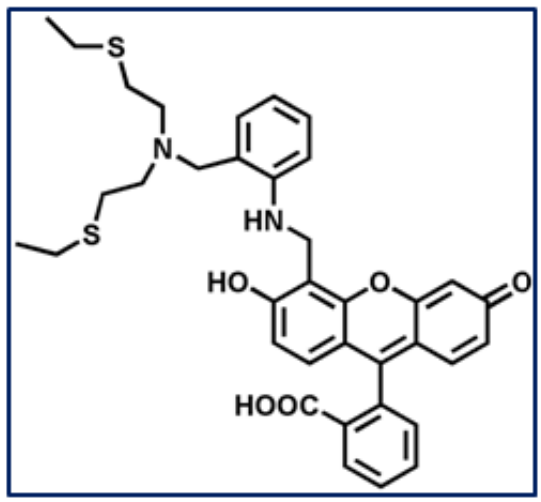

Figure 1.38. Chemical structure of **L**^{18}.

Lippard et.al[113] synthesized seminaphthofluorescein-based chemosensor **L**^{19} **(Figure 1.39)** containing a pyridyl-amine-thioether unit for the detection of Hg^{2+} in 50 mM HEPES, 100 mM KCl at pH 8. It showed an excellent sensitivity and selectivity towards Hg^{2+} over other metal ions. Spectroscopic studies showed 4 fold ratiometric (I_{624}/I_{524}) detection of Hg^{2+} in HEPES buffer upon excitation at 499 nm. The quantum yield of the probe was found to be 0.05 which was doubled upon coordination to Hg^{2+} ion.

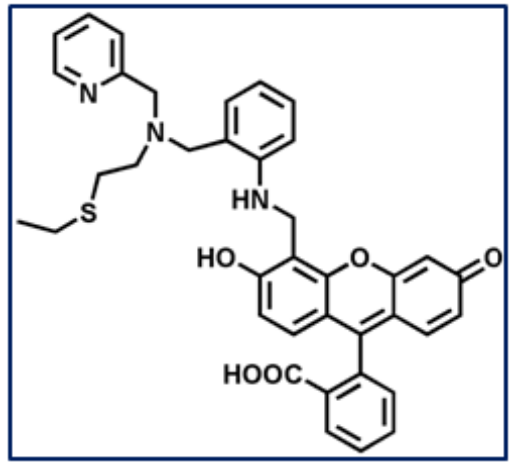

Figure 1.39. Chemical structure of $\mathbf{L^{19}}$.

Nantanit Wanichacheva et al.[114] reported a ratiometric fluorescent chemosensor $\mathbf{L^{20}}$ **(Figure 1.40)** for FRET based detection of Hg^{2+} . The probe is consisting of fluorescein and two rhodamine B units through the hydrazide linker unit. In this probe fluorescein acts as donor and the ring-opened rhodamine act as acceptor. It showed an excellent sensitivity and selectivity towards Hg^{2+}. $\mathbf{L^{20}}$ showed an absorption band at 525 nm in the presence of Hg^{2+} with a change in colour from colourless to pink. The jobs plot revealed 1:1 binding ratio for $\mathbf{L^{20}}$ and Hg^{2+}. The association constant of Hg^{2+} towards r $\mathbf{L^{20}}$ was found to be 1.49×10^{5} M^{-1}. A strong emission band appeared at 575 nm upon excitation at 525. The LOD's was calculated to be 2.02×10^{-8}M. The quantum yield was found to be 0.19 for the complex.

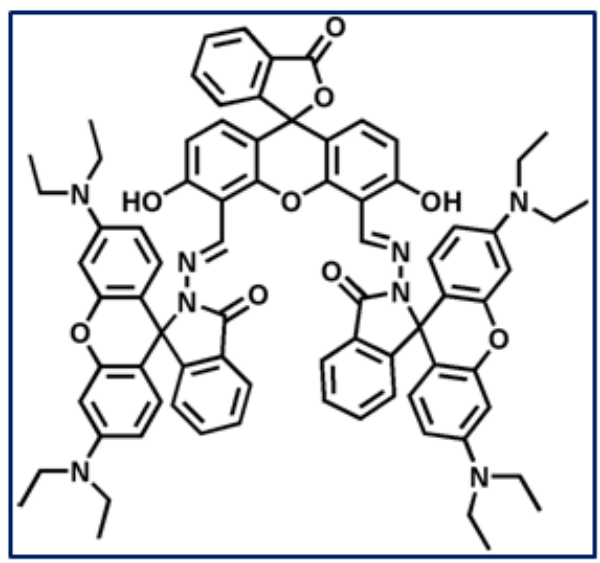

Figure 1.40. Chemical structure of **L**[20].

Zheng's group[115] reported a FRET based chemosensor **L**[21] **(Figure 1.41)** in which resonance energy had been transferred from fluorescein to a rhodamine B moiety on binding with Hg^{2+}. The phenomenon of FRET was evident from generation of dual emission band at 520 and 591 nm on excitation at 490 nm. 65-fold fluorescence enhancement was observed after the addition of Hg^{2+} at 591 nm while the fluorescence intensity decreases at 520 nm simultaneously with the colour change from yellow to magenta.The limit of detection was calculated to be 5×10^{-8} M.

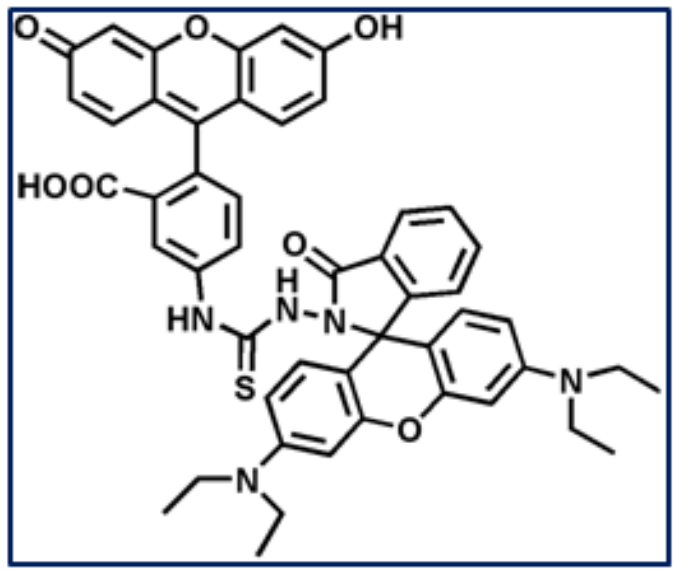

Figure 1.41. Chemical structure of **L**[21].

Chereddy and his group[116] reported a fluorescein-rhodamine conjugate **L**[22] **(Figure 1.42)** which exhibited an "OFF-ON" colorimetric and fluorogenic chemosensor **(**for the simultaneous detection of Hg^{2+} and F^{-} in a (1:1, v/v) CH_3CN : H_2O mixed solvent at pH 7.4 over other biologically important and toxic metal ion. This group showed a gradual enhancement of the emission band at 592 nm in the presence of Hg^{2+} in 0.01 M Tris HCl-CH_3CN, The LOD was calculated as 5.4×10^{-9} M and 5.17×10^{-8} M for Hg^{2+} and F−, respectively. Cytotoxicity studies revealed that the probe had negligible cytotoxicity, cell permeable and suitable for the detection of Hg^{2+} in biological system in NIH 3T3 cells.

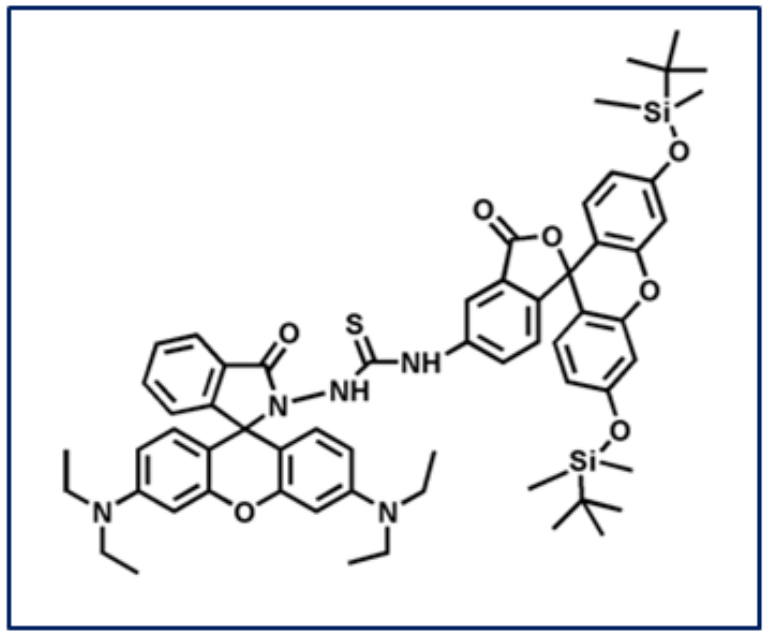

Figure 1.42. Chemical structure of $\mathbf{L^{22}}$.

Helal *et.al*.,[117] developed a fluorescein hydrazide-appended Ni(MOF) composite, FH@Ni(MOF) $\mathbf{L^{23}}$ **(Figure 1.43)** for chromo and fluorogenic recognition of Hg^{2+} ion in aqueous medium. This sensor exhibited high sensitivity towards Hg^{2+} only in the presence of other interfering cations. The probe was thoroughly characterised by PXRD, FT-IR, FESEM, XPS and TGA. The colour of the solution containing this probe changed from colourless to pink in the presence of Hg^{2+} .The binding constant of $\mathbf{L^{23}}$ was determined to be as 6.1 $x10^5$ M^{-1} from UV–vis titration. Remarkable enhancement of fluorescence intensity was observed at 523 nm in the presence of Hg^{2+} upon excitation at 460 nm at pH=7.2. $\mathbf{L^{23}}$ showed a Hg^{2+} induced chelation enhanced fluorescence with spirolactam ring opening. The binding constant was found to be 9.4 $x10^5$ M^{-1} and 1:1 stoichiometric ratio was confirmed from Job's plot. The LOD of $\mathbf{L^{23}}$ was found to be 20 nM. The quantum yield was calculated to be as 0.07 for the probe and 0.46 upon Hg^{2+} binding. This probe $\mathbf{L^{23}}$ was found to be reversible and was applied successfully to detect Hg^{2+} ion water bodies.

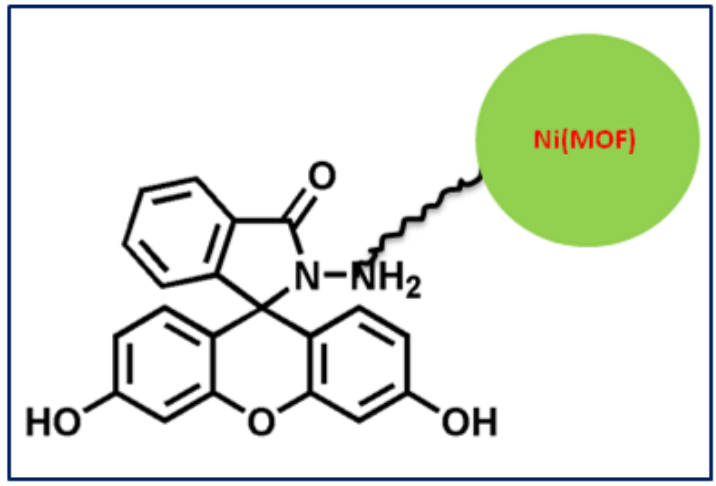

Figure 1.43. Chemical structure of **L**[23].

Chang et.al.[118] reported two sensors based on dichlorofluorescein **L**[24a] and its methyl ester derivative **L**[24b] (**Figure 1.44**) for colorimetric and fluorogenic recognition of Hg^{2+} in acetate buffer [10% DMSO, pH 5.0]. The probe exhibited the fluorescence quenching at 528 nm. The limit of detections were calculated 7.5×10^{-6} M (**L**[24a]) and 1.5×10^{-5} M (**L**[24b]) respectively.

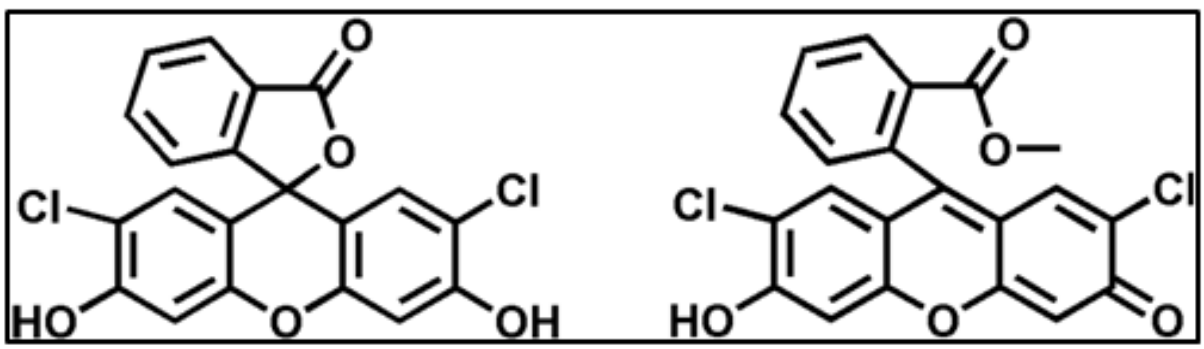

Figure 1.44. Chemical structure of **L**[24a] and **L**[24b].

Wang et al.[119] developed a bonding signaling based fluorescein chemosensor **L**[25] (**Figure 1.45**) by attaching thiol-DNA functionalized AuNPs for the detection of Hg^{2+} in 20 mM Tris-CH_3COOH at pH 7.4. In the presence of Hg^{2+}, the probe produced the hairpin structure of ssDNA which originates from thymine Hg^{2+} thymine (T- Hg^{2+}-T) coordination. It resulted in notable fluorescence quenching due to the FRET process between the energy donor fluorescein

and the energy acceptor AuNPs .The LOD was found to be as 8 nM. This sensor was applied to detect Hg^{2+} in tap water samples.

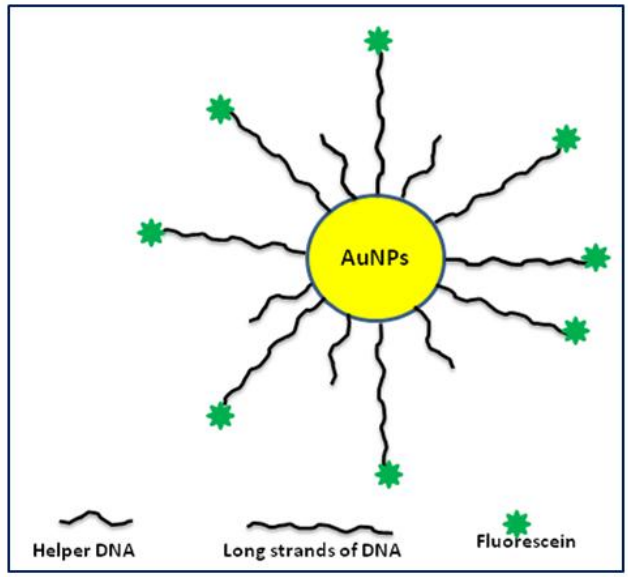

Figure 1.45. Fluorescein probe **L**[25] for Hg^{2+} detection.

Duan et.al.[120] developed fluorescein based chemosensor N-(Fluorescein) lactam-N′-methylethylidene **L**[26] **(Figure 1.46)** for the selective detection of Hg^{2+} ion. An absorption peak appeared at 477 nm in EtOH:H_2O (5/1, v/v) and emission peak at 518 nm after the addition of Hg^{2+} to the solution containing **L**[26]. It is interesting that the probe also displayed fluorescence enhancement at 568 nm in DMSO:H_2O (5/1, v/v) The Hg^{2+} induced fluorescence enhancement occured due to the "PET-off" (Photoinduced Electron Transfer-off) and CHEF (Chela- tion Enhanced Fluorescence) effect. The formation of 1:1 complex was confirmed from Job's plot. Increase in fluorescence intensity shows a good linearity (0.99645) with respect to the Hg^{2+} concentration. They reported LOD of Hg^{2+} as 14.9 nM. It is also applied to environmental water for Hg^{2+}.Then, Chemodosimeter can be applied to prepare novel hydrogel sensor by copolymerization with MBA. AAm, MMA and HEMA. This hydrogels sensor could be used as visual-eye detection of Hg^{2+}.

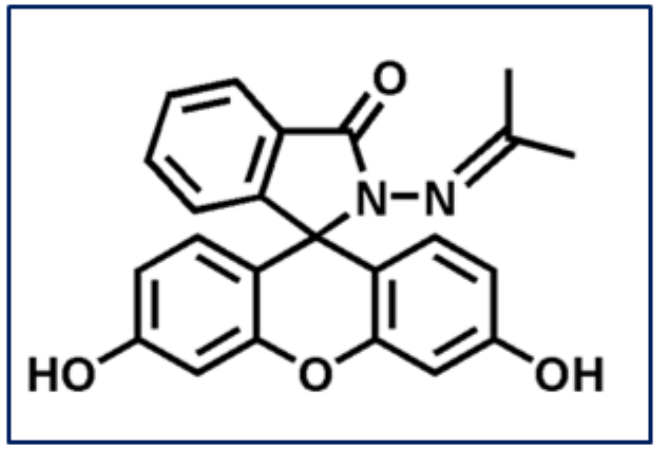

Figure 1.46. Chemical structure of **L**[26].

Feng Huo et al.[121] reported a ratiometric and colorimetric chemosensor **L**[27] **(Figure 1.47)** for the naked eye detection of Hg^{2+} in water. The probe is based on fluorescein and red-emitting bovine serum albumin based golden nano-clusters (BSA-AuNCs). In the presence of Hg^{2+}, the red fluorescence from BSA-AuNCs was quenched while the green fluorescein was inert thus as a reference. It exhibited traffic light-type (red, yellow and green) color in the low, middle and high concentration of Hg^{2+}. A linear correlation was constructed for Hg^{2+} in the concentration range of 10–500 μg L^{-1}. A limit of detection (LOD) of 7.4 μg L^{-1} and a relative standard deviation (RSD, n=7) of 0.4% were obtained, which can be used to monitor the concentration of Hg^{2+}. In visual detection, as low as 0.1 μg L^{-1} of Hg^{2+} can be easily discriminated from the blank with the naked eye. The proposed method was validated by analysis of certified environment and food samples with satisfactory results.

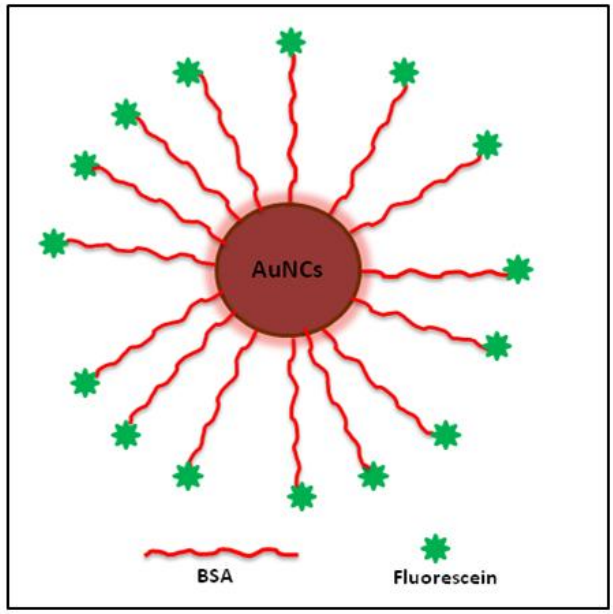

Figure 1.47. Fluorescein probe **L**[27] for Hg^{2+} detection.

1.7 Objective and Aim of the Thesis:

Due to simplicity and low detection limit and convenient implementation for the optical detections of metal ions via fluorescence/absorption changes are the most advantageous. The various effects on the environment as well as aquatic living organisms it is necessary to detect low concentration of metal ions accurately. Fluorescent sensors provide greater specificity than on-line and field monitoring colorimetric sensors, because sometimes colorimeters may miss to identifying colour differences. In terms of sensitivity, response time and local observation by fluorescence imaging spectroscopy, fluorescent molecular sensors offer distinct advantages. Not only that fluorescent sensors are highly specific and less susceptible towards interferences because fewer materials absorb and also emit light (fluorescence). To monitor biologically important metal ions for *in-vitro* and *in-vivo* sensing at a very low concentration the useful tool is fluorescent sensors. Hence to recognize metal ions selectively the fluorescent chemical sensors are developed.

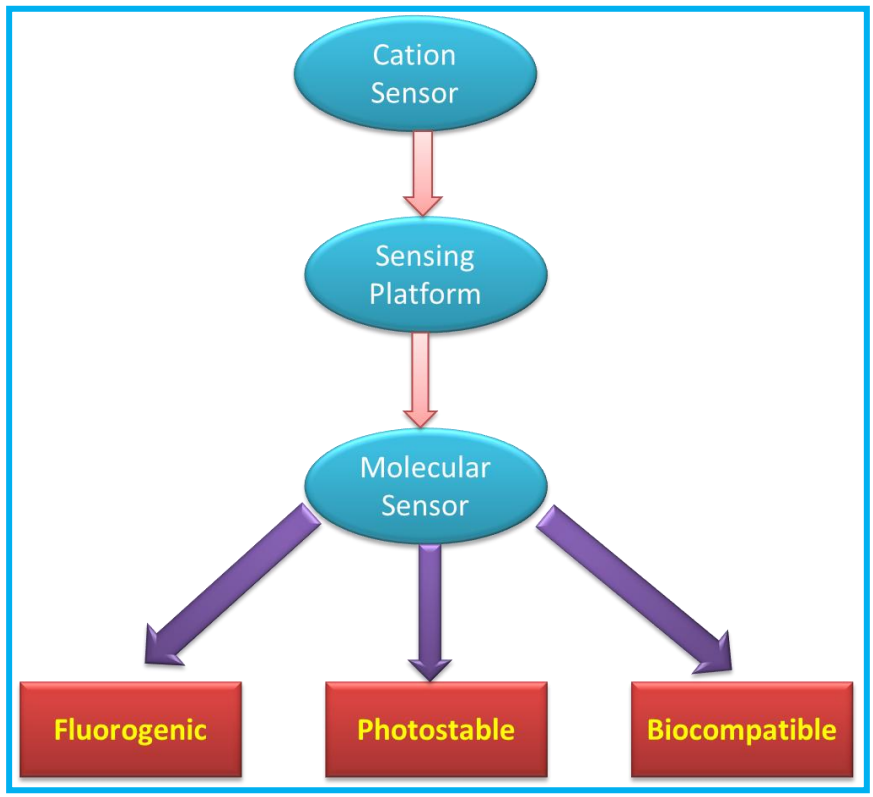

Sceheme 1.1. Schemetic representation of the project.

The fluorescence turn-on (fluorescence enhancement) response for cation is preferred over fluorescence turn-off (fluorescence quenching) response due to false positive responses of the later in the metal-ion–receptor binding phenomenon in real samples. Furthermore fluorescent molecular sensors (reversible probe) are found to be superior to the chemo dosimeters (irreversible probe) for real time practical application due to the distinct advantage in terms of the reusability of the former.

1.8 Present Work:

The main aim of the current works was to easily synthesized Fluorescein based fluorescent molecular probes to recognise Hg^{2+} metal ions in aqueous medium or organo

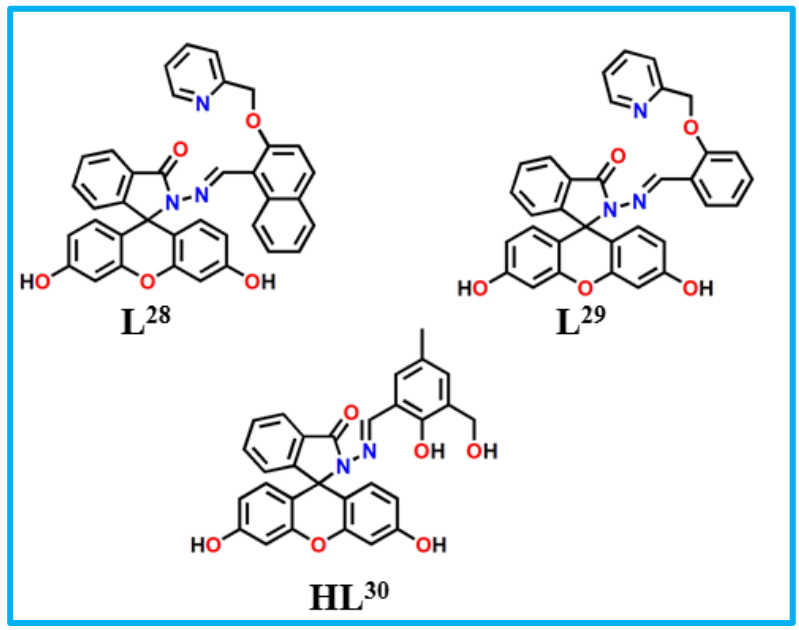

Sceheme 1.2. Design of target molecules.

aqueous medium in a very low concentration range. The fluorophores synthesized and used for the detection of Hg^{2+} in this thesis are enlisted in **Scheme 1.2.**

1.9 Physical measurements:

(i) *FTIR spectra*: Infrared spectra (400–4000 cm^{-1}) were recorded in liquid or solid states on a Nickolet Magna IR 750 series-II FTIR spectrometer.

(ii) *^{1}H NMR spectra*: ^{1}H-NMR spectra were recorded in DMSO-d_6, $CDCl_3$, CD_3OD, CD_3CN on a Bruker 300 MHz NMR spectrometer using tetramethylsilane ($\delta = 0$) as an internal standard.

(iii) *UV-vis spectra*: UV-vis spectra were recorded on an Agilent diode-array spectrophotometer (Model, Agilent 8453).

(iv) *Mass spectra*: ESI-MS^+ (m/z) of the ligand and complexes were recorded on a Waters' HRMS spectrometer (Model: QTOF Micro YA263).

(v) *Fluorescence spectra*: Steady-state fluorescence measurements were performed with a PTI QM-40 spectrofluorometer, Shimadzu spectrofluorometer (Model RF-5301).

(vi) *Life time measurements:* Lifetimes were measured in Horiba–Jobin–Yvon on a Hamamatsu MCP photomultiplier (R3809) and analysed using IBH DAS6 software.

(vii) *DFT calculations:* Ground state electronic structure calculations of the ligand and complexes have been carried out using using Gaussian 09W software package, associated with the conductor-like polarizable continuum model (CPCM).

(viii) *Cell imaging*: Cell imaging studies has been performed under fluorescence microscope. Bright field and fluorescence images of the HepG2 cells, HCT116 cells, were taken using a fluorescence microscope (Leica DM3000, Germany) with an objective lens of 40x, 20x magnification.

(ix) *pH study:* The pH of the solutions was recorded using a Systronics digital pH meter (Model 335, India) with the pH range 2–12. The pH meter was calibrated using standard buffer solutions (Acros Organics) of pH 4.0, 7.0 and 10.0.

References:

1 A. Renzoni, F. Zino and E. Franchi, *Environ. Res.*1998, **77**, 68.

2 H. H. Harris, I. J. Pickering and G. N. George, *Science*, 2003, **301**, 1203.

3 J. J. Gutknecht, *Membr. Biol.*,1981, **61**, 61.

4 P. Grandjean, P. Weihe, R. F. White and F. Debes, *Environ. Res.*, 1998, **77**, 165.

5 X. Zhang, Y. Xiao and X. Qian, *Angew. Chem., Int. Ed*., 2008, **47**, 8025.

6 T. Takeuchi, N. Morikawa, H. Matsumoto and Y. Shiraishi, *Acta Neuropathol*., 1962, **2**, 40.

7 M. Harada, Crit. *Rev.Toxicol.*, 1995, **25**, 1.

8 R. Von Burg, *J. Appl. Toxicol*., 1995, **15**, 483.

9 T. W. Clarkson, L. Magos and G. J. Myers, *N. Engl. J. Med.*, 2003, **349**, 1731.

10 B. Welz and M. Sperling, Atomic Absorption Spectrometry,Weinheim, Germany, *Wiley, 3rd edn*, 1999.

11 V. Iyengar and J. Wolttlez, *Clin. Chem.*, (Washington, D. C.), 1988, **34**, 474.

12 D. Diamond, Chemical Sensors, *John Wiley & Sons, INC*, 1998, 45.

13 A. T. Townsend, K. A. Miller, S. Mc and S. Aldous, *J. Anal. At. Spectrom.*, 1998, **13**, 1213.

14 R. Klockenkämpfer, *Total-Reflection X-ray Fluorescence Analysis, Wiley, New York* (1997).

15 A. P. de Silva, H. Q. N. Gunaratne, T. Gunnlaugsson, A. J. M. Huxley, C. P. McCoy, J. T. Rademacher and T. E. Rice, *Chem. Rev.*, 1997, **97**, 1515.

16 J. F. Zhang, Y. Zhou, J. Yoon and J. S. Kim, *Chem. Soc. Rev.*, 2011, **40**, 3416.

17 M. Formica, V. Fusi, L. Giorgi and M. Micheloni, *Coord. Chem. Rev.*, 2012, **256**, 170.

18 L. Xin, Y. Z. Chen, L. Y. Niu, L. Z. Wu, C. H. Tung, Q. X. Tong and Q. Z. Yang, *Org. Biomol.Chem.*, 2013, **11**, 301427.

19 J. G. Haub, Y. He, R. T. White, "Spectroscopic Applications of Pulsed Tunable Optical Parametric Oscillators", 2016, 17–142, (3rd ed.).

20 L. Bruneau, V. Jakši´, Y. Last, C. A. Pillet, *Commun. Math. Phys.*, 2016, **344 (3),** 959-981.

21 N. A. Sinitsyn, Y. V. Pershin, "The theory of spin noise spectroscopy: A review".cond-mat.mes-hall, 2016.

22 D. L. Pavia, G. M. Lampman, G. S. Kriz, J.R. Vyvyan, “Introduction to Spectroscopy” 5th ed., 2015.

23 W. Kemp, “Organic Spectroscopy”, Palgrave, London,1991.

24 D. C. Harris, M. D. Bertolucci, Symmetry and Spectroscopy: An Introduction to Vibrational and Electronic Spectroscopy, Dover Publications, New edition, 1989.

25 T. H. Roos, W. J. Price, *Spectrochimica Acta Part B: Atomic Spectroscopy*, 1971, **26(5),** 279-284.

26 G. M. Barrow, Introduction to Molecular Spectroscopy, McGraw-Hill, 1962.

27 M. Gorur, F. Yilmaz, A. Kilic, Z. M. Sahin and A. J. Demirci, *Polym. Sci., Part A: Polym.Chem., 2011*, **49**, 3193−3206.

28 M. Gorur, F. Yımaz, A. Kilic, A. Demirci, Y.Ozdemir, A. Kosemen and E. A. J. San, *Polym. Sci., Part A: Polym. Chem., 2010*, **48**, 3668.

29 Z. Tian, C. Chen and H. R. Allcock, *Macromolecules, 2013*, **46**, 2715.

30 H. R. Allcock, *Appl. Organometal. Chem*., 2013, **27**, 620.

31 R. J. Davidson, E. W.Ainscough, A. M. Brodie, G. B. Jameson, M. R.Waterland, H. R.Allcock, M. D.Hindenlang, B.Moubaraki, K. S.Murray, K. C. Gordon, R. Horvath and G. N. L. Jameson, *Inorg. Chem.*, 2012, **51**, 8307.

32 H. A. Alidagi, O. M.Girgic, Y. Zorlu, F. Hacivelioglu, S. U. Celik, A. Bozkurt, A. Kilic, and S. Yesilot, *Polymer, 2013*, **54**, 2250.

33 C. W. Allen, *Chem. Rev*., 1991, **91**, 119.

34 B. Cosut and S. Yesilot, *Polyhedron*, 2012, **35**, 101.

35 K. K. Rohatgi-Mukherjee, *Fundamentals of Photochemistry, Wiley Eastern, New Delhi*, 1992.

36 A. D. Skoog, J. F. Holler and D.M. West, *Fundamentals of Analytical Chemistry*, 7th *ed.,Thomsen learning*, 2007, 601.

37 B. Valeur, *"Molecular Fluorescence: Principles and Applications" Wiley-VCH Verlag GmbH*, 2001.

38 J. R. Lakowicz, *"Principles of Fluorescence Spectroscopy 3rd edition" Springer*, 2006.

39 K. K. Rohatgi-Mukherjee, *Fundamentals of Photochemistry, Wiley Eastern, New Delhi*, (1992).

40 L. Fabbrizzi, M. Licchelli, P. Pallavicini, A. Perotti, A. Taglietti and Donata Sacchi, *Chem. Eur. J.*, 1996, **2**, 1.

41 S. K. Sahoo, D.Sharma, R. K. Bera, G. Crisponi and J. F Callan, *Chem. Soc. Rev.*, 2012, **41**, 7195.

42 K. Kaur, R. Saini, A. Kumar, V. Luxami, N. Kaur, P. Singh and S. Kumar; *Coordination Chemistry Rev.*, 2012, **256** ,1992.

43 S. Cai, Y. Lu, S. He, F. Wei, L. Zhaoab and X. Zeng, *Chem. Commun.*, 2013, **49**, 822.

44 J. T. Yeh , W.C. Chen, S. R. Liu, S. P. Wu, *New J. Chem.*, 2014, **38**, 4434-4439.

45 A. K. Das, K. Aich, A. Manna, S. Maity, K. Khanra and N Bhattacharyy and S. Goswami, *Analyst*, 2013, **138**, 4593.

46 D. Wu, W. Huang, C. Duan, Z. Lin, Q. Meng, *Inorg. Chem*,. 2007, **46**, 1538.

47 W. Jiang, W. Wang, *Chem. Commun*., 2009, 3913.

48 M. H. Lee, T.V. Giap, S.H. Kim, Y. H. Lee, C. Kang, J. S. Kim, *Chem. Commun.*, 2010, 1407.

49 H.Y. Lin, P. Y. Cheng, C. F. Wanb and A. T Wu, *Analyst*, 2012, **137**, 4415.

50 A. Munoz de la Pena, A. Machuca, H. C. Goicoechea , R. Babiano and M. J. Culzoni, *Anal. Methods*, 2013, **5**, 30.

51 M. Suresh, A. K.Mandal, S. Saha, E. Suresh, A. Mandoli, R. D. Liddo, P. P.Parnigotto and A. Das,*Org. Lett.*, 2010,**12**, 5408.

52 A. P. de Silva, T. S. Moody and G. D. Wright, *Analyst*, 2009,**134**, 2385.

53 J. S. Kim and D. T. Quang, *Chem. Rev.*, 2007, **107**, 3780.

54 T. Gunnlaugsson, H. D. P. Ali, M. Glynn, P. E. Kruger, G. M. Hussey, F. M. Pfeffer, C. M. D. Santos and J. Tierney, *J. Fluoresc.*, 2005, **15**, 287.

55 J. F. Callan, A. P. de Silva and D. C. Magri, *Tetrahedron*, 2005, **61**, 8551.

56 R. Martinez-Manez and F. Sancenon, *Chem. Rev.*, 2003, **103**, 4419.

57 B. Valeur and I. Leray, *Coord. Chem. Rev.*, 2000, **205**, 3.

58 Z. C. Xu, J. Yoon and D. R. Spring, *Chem. Soc. Rev.*, 2010, **39**, 1996.

59 W. Rettig and R. Lapouyade, *Fluorescence probes based on twisted intramolecular charge transfer (TICT) states and other adiabatic photoreactions, in Topics in Fluorescence Spectroscopy, Probe Design and Chemical Sensing*, ed. J. R. Lakowicz, Plenum Press, New York, 1994, **4**, 109.

60 Q. Zhao, F. Y. Li and C. H. Huang, *Chem. Soc. Rev.*, 2010, **39**, 3007.

61 K. E. Sapsford, L. Berti and I. L. Medintz, *Angew. Chem., Int. Ed.*, 2006, **45**, 4562.

62 Y. Zhao, Y. Zhang, X. Lv, Y. Liu, M. Chen, P. Wang, J. Liu and W. Guo, J. Mater.*Chem.*, 2011, **21**, 13168.

63 Y. N. Hong, J. W. Y. Lam and B. Z. Tang, *Chem. Commun.*, 2009, 4332.

64 J.R. Lakowicz, Principles of Fluorescence Spectroscopy, Kluwer Academic/Plenum, New York, 1999.

65 C. LODeiro and F. Pina, *Coord. Chem. Rev.*, 2009, **253**, 1353.

66 C. M. G. dos Santos, M. Glynn, T. McCabe, J. S. Seixas de Melo, H. D. Burrows and T. Gunnlaugsson, *Supramol. Chem.*, 2007, **20**, 407.

67 A. P. de Silva and S. A. de Silva, *J. Chem. Soc. Chem. Commun.*, 1986, 1709.

68 L. Yang, Q. Song, K. Damit-Og and H. Cao, *Sens. Actuators B*, 2013, **176**, 181.

69 R. Metivier, I. Leray, B.Valeur, *Chemistry-a European Journal*, 2004, **10**, 4480.

70 G. Bergamini, L. Boselli, P. Ceroni, P. Manca, G. Sanna and M. Pilo, *Eur. J. Inorg. Chem.*, 2011, 4590.

71 H. J. Jeong, Y. Li, M. H. Hyun, *Bulletin of the Korean Chemical Society*, 2011, **32**, 2809.

72 I. Leray, B. Valeur, *Coordination Chemistry Rev.*, 2000, **205**, 3.

73 J. Bourson, J. Pouget, B. Valeur, *Journal of Physical Chemistry*1993, **97**, 4552.

74 W. Jiang, Q. Fu, H. Fan and W. Wang, *Chem.Commun.*, 2008, 259.

75 S. Wagner, K. Brodner, B. A. Coombs, U. H. F. Bunz, *European Journal of Organic Chemistry*, 2012, 2237-2242.

76 T. Iijima , A. Momotake , Y. Shinohara , T. Sato , Y. Nishimura and T. Arai , *J. Phys. Chem. A*, 2010, **114** , 1603-1609.

77 J. Zhao, S. Ji, Y. Chen, H. Guo and P.Yang, *Phys. Chem. Chem. Phys.*, 2012, **14**, 8803.

78 J. Mei, N. L. C. Leung, R. T. K. Kwok, J. W. Y. Lam, and B. Z. Tang, *Chem. Rev.*, 2015, **115,** 11718−11940.

79 W. Chen, Z. Zhang, X. Li, H. Agren and J. Su, *RSC Adv.*, 2015, **5**, 12191.

80 X. Chen, X. Y. Shen, E. Guan, Y. Liu, A. Qin, J. Z. Sun and B. Z. Tang, *Chem. Commun.*, 2013, **49**, 1503.

81 S. Samanta, S. Goswami, Md. N. Hoque, A. Ramesh and G. Das,*Chem. Commun.*, 2014, **50**, 11833.

82 S. Sarkar, S. Roy, A. Sikdar, R. N. Saha and S. S. Panja, *Analyst*, 2013, **138**, 7119.

83 Y. Suzuki, T. Morozumi, H. Nakamura, M. Shimomura, T. Hayashita and R. A. Bartsh, *J. Phys. Chem. B*, 1998, **102**, 7910.

84 L. N. Neupane, J. Y. Park, J. H. Park and K. H. Lee, *Org. Lett.*, 2013, **15**,255.

85 N. Kumar, V. Bhalla and M. Kumar , *Analyst*, 2014, **139**, 543.

86 L. Yuan, W. Lin, B. Chen and Y. Xie, *Org. Lett.*, 2012, **14**, 432.

87 M. Kumar, N. Kumar, V. Bhalla, P. R. Sharma and T. Kaur, *Org. Lett.*, 2011, **13**, 1422.

88 J. B. Grim, L. D. Lavis, *Org Lett.*, 2011, **13,** 6354.

89 F. Ge, H. Ye, H. Zhang, B. X. Zhao, *Dyes Pigm.*, 2013, **99,** 661-665.

90 M. Adamczyk, J. Grote, *Synth Commun*, 2001 **31,** 2681–2690.

91 E. Oliveira, E. Bertolo C. Nunez, V. Pilla, H. M Santos, J, Fernandez-LODeiro, A. Fernandez-LODeiro J. Djafari, J. L. Capelo, C, LODeiro, *Chemistry Open*, 2017, **7,** 9–52.

92 M. Rajasekar, *J Mol Struct*, 2020, **1224,** 129085.

93 W. A. Banks, A. J, Kastin, D. A. Durham, *Brain Res Bull*, 1989, **23,** 433–437.

94 H. N. Kim, M. H. Lee, H. J. Kim, J. S. Kim and J. Yoon, *Chem. Soc. Rev.*, 2008, **37**, 1465.

95 Z. Xie, F. Huo, J. Su, Y. Yang, C. Yin, X. Yan and S. Jin, *Open Journal of Applied Biosensor*, 2012, **1,** 44-52.

96 X. F. Yang, Y. Lia, and Q. Bai, *Analytica Chimica Acta*, 2007, **584,** 95–100.

97 P. Piyanuch, S. Watpathomsub, V. S. Lee, H. A. Nienaber, N. Wanichacheva, *Sensors and Actuators B*, 2016, **224,** 201–208.

98 S. Guang, J. Tian, G. Wei, Z. Yan, H. Pan, J. Fengd, H. Xu, *Talanta*, 2017, **170,** 89–96.

99 Y. Feng, Z. Kuai, Y. Song, J. Guo, Q.Yang, Y. Shan, Y. Li, *Talanta*, 2017, **170,** 103–110.

100 H. J. Kim, J. E. Park, M. G. Choi, S. Ahn, S. K. Chang, *Dyes and Pigments*, 2010, **84,** 54–58.

101 R.V. Rathod, S. Bera, P. Maity, and D. Mondal, *ACS Omega*, 2020, **5,** 4982−4990.

102 L. Huang , Y. Sun, G. Zhao , L.Wang , X. Meng , J. Zhou , H. Duan, *Journal of Molecular Structure*, 2022, **1255,** 132427.

103 W. Shen, L. Wang, M. Wu, X. Bao, *Inorganic Chemistry Communications*, 2016, **70,** 107–110.

104 S. R. Bhatta, A. Pal, U. K. Sarang, A. Thakur, *Inorganica Chimica Acta*, 2019, **498,** 119097.

105 S. Erdemir, O. Kocyigit, *Dyes and Pigments*, 2017, **145,** 72–79.

106 D. Liu, Y. Wang, R. Wang, B. Wang, H. Chang, J. Chen, G.Yang, H. He, *Inorganic Chemistry Communications*, 2018, **89,** 46–50.

107 A. P. Lafond, D. Larivière and D. Boudreau, *ACS Omega*, 2020, **5,** 701−711.

108 Y. Zhanga, Q.Tua, L. Chena, N. Lic, L. Yanga, X. Zhanga, M. S. Yuana, J. Wanga, *Talanta*, 2019, **202,** 323–328.

109 K. Tripathi, A. Rai, A. K. Yadav, S. Srikrishna, N. Kumari and L. Mishra, *RSC Adv.*, 2017, **7,** 2264.

110 K. Sureshkumar, T. Ramakrishnappa, M. Pandurangappa, *Materials Today: Proceedings*, 2022, **49,** 576–582.

111 H. Kang, H. Xu, C. Fan, G. Liu, S. Pu, *Journal of Photochemistry & Photobiology A: Chemistry*, 2018, **367,** 465–470.

112 E. M. Nolan and S. J. Lippard, *J. Am. Chem. Soc.*, 2003, **125,** 14270-14271.

113 E. M. Nolan and S. J. Lippard, *J. Mater. Chem.*, 2005, **15,** 2778–2783.

114 N. Wanichacheva, O. Hanmeng, S. Kraithong, K. Sukrat, *Journal of Photochemistry and Photobiology A: Chemistry*, 2014, **278,** 75– 81.

115 G. Q. Shang, X. Gao, M. X. Chen, H. Zheng and J. G. Xu, *J. Fluoresc.*, 2008, **18,** 1187–1192.

116 N. R. Chereddy, P. Nagaraju, M.V. N. Raju, K. Saranraj, S. Thennarasu, V. J. Rao, *Dyes and Pigments*, 2015, **112,** 201-209.

117 A. Helal, M. Naeem, M. Fettouhi and Md. H. Zahir, *Molecules*, 2021, **26,** 5773.

118 M. G. Choi, D. H. Ryu, H. L. Jeon, S. Cha, J. Cho, H. H. Joo, K. S. Hong, C. Lee, S. Ahn and S. K. Chang, *Org.Lett.*, 2008, **10,** 3717–3720.

119 G. Wang, Y. Lu, C. Yan, Y. Lu, *Sens. Actuat. B Chem*,. 2015, **211,** 1-6.

120 Z. Qua, L. Wangb, S. Fanga, D. Qina, J. Zhoua, G. Yanga, H. Duana, *Microchemical Journal*, 2019,**150,** 104198.

121 W. Deng, R. Dai, P. Hu, Q. Li, X. Xiong, K. Huang, F. Huo, *Microchemical Journal*, 2018, **141,** 163–169.

A fluorescein-based chemosensor for "turn-on" detection of Hg^{2+} and resultant complex as a fluorescent sensor for S^{2-} in semi aqueous medium with cell-Imaging application: Experimental and Computational studies

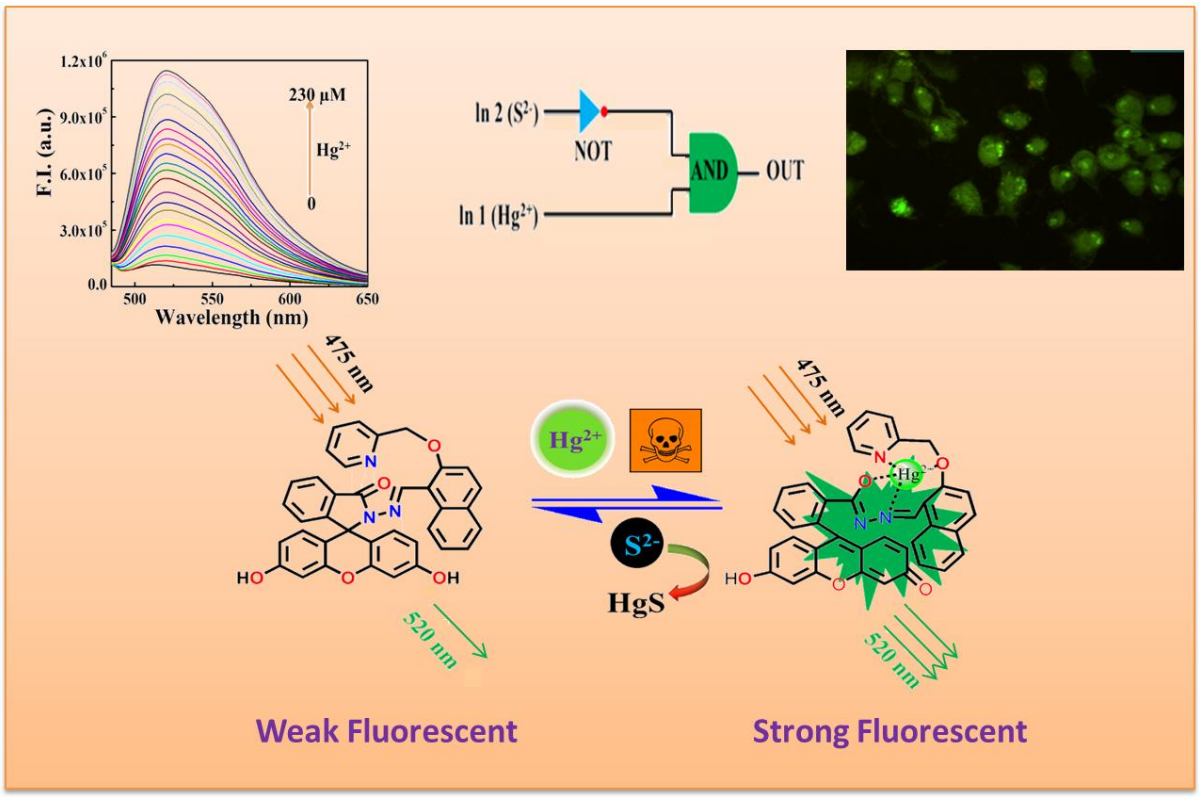

Abstract:

A fluorescein hydrazone based conjugate (**L^{28}**) is synthesized by coupling of fluorescein hydrazide (**1**) with 2-(Pyridin-2-ylmethoxy)-napthlene-1-carbaldehyde (**2**). **L^{28}** is well characterized by several spectroscopic methods such as IR, ^{1}H, ^{13}C-NMR and ESI-MS. The probe **L^{28}** exhibited high selectivity and high sensitivity towards toxic Hg^{2+} ion in semi aqueous medium (pH 7.2, 10 mM HEPES) over other metal ions. The significant enrichment in fluorescence emission centered at 520 nm was attributed to the Hg^{2+}-induced ring opening of the spirolactam moiety in the fluorescein structure. The 1:1 binding of **L^{28}** to Hg^{2+} was established by Job's method and confirmed by ESI-MS^{+} (m/z) studies and the binding constant was calculated as $(0.43 \pm 0.04) \times 10^{4}\ M^{-1}$ with a detection limits of 1.24 µM. Then again, L^{28}-Hg^{2+} complex could be utilized as a reversible fluorescent sensor for S^{2-}. On addition of S^{2-} to the L^{28}-Hg^{2+} complex, the fluorescence intensity was totally quenched because Hg^{2+} in the complex was grabbed by S^{2-}because of the stronger binding force between Hg^{2+} and S^{2-}. The tentative coordination environment in the L^{28}-Hg^{2+} complex was established by DFT studies. The fluorescence "OFF–ON–OFF" mode of **L^{28}** was examined in the presence of Hg^{2+} and S^{2-} and finds applications in devices with logic gate functions. The **L^{28}** also exhibits bio-compatibility and negligible cytotoxicity and is suitable for fluorescence cell imaging of Hg^{2+} ions in live HepG2 cells.

2.1 Introduction

Hg^{2+} and its derivatives are highly toxic pollutants. Mercury pollution, specifically, is a subject of recent worry[1-3]. Contamination with Hg^{2+} originates from a variety of natural and anthropogenic sources, including oceanic and volcanic emission[4-5] gold mining, solid waste incineration[6], and the combustion of fossil fuels[7]. Inorganic mercury can be transformed into methyl mercury by bacteria, and can easily enter into the human body via the food chain.[4,8-11,] Hg^{2+} can accumulate in the human body and leads to severe health problems such as damaging and dysfunction of brain, kidneys, DNA and central nervous system[12-13] and Minamata disease[14]. Owing to its serious toxic effect and wide distribution, the Environmental Protection Agency of United States (USEPA) set a maximum tolerance limit of 2 ppb for Hg^{2+} for drinking water.[15] The typical detection methods such as inductively coupled plasma mass spectrometry, atomic absorption/ emission spectroscopy[16-17] and voltammetry[18] are used to detect Hg^{2+} ions. These traditional methods are not suitable as they are very expensive and need continuous monitoring, skilled personnel and sophisticated instrumentation for on-site detection of Hg^{2+}. The Sol-gel method is also use for heavy metal (e.g Hg^{2+}) detection. Due to the porous nature of the sol–gel network, entrapped species remains accessible and can interact with external chemical species or analytes. Sol–gel based sensors also suffer from some disadvantages, e.g., entrapment in sol–gel glass may change chemical and biological properties of the entrapped species, due to reduced degrees of freedom and interactions with the inner surface of the pores.[19-22] Hence, spectrofluorometric techniques are extensively used to monitor Hg^{2+} due to their faster and cheaper execution with simplicity and easy adaptability. In particular, colorimetric and fluorescent sensors have attracted a lot of attention in the field of heavy metal detection[23-31] due to their advantages of well selectivity, quick response and high sensitivity. Recently, some important fluorescent sensors on Hg^{2+} have been repoted.[32-38] Among various fluorophore, we have selected fluorescein dye to design a Hg^{2+} selective probe owing to its excellent spectroscopic properties with longer absorption and emission wavelengths, high fluorescence quantum yield, well biocompatibility and negligible toxicity.[39] For detection of Hg^{2+} most of the sensors are found on rhodamine compounds.[40-52] However, fluorescein-based probes have acquired comparatively little attention.[53-57] Thus, here fluorescein is used as a constituent to

design a chemosensor with prospective N_2O_2 donor atoms for the selective and rapid recognition of toxic Hg^{2+} ions in semi aqueous medium exhibiting chromo and fluorogenic responses through metal-induced ring opening of the spirolactam moiety. The quenching of fluorescence could be realized by adding of S^{2-}. This OFF–ON–OFF fluorescence behaviour can be applied for the sequential recognition of Hg^{2+} and S^{2-} and can be further extended for biological cell imaging.

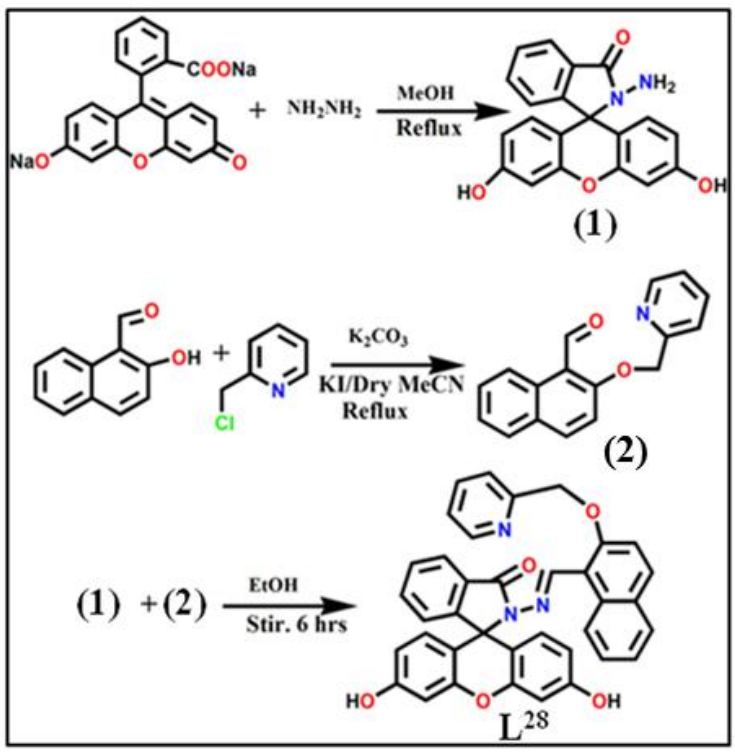

Scheme 2.1. Synthetic route of chemosensor **L**[28]

2.2 Experimental section

2.2.1 Materials and Instruments

Steady-state fluorescence studies were performed with a PTI (QM-40) spectrofluorimeter. UV/Vis absorption spectra were noted with an Agilent 8453 diode array spectrophotometer. Bruker spectrometers of 400 and 500 MHz were used for ^{1}H and ^{13}C NMR studies. The ESI-MS^{+} spectra were documented on a Waters XEVO G2QTof (Micro YA263) mass spectrometer.

Solvents like methanol and ethanol (Merck, India) were of reagent grade and dried before experiment. Deionized water from MiliQ Millipore was used for UV/Vis and fluorescence studies. Fluorescein sodium salt, 2-chloromethylpyridine, $Hg(ClO_4)_2.3H_2O$ and metal salts such as the perchlorates of Zn^{2+}, Mg^{2+}, $Co^{2,}$, Ni^{2+}, Cu^{2+}, Pb^{2+}, Al^{3+}, Cr^{3+}, Cd^{2+}, Pd^{2+}, Fe^{2+} Fe^{3+}, Mn^{2+}, Na^{+}, K^{+}, Ca^{2+}, and Ag^{+} were bought from Sigma–Aldrich and used as received. Sodium salts of anions like SO_4^{2-}, $S_2O_4^{2-}$ SO_3^{2-}, $S_2O_3^{2-}$, PO_4^{3-}, S^{2-}, Cl^{-}, F^{-}, Br^{-}, I^{-}, $H_2PO_4^{-}$, CN^{-}, NO_2^{-}, CO_3^{2-}, ClO_4^{-} and N_3^{-} were of reagent grade and used as received. All other compounds were bought from commercial sources.

2.2.2 Solution preparation for UV-Vis/fluorescence studies

For UV-Vis and fluorescence experiments, a 10 ml 1.0 x 10^{-3} M stock solution of **L**[28] (5.91 mg) was made by dissolving required amount of ligand in DMF-MeOH (1:9 v/v). In a similar way, standard solutions of 1.0 x 10^{-3} M $Hg(ClO_4)_2.3H_2O$ and 1.0 x 10^{-3} M of sodium sulphide (Na_2S) in water were also prepared. The standard solutions of other cations and anions were made in $MeOH/H_2O$. A 250 mL of 10 mM HEPES buffer in water was prepared and pH was maintained to 7.2 by using HCl and NaOH. 2.5 mL of this buffer solution was pipetted out into a cuvette to which required volume (50 µL in T-200) of 1.0 x 10^{-3} M probe was transferred to achieve 20 µM final concentrations for fluorescence titration. In a regular interval of volume Hg^{2+} ions were transferred incrementally beginning from 0 to 230 µM and fluorescence spectra was collected for each solution. The cuvettes of 1 cm path length were used for absorption and emission studies. Fluorescence experiments were done using 5 nm x 3 nm slit width.

2.2.3 Synthesis

2.2.3.1 Preparation of Fluorescein Hydrazide (1)

Fluorescein Hydrazide (L^1) was prepared in high yield by reacting fluorescein with hydrazine hydrate in methanol (**Scheme 2.1**) according to the literature[58]. An excessive hydrazine hydrate (85%, 1.2 mL) was added to a 0.35 g of fluorescein dissolved in 20 ml of ethanol, and the reaction solution was refluxed in oil bath for 8 h. A brown oily product resulted from evacuating ethanol under reduced pressure. The solid product was precipitated by adding water and recrystallized from ethanol/water mixture, producing the fluorescein hydrazide as a yellow powder with 72% yield (0.25 g).

2.2.3.2 Preparation of 2-(Pyridin-2-ylmethoxy)-napthlene-1-carbaldehyde (2)

L^2 was synthesized by a modification of a literature method. [43] 2-Hydroxy-napthaldehyde (10 mmol, 1.72 g) and K_2CO_3 (18 mmol, 2.52 g) were poured to dry MeCN (50 ml). The mixture was allowed to reflux for 1 h. After that, a catalytic amount of KI (0.10 g) and 2-Picolyl chloride (10 mmol, 1.64 g) were added to the reaction mixture. Furthermore, the reaction mixture was reflux for 8 h and then filtered after cooling the solution to room temperature. The volume of filtrate was concentrated and diluted with water. Then, 1 M HCl solution was poured to maintain the pH at 4.Then extracted with dichloromethane (DCM; 2 x 30 ml). The pH of the aqueous solution was further adjusted to 8 by adding of 4.0 mmol Na_2CO_3 solutions and extracted with DCM (3 x 20 mL). Then the combined organic phase was evaporated to dryness after drying with anhydrous Na_2SO_4 to get solid residue. Finally, the crude solid product was recrystallized from MeOH/DCM (6:4, v/v) to achieve the desired product as an off-white crystalline solid. Yield: 72%. ^{1}H-NMR (in $CDCl_3$): (δ ppm) 11.06 (1H, s, –ArCHO), 9.3 (1H, d, –ArH), 8.64 (1H, d, –ArH), 8.05 (1H, d, –ArH), 7.79 (2H, t, –ArH), 7.63 (1H, d,–ArH), 7.56 (1H, d, –ArH), 7.46 (2H, t, –ArH)7.35 (1H, t, –ArH),(**Figure 2.1**). ESI-MS$^+$: m/z= 264.02 (**$C_{17}H_{13}NO_2$ + H^+**) (**Figure2.2**).

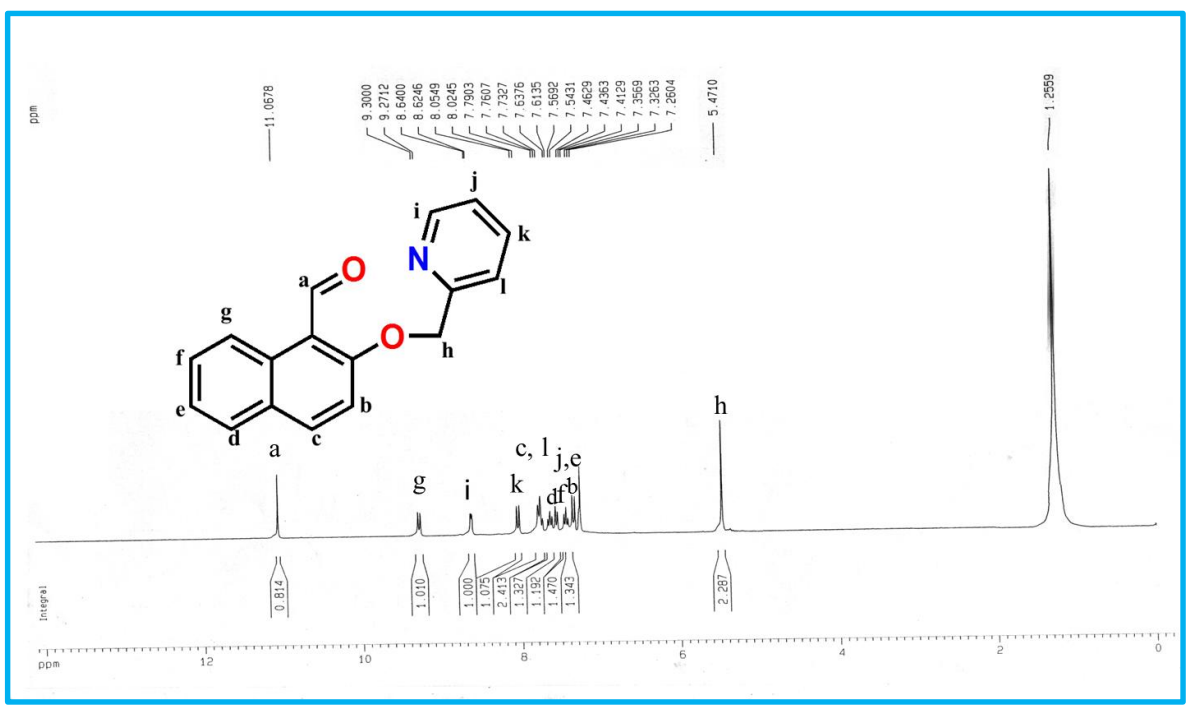

Figure 2.1. ^{1}H-NMR spectrum of **2** in DMSO-d_6.

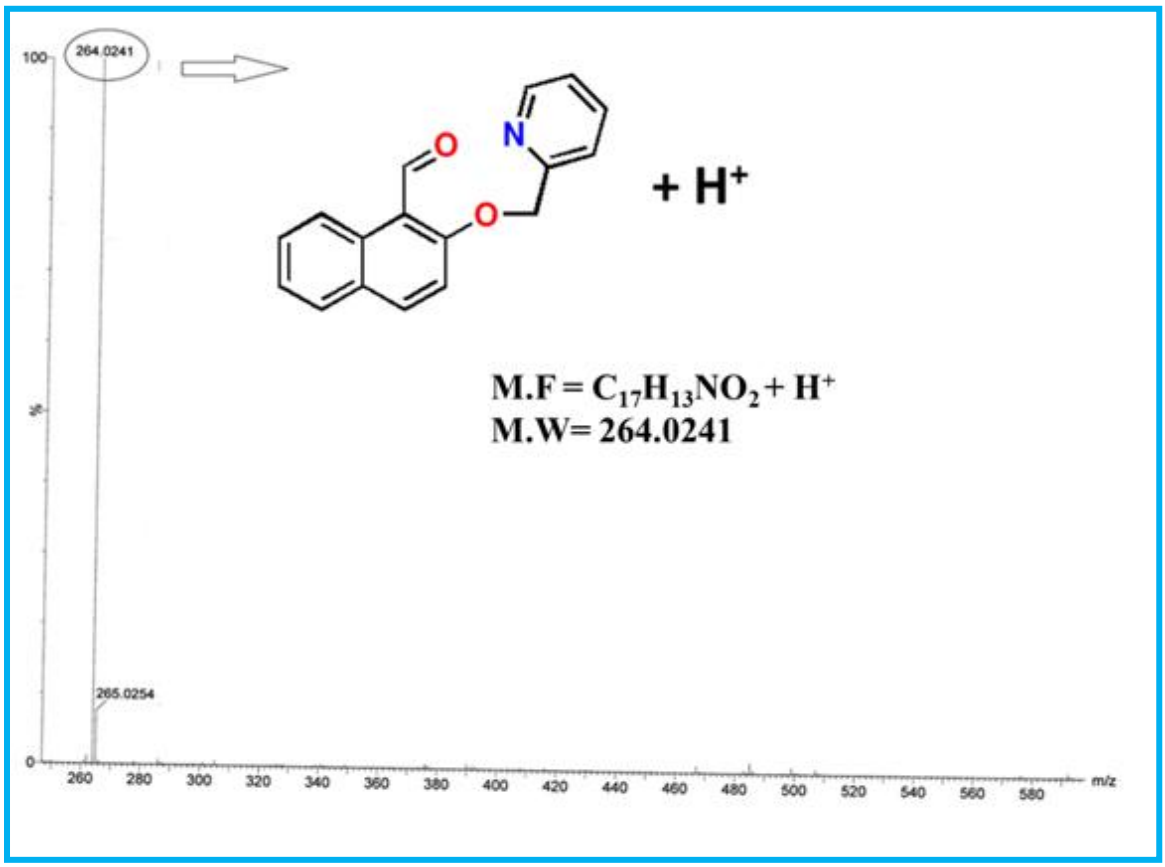

Figure 2.2. Mass spectrum of **2** in MeOH.

2.2.3.3 Preparation of Probe (L²⁸)

In a 250 mL round-bottom flask, Fluorescein Hydrazide (0.692 g, 2 mmol) and 2-(Pyridin-2-ylmethoxy)-napthlene-1-carbal dehyde (0.5262 g, 2 mmol) were suspended in 20 mL ethanol. The mixture was refluxed for 6 h with stirring to get a clear solution. Following the reaction, the mixture was permitted to cool to room temperature. The pale yellow precipitate formed was separated by filtration and finally, washed with 3X10 ml ethanol. 70% yield was obtained.^{1}H-NMR (DMSO-d_6): δ = 9.93 (d, 3 H), 8.56 (s, 1 H), 8.43 (d,1H), 8.19(s, 2 H), 7.90 (d, 2 H), 7.63 (d, 2 H), 7.43(d, 2 H), 7.30 (s, 3 H), 7.17 (d, 1 H), 6.60 (s, 2 H), 6.54 (d, 2 H), 6.46 (d, 2 H), 5.33 (s, 2 H),**(** **Figure 2.3)**.^{13}C-NMR (DMSO-d_6): δ = 164.07, 159.08,156.90,152.79,150.69, 149.55, 147.60, 137.52, 134.38, 133.17, 130.81, 130.28, 129.63, 129.36, 128.74, 128.02, 125.92, 124.51, 124.42, 123.60, 123.47, 121.80, 115.67, 114.85, 112.82, 110,71, 102.89, 71.72, 65.96 **(Figure 2.4) FT**-IR spectrum:-OH (3123 cm^{-1}),-

C=N (1610 cm^{-1}), -ArH (2919 Cm^{-1}), -C=O (1647 Cm^{-1}).(**Figure 2.5**). ESI-MS^{+}: *m/z*= 592.07 (**$C_{37}H_{25}N_3O_5$ + H^{+}**)(**Figure 2.6**).

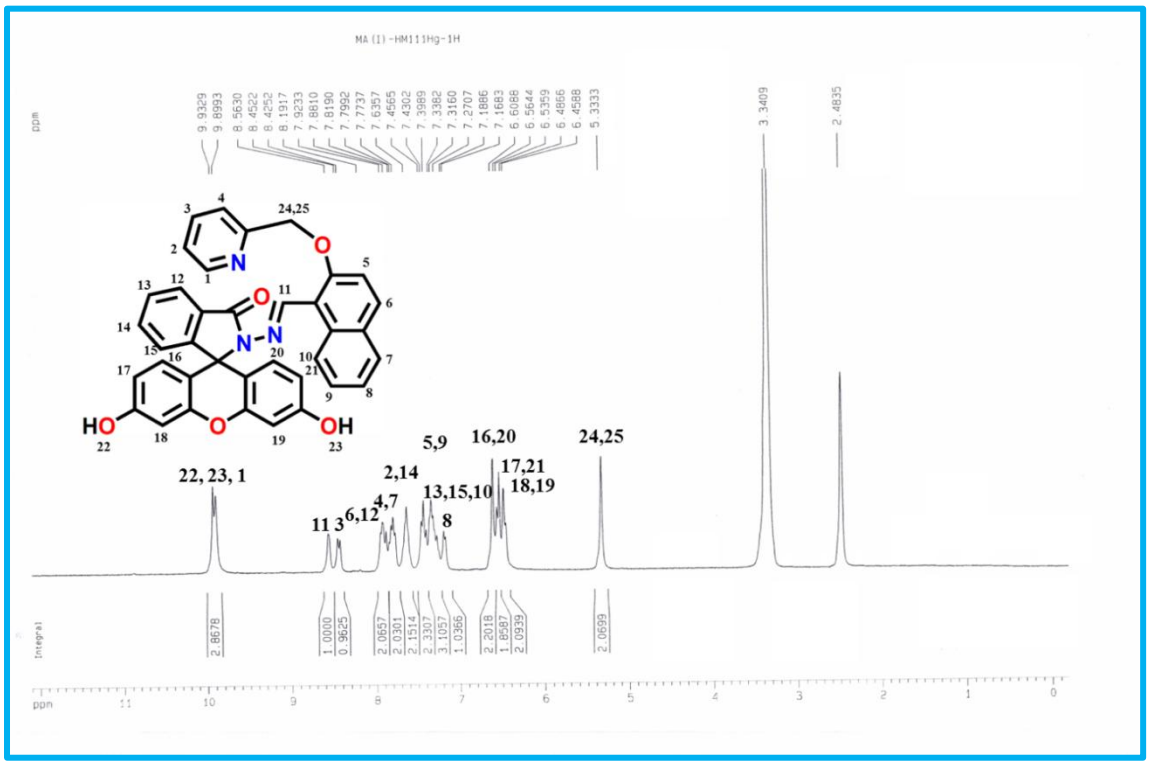

Figure 2.3. ^{1}H-NMR spectrum of **L**^{28}

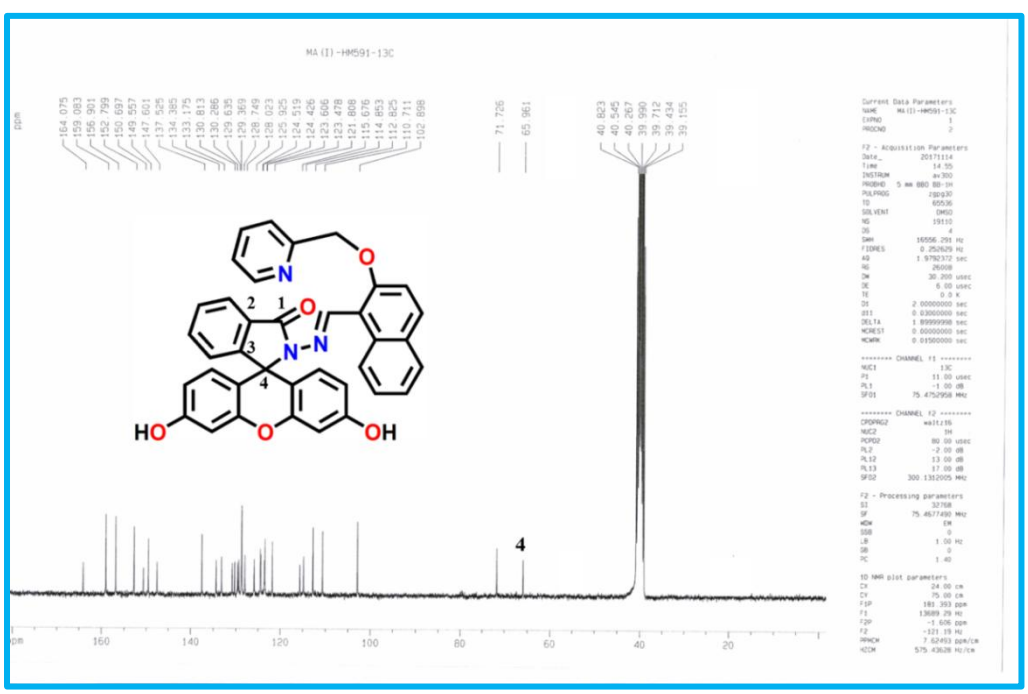

Figure 2.4. ^{13}C-NMR spectrum of **L**^{28} in DMSO-d_6.

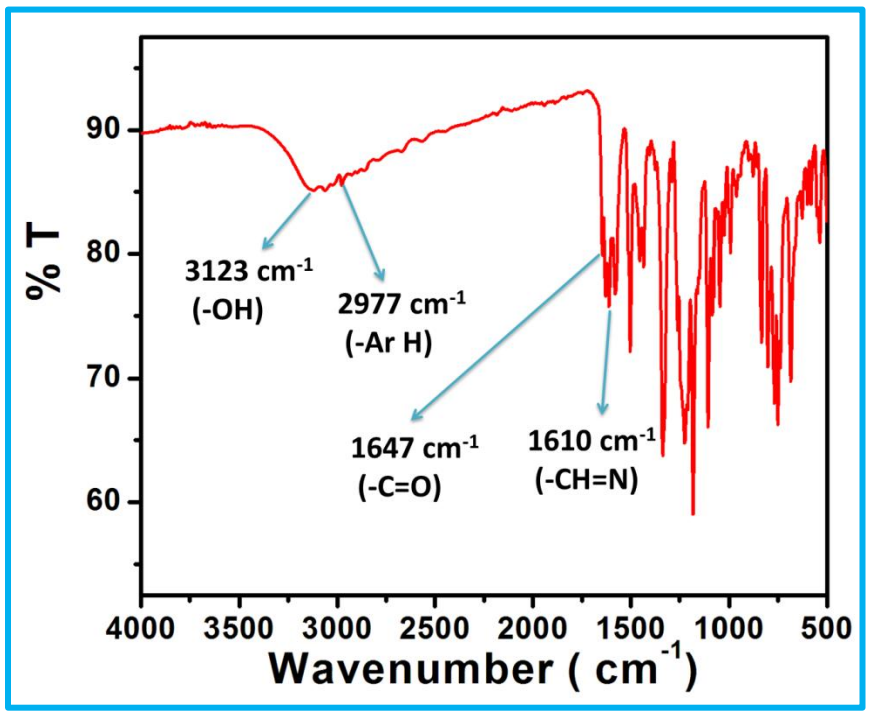

Figure 2.5. IR spectrum of $\mathbf{L}^{28}$.

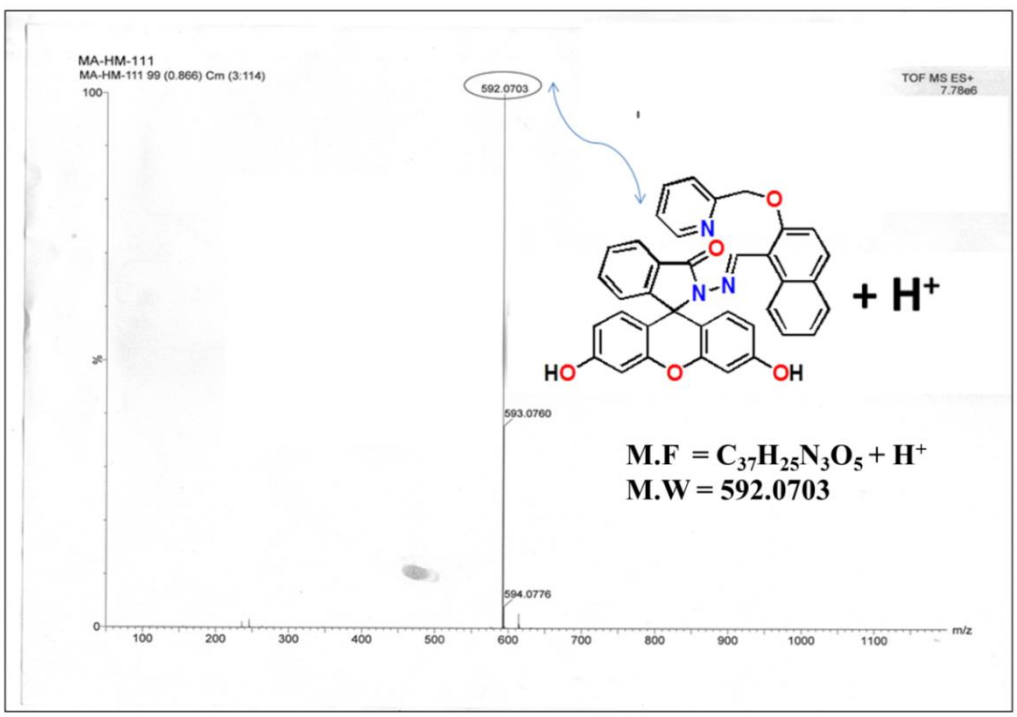

Figure 2.6. Mass spectrum of $\mathbf{L}^{28}$ in MeOH.

2.2.3.4 Preparation of complex L^{28}-Hg^{2+}

$Hg(ClO_4)_2$ (0.272 g, 0.6 mmol) was added to a 10 mL MeOH solution of **L^{28}** (0.295g, 0.5 mmol) and the mixture was stirred for about 30 minutes. It was then filtered and allowed to evaporate slowly at ambient temperature to get a crystalline solid product. ^{1}H-NMR (DMSO-d_6): δ = 9.78(s, 1 H), 8.68 (s, 1 H), 7.95 (m, 1 H), 7.93 (m, 1 H), 7.90 (m, 1 H), 7.81(m, 2 H), 7.78(m, 1 H), 7.62(m, 4 H), 7.42(m, 1 H), 7.35(m, 4 H), 7.28(m, 1H), 6.61(s, 1 H), 6.53(m, 2 H), 6.45(m, 2 H), 5.43(s, 2 H), ppm (**Figure 2.7**).^{13}C NMR (DMSO-d_6): δ =164.45, 161.16, 159.22, 155.51, 154.20, 152.21, 151.03, 150.87, 147.84, 147.08, 134.83, 133.48, 131.08, 129.79, 129.52, 128.94, 128.64, 128.22, 126.04, 124.92, 123.78, 118.10, 115.49, 114.84, 113.01, 112.57, 110.11, 103.36, 102.99, 79.58, 79.38, 69.16 (**Figure 2.8**). FTIR spectrum:- OH (3261 cm^{-1}), -C=N (1587 cm^{-1}), -C=O (1617 Cm^{-1}) (**Figure 2.9**). ESI-MS$^+$: *m*/*z*= 791.07 (**$C_{37}H_{24}N_3O_5$**) (**Figure 2.10**).

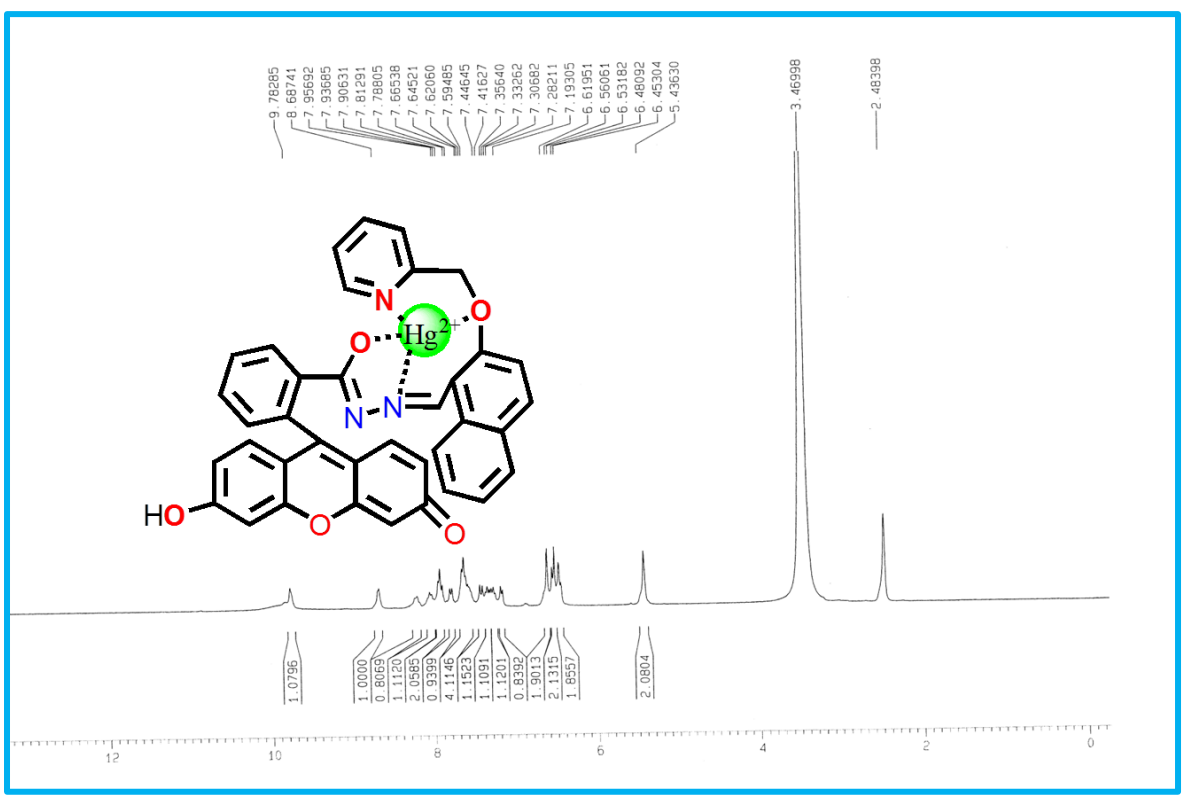

Figure 2.7. ^{1}H-NMR spectrum of L^{28}-Hg^{2+} Complex

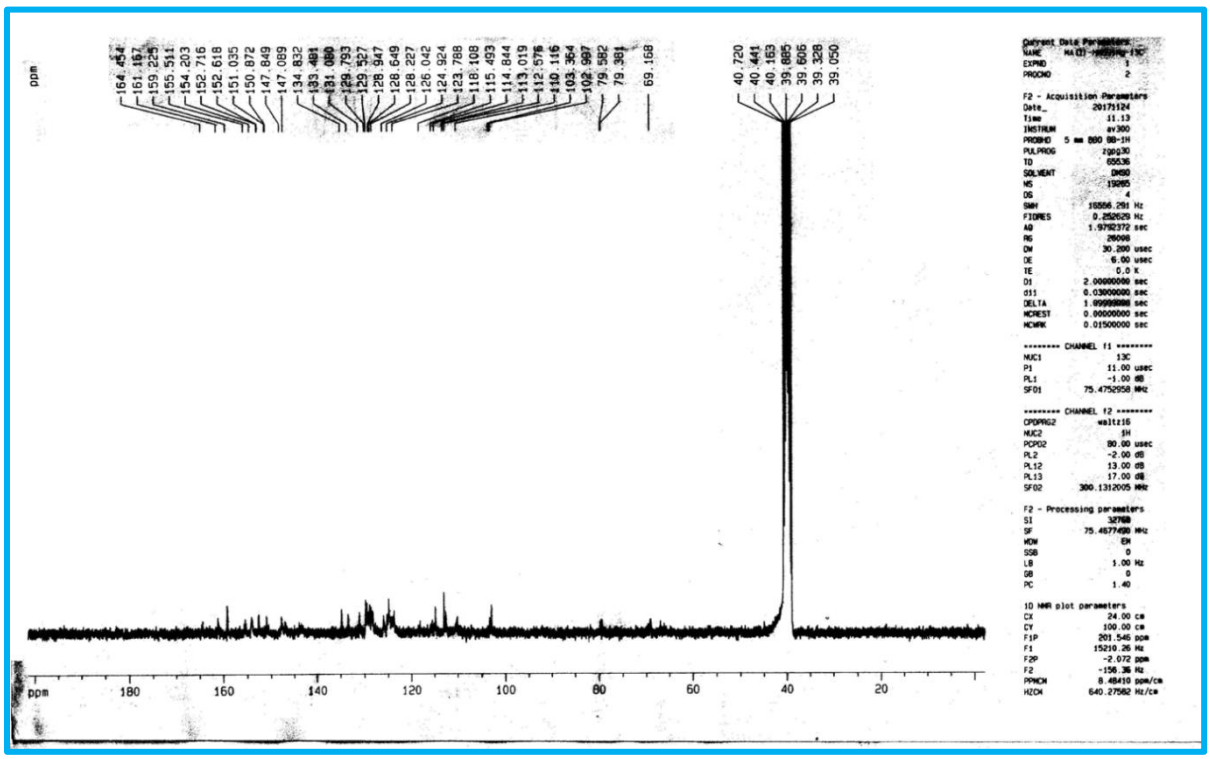

Figure 2.8. ^{13}C-NMR spectrum of L^{28}-Hg^{2+} Complex in DMSO-d_6.

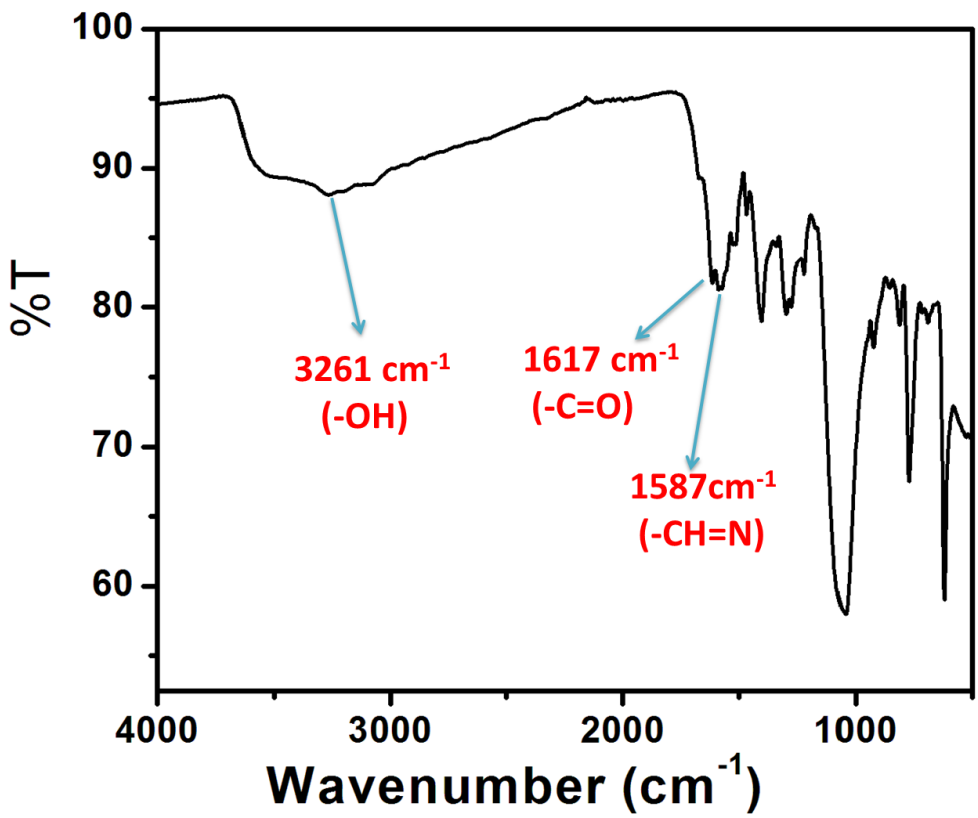

Figure 2.9. IR spectrum of L^{28}-Hg^{2+} complex.

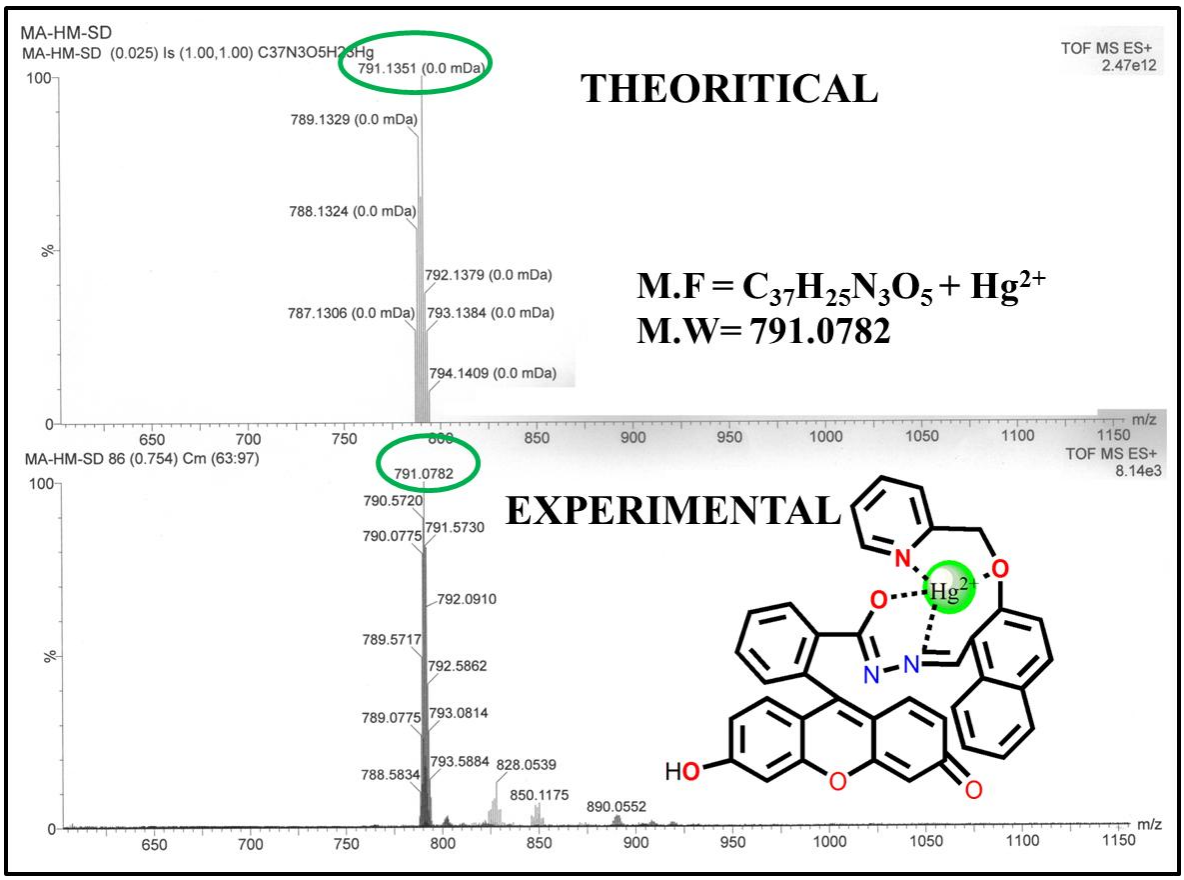

Figure 2.10. Mass spectrum of L^{28}-Hg^{2+} complex in MeOH.

2.2.4 Computational studies

To get better insights into geometry, electronic structure and optical properties, DFT study is an important tool. The calculation of the ground state electronic structure of both the legend and its Hg^{2+} complex has been performed using DFT[59] method associated with conductor like polarizable continuum model (CPCM).[60] For this study Becke's hybrid function[61] with the Lee-Yang-Parr (LYP) correlation function[62] was used. The ligand and complex were fully optimized without any symmetry constraints. In this work we choose 6-31G basis set for Ligand and LanL2DZ basis set for Hg atom for the optimization of the ground state. All the calculations were achieved with the Gaussian 09W software package.[63]

2.2.4 Cell Imaging Experiment and Cytotoxicity Studies

2.2.4.1 Cell culture

Human hepatocellular liver carcinoma (HepG2) cells (NCCS, Pune, India), were grown in DMEM supplemented with 10% FBS and antibiotics (penicillin-100 µg/mL; streptomycin-50 µg/ml). Cells were cultured at 37 ºC in 95% air, 5% CO_2 incubator.

2.2.4.2 Cell Cytotoxicity Assay

Cytotoxicity for $\mathbf{L^{28}}$ was evaluated with the help of 3-(4,5-dimethylthiazol-2-yl)-2,5-diphenyltetra-zolium bromide (MTT) cell viability assay. HepG2 cells (1×10^5 cells/well) were cultured in a 96-well plate and incubated at 37°C, and were exposed to varying concentrations of $\mathbf{L^{28}}$ (1, 5, 10, 20, 30, 40, 50, 60, 70, 80, 90 and 100 µM) for 24 h. After the incubation, 10 µL of MTT solution [5 mg/mL, dissolved in 1X phosphate-buffered saline (PBS)] was added to each well of a 96-well culture plate, and then the cells were incubated at 37 ^{0}C for 4 h. Media were decanted from wells and 100 µL of 0.04 N acidic isopropyl alcohol was added into each well to solubilize the intracellular formazan crystals (blue-violet) formed. Absorbance of the solution was measured at 595 nm wavelength (EMax Precision MicroPlate Reader, Molecular Devices, USA). Values were calculated as means ± standard errors of three independent experiments. The cell viability was expressed as the optical density ratio of the treatment to control.

2.2.4.3 Cell Imaging Study

HepG2 Cells were cultured in 35 x 10 mm culture dish on coverslip for 24 h at 37 ^{0}C. The cells were treated with 5 µM solutions of $\mathbf{L^{28}}$, prepared by dissolving $\mathbf{L^{28}}$ to the mixed solvent DMSO: water = 1:9 (v/v) and incubated for 1 h at 37 ^{0}C. For Hg^{2+} complex formation study, HepG2 cells were pre-incubated with varying concentrations of Hg^{2+} (5 µM, 10 µM and 20 µM) for 60 min at 37 ^{0}C followed by washing for three times with 1X PBS and then incubated with 5 µM of $\mathbf{L^{28}}$ for 60 min at 37^{0}C and washed with 1X PBS for two times. For quenching study, HepG2 cells were pre-incubated with 20 µM of Hg^{2+} for 60 min at 37 ^{0}C followed by washing for three times with 1X PBS and then incubated with 5µM of $\mathbf{L^{28}}$ for 60 min at 37 ^{0}C and then further incubated with 5µM of Na_2S, and subsequent washing for three times with 1X PBS. Fluorescence images of HepG2 cells were taken by a fluorescence microscope (Leica DM3000, Germany) with an objective lens of 40X magnification.

2.3 Results and Discussion

A simple reaction between fluorescein hydrazide (L^1) with 2-(Pyridin-2-ylmethoxy)-napthlene-1-carbaldehyde (L^2) in ethanol leads to the formation of **L^{28}** in quantitative yield (**Scheme 2.1**) which was thoroughly characterized by ^{1}H-NMR, ^{13}C-NMR, ESI-MS$^+$, and IR studies. The unique peak at δ = 65.96 ppm in the ^{13}C-NMR spectrum corresponding to **C4** **(Figure 2.4)** in **L^{28}** supports that the probe exists in solution predominantly in its fluorescence inactive spiro-lactam form.

2.3.1 UV-Vis recognition of Hg^{2+}

The spectrophotometric titration was performed to analyze the interaction of Hg^{2+} (0–70 μM) with **L^{28}** in 10 mM HEPES buffer at pH 7.2. The absorption titration of **L^{28}** as a function of Hg^{2+} concentration performed at room temperature. Upon addition of Hg^{2+} ion in the range 0-70 μM the absorption band at 370 nm is decreased rapidly and the absorption change occurred around 475 nm and the absorption becomes saturated at about 70 μM Hg^{2+} ion, keeping the concentration of **L^{28}** fixed at 20.0 μM and also performed the dilution effect study where we see that the two spectra almost same **(Figure 2.11)**. So, we can say that the absorption change of **L^{28}** is occurred due to dilution effect.

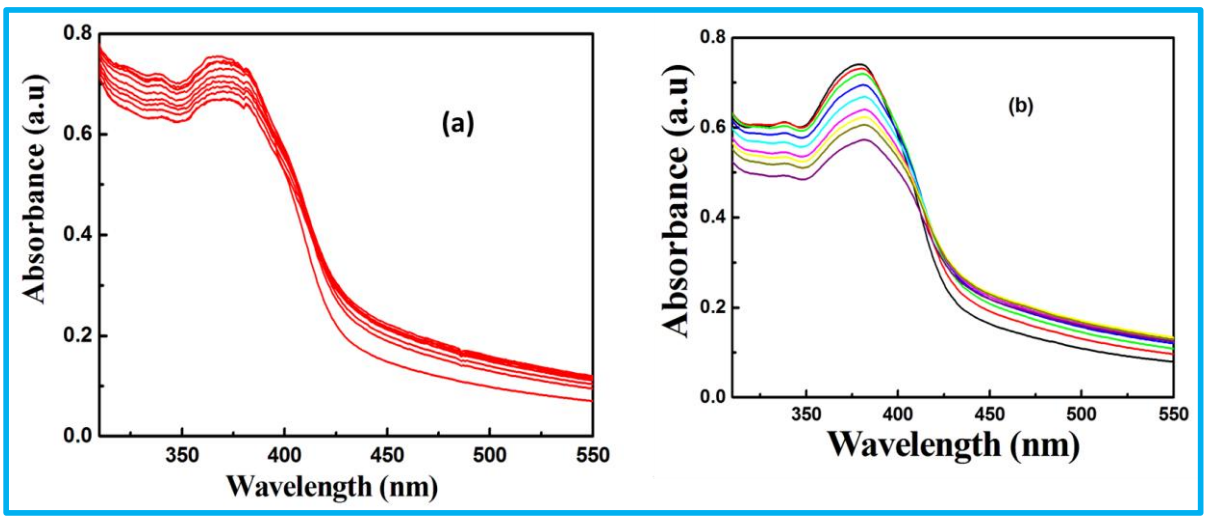

Figure 2.11. (a) Absorption titration of **L^{28}** with gradual addition of Hg^{2+} solution (b) Absorption titration of **L^{28}** with gradual addition of water.

2.3.2 Fluorescence recognition of Hg^{2+}

The emission spectra of **L^{28}** and fluorescence titration with Hg^{2+} were recorded in 10 mM HEPES buffer at pH 7.2. Free **L^{28}** displayed very weak-fluorescence, however, on gradual addition of Hg^{2+} (0-230 μM) to the aqueous solution of **L^{28}** (20.0 μM) a significant enhancement of the fluorescence intensity with a band centered at λ_{em} = 520 nm, on excitation at λ_{ex} = 475 nm was displayed (**Figure 2.12**). The specific response of **L^{28}** towards Hg^{2+} was supposed to be based on the opening of the spirolactam ring. Meanwhile, it may be because the reaction of Hg^{2+} with the chelating probe leads to a rigid complex L^{28}-Hg^{2+} and tends to attribute to a chelation enhanced fluorescence (CHEF).[64-66] These results demonstrate that **L^{28}** could serve as alluring "turn on'' chemosensor for detecting toxic Hg^{2+} ion. A plot of FI vs. [Hg^{2+}] gives a straight line up to 230 μM where nonlinear eqn. (1) [67] becomes y = a + b*c*x under the conditions 1 ≫ c*x with n = 1 and the linear dependence of such a plot gives a slope = b × c, where b = fluorescence maximum (F_{max}) and c = K_f = apparent formation constant. So, slope/F_{max} gives K_f =(0.43 ± 0.04) × 10^4 M^{-1}.

$$y = \frac{a+b\times c\times x^n}{1+c\times x^n} \qquad \text{(Eqn. 1)}$$

The mole fraction at 0.5 for Hg^{2+} in Job's plots (**Figure 2.13**) indicated 1:1 binding stoichiometry between **L^{28}** and Hg^{2+}. The bindings were further supported by mass spectrometry. The unique peak assigned at m/z 791.07 (calculated for L^{28}-Hg^{2+} = 791.13) corresponds 1:1 stoichiometry between probe and Hg^{2+} (**Figure 2.10**). Limit of detection (LOD) of Hg^{2+} was calculated by 3σ method and found to be 1.24 μM (**Figure 2.14**). The quantum yield of **L^{28}** (ϕ=0.0132) is enhanced upon binding with the Hg^{2+} ions (ϕ =0.1122) using fluorescein as a standard (0.5 in ethanol). Fluorescence quantum yields (Φ) were estimated by integrating the area under the fluorescence curves using the equation, eqn. (2)

$$\Phi_{sample} = (OD_{std} \times A_{sample})/(OD_{sample} \times A_{std}) \times \Phi_{std} \qquad \text{(Eqn. 2)}$$

Where Asample and Astd are the area under the fluorescence spectral curves and ODsample and ODstd are the optical densities of the sample and standard, respectively at the excitation wavelength. Fluorescein has been used as the standard with Φstd = 0.5 in ethanol for measuring the quantum yields of L^{28} and of L^{28}-Hg^{2+} complex.

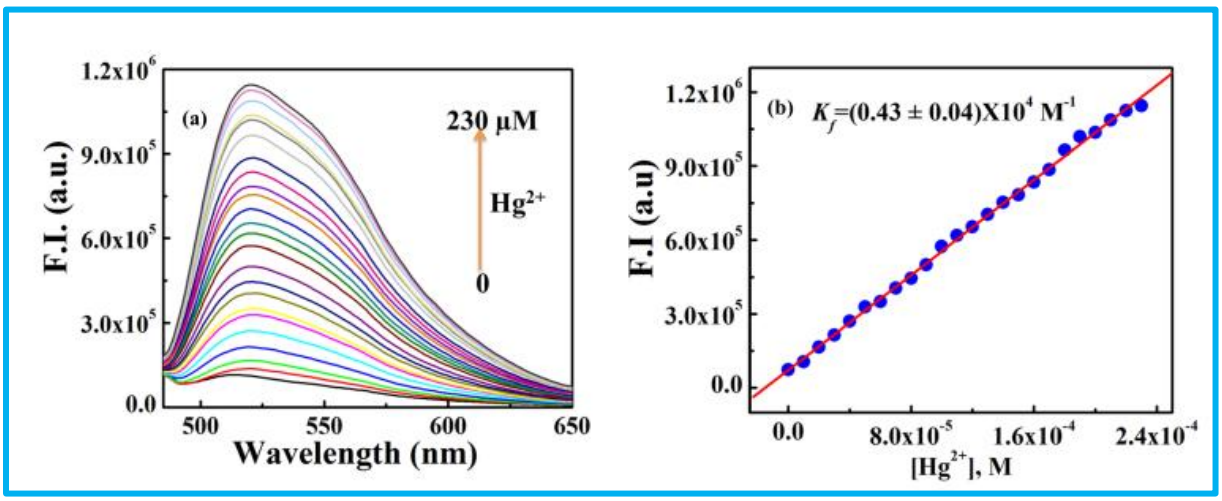

Figure 2.12. (a) Fluorescence titration of **L**[28] (20.0 μM) in 10mM HEPES buffer at pH 7.2 by the gradual addition of Hg^{2+} with λ_{ex} = 475 nm and λ_{em} = 520 nm. (b) linear fit plot of FI vs. [Hg^{2+}].

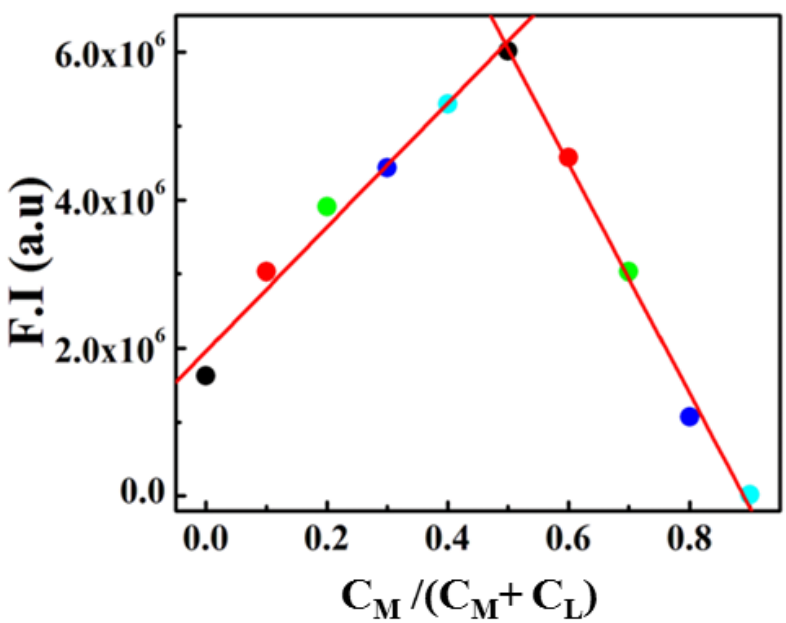

Figure 2.13. JOB's plot for Hg^{2+}.

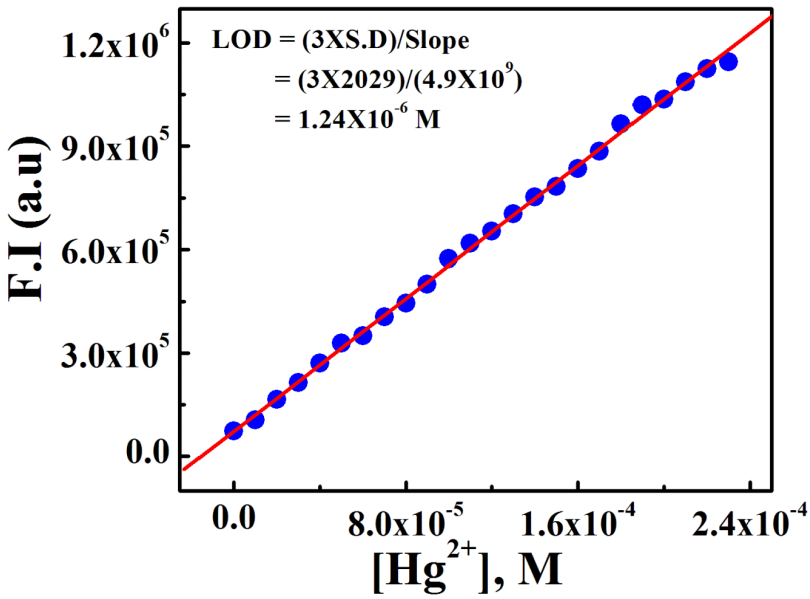

Figure 2.14. LOD of Hg^{2+}

2.3.3 Probable mechanism of recognition of Hg^{2+}

The plausible mechanism proposed for the formation of the L^{28}-Hg^{2+} complex by opening of the spiro-lactam ring was established through IR, ^{1}H and ^{13}C-NMR studies. The characteristic stretching frequency at 1610 cm^{-1} in the free $\mathbf{L^{28}}$ due to (-CH=N) is shifted significantly to 1587 cm^{-1}. This supports the participation of azomethine nitrogen of $\mathbf{L^{28}}$ in bonding with Hg^{2+}. The band at 1647 cm^{-1} can be assigned to the ν (-C=O) of cyclic spiro form of fluorescein. This peak moves to a lower frequency at 1617 cm^{-1} indicating the opening of spirolactam ringon coordination to Hg^{2+}. The cation recognition mechanism of the probe with Hg^{2+} was also substantiated by ^{1}H-NMR experiments. The ^{1}H-NMR titration was performed independently with $\mathbf{L^{28}}$ and L^{28}-Hg^{2+} in DMSO-d_6. Upon addition of Hg^{2+}, the imine proton (-CH=N) shifted downfield by δ = 0.18 ppm (8.68 to 8.50 ppm) signifying the coordination of azomethine-N to Hg^{2+}. The two separate phenolic proton signals (-OH) of $\mathbf{L^{28}}$ now appeared to be one and moved up-field from 9.9 ppm to 9.78 ppm. These results clearly demonstrate the spirolactam ring opening mechanism of the probe and one of the phenolic C–OH tautomerized to –C=O.[68] Also, the disappearance of the signal at δ = 65.96 ppm from the ^{13}C-NMR spectrum for the sp^3-hybridized tertiary carbon of the spiro-lactam ring of $\mathbf{L^{28}}$ (**labelled as 4, Figure 2.15**) upon addition of Hg^{2+} strongly supports the opening of the spiro-lactam ring and coordination through O atom.[69] Thus, based on ^{1}H-NMR, ^{13}C-NMR, IR, ESI-MS^{+} and Job's plot, we proposed a probable mechanism of binding of Hg^{2+} ions to $\mathbf{L^{28}}$ as shown in (**Scheme 2.2**).

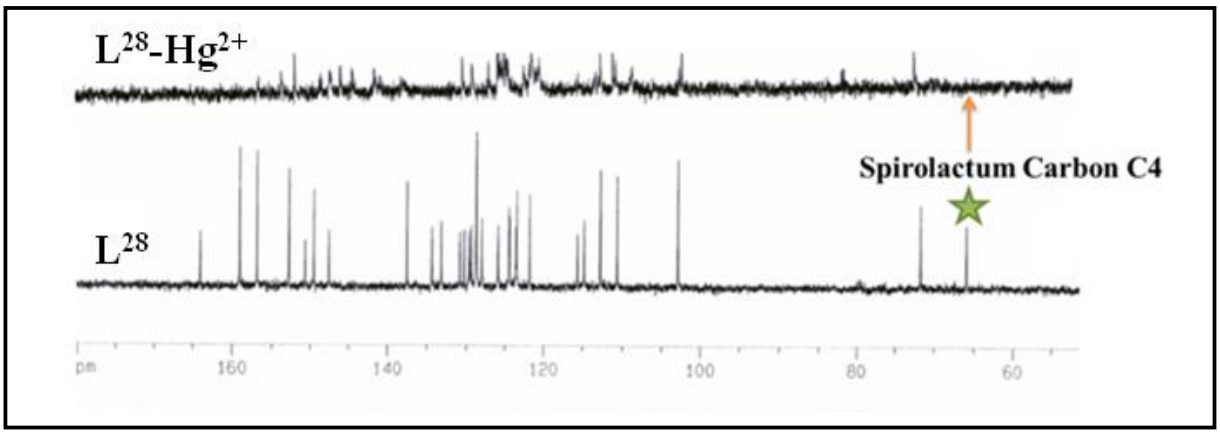

Figure 2.15. ^{13}C NMR spectra of **L^{28}** and **L^{28}-Hg^{2+}** in DMSO-d_6 recorded on a Bruker 500 MHz spectrometer.

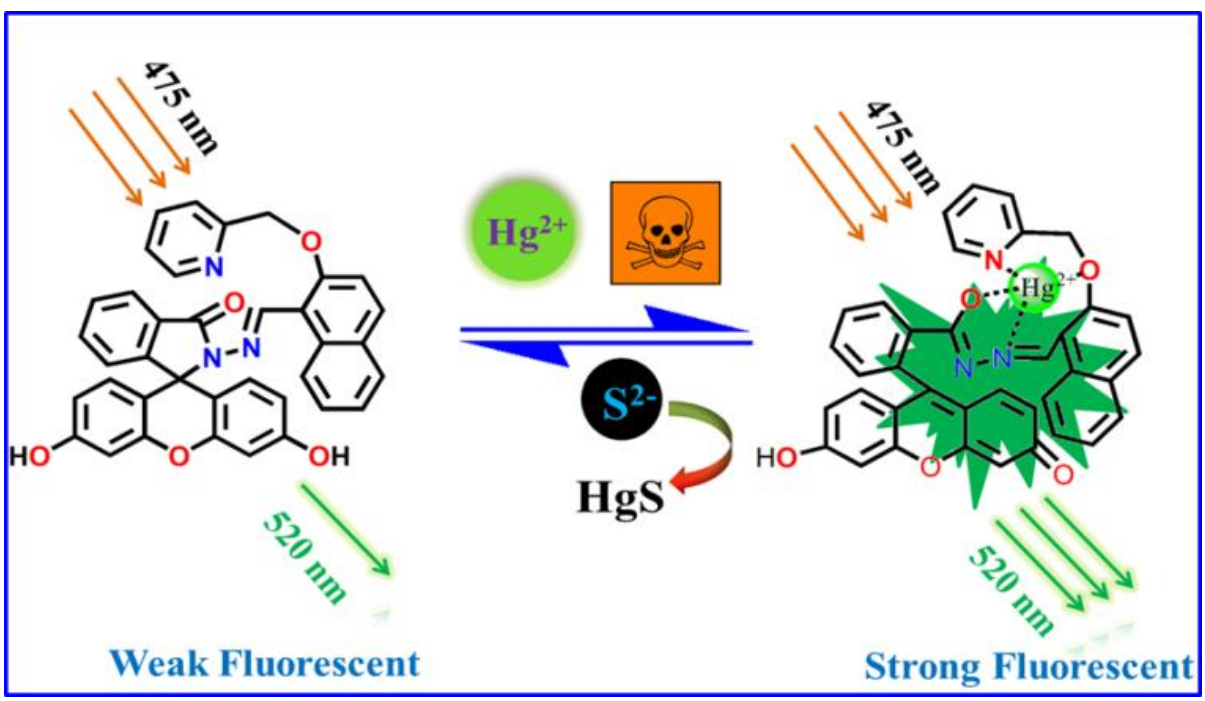

Scheme 2.2. Proposed mechanism for the recognition of Hg^{2+}.

2.3.4 Selectivity

Selectivity is one of the important parameters to scrutinize the practical applicability of a probe. Thus, competitive reactions of **L^{28}** (20 μM) towards Hg^{2+} ion in the presence of 10 equivalent of various cations like Zn^{2+}, Mg^{2+}, Co^{2+}, Ni^{2+}, Cu^{2+}, Pb^{2+}, Al^{3+}, Cr^{3+}, Cd^{2+}, Pd^{2+}, Fe^{2+} Fe^{3+}, Mn^{2+}, Na^{+}, K^{+}, Ca^{2+}, and Ag^{+} in 10 mM HEPES buffer were carried out. As shown in **Figure 2.16** and **Figure 2.17** the competitive cations did not reveal any noticeable

interference in the detection of Hg^{2+} ions. So, **L**[28] serves as a highly sensitive 'naked-eye sensor' for the selective detection of Hg^{2+} in aqueous buffer solution.

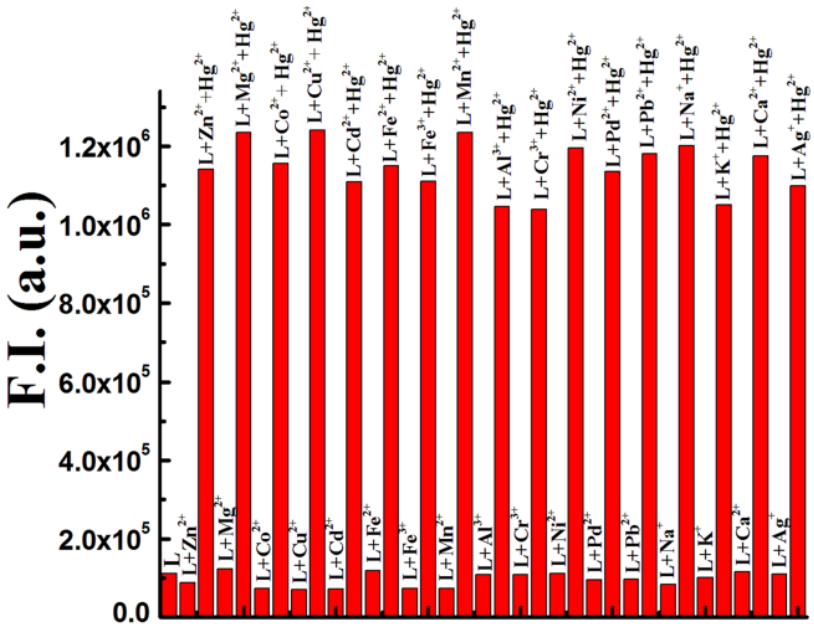

Figure 2.16. Competitive fluorescent responses of **L**[28] to diffent metal ions in 10 mM HEPES buffer at pH 7.2.

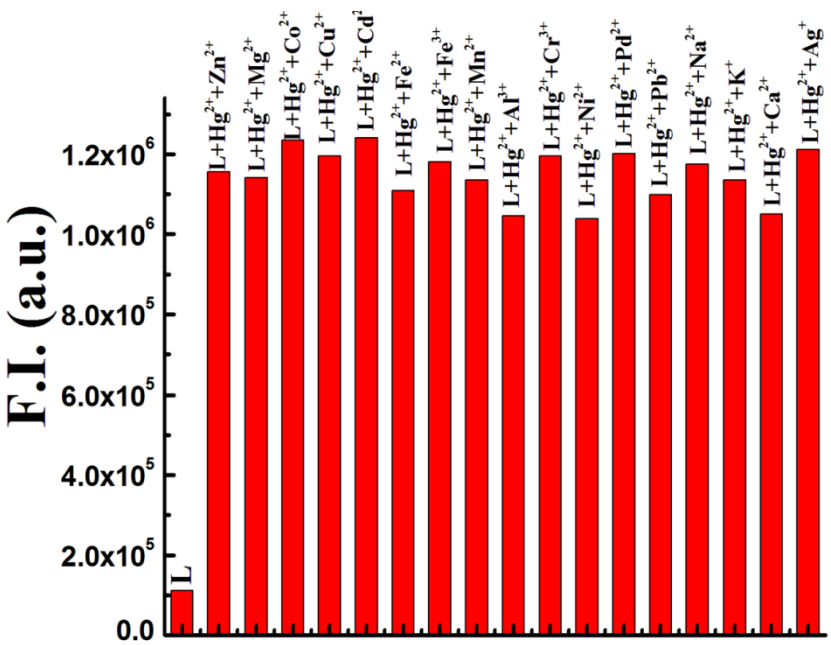

Figure 2.17. Selectivity study of Hg^{2+} in presence of different cations

2.3.5 Fluorescence spectral responses for S^{2-}

To observe the performance of the L^{28}-Hg^{2+}complex in anion sensing, the fluorescence changes of the complex were recorded in the presence of various anions. **Figure 2.18** displays the changes in the fluorescence emissions of L^{28}-Hg^{2+} upon the addition of 10 equivalent of a series of anions like SO_4^{2-}, $S_2O_4^{2-}$, SO_3^{2-}, $S_2O_3^{2-}$, PO_4^{3-}, S^{2-}, Cl^-, F^-, Br^-, I^-, $H_2PO_4^-$, CN^-, NO_2^-, CO_3^{2-}, ClO_4^- and N_3^-. It is very exciting to note that only S^{2-} causes a significant fluorescence quenching. This indicates that L^{28}-Hg^{2+} complex can selectively detect S^{2-}. Besides, the detection of S^{2-} was not perturbed by the presence of other sulphur species like SO_4^{2-}, $S_2O_4^{2-}$, SO_3^{2-}, $S_2O_3^{2-}$.

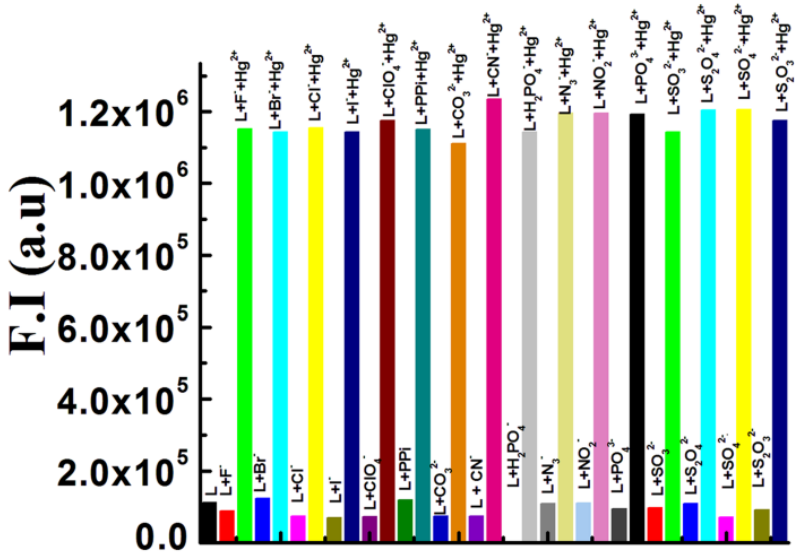

Figure 2.18. Competitive test for the fluorescent responses of **L^{28}** to various anions in 10 mM HEPES buffer at pH 7.2.

A competitive experiment was subsequently performed by adding S^{2-} to L^{28}-Hg^{2+} complex containing other anions (**Figure 2.18**). Before the addition of S^{2-}, there was an almost negligible fluorescence change at 520 nm in the presence of other unions. The fluorescence emission intensity at 520 nm disappeared completely upon addition of 210 µM of S^{2-} to the L^{28}-Hg^{2+} solution. This clearly demonstrates that any anions considered in this study did not interfere with the detection of S^{2-}. Thus L^{28}-Hg^{2+} complex displays high specificity for S^{2-}. A fluorescence titration was carried out to investigate the interaction between L^{28}-Hg^{2+} and S^{2-}. As shown in (**Figure 2.19**), the fluorescence intensity of L^{28}-Hg^{2+} gradually decreases as the concentration of S^{2-} was

increased. The Lod of S^{2-} was determined to be 2.35 µM **(Figure 2.20)**. The mass spectrum of L^{28}-Hg^{2+} complex in the presence of S^{2-} was compared with those of $\mathbf{L^{28}}$ and free L^{28}-Hg^{2+} complex to determine the interaction between L^{28}-Hg^{2+} and S^{2-}. In mass spectrum the peak at m/z = 592.06 corresponds to $\mathbf{L^{28} \approx C_{17}H_{13}NO_2 + H^+}$ (**Figure 2.6**) indicating the S^{2-} induced displacement of Hg^{2+} from L^{28}-Hg^{2+} complex. This is attributed to the stronger binding force between Hg^{2+} and S^{2-}. These results clearly demonstrate that L^{28}-Hg^{2+} complex could serve as secondary sensor for S^{2-} via displacement approach (**scheme 2.2**). This proves the reversibility between L^{28}-Hg^{2+} and S^{2-}.

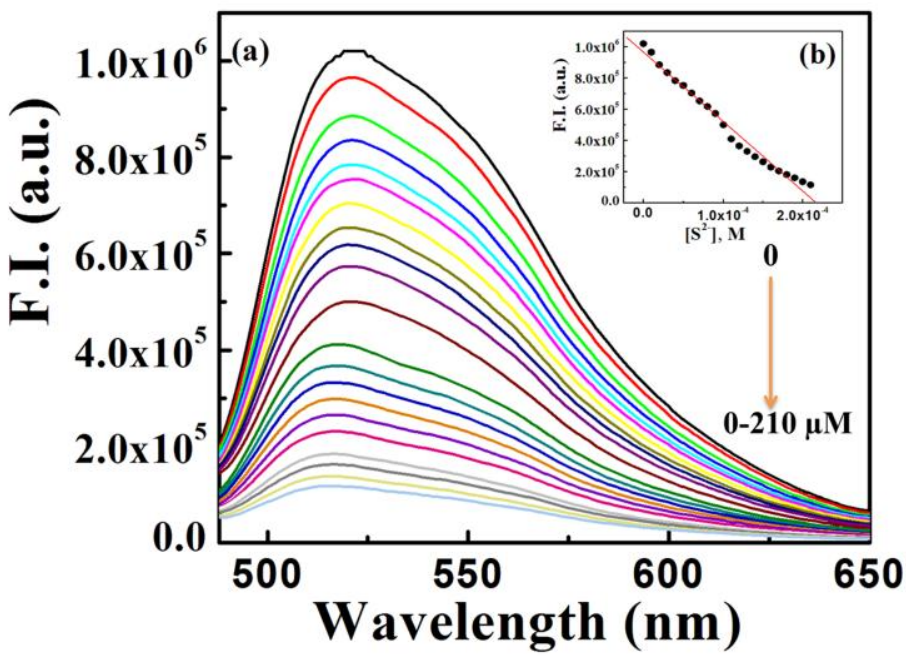

Figure 2.19. (a) Fluorescence titration of L^{28}-Hg^{2+} by adding S^{2-} in 10mM HEPES buffer at pH 7.2 (b) Fluorescence intensity at 520 nm was linearly related to the concentration of S^{2-}.

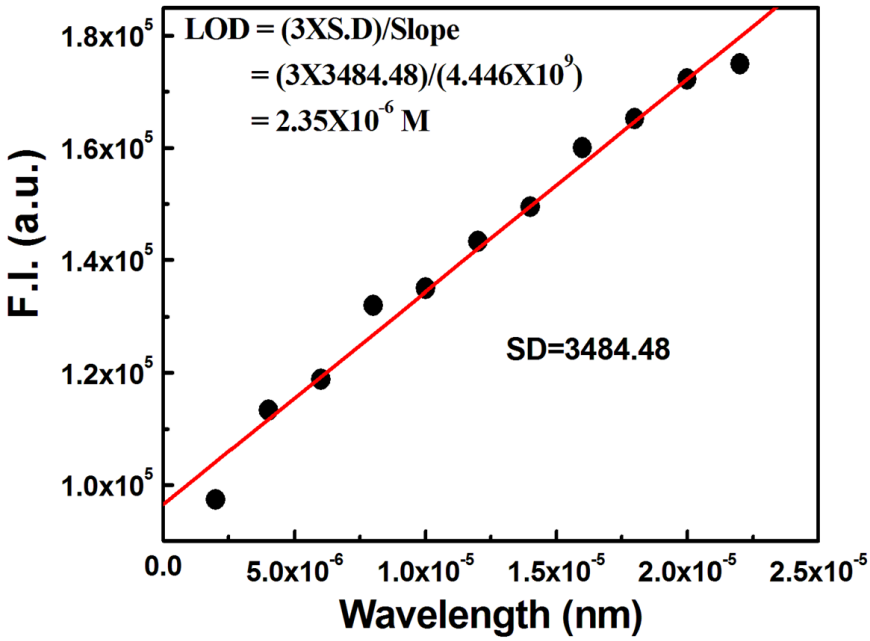

Figure 2.20. LOD of S^{2-}

2.3.6 Reversibility of L^{28} for sensing Hg^{2+}

The reversibility of the chemosensor is an essential aspect for sensory applications. We have carried out reversibility experiments by using Na_2S for Hg^{2+} in aqueous solution. Addition of 210 µM of S^{2-} into the solution containing 20 µM $\mathbf{L^{28}}$ and 230 µM Hg^{2+}, a notable decrease of the fluorescence emission intensity at 520 nm was observed (**Figure 2.21**). It can be attributed to the fact that S^{2-} anion has a strong affinity towards Hg^{2+} and their binding constants may be much higher than that towards $\mathbf{L^{28}}$. Thus, the addition of S^{2-} causes demetallation of Hg^{2+} from the L^{28}-Hg^{2+} complex, releasing free $\mathbf{L^{28}}$ with the re-establishment of spirolactam ring. With further addition of Hg^{2+} in slight excess (230 µM) the fluorescence intensity was revived again. This reversible process is repeated three times with a little loss of sensitivity. **(Figure 2.22)** This clearly demonstrates that $\mathbf{L^{28}}$ is a reversible sensor towards Hg^{2+} ions. This restoration capability indicates that $\mathbf{L^{28}}$ could be re-used with suitable management and L^{28}-Hg^{2+} could be used as a secondary sensor for S^{2-}.

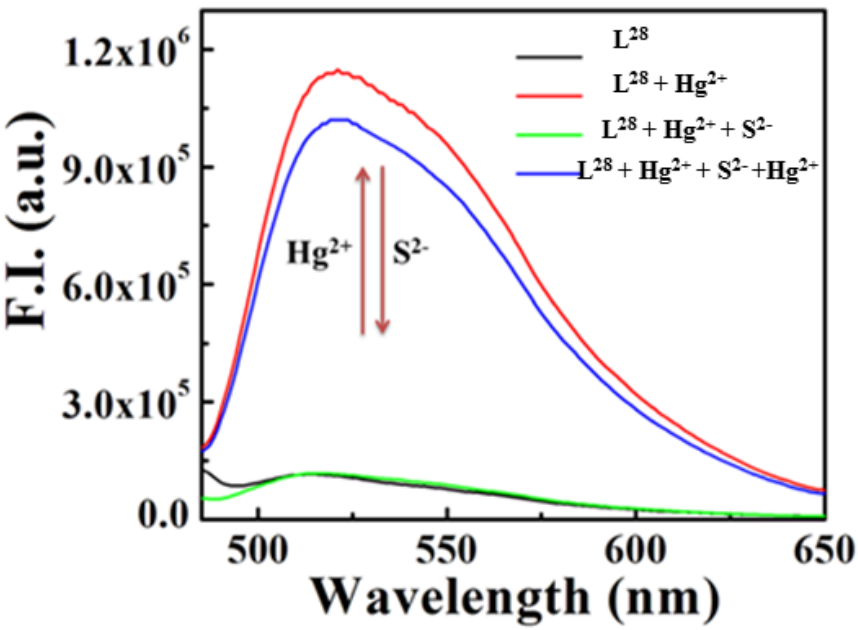

Figure 2.21. Reversibility of Hg^{2+}coordination to $\mathbf{L^{28}}$ by Na_2S. The black curve represents the fluorescence intensity of free $\mathbf{L^{28}}$; the red line represents the fluorescence enhancement after the addition of 230 µM Hg^{2+}, the green line represents the fluorescence decrease after the addition of 210 µM S^{2-} into the solution of L^{28}-Hg^{2+} species, the blue line represents the fluorescence enhancement again after the addition of 230 µM Hg^{2+} into the [(L^{28}-Hg^{2+})+ S^{2-}] solution.

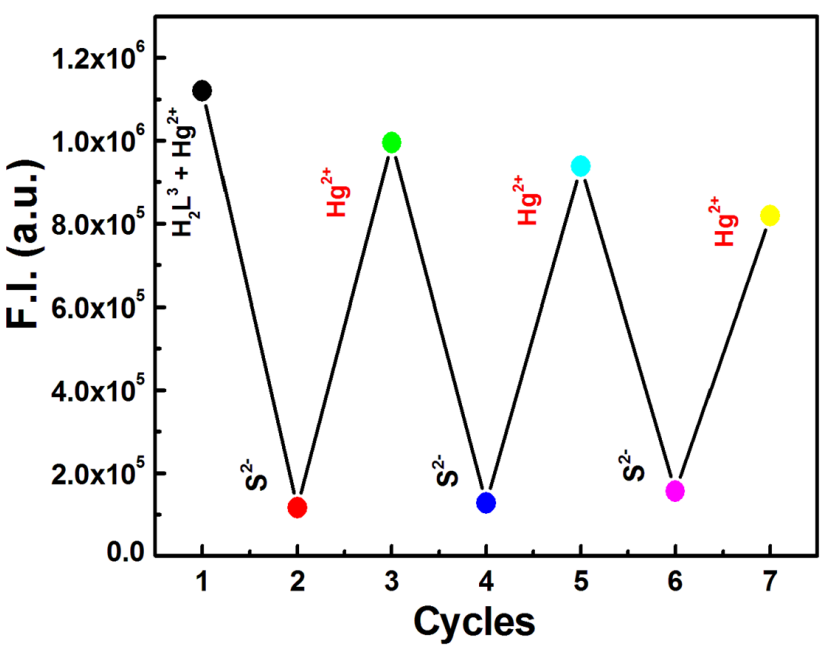

Figure 2.22. Cascade fluorescence ON-OFF-ON response of $\mathbf{L^{28}}$ with sequential addition of Hg^{2+} and S^{2-}.

2.3.7 pH Dependance

For the biological application, the dependence of fluorescence emission intensity of **L**^{28} and the pH of the reaction solution was investigated in details. As shown in **Figure 2.23**, the fluorescence intensity of **L**^{28} was almost no change in the pH range of 2.0-7.0. However, there is a slight enhancement in fluorescence intensity at pH>7.0. This can be attributed to the deprotonation of aromatic –OH group[70-73] at high pH. As demonstrated in (**Figure 2.23**) upon addition of 230 µM of Hg^{2+}, fluorescence intensity of **L**^{28} at 520 nm is significantly enhanced at pH = 6.0-9.0 which indicates that the Hg^{2+} ions induce the formation of the ring-opened L^{28}-Hg^{2+} complex. In the present work, 10 mM HEPES buffer solution at pH 7.2 was chosen for potential application throughout the experiment for the detection of Hg^{2+} ions.

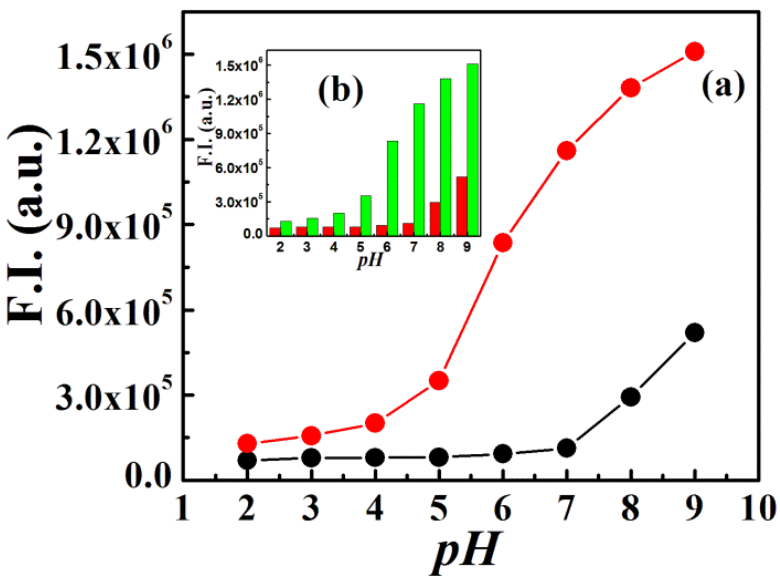

Figure 2.23. (a) Fluorescence intensity vs. pH plot at 520 nm with **L**^{28} (20 µM; denoted by black circles) and L^{28}-Hg^{2+} complex (denoted in red circles). (b) Corresponding histogram plot.

2.3.8 Geometry optimization and electronic structure

The ground state geometry optimization for **L^{28}** and L^{28}-Hg^{2+} complex was performed using (B3-LYP). The global minima of all these species are confirmed by the positive vibrational frequencies. Both **L^{28}** and L^{28}-Hg^{2+} complex have C1 point group. Main optimized geometrical parameters of the complex and ligand are listed in **Table 2.1 and 2.2** and the optimized structure of **L^{28}** and L^{28}-Hg^{2+} complex are given in (**Figure 2.24**).

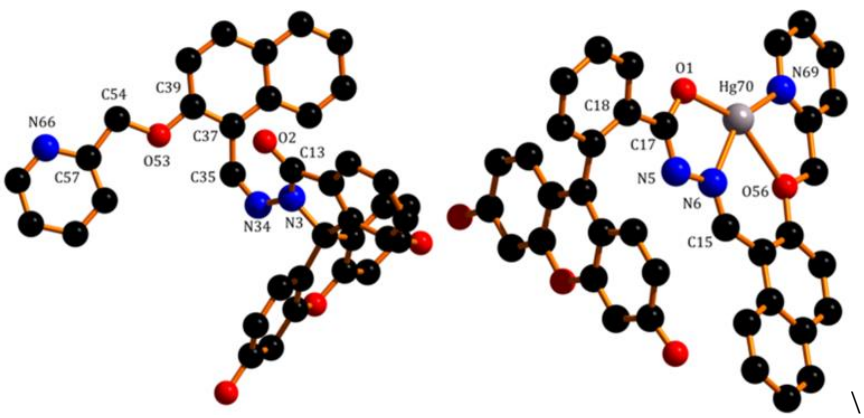

Figure 2.24. Optimized geometry of **L^{28}**and Complex L^{28}-Hg^{2+} under DFT calculation.

Table 2.1. Selected optimized geometrical parameters for **L^{28}** in the ground state calculated at B3LYP Levels.

Bond Distance (A˚)			
C13-C18	1.24404	N34-C35	1.29994
C13-N3	1.40307	C39-O53	1.39060
N3-N34	1.38507	C57-N66	1.35324
Bond Angle (˚)			
C54-O53-C39	120.266	N34-N3-C13	128.646
C37-C35-N34	133.768	N3-C13-O2	126.645
C35-N34-N3	123.773		

Table 2.2. Selected optimized geometrical parameters for complex in the ground state calculated at B3LYP Levels.

Bond Distance (A˚)			
C17-C18	1.49306	O1-Hg70	2.24728
C17-O1	1.33876	N6- Hg70	2.27472
C17-N5	1.40550	N6-C15	1.31663
O56- Hg70	2.53569	N69- Hg70	2.27861
Bond Angle (˚)			
N69- Hg70-O56	72.184	C17-N5-N6	115.635
O56- Hg70-N6	76.878	O1- Hg70-N69	136.108
N6- Hg70-O1	74.535	N5-N6-C15	113.987

The four co-ordinated metal center possesses a distorted tetrahedral geometry around the Hg^{2+} ion. All calculated Hg–O distances fall in the range 2.24-2.53 Å and Hg–N distance is 2.27 Å. In the case of **L**^{28} in the ground state, the electron densities at the HOMO and LUMO mainly reside on the 1-Iminomethyl-naphthalen-2-ol and (2-hydroxy-naphthalen-1-ylmethylene)-hydrazide moieties respectively. The energy difference between the HOMO and LUMO is 3.95 eV in **L**^{28}. In the case of L^{28}-Hg^{2+} the HOMO orbitals are mainly originates from ligand π and π^* orbital contribution while the LUMO orbital is mainly reside on the Pyridin-2-yl-methano moiety. The energy difference between HOMO and LUMO is 1.94 eV (**Figure 2.25**). From this study, it is clear that the energy gap between the highest occupied molecular orbital (HOMO) and the lowest unoccupied molecular orbital (LUMO) are 3.95 and 1.94 eV for the free ligand and its Hg^{2+} complex respectively. As a result, substantial change in fluorescence intensity is observed.

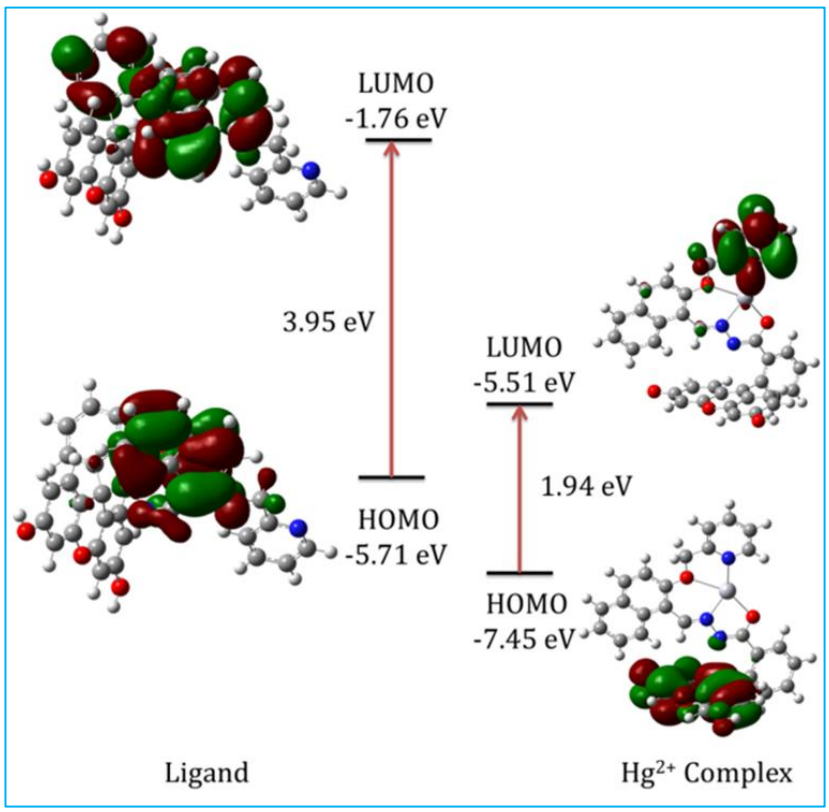

Figure 2.25. Frontier molecular orbital of **Hg^{2+}** complex as well as ligand optimized under DFT.

2.3.9 Design of logic gate

The molecular probe **L^{28}** displays logic gate operation with its spectroscopic properties. We consider the output by consecutive addition of Hg^{2+} and S^{2-} and monitoring their emission. The emission band maxima at 520 nm appeared due to the interaction of **L^{28}** with the analyte Hg^{2+} ion, selected as an output signal (**Figure 2.26.**). When Hg^{2+} is added to the **L^{28}** solution, the emission intensity at 520 nm again decreased. Thus with the two inputs of Hg^{2+} and S^{2-} the sensor **L^{28}** has the capability to exhibit an INHIBIT logic gate function which has been summarised in the truth table (**Figure 2.26d**). Only when Hg^{2+} is present, the output at 520 nm is 1, otherwise the output is 0.

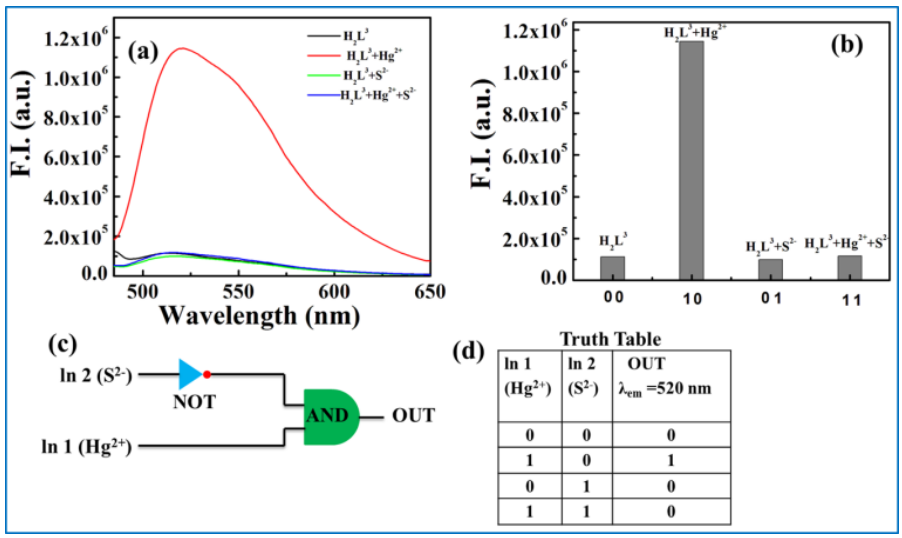

Figure 2.26. (a) Output signals (λ_{em} = 520 nm) of the logic gate in the presence of different inputs with corresponding gray diagram (b). (c) a general representation of an INHIBIT logic gate. (d) corresponding truth table of the logic gate.

2.3.9 Application in bioimaging

Taking into account the highly specific selective nature of **L**^{28} in the detection of **Hg**$^{2+}$ ions, it was further checked for its **Hg**$^{2+}$ sensing ability in living cells. To determine if **L**^{28} has cytotoxic effects, a cell viability assay using MTT was done throughcalculation of % cell viability on HepG2 cells (**Figure 2.27**). There was no significant reduction in the tetrazolium salt (reflected by a decrease in formazine production) for **L**^{28} up to 10 µM, thus suggesting that below 10 µM ligand concentration, **L**^{28} would be much more effective for the analysis of its complex formation with Hg^{2+} ions *in vitro*. A cell viability higher than90% was observed for **L**^{28} at 5 µM, after which the viability of the HepG2 cells decreased. Hence, further experiments were carried out with 5 µM of **L**^{28} for treatment.

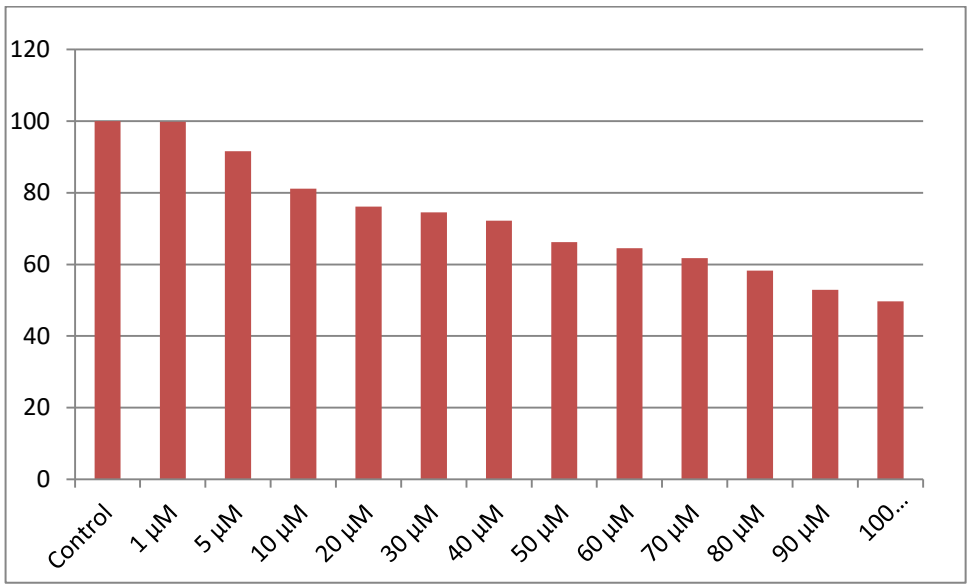

Figure 2.27. Percent (%) cell viability of HepG2 cells treated with different concentrations (1-100 µM) of $\mathbf{L^{28}}$ for 24 hours determined by MTT assay.

The probe $\mathbf{L^{28}}$ exhibited absence of intracellular fluorescence on HepG2 cells treated with 5 µM of the ligand and incubated for 1 h (**Figure 2.28**). However, prominent intracellular green fluorescence signal was observed when the HepG2 cells were incubated with 5 µM of Hg^{2+} for 60 min at 37^0C, followed by incubation with 5 µM of $\mathbf{L^{28}}$. The intracellular fluorescence was found to be prominently localized in the cytoplasmic region, suggesting that $\mathbf{L^{28}}$ specifically produces a complex with the Hg^{2+} ions transported to the cytoplasm. Keeping the ligand $\mathbf{L^{28}}$ concentration constant (5 µM)and increasing the concentration of Hg^{2+} (from 5 µM, 10 µM and 20 µM) displays Hg^{2+} ion concentration-dependent enhancement in the intracellular green fluorescence, caused by formation of complex with $\mathbf{L^{28}}$. Again, in the presence of 5 µM of Na_2S, the fluorescence signal diminished significantly, acting as a quencher for the ligand. Hence, the present ligand with low cytotoxicity and biocompatiblity for cellular cytoplasmic Hg^{2+} ionscan be utilized for Hg^{2+} ion detection in biological samples.

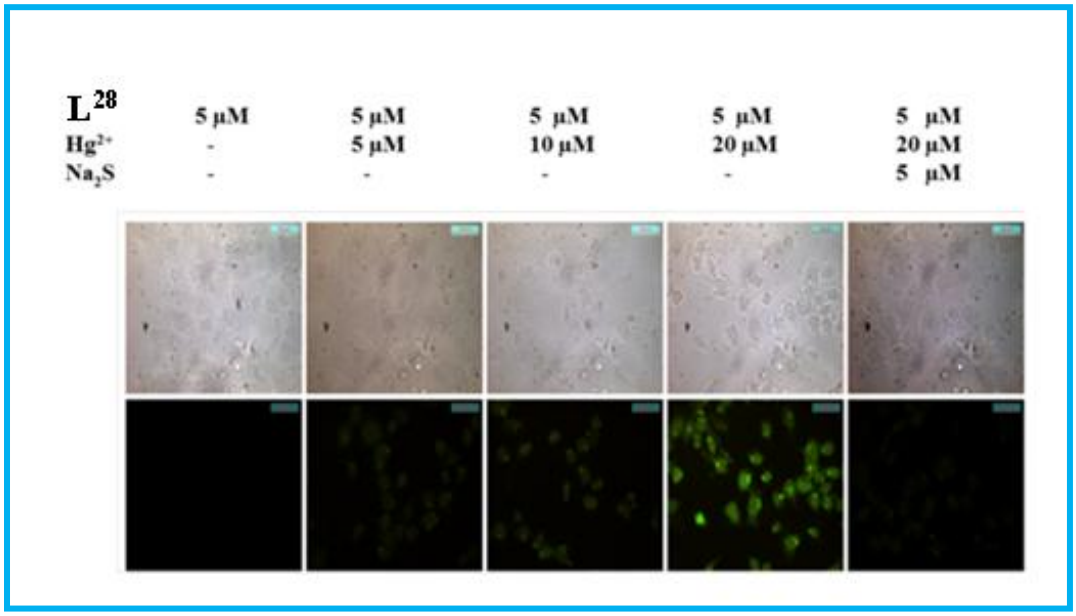

Figure 2.28. The fluorescence images of HepG2 cells were capture (40X) after incubation with 5µM of $\mathbf{L^{28}}$ for 60 min at 37 °C, followed by washing thrice with 1X PBS, and incubation with 5 µM, 10 µM and 20 µM of Hg^{2+} for 60 min at 37°C followed by incubation with 5µM of $\mathbf{L^{28}}$ for 60 min at 37 °C . The fluorescence images show no fluorescence signal by the fluorophore $\mathbf{L^{28}}$ (5 µM) in absence of Hg^{2+} ion, while the fluorescence gradually increases with higher concentration of Hg^{2+} ion; again, the fluorescence emission reduced significantly in presence of 5 µM of Na_2S, acting as a quencher.

2.4 Conclusion

In summary, We have successfully designed and prepared a new fluorescein-based sensor ($\mathbf{L^{28}}$) with potential N_2O_2 donor atoms, which was found to act as fluorogenic sensor for selective recognition of Hg^{2+} (emission at 520 nm) in semi aqueous medium at pH 7.2 (10 mM HEPES buffer) and 25 ^{0}C. The probe has been thoroughly characterized by ^{1}H and ^{13}C NMR, IR, ESI-MS spectroscopy. The fluorescence enhancement was explored due to the configuration transformation of the fluorescein from a spirolactam ring form to the ring-opened amide form on binding with Hg^{2+} in a 1:1 mole ratio which was established by Job's method and ESI-MS+ (m/z) studies. The corresponding LOD was evaluated by the 3σ method and found to be 1.24 µM. The sensor demonstrates a reversible change in fluorescence upon the successive additions

of Hg^{2+} and S^{2-} in **L**[28] solution with negligible interference from other anions. Moreover, it can be applied for the successful fabrication of molecular 'INHIBIT' logic gates. This work would offer a reference for the development of sensors with sequential recognition of Hg^{2+} and S^{2-}. **Table 2.3** has been prepared for quick highlight of few aspects of some recently published chemosensors for the Hg^{2+} ion e.g working medium, biological study, reversibility and quantum yield .[74–83] Most of the studies were not performed biological study and logic gate operation with few exceptions,[75,76,78] Also most of the studies were done organic or mixed organo-aqueous medium.

Table 2.3. Comparison of few aspects of some recently published fluorescent chemosensors for Hg^{2+} ion.

Probe		Working System	Biological Study	Reversibility	Logic Gate	Quantum Yield	Ref
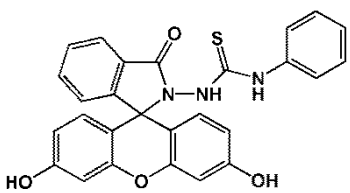	Turn On	Methanol–water (30/70, v/v)	-	-	-	-	74
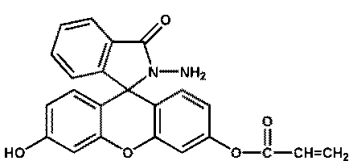	Turn On	Aqueous	Done	-	-	-	75
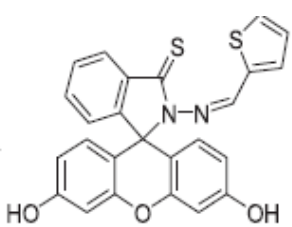	Turn Off	EtOH/HEPES (1:1, v/v,)	Done	Done	-	-	76

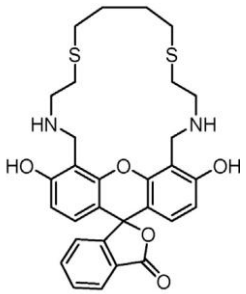	Turn Off	95:5 Tris–HCl buffer:MeOH	-	-	-	0.56	77
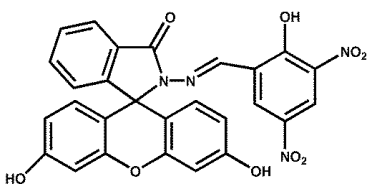	Turn On	aqueous HEPES buffer: MeOH (8 : 2 v/v)	-	Done	Done	0.095	78
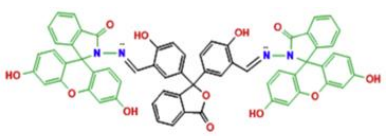	Turn On	EtOH-H_2O (v/v, 8/2).	-	Done	-	0.258	79
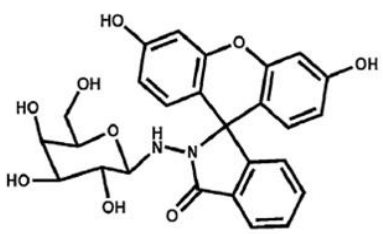	Turn On	H_2O:CH_3CN (70:30,v/v)	-	-	-	-	80
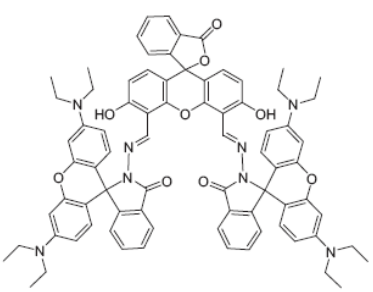	Turn On	DCM	-	Done	-	0.19	81

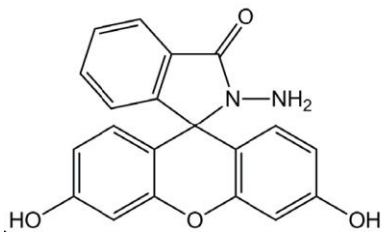	Turn On	Ethanol /HEPES (v/v = 1:1)	-	-	-	-	82
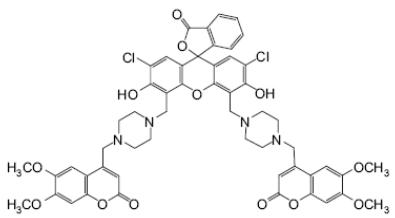	Turn On	aqueous 1% DMSO	-	-	-	-	83
 L^{28}	Turn On	Semi aqueous	Done	Done	Done	0.1122	

References

1 P. M. Bolger and B. A. Schwetz, *N. Engl. J. Med.*, 2002, **347,** 1735-1736.

2 H. H. Harris, I. J. Pickering and G. N. George, *Science*, 2003, **301,** 1203.

3 T. W. Clarkson, L. Magos and G. J. Myers, *N. Engl. J. Med.*, 2003, **349,** 1731-1737.

4 A. Renzoni, F. Zino and E. Franchi, *Environ. Res.*, 1998, **77,** 68-72.

5 D. B. Gil, M. I. Rodriguez-Cáceres, M. del C. HurtadoSánchez and A. M. de la Pena, *Appl. Spectrosc.*, 2010, **64**, 520-527.

6 O. Malm, *Environ. Res.*, 1998, **77,** 73-78.

7 E. M. Nolan and S. J. Lippard, *J. Am. Chem. Soc.*, 2007, **129** 5910-5918.

8 W. F. Fitzgerald, C. H. Lamborg and C. R. Hammerschmidt, *Chem. Rev.*, 2007, **107**, 641-662.

9 Z. C. Zhang, D. Wu, X. F. Guo, X. H. Qian, Z. Lu and Q. Xu, *Chem. Res. Toxicol.*, 2005, **18,** 1814-1820.

10 D. W. Boening, *Chemosphere*, 2000, **40,** 1335-1351.

11 J. Gutknecht, *J. Membr. Biol.* 1981, **61**, 61-66.

12 M. Harada, *Crit. Rev. Toxicol.*, 1995, **25**, 1-24.

13 P. B. Tchounwou, W. K. Ayensu, N. Ninashvili and D. Sutton, *Environ. Toxicol.*, 2003, **18,** 149-175.

14 USEPA, Regulatory Impact Analysis of the Clean Air Mercury Rule Final Report. PA-452/R-05-003, Research Triangle Park, NC, 2005.

15 J. G. Chen, H. W. Chen, X. Z. Jin and H. T. Chen, *Talanta*, 2009, **77,** 1381-1387.

16 L. Ling, Y. Zhao, J. Du and D. Xiao, *Talanta*, 2012, **91,** 65-71.

17 X. Fu, X. Chen, Z. Guo, C. Xie, L. Kong, J. Liu and X. Huang, *Anal. Chim. Acta*, 2011, **685,** 21-28.

18 F. Wang, X. Wei, C.Wang, S. Zhang and B. Ye, *Talanta*, 2010, **80,** 1198-1204.

19 W. Huang, D. Wu, G. Wu and Z. Wang, Dalton Trans., 2012, 41, 2620.

20 S. Jayabal, R. Sathiyamurthi and R. Ramaraj *J. Mater. Chem. A*, 2014, **2,** 8918.

21 A. Panja and K. Ghosh, Supramolecular Chemistry, 2018, **8,** 722–729.

22 S. Xu, L. Chen, J. Li, Y. Guan and H. Lu, *J. Hazard. Mater.*, 2012, **237,** 347– 354.

23 D. T. Quang and J. S. Kim, *Chem. Rev.*, 2010, **110,** 6280-6301.

24 V. K. Gupta, A. K. Jain, G. Maheshwari, Heinrich Lang and Z. Ishtaiwi, *Sens. Actuators B:Chem.*, 2006, **117,** 99-106.

25 V. K. Gupta, A. K. Jain and P. Kumar, *Sens.Actuators B: Chem.*, 2006, **120,** 259-266.

26 H. Zheng, X. Q. Zhan, Q. N. Bian and X. J. Zhang, *Chem. Commun.*, 2013, **49,** 429-447.

27 A. K. Jain, V. K. Gupta, L. P. Singh and J. R. Raisoni, *Electrochim. Acta*, 2006, **51,** 2547-2553.

28 V. K. Gupta, L. P. Singh, R. Singh, N. Upadhyay, S.P. Kaur and B. Sethi, J. *Mol. Liq.*, 2012, **174,** 11-16.

29 J. H. Song, M. X. Huai, C. C. Wang, Z. H. Xu, Y. F. Zhao and Y. Ye, *Spectrochim. Acta A*, 2015, **139,** 549-554.

30 S. K. Srivastava, V. K. Gupta and S. Jain, *Analyst*, 1995, **120,** 495-498.

31 V. K. Gupta, A. K. Jain, S. Agarwal and G. Maheshwari, *Talanta*, 2007, **71,** 1964-1968.

32 Z. Xu, C. Zhang, X. Zheng, Z. Li and S. Xu, *Optik*, 2018, 175 , 54–62.

33 G. Gangatharan V. Kumar, M. P. Kesavan, A. Tamilselvi, G. Rajagopal, J. D. Raja, K. Sakthipandi, J. P. Rajesh and G. Sivaraman *Sens. Actuators B:Chem.*, 2018, **273,** 305–315.

34 K. Tomar, G. Kaur, S. Verma and G. Ramanathan *Tetrahedron Lett.*, 2018, **59,** 3653–3656.

35 A. Han, X. Liu, G. D. Prestwich and L. Zang, *Sens. Actuators B:Chem.*, 2014, **198,** 274–277.

36 A. A. Soares-Paulino, L. Giroldoa, G. Celantea, C. Lodeiro and A. A. Dos Santosa, *Dyes Pigm.*, 2018, **159,** 121–127.

37 A. Sikdar, S. Roy, S. Dasgupta, S. Mukherjee and S. S. Panja *Sens. Actuators B:Chem.*, 2018, **263,** 298–311.

38 Q. Lin, X. M. Jiang, X. Q. Ma, J. Liu, H. Yao, Y. M. Zhang and T. B. Wei, *Sens. Actuators B:Chem.*, 2018, **272,** 139–145.

39 F. Ge, H. Ye, H. Zhang and B. X. Zhao, *Dyes Pigm.*, 2013, **99,** 661-665.

40 Y. Zhou, X. Y. You, Y. Fang, J. Y. Li, K. Liu and C. Yao, *Org. Biomol. Chem.*, 2010, **8,** 4819-4822.

41 J. K. Ni, B. Li, L.M. Zhang, H. F. Zhao and H. Jiang, *Sens. Actuators B: Chem*, 2015, **215**, 174-180.

42 Y. Jiao, L. Zhang and P. Zhou, *Talanta*, 2016, **15,** 14-19.

43 T. Mistri, R. Alam, M. Dolai, S.K. Mandal, P. Guha, A.R. Khuda-Bukhsh and Mahammad Ali, *Eur. J. Inorg. Chem.*, 2013, 5854-5861.

44 K. Bera, A. K. Das, M. Nag, and S. Basak, *Anal. Chem.*, 2014, 86, 2740-2746.

45 A. Sikdar, S. Roy, S. Dasgupta, S. Mukherjee and S.S. Panja, *Sens. Actuators B: Chem*, 2018, **263**, 298-311.

46 S. Lee, B. A. Rao and Y. A. Son, *Sens. Actuators B: Chem*, 2014, **196,** 388-397.

47 H. Ding, C. Zheng, B. Li, G. Liu, S. Pu, D. Jia and Y. Zhou, *RSC Adv.*, 2016, **6,** 80723-80728.

48 M. Wang, F. Y. Yan, Y. Zou, N. Yang, L. Chen and L. G. Chen, *Spectrochimica Acta Part A: Molecular and Biomolecular Spectroscopy*, 2014, **123**, 216-223.

49 Y. Jiao, L. Zhang and P. Zhou, *Talanta*, 2016, **150,** 14-19.

50 M. M. Hong, A. F. Liu, Y. Xu and D. M. Xu, *Chin. Chem. Lett.*, 2016, **27,** 989-992.

51 A. Sikdar, S. Roy, K. Haldar, S. Sarkar and S. S. Panja, *J. Fluoresc.*, 2013, **23**, 495-501.

52 S. Erdemir, O. Kocyigit and S. Malkondu, *J. Photochem. Photobiol. A: Chem.*, 2015, **309,** 15-21.

53 H. J. Kim, J. E. Park, M. G. Choi, S. Ahn and S. K. Chang, *Dyes Pigm.*, 2010, **84,** 54-58.

54 X. F. Yang, Y. Li and Q. Bai, *Anal. Chim. Acta*, 2007, **584,** 95-100.

55 Y. Feng, Z. Kuaib, Y. Song, J. Guo, Q. Yanga, Y. Shanb and Y. Li, *Talanta*, 2017, **170,** 103-110.

56 P. Piyanuch, S. Watpathomsuba, V. S. Lee, H. A. Nienaberc and N. Wanichacheva, *Sens. Actuators B: Chem*, 2016,**224,** 201-208.

57 X. F. Yang, Y. Li and Q. Bai, *Anal. Chim. Acta*, 2007, **584,** 95-100.

58 X. Bao, Q. Cao, X. Wu, H. Shu , B. Zhou , Y. Geng and J. Zhu, *Tetrahedron Lett.*, 2016, **57,** 942-948.

59 R. G. Parr, W. Yang, Density Functional Theory of Atoms and Molecules, Oxford University Press, Oxford, 1989.

60 M. Cossi, N. Rega, G. Scalmani and V. Barone, *J. Comp. Chem.*, 2003, **24,** 669-681.

61 A. D. Becke, Density-functional thermochemistry. III. The role of exact exchange, *J. Chem. Phys.*, 1993, **98,** 5648-5652.

62 C. Lee, W. Yang and R. G. Parr, *Phys. Rev. B* , 1998, **37,** 785-789.

63 M. J. Frisch, G. W. Trucks, H. B. Schlegel, G. E. Scuseria, M. A. Robb, J. R. Cheeseman, G. Scalmani, V. Barone, B. Mennucci, G. A. Petersson, H. Nakatsuji, M. Caricato, X. Li, H.P. Hratchian, A.F. Izmaylov, J. Bloino, G. Zheng, J.L. Sonnenberg, M. Hada, M. Ehara, K. Toyota, R. Fukuda, J. Hasegawa, M. Ishida, T. Nakajima, Y. Honda, O. Kitao, H. Nakai, T. Vreven, J.A. Montgomery Jr., J.E.

Peralta, F. Ogliaro, M. Bearpark, J.J. Heyd, E. Brothers, K.N. Kudin, V.N. Staroverov, R. Kobayashi, J. Normand, K. Raghavachari, A. Rendell, J. C. Burant, S.S. Iyengar, J. Tomasi, M. Cossi, N. Rega, J. M. Millam, M. Klene, J. E. Knox, J. B. Cross, V. Bakken, C. Adamo, J. Jaramillo, R. Gomperts, R.E. Stratmann, O. Yazyev, A.J. Austin, R. Cammi, C. Pomelli, J.W. Ochterski, R.L. Martin, K. Morokuma, V.G. Zakrzewski, G.A. Voth, P. Salvador, J.J. Dannenberg, S. Dapprich, A.D. Daniels, Ö. Farkas, J.B. Foresman, J.V. Ortiz, J. Cioslowski and D.J. Fox, Gaussian 09, (Revision A.1), Gaussian, Inc., Wallingford, CT, 2009.

64 E. M. Nolan and S. J. Lippard, *Chem. Rev.*, 2008, **108,** 3443-3480.

65 A. Tamayo, B. Pedras, C. Lodeiro, L. Escriche, J. Casabo, L. Capelo, B. Covelo, R. Kiveka and R. Sillanpa, *Inorg.Chem.*, 2007, **46,** 7818-7826.

66 Y. Zhang, Y. Yang, J. Hao, C. Yin, F. Huo, J. Chao and D. Liu, *Spectrochim. Acta A*, 2014, **132,** 27-31.

67 C. R. Lohani, J. M. Kim, S. Y. Chung, J. Yoon and K. H. Lee**,** *Analyst*, 2010, **135,** 2079-2084.

68 Y. Gao, H. Liu, Q. Liu and W. Wang, *Tetrahedron Lett.*, 2016, 57, 1852-1855.

69 D. Wang, X. Xiang, X. Yang, X. Wang, Y. Guo, W. Liu and W. Qin, *Sens. Actuators B: Chem*, 2014, **201,** 246-254.

70 V. R. Batistela, J. D. C. Cedran, H. P. M. D. Oliveira, I. S. Scarminio, L. T. Ueno, A. E. D. H. Machado and N. Hioka, *Dyes Pigm.*, 2010, **86,** 15-24.

71 L. N. Bogdanova, N. O. Mchedlov-Petrossyan, N. A. Vodolazkaya, A. V. Lebed, The influence of -cyclodextrin on acid–base and tautomeric equilibrium offluorescein dyes in aqueous solution, *Carbohydr. Res.*, 2010, **345,**

72 N .O. Mchedlov-Petrossyana, O. N. Tychina, T. A. Berezhnaya, V. I. Alekseeva,

73 L. P.Savvina, *Dyes Pigm.*, 1999, **43,** 33-46.R. Sjoback, J. Nygren and M. Kubista, *Spectrochim. Acta A*, 1995, **51,** 7-21.

74 X. F. Yang, Y. Lia and Q. Bai, *Anal. Chim. Acta*, 2007, **584,** 95–100.

75 S. Guanga, J. Tiana, G. Weia, Z. Yanc, H. Pand, J. Fengd and H. Xub, *Talanta*, 2017, **170,** 89–96.

76 Y. Fenga, Z. Kuaib, Y. Songa, J. Guoa, Q. Yanga, Y. Shanb and Y. Li, *Talanta*, 2017, **170,** 103–110.

77 P. Piyanucha, S. Watpathomsuba, V. S. Leeb, H. A. Nienaberc and N. Wanichacheva, *Sens. Actuators B:Chem.*, 2016, **224,** 201–208.

78 K. Tripathi, A. Rai, A. Kumar Yadav, S. Srikrishna, N. Kumari and L. Mishra, *RSC Adv.*, 2017, **7,** 2264.

79 S. Erdemir and O. Kocyigit, *Dyes Pigm.*, 2017, **145**, 72-79.

80 U. Diwan, A. Kumar, V. Kumara, K.K. Upadhyay and P.K. Roychowdhury, *Sens. Actuators B:Chem.*, 2014, 1963, 45–351.

81 N. Wanichacheva, O. Hanmeng, S. Kraithonga, and K. Sukrat, *J. Photochem. Photobiol.*, 2014, **278**, 75– 81.

82 Z. Xie, F. Huo, J. Su, Y. Yang, C. Yin, X. Yan and S. Jin, *open Journal of Applied Biosensor*, 2012, 1, 44-52.

83 H. J. Kim, J. E. Park, M. G. Choi, S. Ahn and S. K. Chang, *Dyes Pigm.*, 2010, **84,** 54–58.

Fluorescein-2-(Pyridin-2-ylmethoxy) benzaldehyde conjugate for fluorogenic turn-ON recognition of Hg^{2+} in water and living cells with logic gate and memory device applications

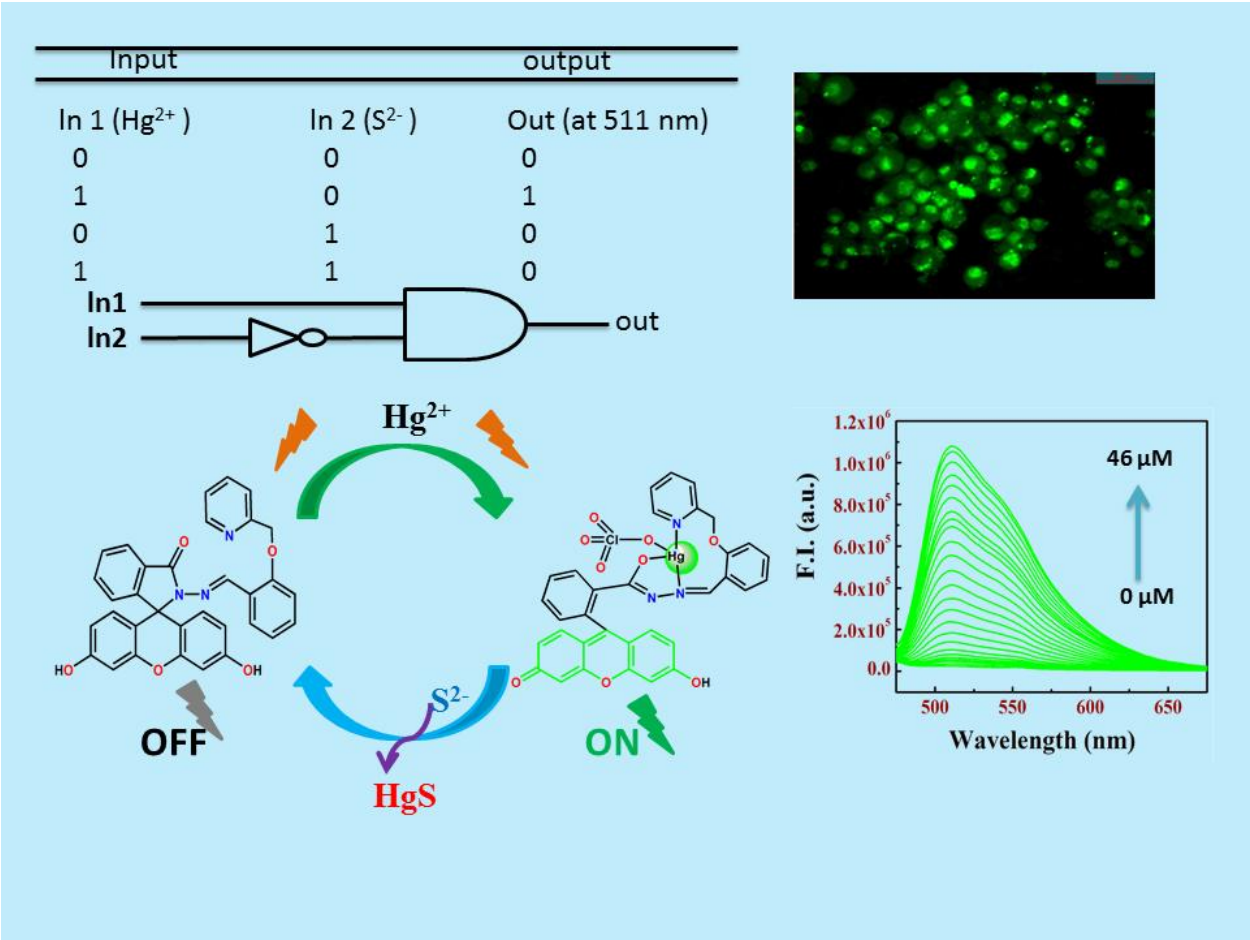

Abstract:

An effective Hg^{2+} specific probe, fluorescein-2-(Pyridin-2-ylmethoxy)-benzaldehyde conjugate (L^{29}), was designed, synthesized and characterized by various instrumental techniques. The sensing behavior of L^{29} was investigated by fluorescence technique which clearly established the high selectivity towards Hg^{2+} through OFF–ON fluorescence response in the presence of other metal ions like Zn^{2+}, Mg^{2+}, Co^{2+}, Ni^{2+}, Cu^{2+}, Pb^{2+}, Al^{3+}, Cr^{3+}, Cd^{2+}, Pd^{2+}, Fe^{2+} and Fe^{3+} in aqueous medium (pH 7.2, 10 mM HEPES buffer). The sensing mechanism could be attributed to the Hg^{2+} triggered spirolactam ring opening of the fluorescein moiety and simultaneous formation of a 1:1 L^{29}–Hg^{2+} complex. The interaction and formation of L^{29}–Hg^{2+} species was supported by the observations gained from fluorescence titrations, Job's plot, ^{1}H NMR and HRMS, and other spectroscopic studies. For the Hg^{2+} interaction towards L^{29} the binding constant was calculated to be $(3.21 \pm 0.05) \times 10^{4}$ M^{-1} with detection limit 92.7 nM. On addition of S^{2-} to the L^{29}–Hg^{2+}complex, the fluorescence intensity was totally quenched due to removal of Hg^{2+} from the complex by S^{2-} ion arising out of stronger affinity of Hg^{2+} towards S^{2-} resulting concomitant formation of ring closed form, L^{29}. The tentative coordination environment in the L^{29}–Hg^{2+}complex was established by DFT studies. L^{29} exhibits low cytotoxicity and cell permeability, which makes it capable for bioimaging applications in living HepG2 cells.

3.1 Introduction

Mercury is known to be one of the most prevalent toxic metals in the environment. Mercury pollution pervades the globe and threatens to human health and the environment. Hg(0), Hg(II) and organic mercury, CH_3Hg are the prevailing forms of Hg in nature and all of them are highly toxic. A living cell can be exposed to mercury through multiple pathways like, air[1] water[2], cosmetic products[3], and even vaccines[4]. More importantly; Hg (0) and Hg (II) ions present in soil or in waste water are assimilated and converted to methyl mercury, a potent neurotoxin, by the lower aquatic organisms which is subsequently bio-accumulated in the human body through food chain[5-7]. Organomercury can easily cross the cell membrane and the blood-brain barrier impairing nefrological and neurological functions. Therefore, mercury exposure, even at very low concentrations, can cause serious metabolic, motor and cognitive disorders and long term diseases in human beings[8-10]. The extreme toxicity of mercury and its derivatives results from their affinity towards thiol groups in proteins and enzymes that lead to malfunctioning of living cells[6] and eventually to serious health hazards.

Therefore, identification and quantification of mercury in numerous circumstances need efficient detection methods. Among various traditional methods, fluorescence spectroscopy might be the best choice for the detection of Hg^{2+} due to its rapid, sensitive, selective, non-destructive and easy operative features. In addition, it allows on-site and remote detections of mercury in the environmental samples[11-13]. Due to high atomic mass (A) and large spin−orbit coupling (ζ) Hg^{2+} mostly acts as a fluorescence quencher[14]. However, an actual 'OFF–ON' fluorescence probe for Hg^{2+} is difficult to realize. Again, an unavoidable background fluorescence signal restricts its application in bio imaging process. Thus, fluorescein-based conjugate supposed to be a suitable choice for building an 'OFF–ON' fluorescent chemosensor exhibiting a special structural feature (spirolactam ring) and excellent photophysical properties of longer absorption and emission wavelengths with larger absorption coefficient[15-20].

S^{2-} is extensively used in the industrial conversion S^{2-} into sulphur and sulphuric acid, in the manufacturing of cosmetic and dyes, in the production of wood pulp etc[21] that may lead to contamination of water. The other sources of S^{2-} in nature are sulphur-containing amino acids in the meat proteins and microbial reduction of sulphate by anaerobic bacteria. Sulphide can irritate mucous membranes and even causes unconsciousness and respiratory paralysis[22-23]. Once protonated, HS^- or H_2S is even more toxic than sulphide (S^{2-}) itself. Abnormal

concentrations of H_2S can cause Down syndrome, Alzheimer's disease, and liver cirrhosis[24]. H_2S can also cause loss of consciousness, permanent brain damage, or even death through asphyxiation[25-26]. So, there is an urgent need to develop a method with high sensitivity and selectivity for detection of sulphide ion in aqueous medium and in biological systems.

In this work, we are disclosing a new fluorescent sensor L^{29} which selectively binds with Hg^{2+} to form L^{29}–Hg^{2+} displaying a 'turn-on' fluorescence response through spirolactam ring opening, and subsequently reacts with S^{2-} displaying a 'turn-off' fluorescence response due to dislodging the Hg^{2+} ion from L^{29}–Hg^{2+} complex selectively over other possible competitive anions leaving behind the ring closed non-fluorescent spirolactam form.

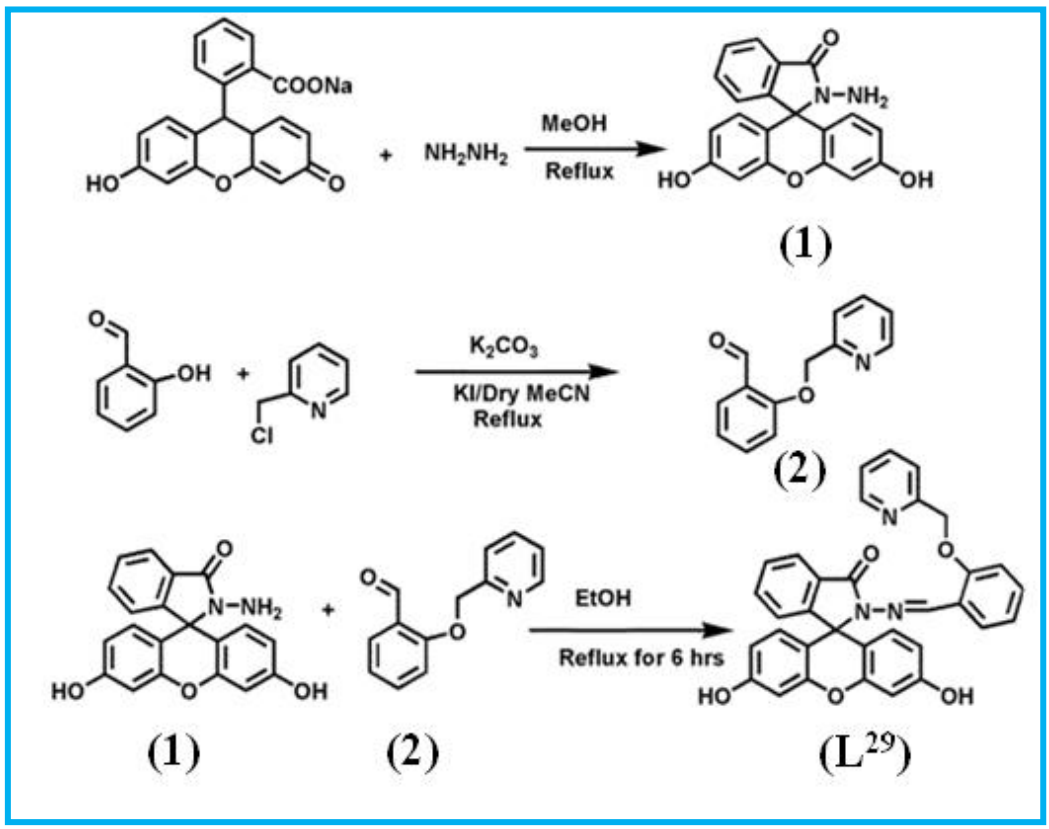

Scheme 3.1: Synthetic route of chemosensor L^{29}

3.2 Experimental section

3.2.1 Materials and reagents

Infrared spectra (400–4000 cm^{-1}) were recorded in solid state on a Nickolet Magna IR 750 series-II FTIR spectrometer. ^1H NMR spectra were generated in DMSO-d_6 and $CDCl_3$ solutions on a Bruker 300 MHz (AVI, 300) NMR spectrometer. Chemical shifts are expressed in parts per million (ppm, δ) and are referenced to tetramethylsilane (δ = 0) as an internal standard. Signal description: s = singlet, d = doublet, t = triplet, m = multiplet, dd =

doublet of doublets, q = quartet. ^{13}C NMR spectra were recorded in DMSO-d_6 with complete proton decoupling. ESI-MS^+ (m/z) studies of the ligand and complex were performed on a Waters' HRMS spectrometer (Model: **XEVO G2QTof**). UV-Vis spectra were generated on an Agilent diode-array spectrophotometer (Model, Agilent 8453). Steady-state fluorescence measurements were carried out with a PTI QM-40 spectrofluorimeter. pH values of the reaction solutions were measured with a digital pH meter (Model: Systronics 335, India) in the pH range 2–10 which was prior calibrated using buffers of pH 4, 7 and 10. Fluorescein sodium salt, 2-chloromethylpyridine, $Hg(ClO_4)_2.3H_2O$ and metal salts such as the perchlorates of Zn^{2+}, Mg^{2+}, $Co^{2,}$, Ni^{2+}, Cu^{2+}, Pb^{2+}, Al^{3+}, Cr^{3+}, Cd^{2+}, Pd^{2+}, Fe^{2+} Fe^{3+}, Mn^{2+}, Na^+, K^+, Ca^{2+}, and Ag^+ were bought from Sigma–Aldrich and used as received (Caution! Perchlorate salts of the complexes are potentially explosive and should be handled in small quantity with care) . Sodium salts of anions like SO_4^{2-}, $S_2O_4^{2-}$ SO_3^{2-}, $S_2O_3^{2-}$, PO_4^{3-}, S^{2-}, Cl^-, F^-, Br^-, I^-, $H_2PO_4^-$, CN^-, NO_2^-, CO_3^{2-}, ClO_4^- and N_3^- were of reagent grade and used as received.

3.2.2 Solution Preparation for UV-Vis/fluorescence studies

For UV-Vis and fluorescence experiments, a 10 ml 1.0 x 10^{-3} M stock solution of L^{29} was prepared by dissolving required amount of ligand in DMF-MeOH (1:9 v/v). In a similar way, standard solutions of 1.0 x 10^{-3} M $Hg(ClO_4)_2.3H_2O$ and 1.0 x 10^{-3} M of sodium sulphide (Na_2S) in water were also prepared freshly at the time of spectroscopic studies. The standard solutions of other cations and anions were made in MeOH/H_2O. A 250 mL of 10 mM HEPES buffer in water was prepared and pH was maintained to 7.2 by using HCl and NaOH keeping ionic strength at 0.1 M with respect to NaCl. 2.5 mL of this buffer solution was pipetted out into a cuvette to which required volume of 1.0 x 10^{-3} M probe was transferred to achieve 10 µM final concentrations for fluorescence titration. In a regular interval of volume Hg^{2+} ions were transferred incrementally beginning from 0 to 46 µM and fluorescence and UV-Vis spectra were collected for each solution. The cuvettes of 1 cm path length were used for absorption and emission studies. Fluorescence experiments were done using 5 nm x 3 nm slit width.

3.2.3 Preparation of Fluorescein Hydrazide (1)

1 was prepared according to the method described in chapter 2[27].

3.2.4 Preparation 2-(Pyridin-2-ylmethoxy)benzaldehyde (2):

2 was synthesized according to the method described in chapter 2[28].

3.2.5 Synthesis of the receptor (L[29])

A mixture of 2-(Pyridin-2-ylmethoxy)benzaldehyde (0.692 g, 2 mmol)) and Fluorescein Hydrazide (0.424 g, 2 mmol) was dissolved in 20 mL of ethanol in the presence of 4 drops of acetic acid and the resulting solution was stirred under reflux for 6 h at an ambient temperature. The product precipitated from the reaction mixture and was collected by filtration. It was washed with cold ethanol and dried under vacuum to afford a white solid. 70% yield was obtained. ^{1}H-NMR (DMSO-d6): δ= 9.87 (S, 2H), 8.91 (s, 1H), 8.59 (d,1H), 7.96(m, 2 H), 7.61 (m, 3H), 7.42 (m, 1H), 7.27 (d, 2 H), 7.05 (s, 2H), 6.94 (m, 1H), 6.55 (d, 2 H), 6.48 (s, 1H), 6.44 (s, 1H), 6.41 (s, 2H), 5.10 (s, 2H), **(Figure 3.1)**. **FT**-IR spectrum:-OH (3143 cm^{-1}),-C=N (1657 cm^{-1}), -C=O (1647 Cm^{-1}) (**Figure 3.2**). ESI-MS^{+}: *m/z*= 542.32 (**$C_{33}H_{23}N_3O_5$ + H^{+}**) **(Figure 3.3)**.

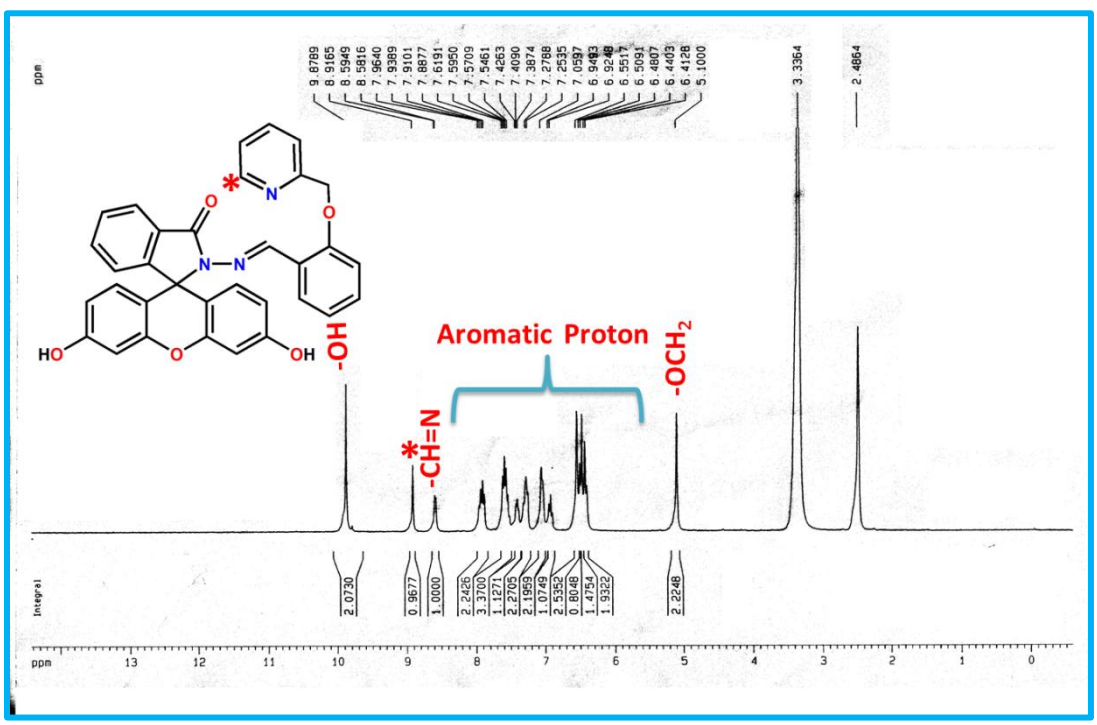

Figure 3.1. ^{1}H-NMR spectrum of L[29] in DMSO-d_6.

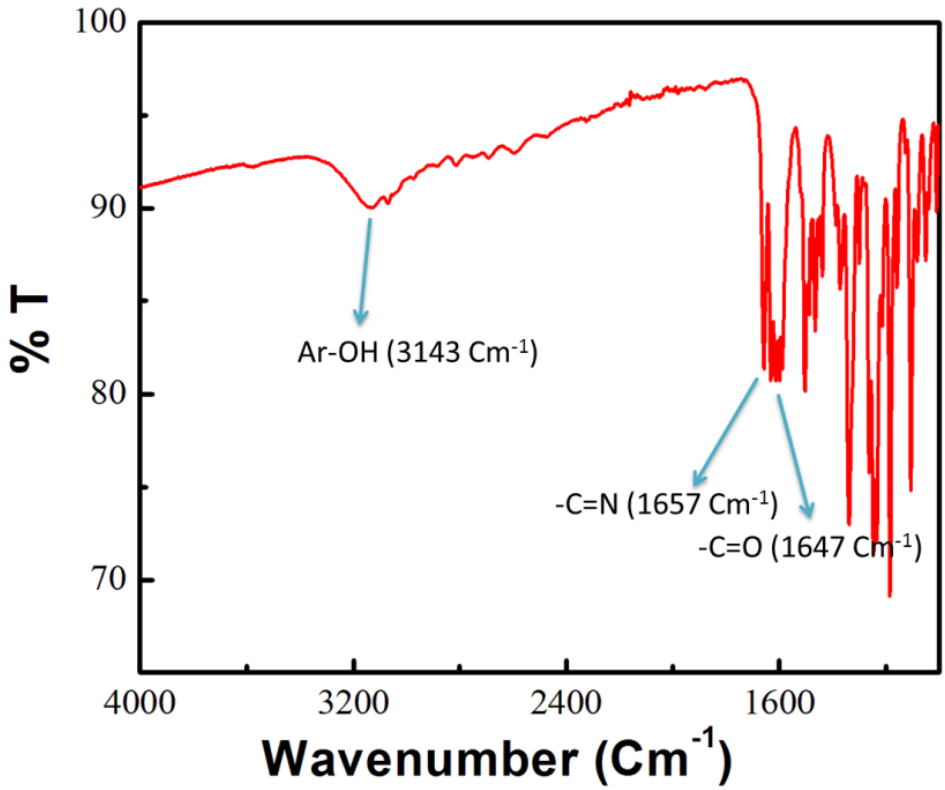

Figure 3.2. IR spectrum of L[29].

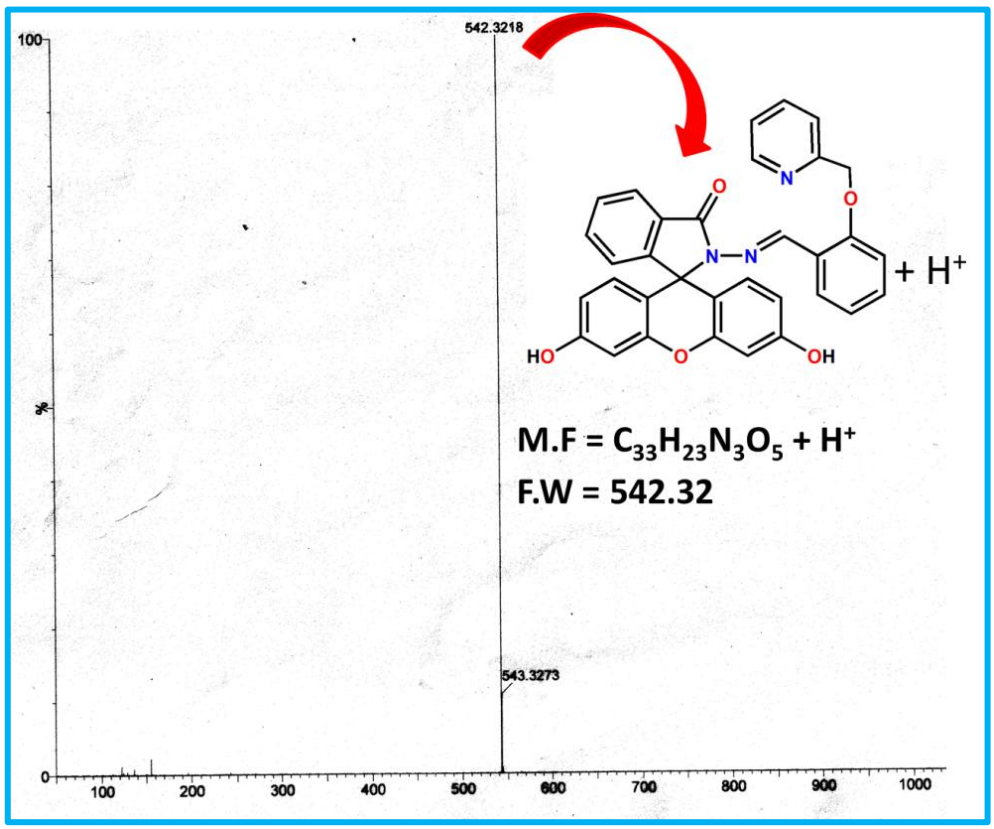

Figure 3.3. Mass spectrum of L^{29} in MeOH.

3.2.6 Synthesis of the L^{29}–Hg^{2+} complex

To a methanolic solution (5 mL) of the ligand (0.424 g, 0.27 mmol), a methanolic solution of $Hg(ClO_4)_2.3H_2O$ (0.272 g, 0.6 mmol) was added. The resulting mixture was stirred for 1 h. The solvent was removed under vacuum and the whole mass was washed with ether several times to afford the complex as orange solid. ^{1}H-NMR (DMSO-d_6): δ= 9.24 (S, 1H), 8.92 (m, 1H), 8.35 (s, 1H), 7.88 (m, 2 H), 7.57 (m, 2H), 7.35 (m, 2H), 7.09 (m, 2 H), 6.60 (m, 10H), 5.43 (d, 2H), (**Figure 3.4**). FTIR spectrum:-OH (3381 cm^{-1}), -C=N (1546 cm^{-1}), -C=O (1601 Cm^{-1}) (**Figure 3.5**). ESI-MS$^+$: *m*/*z*= 840.24 (**$C_{37}H_{22}N_3O_5Hg_1ClO_4$**) (**Figure 3.6**).

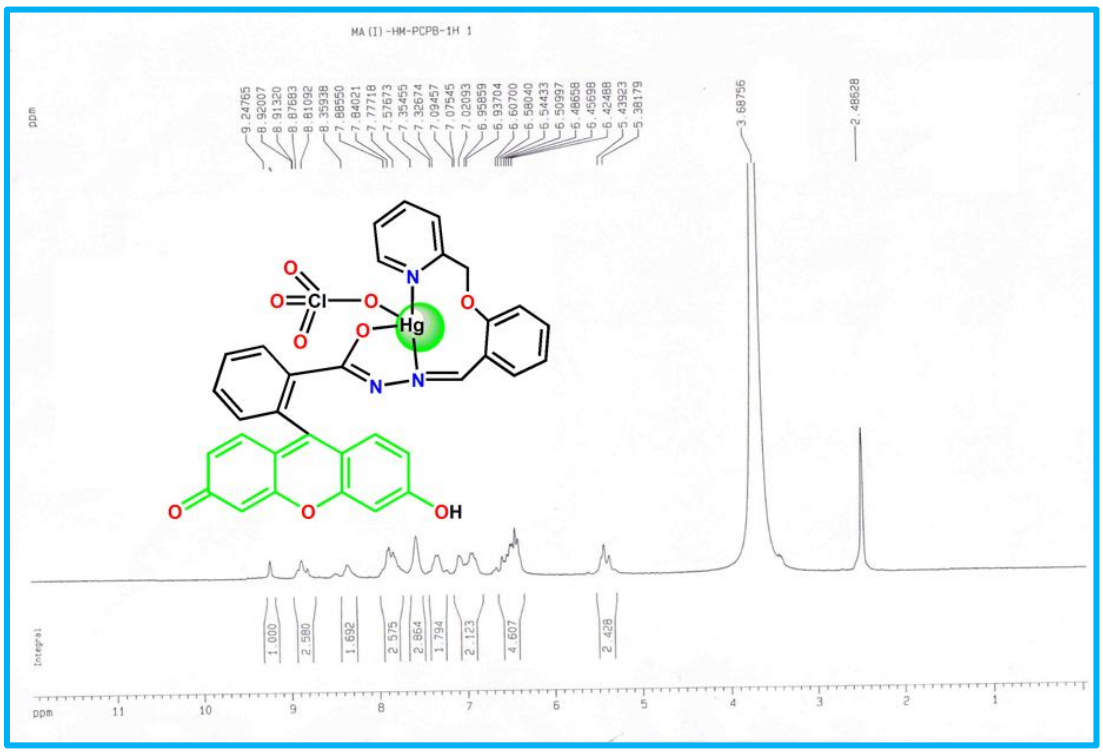

Figure 3.4. ^{1}H-NMR spectrum of L^{29}-Hg^{2+} complex.

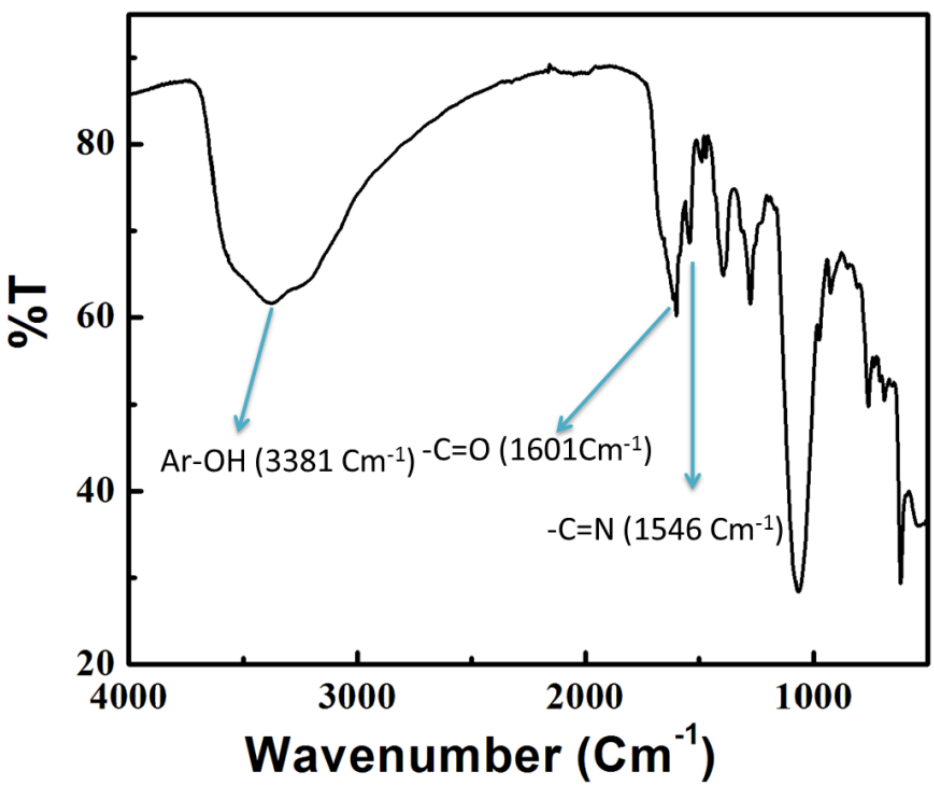

Figure 3.5. IR spectrum of L^{29}-Hg^{2+} complex.

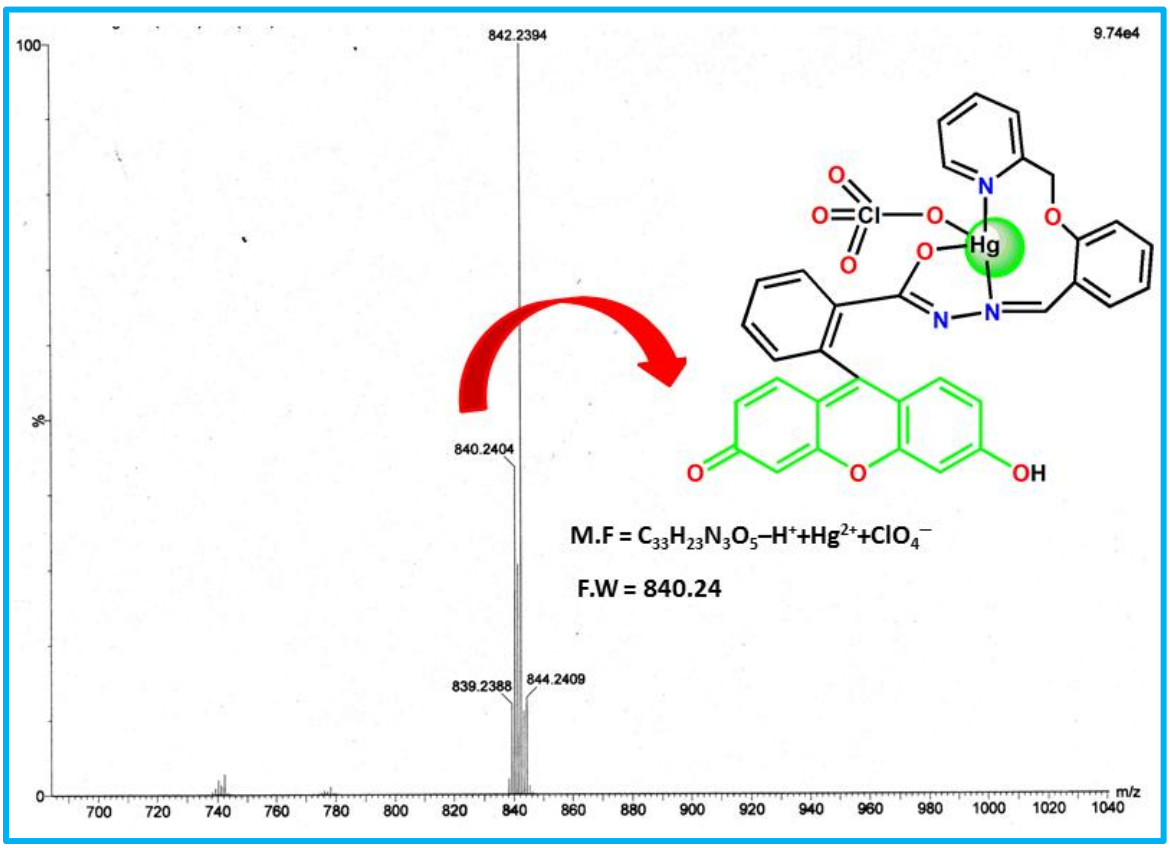

Figure 3.6. Mass spectrum of L^{29}-Hg^{2+} complex in MeOH.

3.2.7 Computational studies

All calculations relating to optimization of geometries of L^{29} and L^{29}-Hg^{2+} were performed with the Gaussian 09 program[29] with the help of the density functional theory (DFT) at the B3LYP[30] level. The calculations were supported by the Gauss View visualization program. All elements except Hg were assigned the 6-31G basis set. For the Hg atom the LanL2DZ basis with effective core potentials was employed. Vibrational frequency calculations were performed to ascertain that the optimized geometries correspond to local minima as reflected by positive eigenvalues.

3.2.8Cell culture

Human hepatocellular liver carcinoma (HepG2) cell lines (NCCS, Pune, India), were grown in DMEM supplemented with 10% FBS and antibiotics (penicillin-100 µg/ml; streptomycin-50 µg/ml). Cells were cultured at 37°C in 95% air, 5% CO_2 incubator.

3.2.9 Cell Cytotoxicity Assay

Cytotoxic effects of L^{29} on living cells were assessed employing 3-(4,5-dimethylthiazol-2-yl)-2,5-diphenyltetrazolium bromide (MTT) by cell viability assay method. HepG2 cells (3 × 104 cells/well) were cultured in a 96-well plate and incubated at 37°C followed by exposure to varying concentrations of L^{29} (1, 5, 10, 20, 40, 50, 60, 70, 80, 90 and 100 μM) for 24 hours. After the incubation, 10 μL of MTT solution [5 mg/ml, dissolved in 1X phosphate-buffered saline (PBS)] was added to each well of a 96-well culture plate, and then incubated at 37°C for 4 hours. Media were decanted from wells and 100 μL of 0.04 N acidic isopropyl alcohol was added into each well to solubilize intracellular formazan crystals (blue-violet) formed and absorbance of each solution was measured at 595 nm on EMax Precision MicroPlate Reader (Molecular Devices, USA). Values were calculated as mean ± standard errors of three independent experiments. The cell viability was expressed as the optical density ratio of the treatment to control.

3.2.10 Cell Imaging Study

HepG2 Cells (1×10^3) were cultured in 35 x 10 mm culture dish on coverslip for 24 h at 37°C. The cells were treated with 10 μM solutions of L^{29}, prepared by dissolving L^{29} to the mixed solvent DMSO: water = 1:9 (v/v) and incubated for 1 hour at 37°C. To study the complex formation ability with Hg^{2+} ions, HepG2 cells were pre-incubated with 10 μM and 20 μM of Hg^{2+} for 60 min at 37°C. Then it was washed three times with 1X PBS and subsequently incubated with 10 μM of L^{29} for 60 min at 37°C. Fluorescence images of HepG2 cells were taken by a fluorescence microscope (Leica DM3000, Germany) with an objective lens of 40X magnification.

3.3 Results and Discussion

As demonstrated in **Scheme 3.1**, the probe L^{29} was readily prepared from the acetic acid mediated condensation reaction between 2-(Pyridin-2-ylmethoxy)-benzaldehyde (**L^1**) and equi-molecular amount of Fluorescein hydrazide in ethanol for 6 h under reflux. The pure product was achieved as an off-white solid in 80% yield. Then, it was thoroughly characterized using ^{1}H NMR, ESI-MS$^+$ and FT-IR spectral analysis (**Figure 3.1-3.3**). In the IR spectrum, the appearance of the characteristic peak of imine (-C=N) at 1657 Cm^{-1} clearly suggests the formation of the Schiff base.

3.3.1 Photophysical characteristics of L^{29}

The UV-Vis spectrum of the probe L^{29} was recorded in 10 mM HEPES buffer at pH 7.2. On addition of Hg^{2+} the absorption band at 370 nm showed a gradual red shift with concomitant increase in absorption around 475 nm without developing a well-defined absorption peak. The dilution effects on spectra were also studied where it was observed that the two spectra are almost same **(Fig.3.7).** So, we can say that the absorption change of L^{29} is occurred due to dilution effect[31].

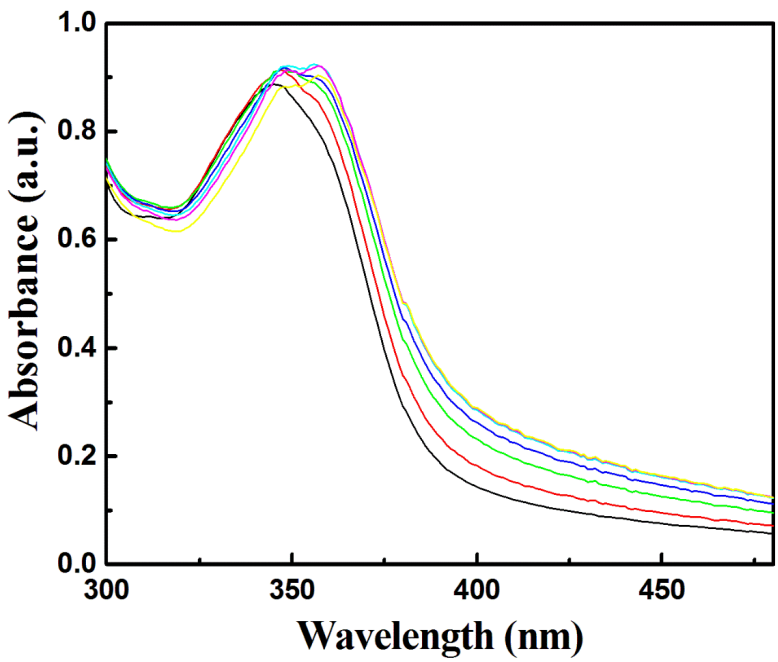

Figure 3.7. Absorption titration of L^{29} with gradual addition of Hg^{2+} solution.

The fluorescence titration of the probe L^{29} was executed in pure aqueous buffer at pH 7.2 using 10 mM HEPES (2-[4-(2-hydroxyethyl)-1-piperazinyl]ethane sulfonic acid). As delineated in **Figure 3.8,** free probe L^{29} itself is very weakly fluorescent due to the Spiro cyclic structure. However, upon addition of increasing concentrations of Hg^{2+} (0-46 μM) to a 10.0 μM solution of L^{29}, an intense new fluorescence emission band at 511 nm was noticed. It displayed a strong green fluorescence with an approximately ~44 fold enhancement in the fluorescence intensity. This enhancement was attributed to Hg^{2+} promoted spirolactam ring opening[18] of L^{29}.

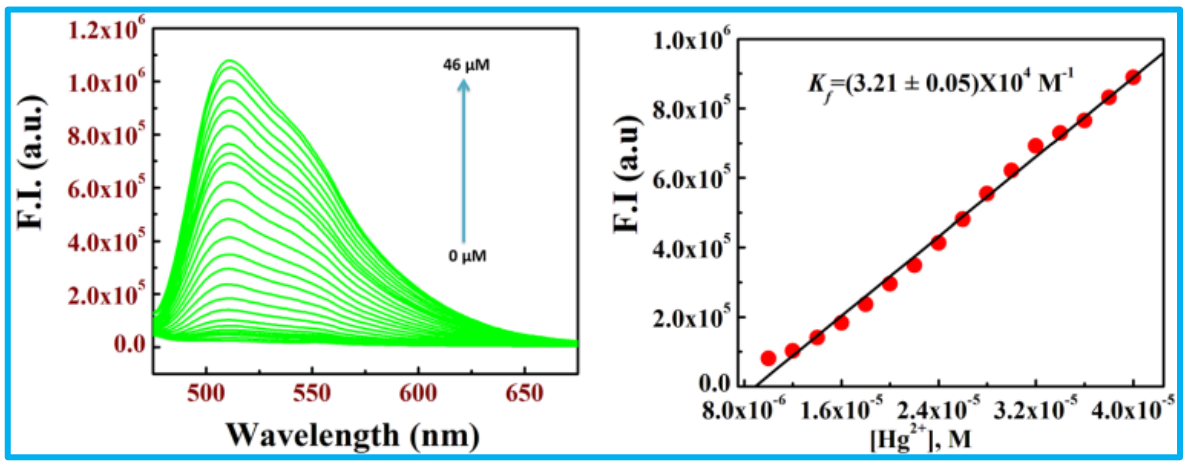

Figure 3.8. (a) Fluorescence titration of L^{29} (10.0 µM) in 10 mM HEPES buffer at pH 7.2 by addition of increasing concentration of Hg^{2+} (0-46 µM) with λ_{ex} = 475 nm and λ_{em} = 511 nm. (b) linear fit plot of FI vs. [Hg^{2+}].

Meanwhile, the reaction of Hg^{2+} with a chelating agent L^{29} induces rigidity in the resulting molecule that produces a large enhancement of the fluorescence intensity (CHEF) [32-34]. The detection of Hg^{2+} was not perturbed by the presence of Zn^{2+}, Mg^{2+}, Co^{2+}, Ni^{2+}, Cu^{2+}, Pb^{2+}, Al^{3+}, Cr^{3+}, Cd^{2+}, Pd^{2+}, Fe^{2+} , Fe^{3+} **(Figure 3.9).** and Ag^{+} **(Figure 3.10).** However, other competitive metal ions like Zn^{2+}, Mg^{2+}, Co^{2+}, Ni^{2+}, Cu^{2+}, Pb^{2+}, Al^{3+}, Cr^{3+}, Cd^{2+}, Pd^{2+}, Fe^{2+} and Fe^{3+} have hardly any response towards enhancement of emission of the probe (**Figure 3.11.**). This establishes the fact that L^{29} binds selectively with Hg^{2+} in the presence of a variety of interfering metal ions present in environmental and biological settings. Furthermore, for the biological application, the effect of pH on the fluorescence response of probe L^{29} upon binding with Hg^{2+} was also scrutinized at varying pH values from 2.0 to 10.0 by fluorescence titration.

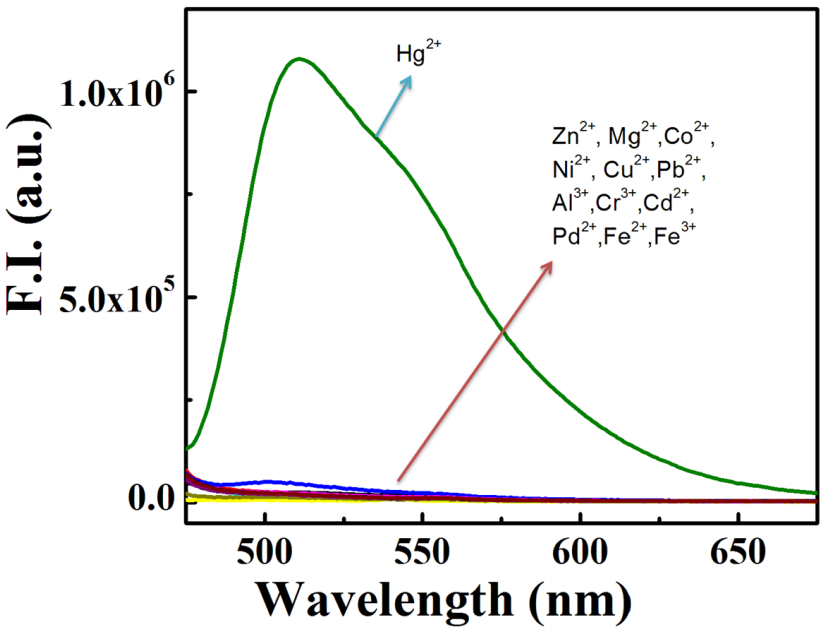

Figure 3.9. Fluorescence spectra of L^{29} (10.0 μM) in the presence of different cations (100 μM) in 10 mM HEPES buffer at pH 7.2 with λ_{ex} = 475 nm and λ_{em} = 511 nm.

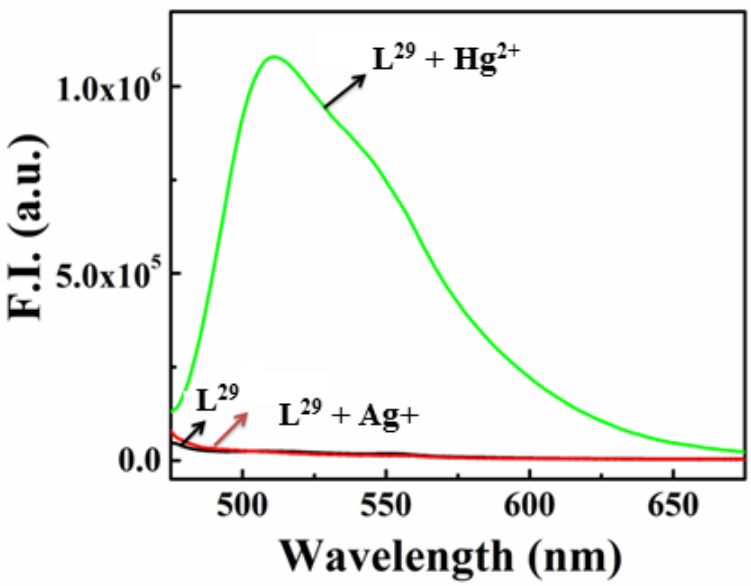

Figure 3.10. Fluorescence spectra of L^{29} (10.0 μM) in the presence of Ag^{+} cations (100 μM) in 10 mM HEPES buffer at pH 7.2 with λ_{ex} = 475 nm and λ_{em} = 511 nm.

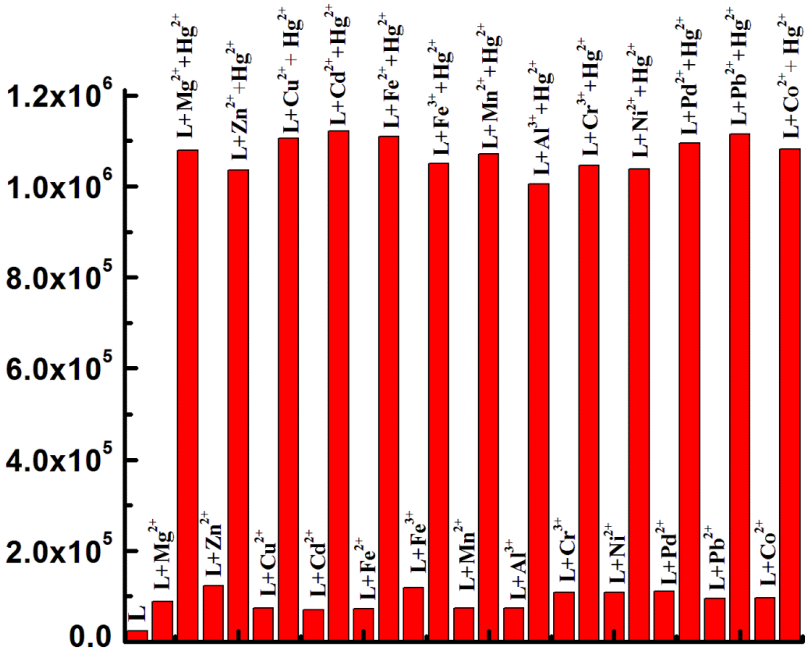

Figure 3.11. Competitive fluorescent responses of L^{29} to different metal ions in 10 mM HEPES buffer at pH 7.2.

As depicted in **Figure 3.12,** the fluorescence intensity of L^{29} is stable in the range pH 2-7 without obvious fluorescence responses. When the pH is greater than 7, the deprotonation of the aromatic hydroxyl group (–OH)[35-38] leads to slight fluorescence enhancement at alkaline conditions. However, upon addition of 46 μM Hg^{2+}, there is a gradual increase in fluorescence intensity on increase in pH of the medium from 4.0 to 10.0, especially from 7.0 to 10.0, which suggests the fact that Hg^{2+} promotes the formation of ring-opened L^{29}–Hg^{2+} complex. Hence, considering the fact that the physiological environment is slightly alkaline, we set pH = 7.2 as the experimental condition to detect Hg^{2+} ions.

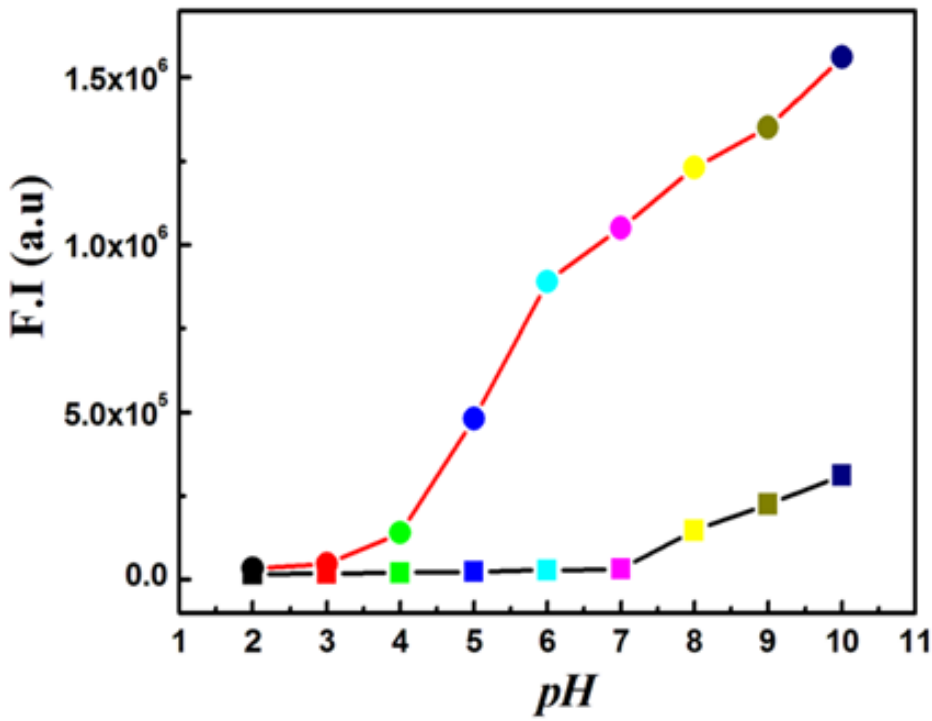

Figure 3.12. Fluorescence intensity vs. pH plot at 511 nm with 10 μM (demonstrated by black line) of L^{29} and L^{29}-Hg^{2+} complex (denoted by red line).

3.3.2 Binding constant and Stoichiometry determination

The binding constant was evaluated by plotting FI versus [Hg^{2+}] that gives an excellent linear curve, which was solved by adopting the equation $y = (a + b \times c \times x^n)/(1 + c \times x^n)$[39], where a = FI of free probe, b = maximum fluorescence (F_{max}), c = K_f, formation constant with the assumption that $1 \gg c \times x^n$ with n = 1. So, slope of the curve is b × c and slope/F_{max} gives $K_f = (3.21 \pm 0.05) \times 10^4\ M^{-1}$ (where b = 1.07894× 10^6) (**Figure 3.8**).

The Job's plot displayed a 1:1 stoichiometry between the probe L^{29} and Hg^{2+} (**Figure 3.13**). Furthermore, ESI-MS^+ were used to confirm the 1:1 coordination mode between L^{29} and Hg^{2+}. Without Hg^{2+}, the m/z 542.32 peak corresponded to $(L^{29} + H)^+$. When, Hg^{2+} was introduced to a solution of L^{29}, a peak appeared at m/z 840.24, which was assigned to the complex (L^{29}–Hg^{2+}−H^+), and this agreed with the calculated value of 840.3 for the 1:1 complex. (**Figure 3.14**).

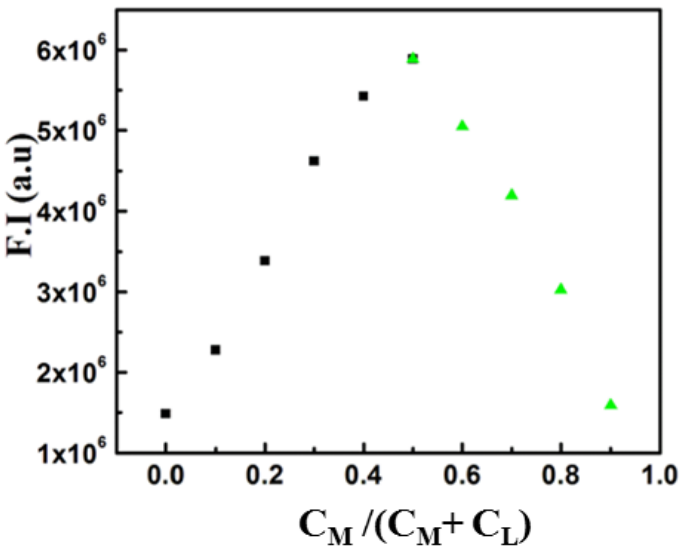

Figure 3.13. JOB's plot for Hg^{2+}.

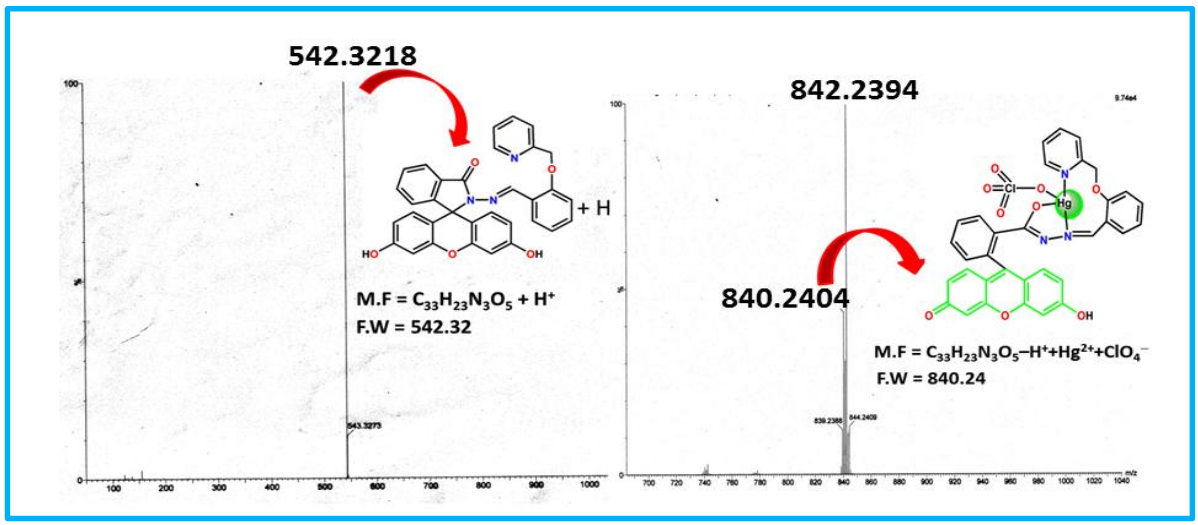

Figure 3.14. HRMS spectrum of L^{29} and the L^{29}–Hg^{2+} complex.

3.3.3 Limit of Detection

The 3σ method was adopted to determine the limit of detection (LOD) of Hg^{2+} and S^{2-}. It was evaluated to be 92.7 nM (**Figure 3.15**) for Hg^{2+} and 0.231 μM (**Figure 3.16**) for S^{2-}. It clearly suggests that L^{29} is an efficient probe for monitoring traces of Hg^{2+} and S^{2-} ions. The present probe has better detection limit as compared to earlier reported probes[40-41].The quantum yields of L^{29} and L^{29}-Hg^{2+} complex were determined to be 0.0041 and 0.1435, respectively

using fluorescein as a standard (0.5 in ethanol). The quantum yield of L^{29} is increased upon binding with the Hg^{2+} ions. However, some of the fluorescent probe reported earlier could not enhance the quantum yield on binding of Hg^{2+} ions[42]. These results suggested that the probe was highly sensitive towards Hg^{2+} ions.

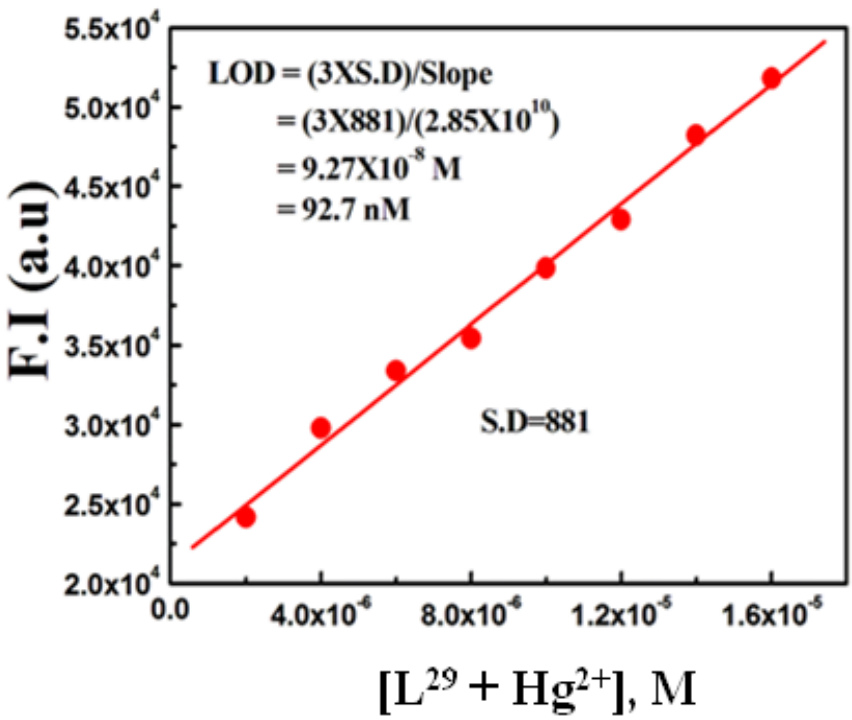

Figure 3.15. LOD of Hg^{2+}.

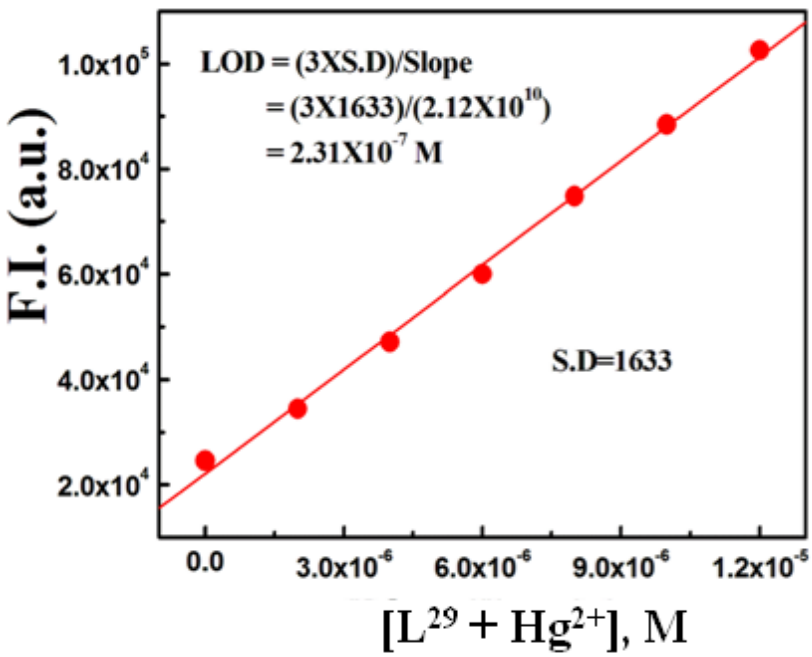

Figure 3.16. LOD of S^{2-}.

3.3.4 S^{2-} induced displacement of Hg^{2+} and S^{2-} sensing

From the above experiment, we can conclude that L^{29} specifically binds with Hg^{2+} to form L^{29}–Hg^{2+} complex with a remarkable enhancement in fluorescence intensity. As Hg^{2+} can coordinate with S^{2-} to form a stable species HgS, we conjectured that the L^{29} –Hg^{2+} ensemble can serve as a candidate for a turn-off fluorescent sensor for S^{2-}. To support this idea, the fluorescence spectra of the L^{29}–Hg^{2+} ensemble were studied in the presence of 5 equivalents of different anions such as SO_4^{2-}, $S_2O_4^{2-}$, SO_3^{2-}, $S_2O_3^{2-}$, PO_4^{3-}, Cl^-, F^-, Br^-, I^-, $H_2PO_4^-$, CN^-, NO_2^-, CO_3^{2-}, ClO_4^- and N_3^- which did not cause any significant change in emission intensity (**Figure 3.17**). However, it is very interesting to note that upon addition of 70 µM S^{2-} to the L^{29}–Hg^{2+} solution only S^{2-} causes a significant fluorescence quenching at 511 nm (**Figure 3.18**). Besides, the detection of S^{2-} was not perturbed by the presence of other sulphur species like SO_4^{2-}, $S_2O_4^{2-}$, SO_3^{2-}, $S_2O_3^{2-}$. It is considered that the decrease in fluorescence intensity is due to the formation of HgS thereby releasing L^{29} in its the spirolactam form indicating the fact that Hg^{2+} has a stronger affinity towards Hg^{2+} compared to that with the receptor L^{29}.

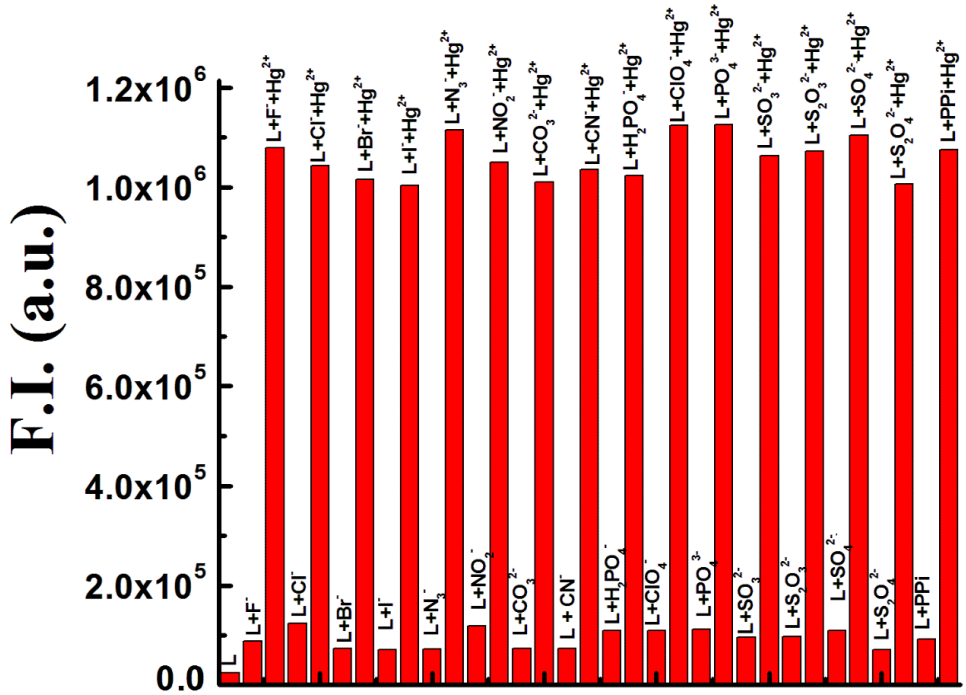

Figure 3.17. Competitive test for the fluorescent responses of L^{29} to various anions in 10 mM HEPES buffer at pH 7.2.

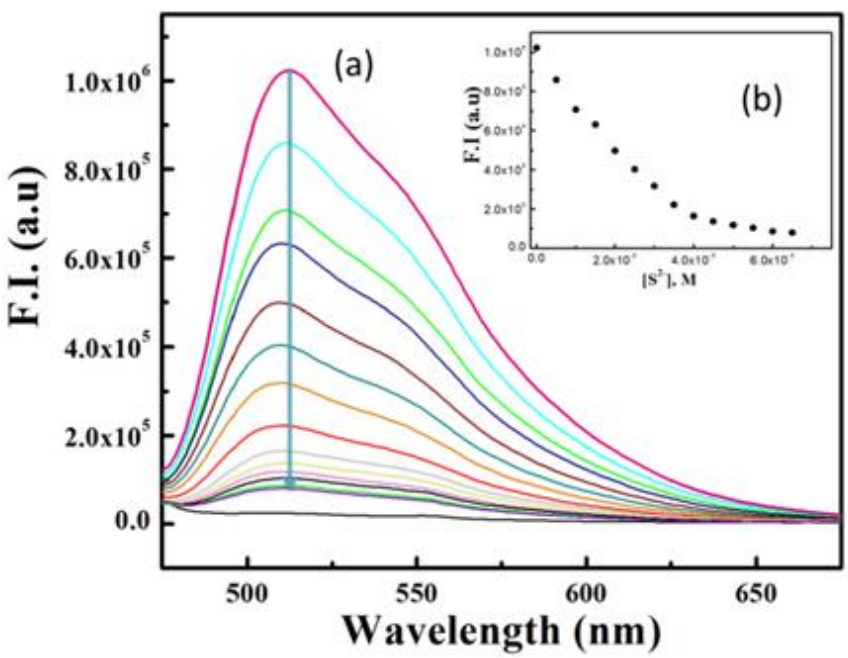

Figure 3.18. (a) Fluorescence titration of L^{29}-Hg^{2+} by adding S^{2-} (70 µM) in 10mM HEPES buffer at pH 7.2 (b) Fluorescence intensity at 511 nm vs concentration of S^{2-}.

3.3.5 Binding Mechanism:

The proposed mechanistic pathway of the formation of **L**^{29}–Hg^{2+} complex via opening of spirolactam ring was investigated through IR and ^{1}H-NMR studies. IR studies revealed that the characteristic stretching frequency for the 'C=O' in amide group of the fluorescein moiety at 1657 cm^{-1} was shifted to lower wave number of 1601 cm^{-1} in the presence of 1.5 equivalent of Hg^{2+}. The larger shift towards lower wave number signifies a higher polarization of the C=O bond upon efficient binding to the Hg^{2+} ion (**Figure 3.5)**. Also, in ^{1}H NMR, the imine proton (-CH=N) showed downfield shift by δ = 0.24 ppm (8.59 to 8.35 ppm) in the presence of 1.5 equiv. Hg^{2+} of ions signifying the coordination of azomethine-N to Hg^{2+} **(Figure 3.4)**. It was confirmed by HRMS analysis and the result was displayed in **Figure 3.14**. Without Hg^{2+}, the m/z 542.32 peak corresponded to [**L**^{29}+H]$^{+}$. When Hg^{2+} was introduced to a solution of **L**^{29}, a peak appeared at m/z 840.23 can be assigned to the complex [**L**^{29}–Hg^{2+}- H]$^{+}$ **(Figure 3.6)**. Thus, based on ^{1}H-NMR, IR, ESI-MS^{+}, Job's plot and HRMS studies, we proposed a probable mechanism of binding of Hg^{2+} ions to **L**^{29} as shown in (**Scheme 3.2).**

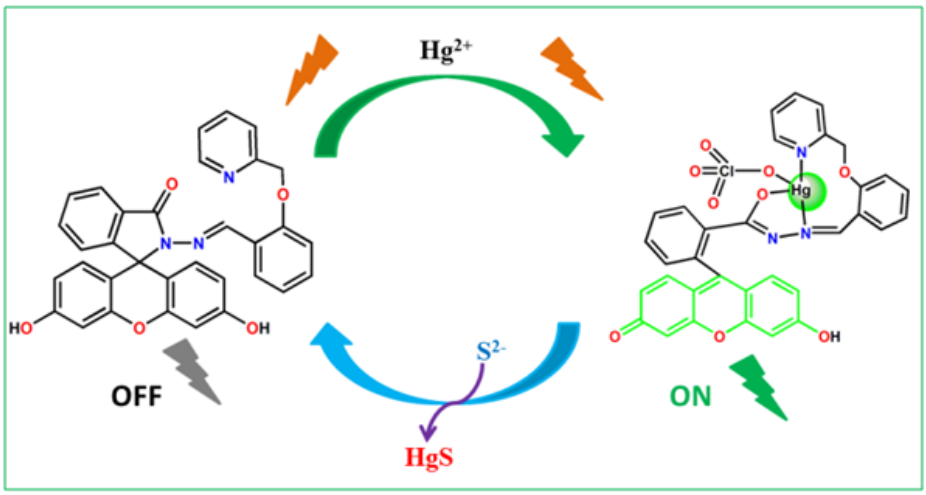

Scheme 3.2. A proposed binding mechanism between the receptor L^{29} and Hg^{2+}.

3.3.6 Reversibility

Reversibility and regeneration are another important factor for the development of devices for sensing of analytes for practical applications. The reversibility of the binding process between L^{29} and Hg^{2+} was established when the introduction of 70 µM of S^{2-} into a solution containing L^{29} (10 µM) and Hg^{2+} (46 µM) resulted in quenching of emission intensity at 511 nm (**Figure 3.19**). Due to strong affinity of S^{2-} for the Hg^{2+} ions, demetallation of the

receptor–Hg^{2+} complex occurred causing the fluorescence quenching. Then further addition of Hg^{2+} (80 μM) ions under the same condition, immediately revived the fluorescence. Therefore, this study renders the probe as a reversible sensor for the selective recognition of Hg^{2+} ions in pure aqueous medium under physiological conditions.

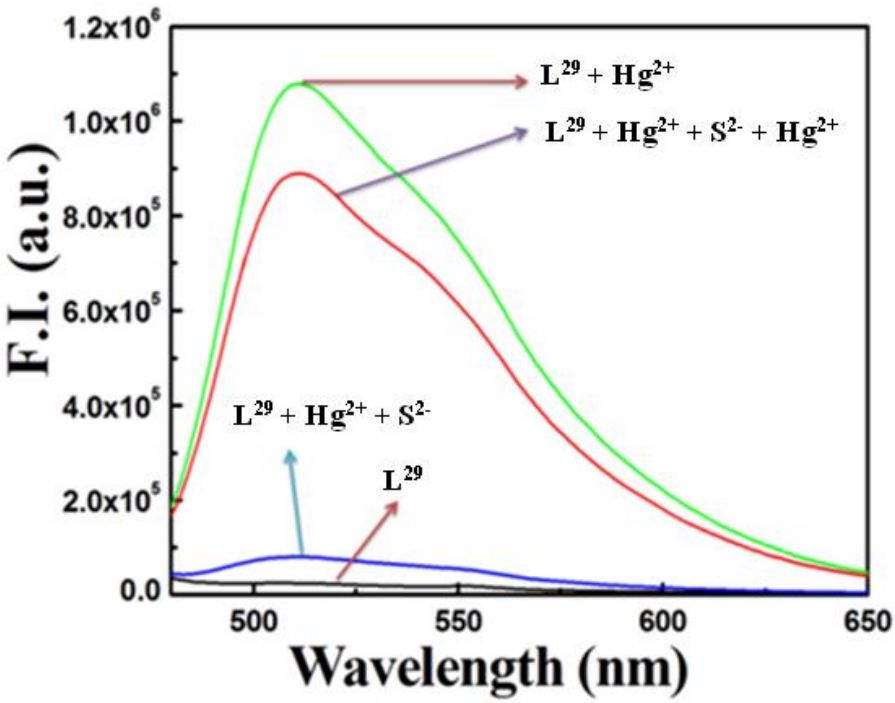

Figure 3.19. Reversibility checking of Hg^{2+} coordination to L^{29} and subsequent displacement by Na_2S. The black curve represents the fluorescence intensity of free L^{29}; the green line represents the fluorescence enhancement after the addition of 46 μM Hg^{2+}, the blue line represents the fluorescence decrease after the addition of 70 μM S^{2-} into the solution of L^{29}–Hg^{2+} species and the red line represents the fluorescence enhancement again after the addition of 80 μM Hg^{2+} into the [L^{29}–Hg^{2+} + S^{2-}] solution.

3.3.7 Geometry optimization and electronic structure

Both probe (L^{29}) and the complex (L^{29}–Hg^{2+}) have the *C1* point group. The main optimized geometrical parameters of the complex and ligand are listed in **Tables 3.1** and **3.2** and the optimized structures of probe (L^{29}) and the complex (L^{29}–Hg^{2+}) are given in (**Figure 3.20**).

Table 3.1. Selected optimized geometrical parameters for L^{29} in the ground state calculated at B3LY Levels.

Bond Distance (A˚)			
C13-O2	1.24	N34-C35	1.29
C13-N3	1.39	C35-C37	1.47
N3-N34	1.40	C39-O45	1.38
O45-C46	1.46	C46-C49	1.50
C49-N58	1.35		
Bond Angle (˚)			
C5-C13-O2	128.05	C39-O45-C46	120.37
C5-C13-N3	105.51	C46-C49-N58	115.71
C13-N3-C35	118.65		

The tetra coordinated Hg^{2+}complex was found to adopt a distorted tetrahedral geometry. The calculated Hg–O bond distances fall in the range 2.30–2.48 Å and Hg–N is 2.42 Å which are comparable to the previously reported respective bond distance values[1]. So after the formation of Hg-complexation (L^{29}–Hg^{2+}) there is a slight change in C–N, N–N and N–O bond distances observed with respect to the free probe (L^{29}) (**Table 3.1** and **3.2**).

Table 3.2. Selected optimized geometrical parameters for (L^{29}–Hg^{2+}) complex in the ground state calculated at B3LYP Levels

Bond Distance (A˚)			
C17-O1	1.31	O1-Hg62	2.30
C17-N5	1.34	O65- Hg62	2.48
N5-N6	1.40	N61- Hg62	2.42
N6- Hg62	2.37		
Bond Angle (˚)			
O1- Hg62-N5	71.11	O1-C17-N5	126.58
O1- Hg62-O65	149.85	C57-N5-N6	114.57
O1- Hg62-N61	112.21	N61-Hg62-O65	90.40
O65-Hg62-O48	71.91		

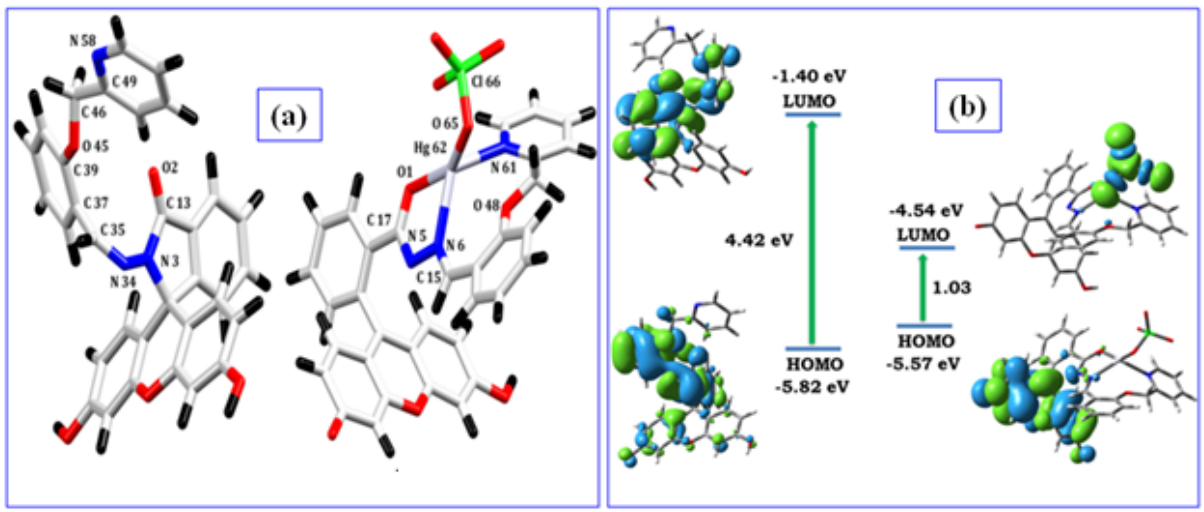

Figure 3.20. (a) Optimized geometries of probe (L^{29}) and the complex (L^{29}–Hg^{2+}) in DFT calculation. (b) Frontier molecular orbital of L^{29} as well as (L^{29}–Hg^{2+}) $^{+}$ complex optimized under DFT.

In the ground state of L^{29} the HOMO and LUMO electron densities mainly spreaded over the formic acid (2-methoxy-benzylidene)-hydrazide and 2-Methyleneamino-2,3-dihydro-isoindol-1-one moieties respectively with a HOMO−LUMO energy gap of 4.24 eV. In the case of L^{29}–$Hg^{2+}$the HOMO mainly has ligand π and π* orbital contributions, while the LUMO resides mainly on the Mercuric perchlorate part with a HOMO – LUMO energy gap of 1.03 eV (**Figure 3.20**). As a result, a substantial change in fluorescence intensity is observed on moving from free ligand to its Hg^{2+} complex.

3.3.8 Molecular logic operation

It has been observed that L^{29} itself is in fluorescence OFF state which on coordination with Hg^{2+} forms L^{29}–Hg^{2+} complex, resulting in the fluorescence "**ON**" state; while on further addition of S^{2-} TO L^{29}–Hg^{2+} complex restoration of fluorescence 'OFF' state occurs. Based on this principle, we can make a correlation by taking two inputs, namely input 1 (Hg^{2+}) and input 2 (S^{2-}), along with fluorescence intensity changes of the probe L^{29} at 520 nm as the outputs. For the input 1, output is assigned as 1 (ON state) while for input 1 and then input 2 the output is 0 (OFF state). The four possible input combinations are possible as (0, 0), (1, 0), (0, 1) and (1, 1), as shown in the truth table (Fig. 11d). Again, with no input, or with S^{2-} input alone, the output was 0. With Hg^{2+} input alone the output signal was 1. Therefore, monitoring

the fluorescence at 520 nm, upon addition of Hg^{2+} and S^{2-} and their combined mixture satisfies an INHIBIT logic gate function (**Figure 3.21**).

Input		output
In 1 (Hg^{2+})	In 2 (S^{2-})	Out (at 511 nm)
0	0	0
1	0	1
0	1	0
1	1	0

(a)

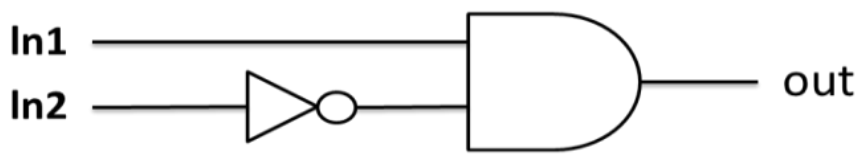

(b)

Figure 3.21. (a) Truth table of the logic gate. (b) a general representation of an INHIBIT logic gate.

3.3.8 Cell imaging studies

Considering the selective binding property of L^{29} with Hg^{2+} ion, it tempted us check its sensing ability of Hg^{2+} in living cells. Before doing this, we checked the cytotoxicity of L^{29} on living cells using MTT assay on HepG2 cells (**Figure 3.22**). It is interesting to note that at 10 µM of L^{29} ~80% cell viability could be achieved; as evidenced from a decrease in formazan production by L^{29} up to 10 µM, thus suggesting that below 10 µM concentration L^{29} would be much more effective for *in vitro* tracking of Hg^{2+} ion. Hence, further experiments were carried out with 10 µM of L^{29}.

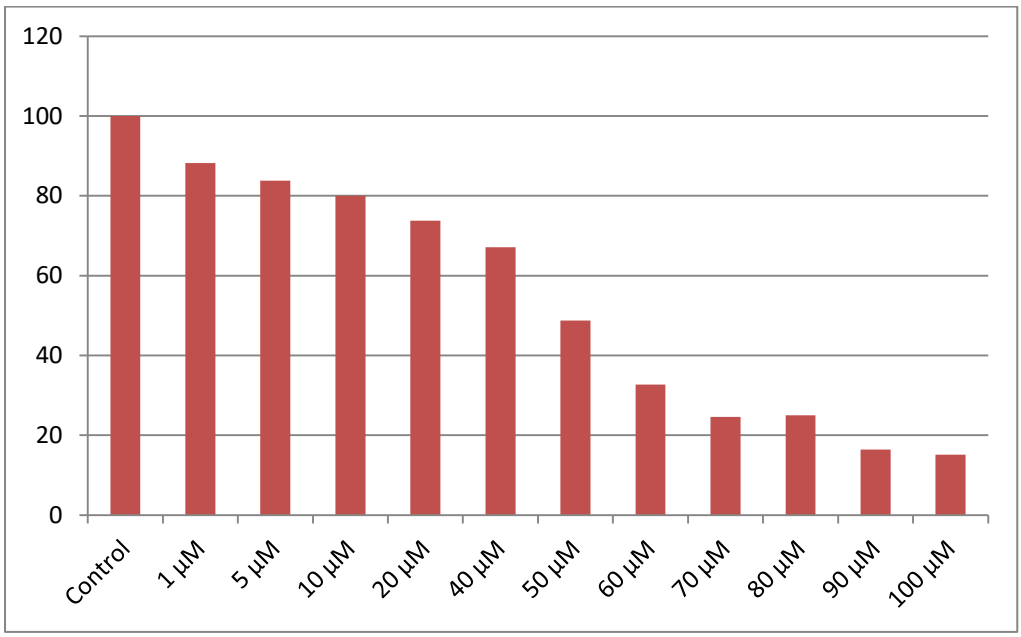

Figure 3.22. Percent (%) cell viability of HepG2 cells treated with different concentrations (1-100 µM) of 10µM of L^{29} for 24 hours determined by MTT assay.

When excited at 465 nm, the ligand L^{29} exhibited absence of intracellular fluorescence on HepG2 cells. However, on treatment with 10 µM of L^{29} for 1 h (**Figure 3.23**) followed by incubation with 10 µM of Hg^{2+} for 1 h at 37°C HepG2 cells showed a prominent green intracellular fluorescence, predominantly localized in the cytoplasmic region. Keeping the ligand L^{29} concentration constant at 10 µM, and increasing concentration of Hg^{2+} ions (from 10 µM to 20 µM) a concentration-dependent enhancement in the intracellular green fluorescence is prevalent. Again, upon incubation with 20 µM of Hg^{2+} towards 10 µM L^{29} for 1 h followed by washing and then incubation with 10 µM S^{2-} exhibited a tremendous reduction in the intracellular fluorescence. Hence the present ligand with low cytotoxicity can be used as a potential *in vitro* selective tracker of Hg^{2+}.

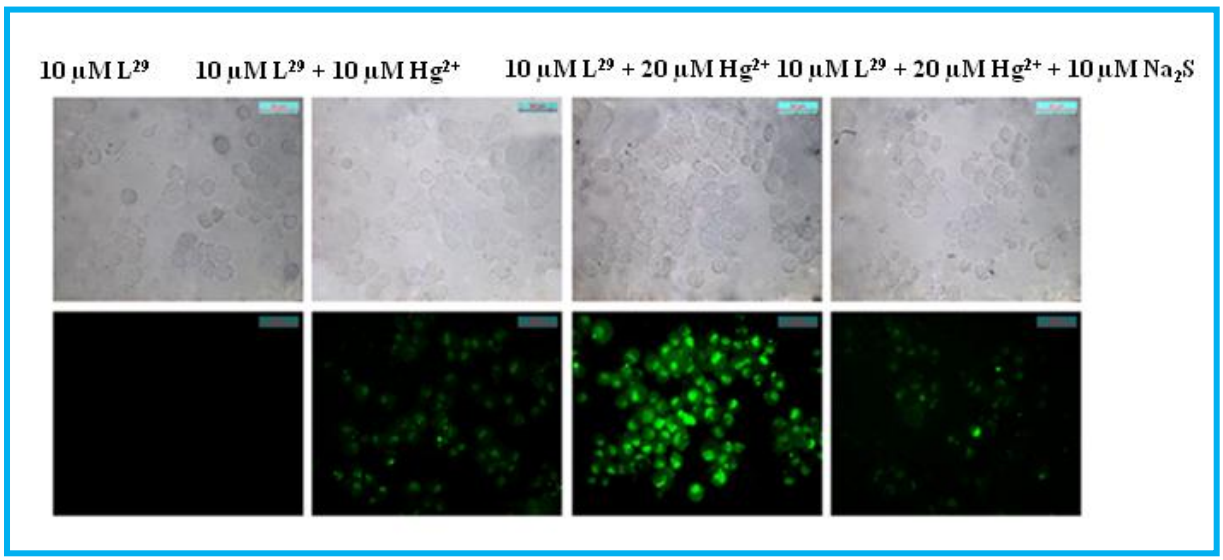

Figure 3.23. The fluorescence images of HepG2 cells were captured (40X) after incubation with 10 μM of L^{29} for 1 h at 37°C followed by washing thrice with 1X PBS. Incubation separately with 10 μM and 20 μM of Hg^{2+} for 1 h at 37°C and then washing with 1X PBS followed by incubation with 10 μM of L^{29} for 1 h at 37°C. Again, the fluorescence emission reduced significantly in presence of 10 μM of Na_2S, acting as a quencher.

3.4. Conclusions

A simple fluorescein-based reversible chemosensor L^{29} has been developed which selectively and sensitively recognises Hg^{2+} over other competing metal ions in 100% aqueous medium at pH 7.2 (10 mM HEPES buffer), temperature 25^0C with 44 fold fluorescence enhancement due to spirolactam ring opening upon coordination with Hg^{2+} in a 1:1 mole ratio as evidenced from Job's method and ESI-MS^+ (m/z) studies. The corresponding LOD was found to be 92.7 nM. Theoretical calculations established the metal–ligand binding through optimizing their structures. The cell imaging and MTT assay experiments further demonstrated the cell permeability and negligible cytotoxicity making the probe suitable for the assessment of Hg^{2+} in biological systems. Thus, L^{29} meets all the requirements to be an excellent fluorescent probe for wide applications in the field of bio-labelling, bio sensing, imaging and so on. **Table 3.3** has been prepared to compare a few aspects e.g working medium, limit of detection, biological study, reversibility and quantum yield of some recently published chemosensors for the Hg^{2+} ion[43-48]. Most of the biological studies and logic gate operation were not done. Also most of the studies were done mixed organo-aqueous or organic medium.

Table 3.3. Comparison of few aspects of some recently published fluorescent chemosensors for Hg^{2+} ion

Probe		Working System	LOD	Biological	Reversibility	Logic Gate	Quantum Yield	Ref
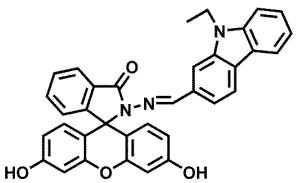	Turn On	EtOH/H_2O (1/1, v/v)	40 nM		-	-	-	43
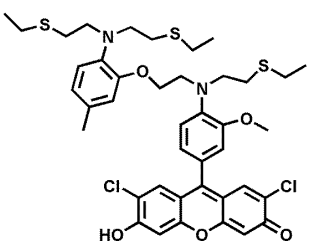	Turn On	H_2O/Methanol (95/5, v/v)	22.06 ppb	done	-	-	-	44
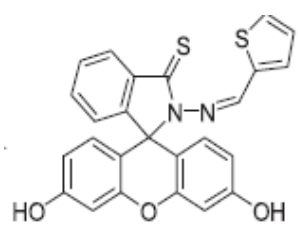	Turn Off	EtOH/HEPES (1:1, v/v,)	37 nM	Done	Done	-	-	45
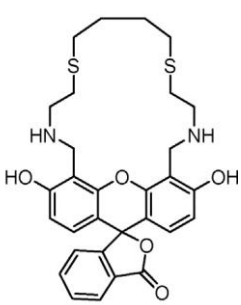	Turn Off	95:5 Tris–HCl buffer:MeOH	7.38 nM		-	-	0.56	46

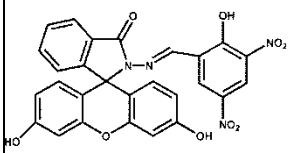	Turn On	aqueous HEPES buffer: MeOH (8 : 2 v/v)	4.13X10^{-7} M		Done	Done	0.095	47
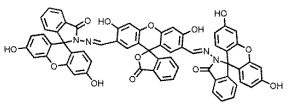	Turn On	EtOH-H_2O (v/v, 8/2).	1.16 µM	-	Done	-	0.258	48
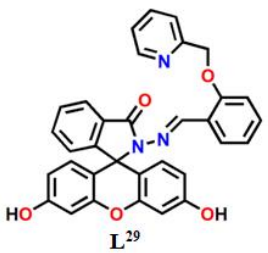 L^{29}	Turn On	aqueous	92.7 nM	Done	Done	Done	0.143	

References

1 S. A. Counter and L. H. Buchanan, *Toxicol Appl. Pharmacol.*, 2004, **198,** 209–30.

2 H. Kariyanna and G. S. Sitaram, *J. Appl. Geochem.*, 2007, **9,** 142–9.

3 I. Al-Saleh, I. Al-Doush, *J Toxicol Environ Health.*, 1997, **51,** 123–30.

4 E. K. Silbergeld, *Am. J. Public Health.*, 2008, **98,**1350.

5 H. H. Harris, I. J. Pickering and G. N. George, *Science*, 2003, **301,** 1203.

6 S. Yoon, A. E. Albers, A. P. Wong and C. J. Chang, *J. Am. Chem. Soc.*, 2005, **127,** 16030.

7 E. M. Nolan and S. J. Lippard, *Chem. Rev.*, 2008, 108, 3443.

8 H. H. Harris, I. J. Pickering and G. N. George, *Science*, 2004, **303,** 764.

9 S. K. Arya and S. Bhansali, *Chem. Rev.*, 2011,**111,** 6783.

10 A. K. Manna, J. Mondal, R. Chandra, K. Rout and G. K. Patra, *J. Photochem. Photobiol. A: Chemistry* 2018, **356,** 477- 488.

11 N. Wanichacheva, M. Siriprumpoonthum, A. Kamkaew and K. Grudpan, *Tetrahedron Letters*, 2009, **50,** 1783– 1786.

12 W. Liu, J. Chen, L. Xu, J. Wu, H. Xu, H. Zhang and P. Wang, *Spectrochimica Acta Part A: Molecular and Biomolecular Spectroscopy*, 2012, **85,** 38–42.

13 X. Hu, X. Zhang, G. He, C. He, and C. Duan, *Tetrahedron*, 2011, **67,** 1091–1095.

14 J. F. Zhang, J. S. Kim, *Anal. Sci.*, 2009, **25,** 1271−1281.

15 A. Ajaya ghosh, P. Carol and S. Sreejith, *J. Am. Chem. Soc.*, 2005, **127,** 14962.

16 J. W. Lee, H. S. Jung, P. S. Kwon, J. W. Kim, R. A. Bartsch, Y. Kim, S. Kim and J. S. Kim, *Org. Lett.*, 2008, **10,** 3801.

17 L. Xue, Q. Liu and H. Jiang, *Org. Lett.*, 2009, **11,** 3454.

18 M. Leermakers, W. Baeyens, P. Quevauviller and M. Horvat, Trends, *Anal. Chem.*, 2005, **24,** 383.

19 C. C. Huang and H. T. Chang, *Anal. Chem.*, 2006, **78,** 8332.

20 S. Cai, Y. Lu, S. He, F. Wei, L. Zhao and X. Zeng, *Chem. Commun.*, 2013, **49,** 822.

21 Hydrogen Sulfide; World Health Organization: Geneva, 1981(Environmental Health Criteria, No. 19).

22 R. E. Gosselin, R. P. Smith, H. C. Hodge, Hydrogen Sulfide. In Clinical Toxicology of Commercial Products, Williams and Wilkins: Baltimore, MD, 1984; pp. III-198−III-202.

23 S. A. Patwardhan and S. M. Abhyankar, *Colourage*, 1988, **35,** 15−18.

24 R. Wang, F. Yu, L. Chen, H. Chen, L. Wang and W. Zhang, *Chem. Commun.*, 2012**, 48,** 11757.

25 P. A. Patnaik, Wiley: New York, 2007.

26 A. K. Manna, J. Mondal, R. Chandra, K. Rout and G. K. Patra, *Analytical Methods* , 2018, **10 (20),** 2317-2326.

27 X. Bao, Q. Cao, X. Wu, H. Shu, B. Zhou, Y. Geng and J. Zhu, Tetrahedron *Tet. Lett.*, 2016, **57,** 942-948.

28 A. S. M. Islam, R. Bhowmick, H. Mohammad, A. Katarkar, K. Chaudhuri and M. Ali, *New J. Chem.*, 2016, **40,** 4710.

29 M. J. Frisch, G. W. Trucks, H. B. Schlegel, G. E. Scuseria, M. A. Robb, J. R. Cheeseman, G. Scalmani, V. Barone, B. Mennucci, G. A. Petersson, H. Nakatsuji, M. Caricato, X. Li, H. P. Hratchian, A. F. Izmaylov, J. Bloino, G. Zheng, J. L. Sonnenberg, M. Hada, M. Ehara, K. Toyota, R. Fukuda, J. Hasegawa, M. Ishida, T. Nakajima, Y. Honda, O. Kitao, H. Nakai, T. Vreven, J. A. Montgomery Jr., J. E. Peralta, F. Ogliaro, M. Bearpark, J. J. Heyd, E. Brothers, K. N. Kudin, V. N. Staroverov, R. Kobayashi, J. Normand, K. Raghavachari, A. Rendell, J. C. Burant, S. S. Iyengar, J. Tomasi, M. Cossi, N. Rega, J. M. Millam, M. Klene, J. E. Knox, J. B. Cross, V. Bakken, C. Adamo, J. Jaramillo, R. Gomperts, R. E. Stratmann, O. Yazyev, A. J. Austin, R. Cammi, C. Pomelli, J. W. Ochterski, R. L. Martin, K. Morokuma, V. G. Zakrzewski, G. A. Voth, P. Salvador, J. J. Dannenberg, S. Dapprich, A. D. Daniels, Ö. Farkas, J. B. Foresman, J. V. Ortiz, J. Cioslowski and D. J. Fox, Gaussian 09 (Revision A.1), Gaussian, Inc., Wallingford, CT, 2009.

30 (a) M. Cossi, N. Rega, G. Scalmani and V. Barone, Energies, structures, and electronic properties of molecules in solution with the C-PCM solvation model, *J. Comput. Chem.*, 2003, 24, 669–681 Cross Ref CAS PubMed. (b) A. D. Becke, Density-functional thermochemistry. III. The role of exact exchange, J. Chem. Phys., 1993, 98, 5648–5652 Cross Ref CAS. (c) C. Lee, W. Yang and R. G. Parr, Phys. Rev. B: *Condens. Matter Mater. Phys*., 1998, **37,** 785–789.

31 H. Mohammad, A. S. M. Islam, R. Bhowmick, C. Prodhan and M. Ali, *New J. Chem.*, 2019, **43,** 4710.

32 E. M. Nolan and S. J. Lippard, *Chem. Rev.*, 2008, **108,** 3443-3480.

33 A. Tamayo, B. Pedras, C. Lodeiro, L. Escriche, J. Casabo, L. Capelo, B. Covelo, R. Kiveka and R. Sillanpa, *Inorg. Chem.*, 2007, **46,** 7818-7826.

34 Y. Zhang, Y. Yang, J. Hao, C. Yin, F. Huo, J. Chao and D. Liu, *Spectrochim. Acta A*, 2014, **132,** 27-31.

35 V. R. Batistela, J. D. C. Cedran, H. P. M. D. Oliveira, I. S. Scarminio, L. T. Ueno, A. E. D. H. Machado and N. Hioka, *Dyes Pigm.*, 2010, **86,** 15-24.

36 L. N. Bogdanova, N. O. Mchedlov-Petrossyan, N. A. Vodolazkaya and A. V. Lebed, *Carbohydr. Res.*, 2010, **345,** 1882-1890.

37 N. O. Mchedlov-Petrossyana, O. N. Tychina, T. A. Berezhnaya, V. I. Alekseeva and L. P. Savvina, *Dyes Pigm.*, 1999, **43,** 33-46.

38 R. Sjoback, J. Nygren and M. Kubista, *Spectrochim. Acta A*, 1995, **51,** 7-21.

39 C. R. Lohani, J. M. Kim, S. Y. Chung, J. Yoon and K. H. Lee**,** *Analyst*, 2010, **135,** 2079-2084.

40 Y. Yang, F. Huo, C. Yin, Y. Chu, J. Chao, Y. Zhang, J. Zhang, S. Li, H. Lv, A. Zheng and D. Liu, *Sens. Actuators, B*, 2013, **177,** 1189.

41 K. Tripathi, A. Rai, A. K. Yadav, S. Srikrishna, N. Kumari and L. Mishra, *RSC Adv.*, 2017, **7,** 2264.

42 E. M. Nolan, M. E. Racine and S. J. Lippard, *Inorg. Chem.*, 2006, **45,** 2742.

43 L. Huanga , Y. Suna , G. Zhaoa , L. Wang , X. Menga , J. Zhoua and H. Duan, *Journal of Molecular Structure*, 2022, **1255,** 132427.

44 D. Liu, Y. Wang , R. Wang , B. Wang , H. Chang , J. Chen , G. Yang , H. He, *Inorganic Chemistry Communications*, 2018, **89,** 46–50.

45 Y. Fenga, Z. Kuaib, Y. Songa, J. Guoa, Q. Yanga, Y. Shanb and Y. Li, *Talanta*, 2017, 170, 103–110.

46 P. Piyanucha, S. Watpathomsuba, V. S. Leeb, H. A. Nienaberc and N. Wanichacheva, *Sens. Actuators B:Chem.*, 2016, **224,** 201–208.

47 K. Tripathi, A. Rai, A. Kumar Yadav, S. Srikrishna, N. Kumari and L. Mishra, *RSC Adv.*, 2017, **7,** 2264.

48 S. Erdemir and O. Kocyigit, *Dyes Pigm.*, 2017, **145**, 72-79.

A Fluorescein-2-Hydroxy-3-hydroxymethyl-5-methyl-benzaldehyde conjugate as a highly selective and sensitive chemosensor for Hg^{2+} ions with cell imaging possibility

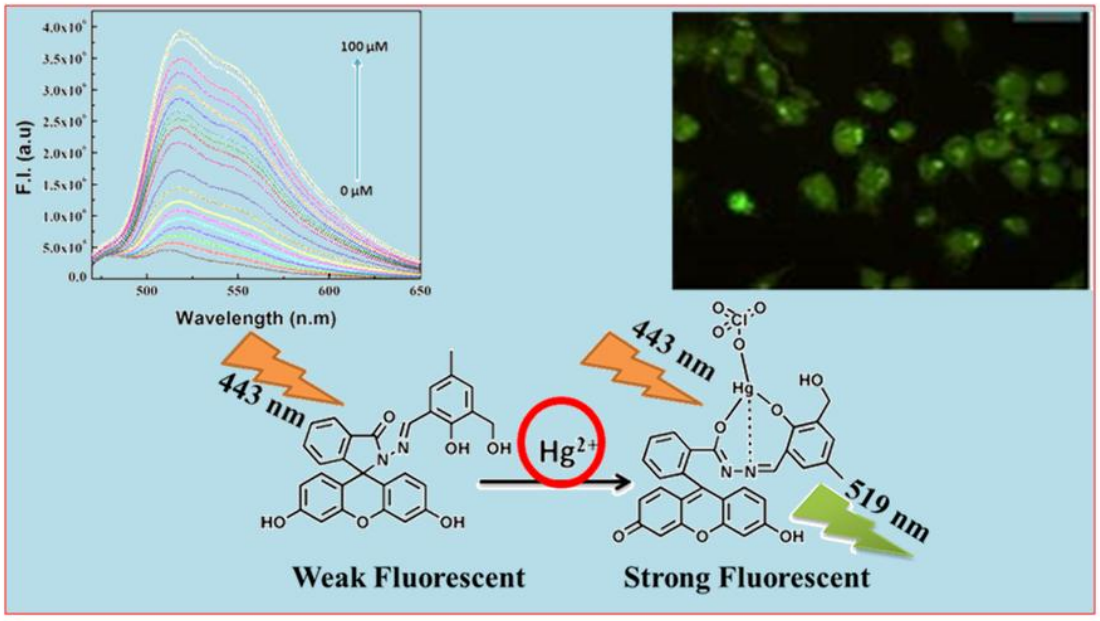

Abstract:

The design and synthesis of an effective Hg^{2+-} specific probe HL^{30} based on Fluorescein-2-Hydroxy-3-hydroxymethyl-5-methyl-benzaldehyde conjugate is reported in this chapter. The sensing performance of HL^{30} was investigated by fluorescence spectroscopy. The probe displayed excellent sensitivity and selectivity towards Hg^{2+} over other tested metal ions in CH_3OH : H_2O 7:3 medium (pH 7.2, 10 mM HEPES), which could be ascribed to the Hg^{2+} induced opening of the spirolactam ring of the flourescein moiety. The 1:1 binding of HL^{30} to Hg^{2+} was recognized by Job's method and confirmed by ESI-MS^+ (m/z) studies. The LOD value was determined by 3σ method and found to be 0.46 µM. The HL^{30} also showed bio-compatibility and low cytotoxicity and is suitable for fluorescence cell imaging of Hg^{2+} ions in live HepG2 cells.

4.1 Introduction

Heavy metal pollution has been identified as one of the major concerns of global environmental pollution problems. [1] Due to exhaust emissions, mining, sewage irrigation and the excessive use of heavy metal products, the content of heavy metal ion has surpassed the normal range which might cause damage to human health and lowers the environmental quality.[2–5] Mercury is one of the most hazardous and prevalent global pollutant.[6] The temporal and spatial distribution of Hg in the atmosphere and its transport to aquatic and terrestrial ecosystems depend primarily on its physical and chemical forms. Elemental Hg (Hg^0) may remain in atmosphere for several months to a year before oxidation and can be transported long distances. On the other hand, reactive gaseous Hg (RGM) and particulate bound Hg^{2+} have a shorter atmospheric residence resulting local or regional deposition. The Hg pollution occurs through the input of Hg largely as Hg^{2+} to ecosystems which are converted to CH_3Hg within ecosystems by bacteria.[7]

In the marine system, both elemental (Hg) and ionic (Hg^{2+}) mercury can be converted into methyl mercury, which then will be absorbed into biological membranes and entered into human food chain.[8–11] Then human, the final consumer, will accumulate mercury causing dysfunction of cells leading to various health problems in the brain, kidney, central nervous, mitosis and endocrine system, even at a very low concentration of Hg^{2+}.[12-13] Thus, developing of rapid and sensitive alytical methods are critical for monitoring the level of Hg^{2+} in the environment and biological systems.[14-15]

Nowadays, many detection methods have been developed and applied such as atomic absorption spectroscopy (AAS), inductively coupled plasma mass spectrometry (ICP-MS), electrochemical analysis etc.[16-19] However, most of these conventional methods are expensive and time-consuming, as they need sophisticated experimental apparatus and tediously long sample preparation steps. In contrast, due to less expensive, easy handing, rapid response and more importantly excellent sensitivity and selectivity, the fluorescent sensors are getting more and more attention in the field of heavy metal detection.[20–28] Various Hg^{2+} probes involving coumarin[29], pyrene [30], 1,8-naphthalimide[31], xanthenes[32], cyanine [33] and BODIPY[34] as fluorophore platform have been developed over the past few years . For detection of Hg^{2+}, most of the sensors are based on rhodamine compounds.[35–37] Among the various fluorophores, fluorescein is very common having some excellent spectroscopic properties of

longer wavelengths absorption and emission, longer, high fluorescence quantum yield, easy to prepare, fast response, good biocompatibility and low toxicity.[38] However, fluorescein-based probes have received comparatively little attention.[39-40] Herein, we have synthesized (**Scheme 4.1**) a chemosensor, HL^{30} which exhibited significant fluorescence enhancements on treatment with Hg^{2+} showing very high sensitivity and selectivity. In addition, cellular imaging experiment showed that HL^{30} could be used as a fluorescent sensor for reliably detecting Hg^{2+} in living cells.

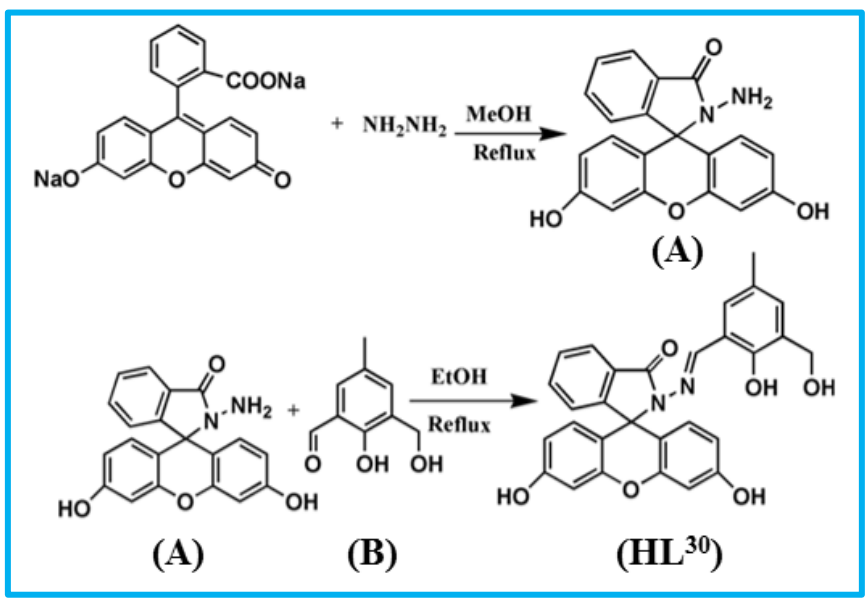

Scheme 4.1: Synthetic route of HL^{30}

4.2 Experimental section

4.2.1 Materials and Instruments

Fluorescein Sodium salt and metal salts such as perchlorates of Na^+, K^+, Ca^{2+}, Fe^{2+}, Co^{2+}, Ni^{2+}, Zn^{2+}, Pb^{2+}, Cd^{2+}, Hg^{2+} and Cu^{2+} and sodium salts of anions such as SO_4^{2-}, NO_3^-, PO_4^{3-}, S^{2-}, Cl^-, F^-, Br^-, OAc-, H_2AsO_4-, N_3^-, ClO4-, PPi, $S_2O_4^{2-}$, HCO_3^-, SCN^-, CO_3^{2-}, $P_2O_7^{4-}$ and NO_2^- were purchased from Sigma–Aldrich and used as received. All solvents used for the synthetic purposes were of reagent grade (Merck) unless otherwise mentioned. For spectroscopic (UV/Vis and fluorescence) studies HPLC-grade MeCN and deionized water from Milli-Q Millipore were used.

UV/Vis absorption spectra were recorded on an Agilent 8453 diode array spectrophotometer. Steady-state fluorescence studies were carried out with a PTI (QM-40) spectrofluorimeter.

NMR spectra were recorded on a Bruker spectrometer at 300 MHz. The ESI-MS^+ spectra were recorded on a Waters XEVO G2QTof mass spectrometer.

4.2.2 Solution Preparation for UV-Vis/fluorescence studies

For fluorescence studies, a stock solution 1.0 x 10^{-3} M of HL^{30} was prepared by dissolving required amount of ligand in 9 ml MeOH and finally the volume was adjusted to 10 ml by de-ionized water. In a similar way, 1.0 x 10^{-3} M stock solution of Hg^{2+} was prepared in MeOH. A 250 mL 10 mM HEPES buffer solution in 7:3 MeOH: H_2O (v/v) was prepared and pH was adjusted to 7.2 by using HCl and NaOH. 2.5 ml of this buffer solution was pipetted out into a cuvette to which required volume of 1.0 x 10^{-3} M probe was added to achieve 20 µM final concentrations for fluorescence titration. In a regular interval fixed volume of Hg^{2+} ions were added incrementally and fluorescence spectra were recorded for each solution. The cuvettes of 1 cm path length were used for absorption and emission studies. Fluorescence measurements were performed using 3 nm x3 nm slit width.

4.2.3 Preparation of Fluorescein Hydrazide (A)

Fluorescein Hydrazide was prepared according to the method described in Chapter 2.[41]

4.2.4 Preparation of 2-Hydroxy-3-hydroxymethyl-5-methyl-benzaldehyde (B):

2-Hydroxy-3-hydroxymethyl-5-methyl-benzaldehyde was prepared according to a literature method.[42] 2,6-Bis(hydroxymethyl)-4-methylphenol (20g, 0.12mol) was placed in a 500 mL flask and stirred witha suspension of MnO_2 (100g, 1.14mol) in $CHCl_3$ (300mL) for 16 h at room temperature. The mixturewas filtered and washed with $CHCl_3$ for several times until the filtrate became colourless. The solventwas removed and the residue was recrystallized from EtOH/H_2O (1:3, v:v) to give yellowish needles (yield: 7.6g, 38).

4.2.5 Synthesis of the receptor (HL^{30}):

In a 250 mL RB flask Fluorescein Hydrazide (0.692 g, 2 mmol) and 2-Hydroxy-3-hydroxymethyl-5-methyl-benzaldehyde (0.332 g, 2 mmol) were suspended in 20 mL ethanol. The mixture was refluxed for 6 hr with stirring to form a clear solution. Following the reaction, the mixture was allowed to cool to room temperature. The pale yellow solid precipitated was separated by filtration and washed with 3x 10 mL ethanol. 70% yield was obtained.

Analysis: ^{1}H NMR (DMSO-d_6): δ = 10.527(s, 1 H), 10.0316 (s, 2 H), 8.929 (s, 1 H), 7.962 (d, 1 H), 7.65 (m, 2 H), 7.189(s, 1 H), 7.133(d, 2 H), 6.930 (s, 1 H), 6.687 (d, 2 H), 6.572(m, 4 H), 5.06 (t, 1 H), 4.417 (d, 2 H), 2.118(s, 3 H) ppm **(Figure 4.1)**.. IR: ṽ = 1613 cm^{-1} (–C=N), -OH (3188 cm^{-1}), -C=O (1667 Cm^{-1}) (**Figure 4.2**). ESI-MS^{+} : m/z= 495.1458 (**$C_{29}H_{22}N_2O_6$ + H^{+}**) (**Figure 4.3**).

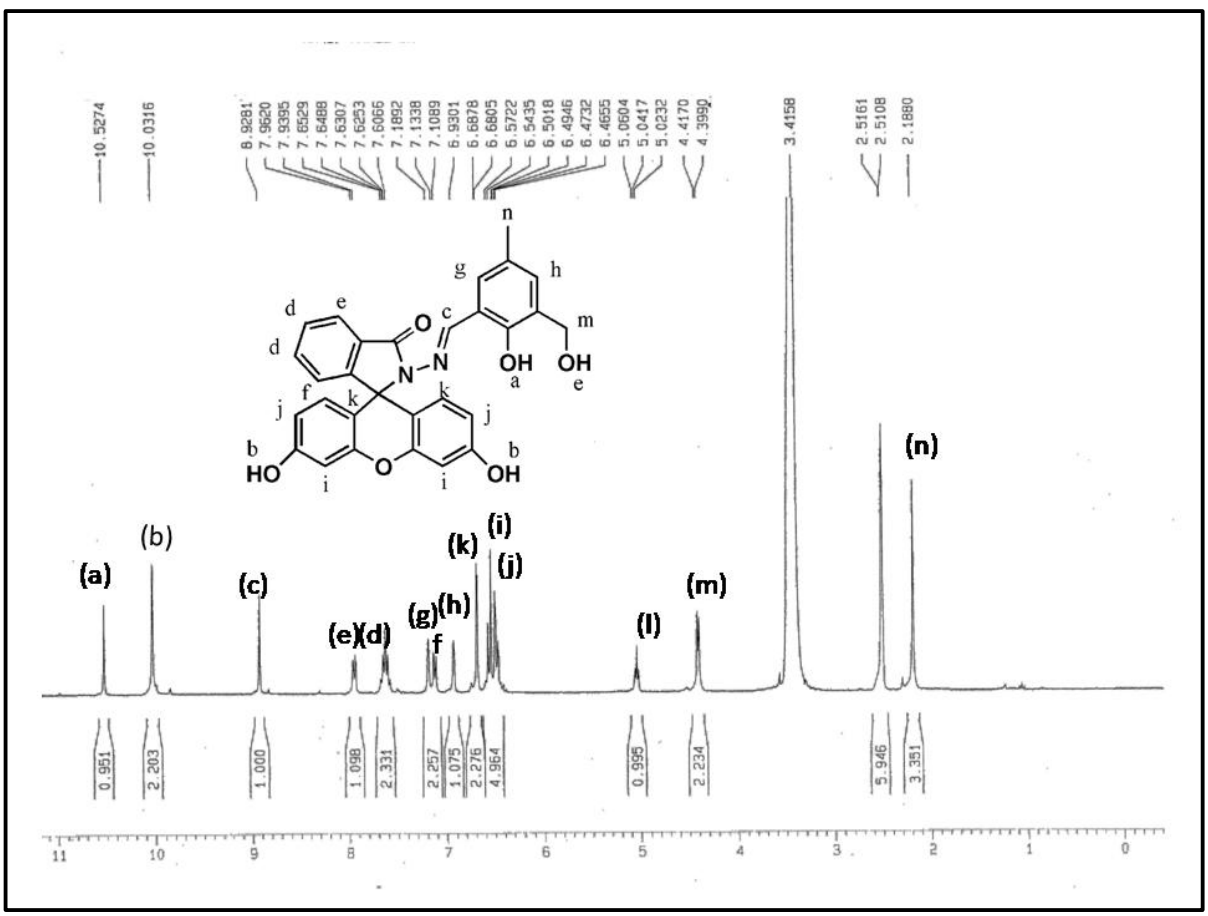

Figure 4.1. ^{1}H-NMR spectrum of HL[30] in DMSO-d_6.

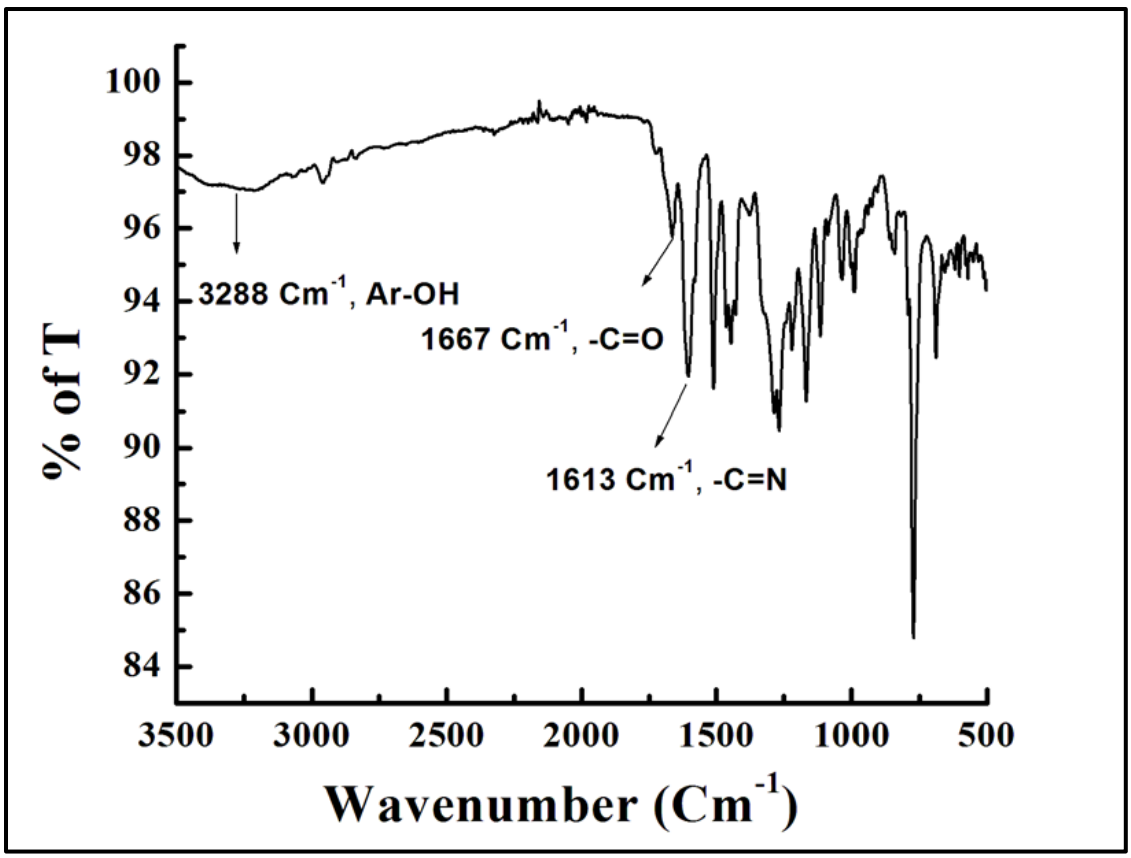

Figure 4.2. IR spectrum of HL^{30}.

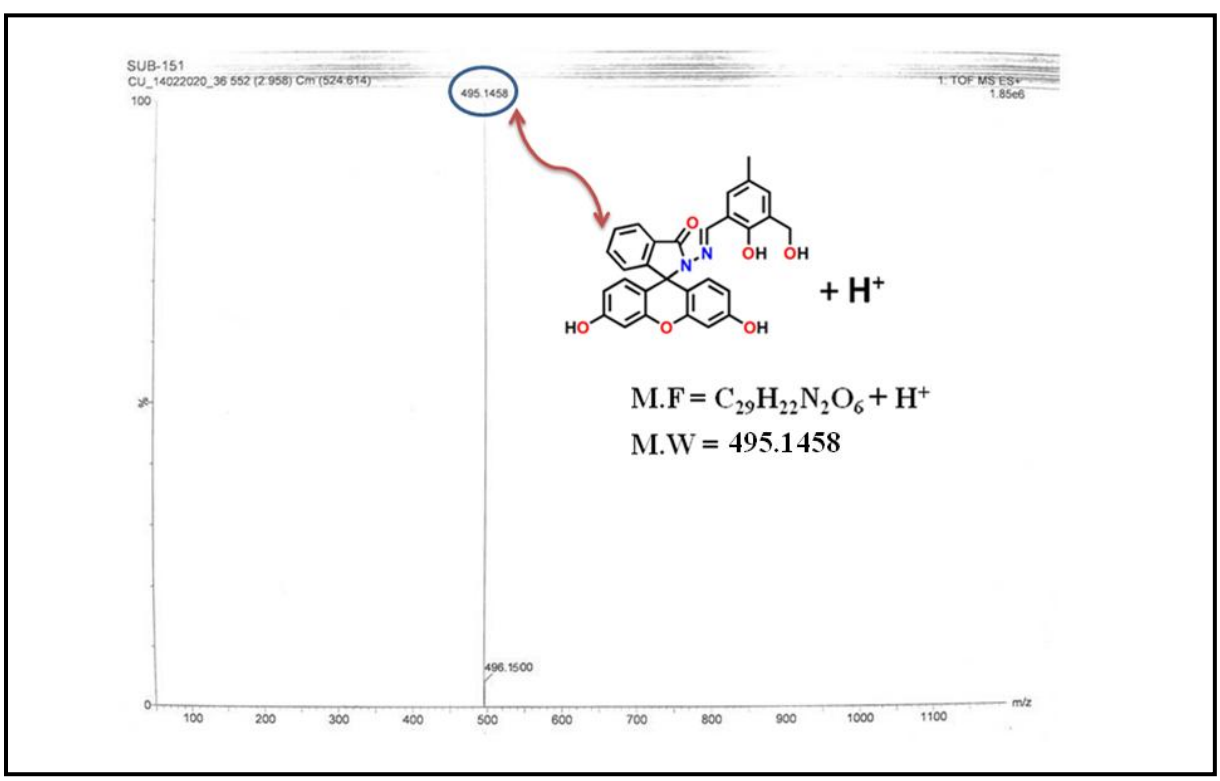

Figure 4.3. Mass spectrum of HL^{30} in MeOH.

4.2.6 Preparation of complex HL^{30}-Hg^{2+}:

$Hg(ClO_4)_2$ (0.272 g, 0.6 mmol) was added to a 10 mL MeOH solution of HL^{30} (0.255 g, 0.5 mmol) and the mixture was stirred for about 30 minutes. It was then filtered and allowed to evaporate slowly at ambient temperature to get crystalline solid product.

Analysis : ^{1}H NMR (DMSO-d_6): δ = 10.215 (s, 1 H), 10.000 (s, 1 H), 8.824 (s, 1 H), 7.927 (d, 1 H), 7.50 (m, 3 H), 7.27 (s, 1 H), 7.103 (d, 2 H), 6.746 (s, 1 H), 6.642 (m, 2 H), 6.467 (m, 4 H), 4.566 (t, 1 H), 4.511 (s, 2 H), 2.082 (s, 3 H) ppm (**Figure 4.4**). IR: $\tilde{\nu}$ = 1578 cm^{-1} (–C=N), -OH (3372 cm^{-1}), -C=O (1613 Cm^{-1}) (**Figure 4.5**). ESI-MS$^-$: *m*/*z*= 793.0594 (**$C_{29}H_{22}ClHgN_2O_{10}$**) (**Figure 4.6**).

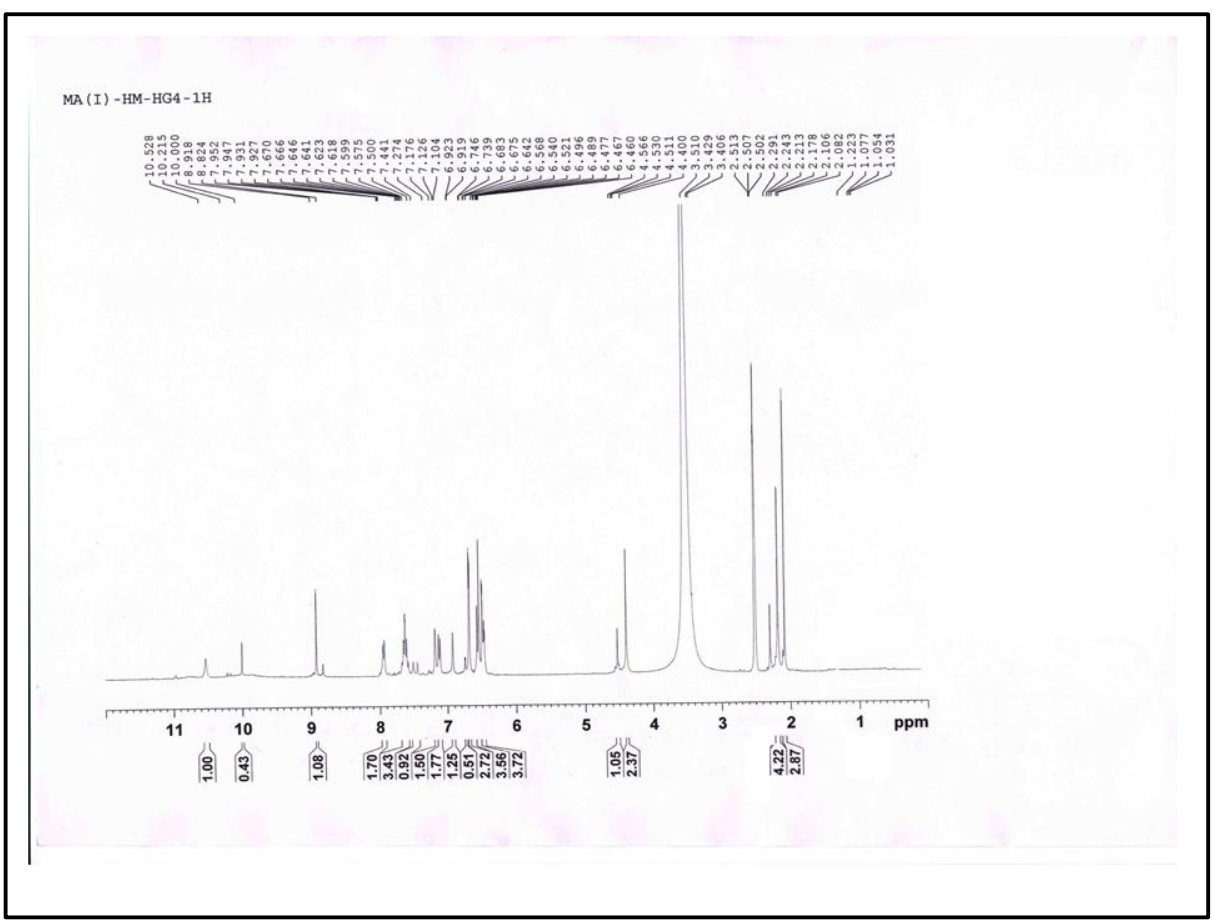

Figure 4.4. ^{1}H-NMR spectrum of HL^{30}-Hg^{2+} in DMSO-d_6.

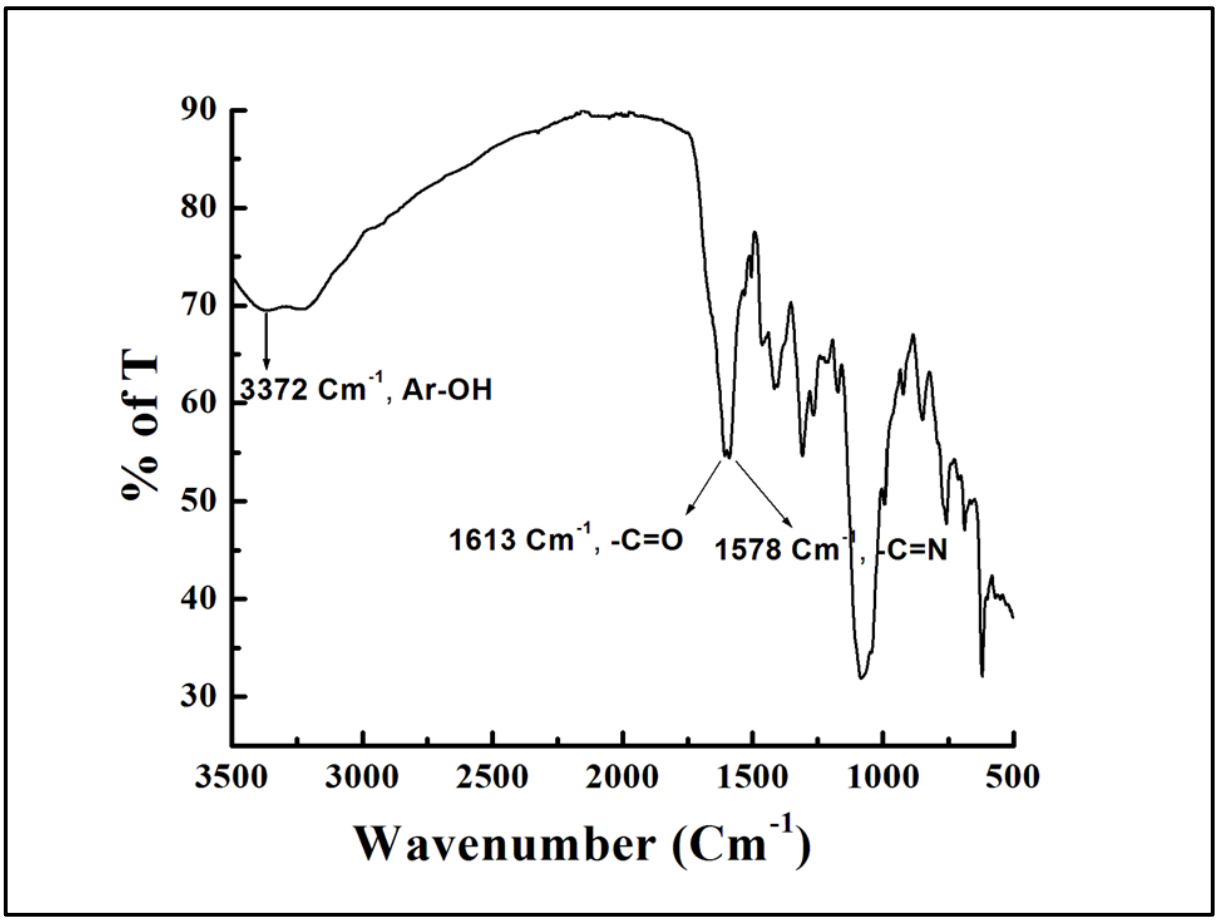

Figure 4.5. IR spectrum of HL^{30}-Hg^{2+}.

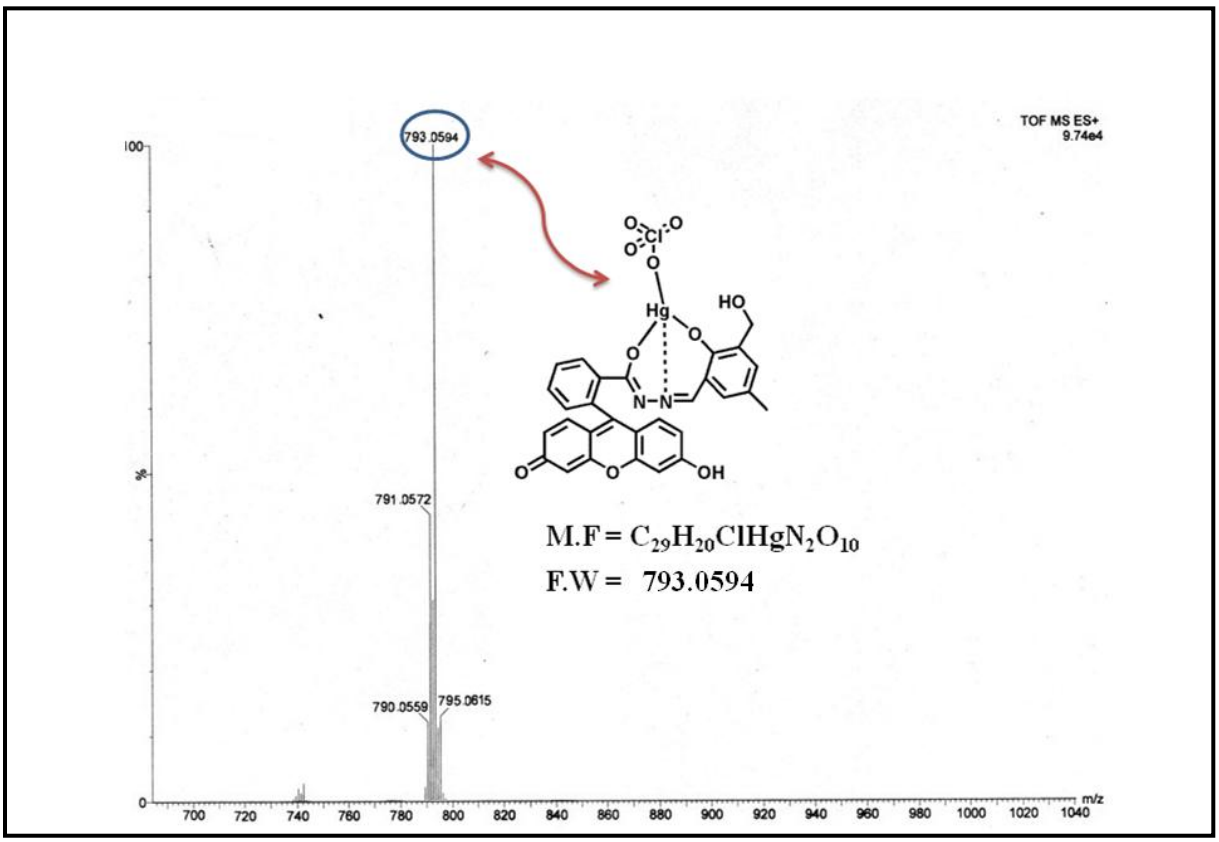

Figure 4.6. ESI-MS^{-}(m/Z) mass spectrum of $[HL^{30}\text{-}Hg^{2+}]^{-}$ complex in MeOH.

4.2.7 Cell culture

Human hepatocellular liver carcinoma cells (HepG2) (NCCS, Pune, India), were grown in DMEM supplemented with 10% FBS and antibiotics (penicillin-100 µg/ml; streptomycin-50 µg/ml). Cells were cultured at 37ºC in 95% air, 5% CO_2 incubator.

4.2.8Cell Cytotoxicity Assay

Cytotoxicity for ligand HL^{30} was evaluated with the help of 3-(4,5-dimethylthiazol-2-yl)-2,5-diphenyltetrazolium bromide (MTT). HepG2 cells (1 × 105 cells/well) were cultured in a 96-well plate at incubated at 37°C, and were exposed to varying concentrations of HL^{30} (1, 5, 10, 20, 30, 40, 50, 60, 70, 80, 90 and 100 µM) for 24 hours. After the incubation, 10 µl of MTT solution [5 mg/ml, dissolved in 1X phosphate-buffered saline (PBS)] was added to each well of a 96-well culture plate, and then incubated at 37 ^{0}C for 4 hours. Media were decanted from wells and 100 µL of 0.04 N acidic isopropyl alcohol was added into each well to solubilize the intracellular formazan crystals (blue-violet) formed. Absorbance of the solution was

measured at 595 nm wavelength (EMax Precision MicroPlate Reader, Molecular Devices, USA). Values were calculated as mean ± standard errors of three independent experiments. The cell viability was expressed as the optical density ratio of the treatment to control.

4.2.9 Cell Imaging Study

HepG2 Cells were cultured in 35 x 10 mm culture dish on a cover slip for 24 h at 37°C. The cells were treated with 5µm solutions of HL^{30}, prepared by dissolving HL^{30} to the mixed solvent DMSO: water = 1:9 (v/v) and incubated for 1 hour at 370C. For Hg^{2+} complex formation study, HepG2 cells were pre-incubated with varying concentrations of Hg^{2+} (5 µM, 10 µM and 20 µM) for 60 min at 37 ^{0}C followed by incubation with 5µM of HL^{30} for 60 min at 37 °C, and subsequent washing for three times with 1X PBS. Fluorescence images of HepG2 cells were taken by a fluorescence microscope (Leica DM3000, Germany) with an objective lens of 40X magnification.

4.3 Results and Discussion

A Schiff base condensation between **A** and **B** in methanol (Scheme 1) under refluxing conditions affords HL^{30}, which was thoroughly characterized by ^{1}H-NMR, IR and ESI-MS^{+} studies. The spectral data were in agreement with the desired structures.

4.3.1 Fluorescence Studies:

We executed fluorescence titration to examine the interaction between HL^{30} and Hg^{2+} in methanol and 10 mM HEPES buffer at pH 7.2. (H_2O:CH_3OH = 3:7). The solution of free HL^{30} displayed a very weak fluorescence in the visible region at around 519 nm. However, on incremental addition of Hg^{2+}, the same solution exhibited notable enhancement of increasing fluorescence intensity with band centered at λ_{em} = 519 nm, on excitation at λ_{ex} = 443 nm. (**Figure 4.7**).This has been attributed to the opening of the spirolactam ring.

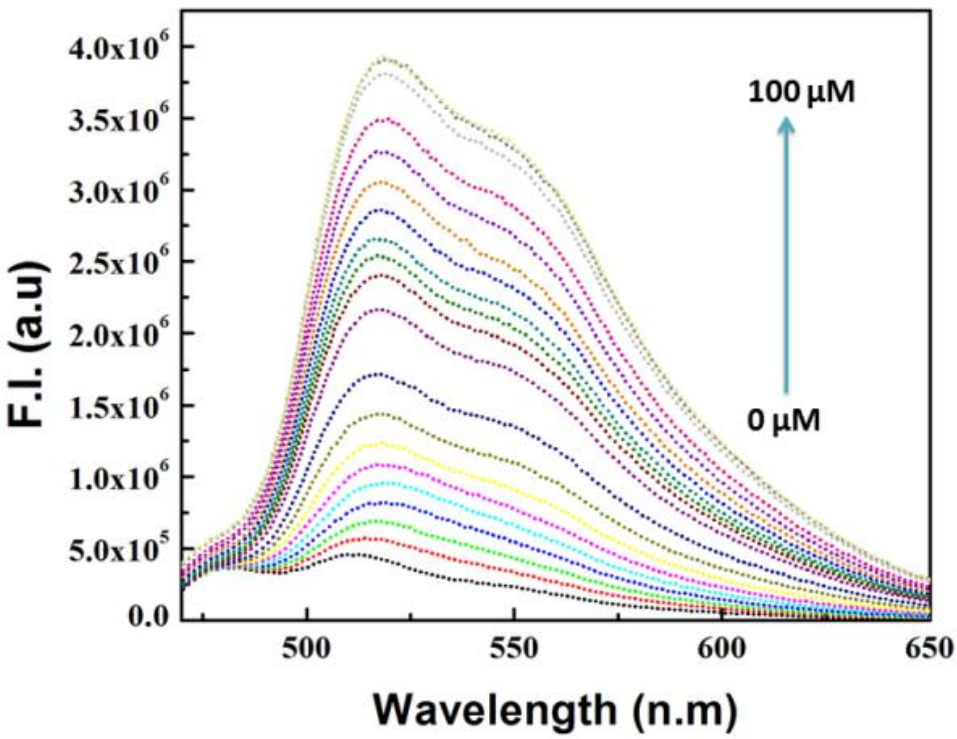

Figure 4.7. Fluorescence titration of HL^{30} (20.0 µM) in HEPES buffer with H_2O:CH_3OH = 3:7(v/v) at pH 7.2, λ_{em} = 519 nm on excitation at λ_{ex} = 443 nm.

A Benesi-Hildebrand plot of $(F_{max}-F_0)/(F-F_0)$ vs $1/[Hg^{2+}]$ gives a straight line with a slope K_d= (1.18 ± 0.01) x 10^{-4}) suggesting a moderately binding of HL^{30} towards Hg^{2+} (**Figure 4.8**). The 1:1 stoichiometry of the Hg^{2+} complex with HL^{30} was determined by Job's method (**Figure 4.9**).

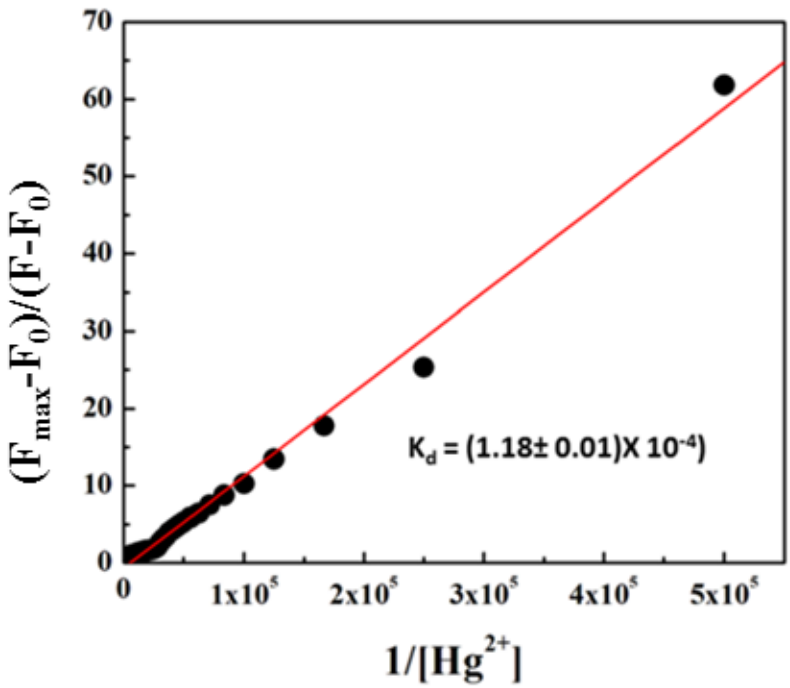

Figure 4.8. Benesi–Hildebrand plot of F.I (at 519 nm) vs [Hg^{2+}] for the corresponding emission titration.

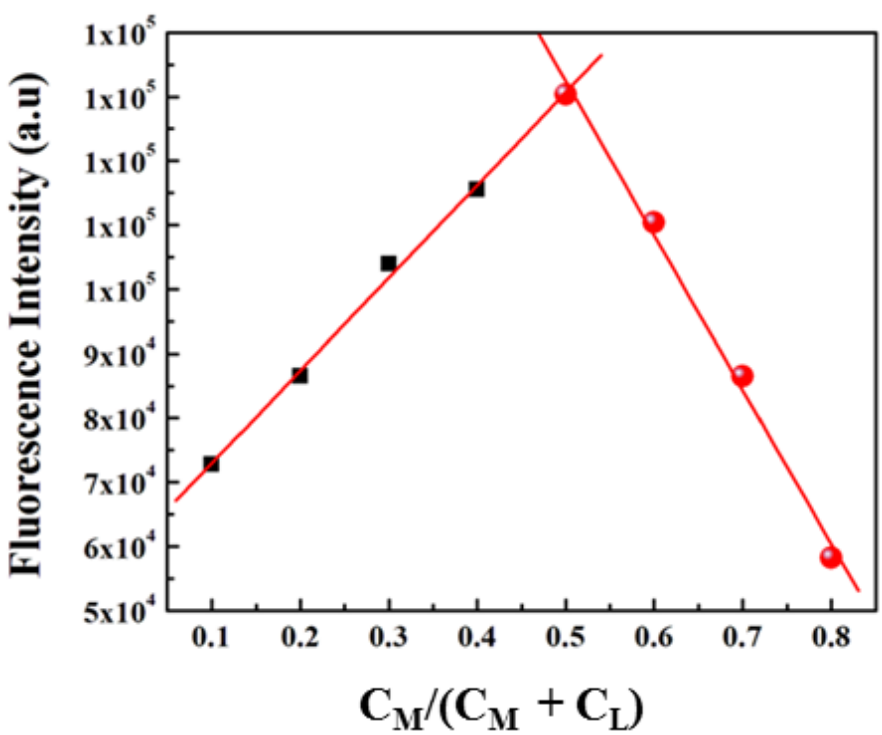

Figure 4.9. 1:1 binding stoichiometry shown by Job's plot.

4.3.2 Selectivity

The detection of Hg^{2+} was not affected by the presence of biologically abundant metal ions like Na^{+}, K^{+}, Ca^{2+} and Mg^{2+}. Likewise, under identical reaction conditions no significant colour or spectral change was observed for transition-metal ions, namely Cr^{3+}, Mn^{2+}, Fe^{2+}, Fe^{3+}, Co^{2+}, Cu^{2+}, Ni^{2+} and Zn^{2+}, and heavy-metal ions, like $Cd^{2+}$and Pb^{2+} (**Figure 4.10**) and also anions like SO_4^{2-}, NO_3^{-}, PO_4^{3-}, S^{2-}, Cl^{-}, F^{-}, Br^{-}, OAc^{-}, H_2AsO^{4-}, N_3^{-}, ClO_4^{-}, PPi, $S_2O_4^{2-}$, HCO_3^{-}, SCN^{-}, CO_3^{2-}, $P_2O_7^{4-}$ and NO_2^{-} (**Figure 4.11**).

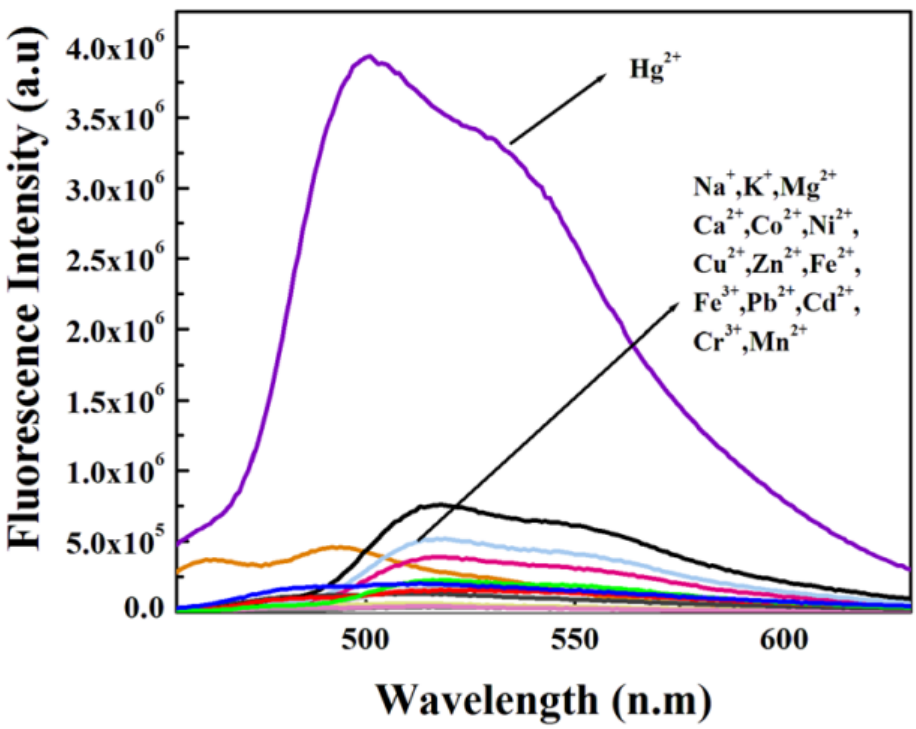

Figure 4.10. Fluorescence spectra of HL^{30} (20.0 μM) in the presence of different cations (100 μM) at pH 7.2 with H_2O:CH_3OH = 3:7(v/v), λ_{em} = 519 nm on excitation at λ_{ex} = 443 nm.

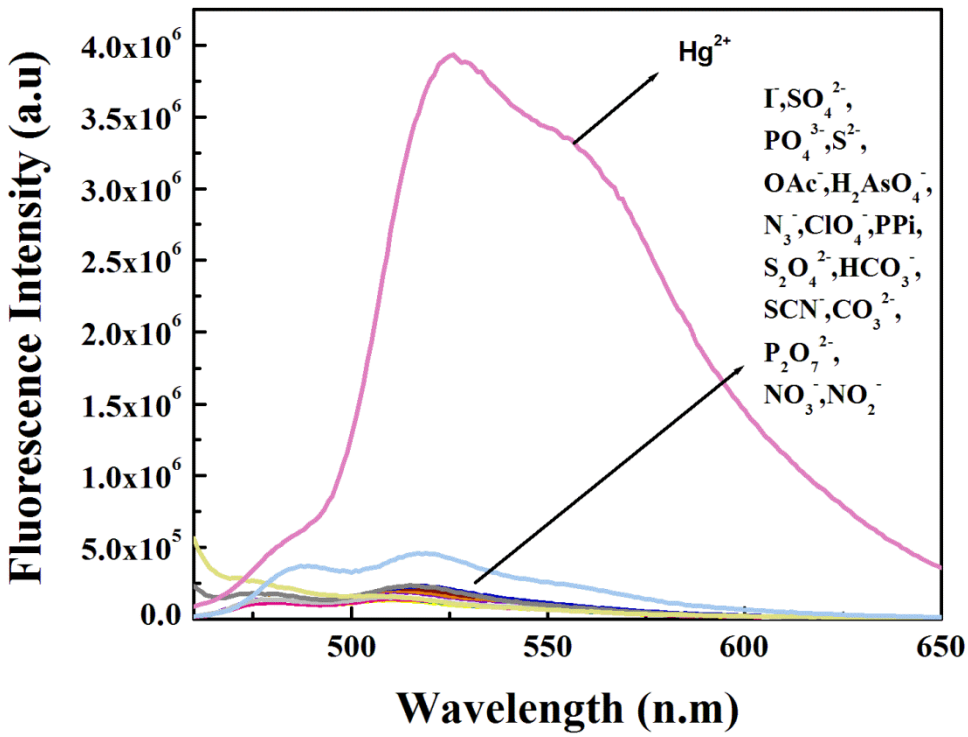

Figure 4.11. Fluorescence spectra of HL^{30} (20.0 μM) in the presence of different anions (100 μM) at pH 7.2, λ_{em} = 519 nm on excitation at λ_{ex} = 443 nm.

4.3.3 Mechanism of ring opening:

The characteristic stretching frequency of the –C=O bond of the flourescein moiety at 1667cm^{-1} is shifted to a lower wave number (1613 cm^{-1}) with the addition of of Hg^{2+} (**Figure 4.5**) indicating a strong polarization of the –C=O bond upon efficient binding to the Hg^{2+} ion and also the stretching frequency of the (-CH=N) bond at 1613 cm^{-1} is significantly shifted to a lower wave number (1588 cm^{-1}). This supports the participation of azomethine nitrogen of HL^{30} in bonding with Hg^{2+}. To further explore the complexation between HL^{30} with Hg^{2+}, ^{1}H NMR spectrum was generated (**Figure 4.4**) in DMSO-d_6. The one of the two separate phenolic -OH proton (b proton) signals of HL^{30} vanishes. These results clearly validate the spirolactam ring opening mechanism of the probe and one of the phenolic –OH tautomerized to –C=O.[43] Thus, based on ^{1}H-NMR, IR, ESI-MS$^+$ and Job's plot, we proposed a probable mechanism of binding of Hg^{2+} ions to HL^{30} as shown in (**Scheme 4.2**).

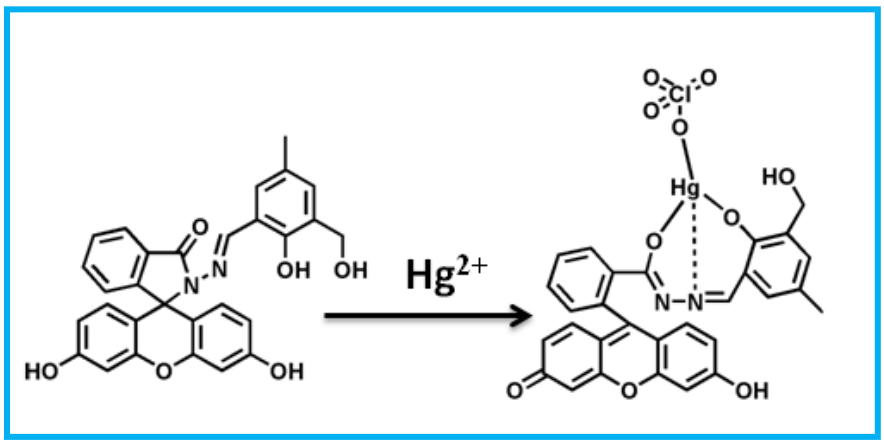

Scheme 4.2. Proposed mechanism for the recognition of Hg^{2+}.

4.3.4 pH Stability Check:

The pH-titration was performed to investigate the practical applicability of HL^{30}. The effect of pH on the fluorescence response of HL^{30} towards Hg^{2+} ions was examined in a series of solution with different pH values, ranging from 2.0 to 10.0. In the absence of Hg^{2+}, it reveals no obvious fluorescence emission of HL^{30} between pH 2.0 to 10.0, indicating that the spirolactam form of HL^{30} was the dominant conformation and the sensor was stable in a wide range of pH. However, in the presence of Hg^{2+}, the fluorescence intensity was enhanced under different pH values from 6.0 to 8.0, especially from 7.0 to 8.0, which suggested that the Hg^{2+} ions induces the formation of the ring-opened HL^{30}-Hg^{2+}complex (**Figure 4.12**).Therefore, considering that the physiological environment is slightly alkaline, so we chose pH 7.2, as it becomes fluorescent between the pH 6.5-8.0 suggesting a convenient application of this probe under physiological conditions.

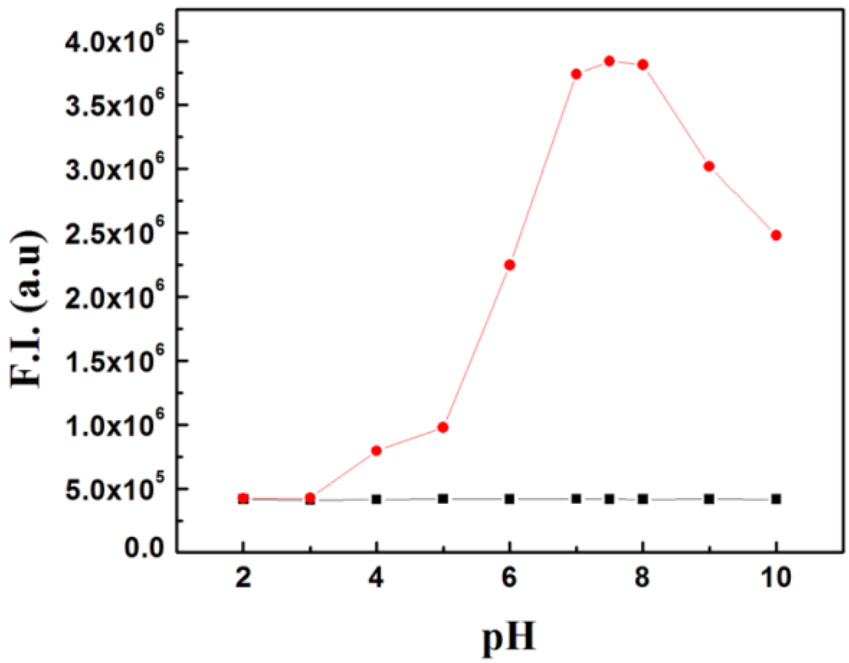

Figure 4.12. pH dependence of the Fluorescence Intensity of the free ligand HL^{30} (black) and the [HL^{30}-Hg^{2+}] complex (red) in the HEPES buffer medium with λ_{em} = 519 nm with H_2O: CH_3OH = 3:7(v/v) on excitation at λ_{ex} = 443 nm.

4.3.5 Determination of LOD:

The 3σ method was adopted to determine the limit of detection (LOD) of Hg^{2+} and was found to be as low as 0.46 μM (**Figure 4.13**) which indicates that HL^{30} is an ideal chemosensor for Hg^{2+} ion.

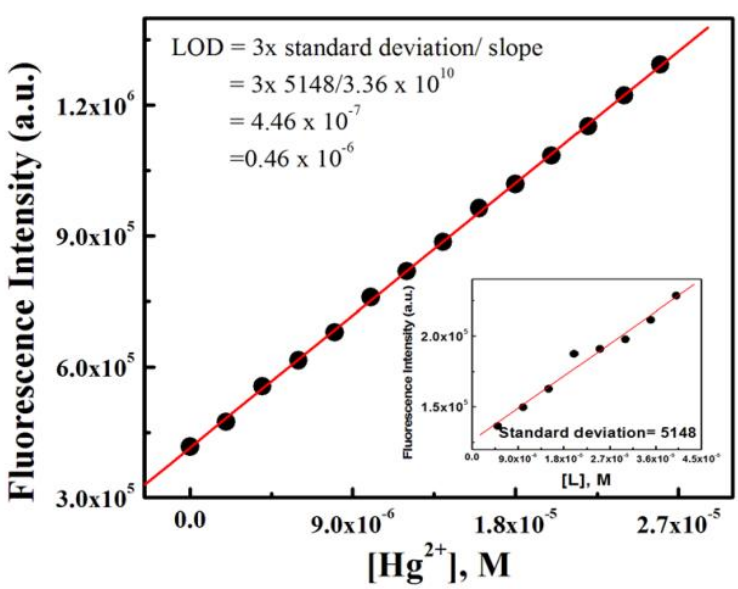

Figure 4.13. LOD of Hg^{2+} with H_2O:CH_3OH = 3:7(v/v) in HEPES buffer medium with λ_{em} = 519 nm on excitation at λ_{ex} = 443 nm.

4.3.6 Cell imaging studies:

Taking into account the highly specific selective nature of HL^{30} in the detection of Hg^{2+} ions, it has been further checked for its Hg^{2+} sensing ability in living cells. To determine whether HL^{30} has any cytotoxic effects, a cell viability assay using MTT was performed by calculating % cell viability on HepG2 cells (**Figure 4.14**). There was no significant reduction in the tetrazolium salt (reflected by a decrease in formazan production) for HL^{30} up to 10 µM, thus suggesting that bellow 10 µM concentration of HL^{30} the probe would be much more effective for the analysis of its complex formation with Hg^{2+} ions *in vitro*. A cell viability higher than 90% was observed for HL^{30} at 5 µM, after which the viability of the HepG2 cells decreases. Hence, further experiments were carried out with 5 µM of HL^{30} for treatment.

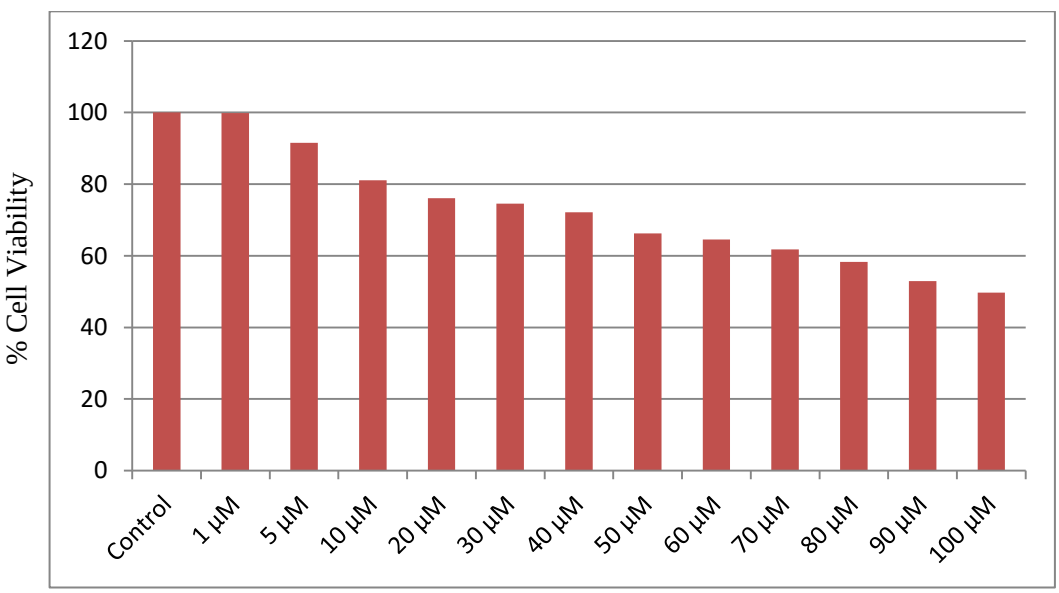

Figure 4.14. Percent (%) cell viability of HepG2 cells treated with different concentrations (1-100 µM) of HL^{30} for 24 hours determined by MTT assay.

The ligand HL^{30} exhibited no intracellular fluorescence on HepG2 cells treated with 5µM of the ligand and incubated for 1 hour (**Figure 4.15**), however, prominent intracellular green fluorescence signal was observed when the HepG2 cells were incubated with 5 µM of Hg^{2+} for 60 min at 37 ^{0}C, followed by incubation with 5 µM of HL^{30}. The intracellular

fluorescence was found to be prominently localized in the cytoplasmic region, suggesting that HL^{30} is specifically making complex with the Hg^{2+} ions transported to the cytoplasm. Keeping the ligand HL^{30} concentration constant (5μM), and increasing concentration Hg^{2+} (from 5 μM, 10 μM and 20 μM) shows Hg^{2+} ion concentration-dependent enhancement in the intracellular blue fluorescence, caused by the more and more formation of complex with HL^{30} with increasing concentration of Hg^{2+}. Intense intracellular fluorescence was observed due to complex formation between Hg^{2+} and the ligands HL^{30} nearly at 20 μM of Hg^{2+}. Hence the present ligand with low cytotoxicity and biocompatiblility for cellular cytoplasmic Hg^{2+} ion detection, can be used for Hg^{2+} ion detection in biological samples.

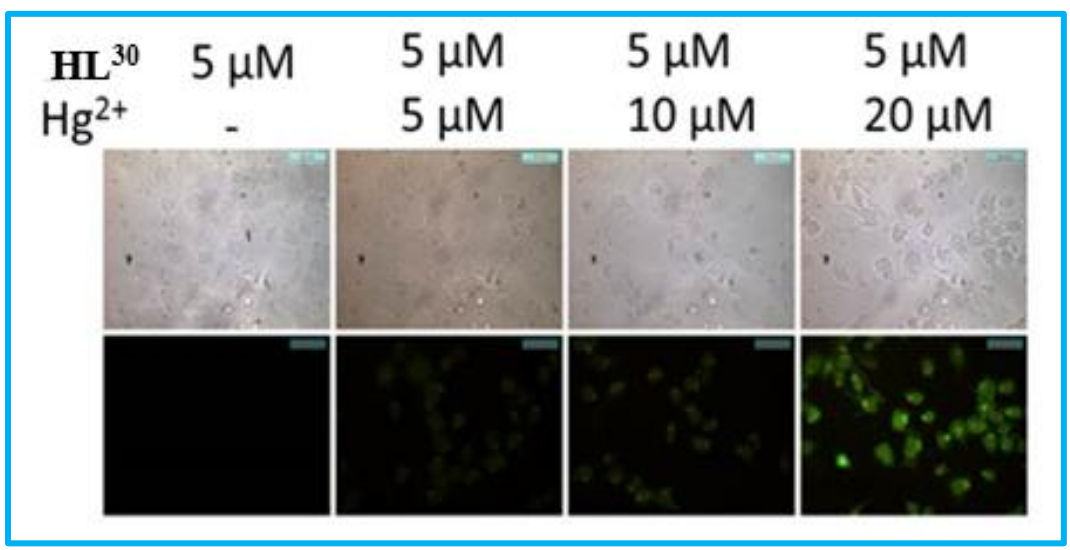

Figure 4.15. The fluorescence images of HepG2 cells were capture (40X) after incubation with 5 μM of HL^{30} for 60 min at 37 °C, followed by washing thrice with 1X PBS, and incubation with 5 μM, 10 μM and 20 μM of Hg^{2+} for 60 min at 37 °C followed by incubation with 5μM of HL^{30} for 60 min at 37 °C . The fluorescence images show no fluorescence signal by the fluorophore HL^{30} (5 μM) in the absence of Hg^{2+} ion, while the fluorescence gradually increases with higher concentration of Hg^{2+} ion.

3.4. Conclusions

A novel fluorescein derivative, HL^{30} was synthesized successfully by a simple two-step methods and characterized by various spectroscopic methods. Their ring-opening reaction

mechanisms were proposed and the HL^{30} bound with Hg^{2+} in a 1:1 stoichiometric ratio as evidenced by fluorescence titration experiments and Job's plot. Moreover, HL^{30} possesses a good selectivity and sensitivity towards Hg^{2+} over other common competitive alkali, alkaline earth and transition metal ions. Experimental results indicated that HL^{30} was a good candidate and had a potential application for rapid, selective and sensitive detection Hg^{2+}in methanol-aqueous media.The MTT assay revealed that HL^{30} exhibits low cytotoxicity toward living HepG2 cells.

References

1 T.W. Clarkson, L. Magos and G. J. Myers, *N. Engl. J. Med.*, 2003, **349,** 1731–1737.

2 J. Gutknecht, *J. Membr. Biol.*, 1981, **61,** 61–66.

3 S. K. Ko, Y.K. Yang, J. Tae and I. Shin, *J. Am. Chem. Soc.*, 2006, **128,** 14150–14155.

4 Y. P. Zhu, T.Y. Ma, T. Z. Ren and Z.Y. Yuan, *ACS Appl. Mater. Interfaces*, 2014, ***6,*** 16344–16351.

5 Z. Yang, L. Hao, B. Yin, M. She, M. Obst and A. Kappler, et al., *Org. Lett.*, 2013, **15,** 4334–4337.

6 U.S. EPA, Regulatory Impact Analysis of the Clean Air Mercury Rule: EPA-452/R-05-003, 2005.

7 D. W. Boening, *Chemosphere*, 2000, **40,** 1335-1351.

8 P. Piyanuch, S. Watpathomsuba, V.S. Lee, H. A. Nienaberc and N. Wanichacheva, *Sens. Actuators B Chem.*, 2016, **22,** 4201–208.

9 H. H. Harris, I. J. Pickering and G. N. George, *Science*, 2003 **301,** 1203.

10 M. Harada, *Crit. Rev. Toxicol.*, 1995, **25,** 1–24.

11 H. Khani, M. K. Rpfouei, P. Arab, V.K. Gupta and Z. Vafaei, *J. Hazard. Mater.*, 2010, **183,** 402–409.

12 E. M. Nolan and S. J. Lippard, *Chem. Rev.*, 2008, **108,** 3443–3480.

13 Z. X. Han, B. S. Zhu, T. L. Wua, Q. Q. Yang, Y. L. Xue, Z. Zhang, X. Y. Wu and A. Chin. *Chem. Lett.*, 2014, **25,** 73–76.

14 H. N. Kim, M. H. Lee, H. J. Kim and J. S. Kim, *Chem. Soc.Rev.*, 2008, **37,** 1465–1472.

15 M. Yuan, Y. Li, J. Li, C. Li, X. Liu, J. Lv, J. Xu, H. Liu, W. Su and D. Zhu, *Org. Lett.*, 2007, **92,** 313–2316.

16 N. H. Bings, A. Bogaerts and A. C. Broekaert, *Anal. Chem.*, 2006, **78,** 3917.

17 O.T. Butler, W. R. Cairns, J. M. Cook and C. M. Davidson, *J. Anal. At. Spectrom.*, 2012, **27,** 187.

18 F. Xuan, X.T. Luo and I. M. Hsing, *Anal. Chem.*, 2013, **85,** 4586.

19 V. K. Gupta, S. Jain and U. Khurana, *Electroanalysis*,1997, 9478–480.

20 D.T. Quang and J. S. Kim, *Chem. Rev.*, 2010, **110,** 6280–6301.

21 V. K. Gupta, A. K. Jain, G. Maheshwari, Heinrich Lang and Z. Ishtaiwi, *Sens. Actuators B: Chem.*, 2006, **117,** 99–106.

22 V. K. Gupta, A. K. Jain and P. Kumar, *Sens. Actuators B: Chem.* 2006, **120,** 259–266.

23 H. Zheng, X. Q. Zhan, Q. N. Bian and X. J. Zhang, *Chem. Commun.*, 2013, **49,** 429–447.

24 A. K. Jain, V. K. Gupta, L. P. Singh and J. R. Raisoni, *Electrochim. Acta.*, 2006, **51,** 2547–2553.

25 V. K. Gupta, L. P. Singh, R. Singh, N. Upadhyay, S. P. Kaur and B. Sethi, *J. Mol. Liq.*, 2012, **174,** 11–16.

26 J. H. Song, M. X. Huai, C. C. Wang, Z. H. Xu, Y. F. Zhao and Y. Ye, *Spectrochim. Acta*, 2015, **139,** 549–554.

27 S. K. Srivastava, V. K. Gupta and S. Jain, *Analyst*, 1995, **120,** 495–498.

28 V. K. Gupta, A. K. Jain, S. Agarwal and G. Maheshwari, *Talanta*, 2007, **71,** 1964–1968.

29 L. He, Q. Xu, Y. Liu, H. Wei, Y. Tang and W. Lin, *Appl. Mater. Interfaces,* 2015, **7,** 12809.

30 B. Tang, Y. Yang, G. Wang, Z. Yao, L. Zhang and H. C. Wu, *Org. Biomol. Chem.,* 2015, **13,** 8708.

31 J. C. Spiteri, J. S. Schembri and D. C. Magr, *New J. Chem.,* 2015, **39,** 3349.

32 N. Kumar, V. Bhalla and M. Kumar, *Analyst,* 2014, **139,** 543.

33 M.V. Kuperman, S.V. Chernii, M.Y. Losytskyy, D.V. Kryvorotenko, N.O. Derevyanko, Y. L. Slominskii, V. B. Kovalska and S. M. Yarmoluk, *Anal. Biochem.,* 2015, **484,** 9–17.

34 S. Wang, H. Liu, J. Mack, J. Tian, B. Zou, H. Lu, Z. Li, J. Jiang and Z. Shen, *Chem. Commun.,* 2015, 13389.

35 Y. Zhou, X.Y. You, Y. Fang, J.Y. Li, K. Liu and C. Yao, *Org. Biomol., Chem.,* 2010, **8,** 4819–4822.

36 J. K. Ni, B. Li, L. M. Zhang, H. F. Zhao and H. Jiang, *Actuators B: Chem* , 2015, **215,** 174–180.

37 Y. Jiao, L. Zhang and P. Zhou, *Talanta,* 2016, **15,** 14–19.

38 F. Ge, H. Ye, H. Zhang and B.X. Zhao, *Dyes Pigm.,* 2013, **99,** 661–665.

39 H. J. Kim, J.E. Park, M.G. Choi, S. Ahn and S.K. Chang, *Dyes Pigm.,* 2010, **84,** 54–58.

40 X. F. Yang, Y. Li and Q. Bai, *Anal. Chim. Acta,* 2007, **584,** 95–100.

41 X. Bao, Q. Cao, X. Wu, H. Shu, B. Zhou, Y. Geng and J. Zhu, *Tetrahedron Lett.,* 2016, **57,** 942-948.

42 G. C. Sun, Z. H. He, Z. J. Li, X. D. Yuan, Z. J. Yang, G. Xi. Wang, L. F.Wang and C.R. Liu, *Molecules,* 2001, ***6,*** 1001-1005.

43 Y. Gao, H. Liu, Q. Liu and W. Wang, *Tetrahedron Lett.,* 2016, **57,** 1852-1855.

HIGHLIGHTS

In the present thesis, some simple sensitive, selective and bio-compatible with low toxicity fluorescent molecular probes have been developed for the recognition of cations in purely aqueous or mixed organo- aqueous medium. The major emphasis has been given to their synthesis, characterization and studies on photophysical properties, DFT calculation and biological applications.

Chapter 1 contains a short introduction of fluoresceine based fluorescent molecular probes, their synthesis, characterization and studies on photophysical properties involving selective sensing of Hg(II). Additionally, a very brief overview of the present work is highlighted.

Chapter 2 describes the synthesis and characterization of fluorescein-based sensor L^{28} with potential N_2O_2 donor atoms which was found to act as fluorogenic sensor for selective recognition of Hg^{2+} emitting at 520 nm in semi-aqueous medium at pH 7.2 (10 mM HEPES buffer), temperature 25 ^{0}C. The fluorescence enhancement arises due to the configurational transformation (from sp^3 to sp^2 at C_4*) of the fluorescein moiety resulting opening of a spirolactam ring on binding with Hg^{2+}. A 1:1 binding mole ratio was established by Job's method and ESI-MS^+ (m/z) studies. The corresponding LOD was evaluated by the 3σ method and found to be 1.24 µM. The tentative coordination environment in the L^{28}-Hg^{2+}complex was established by DFT studies. The sensor demonstrates a reversible change in fluorescence upon the successive addition of Hg^{2+} and S^{2-} in L^{28} solution with negligible interference with other anions. The fluorescence "OFF–ON–OFF" mode of L^{28} was examined in the presence of Hg^{2+} and S^{2-} and finds applications in devising logic gate functions. The L^{28} also exhibits bio-compatibility and negligible cytotoxicity making it suitable for fluorescence cell imaging of Hg^{2+} ions in live HepG2 cells.

Chapter 3 introduces the synthesis, characterization and photophysical studies on a simple fluorescein-based reversible chemosensor L^{29} which selectively and sensitively recognises Hg^{2+} over other competing metal ions in 100% aqueous medium at pH 7.2 (10 mM HEPES buffer), temperature 25^{0}C with 44 fold fluorescence enhancement. The sensing mechanism is based on spirolactam ring opening upon coordination with Hg^{2+}. A 1:1 binding mole ratio was established through Job's method and ESI-MS^+ (m/z) studies. For the Hg^{2+} interaction towards L^{29} the binding constant was calculated to be (3.21 ± 0.05) x 10^4 M^{-1} with detection limit 92.7 nM. On addition of S^{2-} to the L^{29}–Hg^{2+}complex, the fluorescence intensity was totally quenched due to removal of Hg^{2+} from the complex by S^{2-}ion arising out of stronger

affinity of Hg^{2+} towards S^{2-} resulting concomitant formation of ring closed form, L^{29}. The tentative coordination environment in the L^{29}–Hg^{2+}complex was established by DFT studies. L^{29} exhibits low cytotoxicity and cell permeability, which makes it capable for bioimaging applications in living HepG2 cells.

Chapter 4 describes the synthesis and characterization a novel fluorescein derivative (HL^{30}). The probe displayed excellent sensitivity and selectivity towards Hg^{2+} over other tested metal ions in CH_3OH : H_2O 7:3 medium (pH 7.2, 10 mM HEPES), which could be ascribed to the Hg^{2+} mediated opening of the spirolactam ring of the flourescein moiety. The 1:1 binding of HL^{30} to Hg^{2+} was established by Job's method and confirmed by ESI-MS^{-} (m/z) studies. The Lod value was calculated to be 0.46 µM. The MTT assay revealed that HL^{30} exhibits low cytotoxicity toward living HepG2 cells.

List of Publications

1. Fluorescein-2-(Pyridin-2-ylmethoxy) benzaldehyde conjugate for fluorogenic turn-ON recognition of Hg^{2+} in water and living cells with logic gate and memory device applications.
   H. Mohammad, A. S. M. Islam, M. Sasmal, C. Prodhan, and M. Ali, *Inorganica chimica Acta*, 2022, **543**, 121165 **DOI:**10.1016/j.ica.2022.121165 Paper.
2. A fluorescein-based chemosensor for "turn-on" detection of Hg^{2+} and resultant complex as a fluorescent sensor for S^{2-} in semi aqueous medium with cell-Imaging application: Experimental and Computational studies.
   H. Mohammad, A. S. M. Islam, C. Prodhan, K. Chaudhuri and M. Ali, ***New J. Chem.***, 2019, **43**, 5297 **DOI:** 10.1039/C8NJ05418E Paper.
3. A Fluorescein-2-Hydroxy-3-hydroxymethyl-5-methyl-benzaldehyde conjugate as a highly selective and sensitive chemosensor for Hg^{2+} ions with cell imaging possibility.
   H. Mohammad, A. S. M. Islam, M. Sasmal, C. Prodhan, and M. Ali, ***Communicated,*** Paper.
4. A hydrazone based probe for the selective fluorescent detection of Al(III) and Al(III)-probe complex mediated secondary PPi sensing:computational studies, interpretation of molecular logic circuit and memory device and intracellular application.
   H. Mohammad, A. S. M. Islam, C. Prodhan, K. Chaudhuri and M. Ali, ***Photochem. Photobiol. Sci.,*** 2018, **17,** 200, **DOI:** 10.1039/c7pp00286f.
5. A novel 8-hydroxyquinoline-pyrazole based highly sensitive and selective Al(III) sensor in a purely aqueous medium with intracellular application: experimental and computational studies.
   A. S. M. Islam, R. Bhowmick, **H. Mohammad,** A. Katarkar, K. Chaudhuri and M. Ali, ***New J. Chem.***, 2016,**40**, 4710-4719, **DOI:** 10.1039/C5NJ03153B, Paper.
6. Uptake of Azo Dyes into Silk Glands for Production of Colored Silk Cocoons Using a Green Feeding Approach.
   A. Nisal, K. Trivedy, **H. Mohammad,** S. Panneri, S. S. Gupta, A. Lele, R. Manchala, N. S.
   B. Kumar, M. Gadgil, H. Khandelwal,S. More, and R. Seeta Laxman, *ACS Sustainable Chem. Eng.* 2014, **2,** 312−317. **DOI:**10.1021/sc400355k.

NJC

PAPER

View Article Online
View Journal | View Issue

Check for updates

Cite this: *New J. Chem.*, 2019, 43, 5297

A fluorescein-based chemosensor for "turn-on" detection of Hg^{2+} and the resultant complex as a fluorescent sensor for S^{2-} in semi-aqueous medium with cell-imaging application: experimental and computational studies†

Hasan Mohammad,[a] Abu Saleh Musha Islam,[a] Chandraday Prodhan[b] and Mahammad Ali *[ac]

A fluorescein hydrazone based conjugate (**H_2L^3**) was synthesized by coupling fluorescein hydrazide (**L^1**) with 2-(pyridin-2-ylmethoxy)-naphthalene-1-carbaldehyde (**L^2**). **H_2L^3** was well characterized by several spectroscopic methods such as IR, ^{1}H, ^{13}C-NMR and ESI-MS. The probe **H_2L^3** exhibited high selectivity and high sensitivity towards toxic Hg^{2+} ions in semi-aqueous medium (pH 7.2, 10 mM HEPES) over other metal ions. The significant enhancement in fluorescence emission centered at 520 nm was attributed to the Hg^{2+}-induced ring opening of the spirolactam moiety in the fluorescein structure. The 1:1 binding of **H_2L^3** to Hg^{2+} was established by Job's method and confirmed by ESI-MS$^+$ (*m*/*z*) studies and the binding constant was calculated as $(0.43 \pm 0.04) \times 10^4$ M^{-1} with a detection limit of 1.24 μM. Then again, the **$[Hg(HL^3)]^+$** ensemble could be utilized as a reversible fluorescent sensor for S^{2-}. On addition of S^{2-} to the **$[Hg(HL^3)]^+$** complex, the fluorescence intensity was totally quenched because Hg^{2+} in the complex was grabbed by S^{2-} because of the stronger binding force between Hg^{2+} and S^{2-}. The tentative coordination environment in the **$[Hg(HL^3)]^+$** complex was established by DFT studies. The fluorescence "OFF–ON–OFF" mode of **H_2L^3** was examined in the presence of Hg^{2+} and S^{2-} and finds applications in devices with logic gate functions. **H_2L^3** also exhibits bio-compatibility and negligible cytotoxicity and is suitable for fluorescence cell imaging of Hg^{2+} ions in live HepG2 cells.

Received 28th October 2018,
Accepted 8th February 2019

DOI: 10.1039/c8nj05418e

rsc.li/njc

Published on 09 February 2019. Downloaded by Jadavpur University on 12/5/2022 5:01:18 AM.

Introduction

Hg^{2+} and its derivatives are highly toxic pollutants. Mercury pollution, in particular, is a subject of recent concern.[1–3] Contamination with Hg^{2+} originates from a variety of natural and anthropogenic sources, including oceanic and volcanic emission,[4,5] gold mining, solid waste incineration,[6] and the combustion of fossil fuels.[7] Inorganic mercury can be transformed into methyl mercury by bacteria, and can easily enter into the human body *via* the food chain.[4,8–11] Hg^{2+} can accumulate in the human body and leads to severe health problems such as damage to and dysfunction of the brain, kidneys, DNA and central nervous system[12,13] and Minamata disease.[14] Owing to its serious toxic effect and wide distribution, the United States Environmental Protection Agency (USEPA) set a maximum tolerance limit of 2 ppb for Hg^{2+} for drinking water.[15] Typical detection methods such as inductively coupled plasma mass spectrometry, atomic absorption/emission spectroscopy[16,17] and voltammetry[18] are used to detect Hg^{2+} ions. These traditional methods are not suitable as they are very expensive and need continuous monitoring, skilled personnel and sophisticated instrumentation for on-site detection of Hg^{2+}. The sol–gel method is also used for heavy metal (*e.g.* Hg^{2+}) detection. Due to the porous nature of the sol–gel network, entrapped species remain accessible and can interact with external chemical species or analytes. Sol–gel based sensors also suffer from some disadvantages: for example, entrapment in sol–gel glass may change the chemical and biological properties of the entrapped species, due to the reduced degrees of freedom and interactions with the inner surfaces of the pores.[19–22] Hence, spectrofluorometric techniques are extensively used to monitor Hg^{2+} due to their faster and cheaper execution with simplicity

[a] *Department of Chemistry, Jadavpur University, Kolkata 700 032, India. E-mail: m_ali2062@yahoo.com, mali@chemistry.jdvu.ac.in*
[b] *Department of Molecular & Human Genetics Division, CSIR-Indian Institute of Chemical Biology, 4 Raja S.C. Mallick Road, Kolkata-700032, India*
[c] *Vice-Chancellor, Aliah University, ll-A/27, Action Area II, Newtown, Action Area II, Kolkata, West Bengal 700160, India*

† Electronic supplementary information (ESI) available. See DOI: 10.1039/c8nj05418e

Published on 09 February 2019. Downloaded by Jadavpur University on 12/5/2022 5:01:18 AM.

and easy adaptability. In particular, colorimetric and fluorescent sensors have attracted a lot of attention in the field of heavy metal detection[23–31] due to their advantages of good selectivity, quick response and high sensitivity. Recently, some important fluorescent sensors for Hg^{2+} have been reported.[32–38] Among various fluorophores, we have selected fluorescein dye to design a Hg^{2+} selective probe owing to its excellent spectroscopic properties with longer absorption and emission wavelengths, high fluorescence quantum yields, good biocompatibility and negligible toxicity.[39] For detection of Hg^{2+} most of the sensors are based on rhodamine compounds.[40–52] However, fluorescein-based probes have attracted comparatively little attention.[53–57] Thus, here fluorescein is used as a constituent to design a chemosensor with prospective N_2O_2 donor atoms for the selective and rapid recognition of toxic Hg^{2+} ions in semiaqueous medium exhibiting chromo- and fluorogenic responses through metal-induced ring opening of the spirolactam moiety. The quenching of fluorescence could be realized by adding S^{2-}. This OFF–ON–OFF fluorescence behavior can be applied for the sequential recognition of Hg^{2+} and S^{2-} and can be further extended to biological cell imaging.

Experimental

Materials and instruments

Steady-state fluorescence studies were performed with a PTI (QM-40) spectrofluorimeter. UV/vis absorption spectra were recorded with an Agilent 8453 diode array spectrophotometer. Bruker spectrometers of 400 and 500 MHz were used for ^{1}H and ^{13}C NMR studies. The ESI-MS$^+$ spectra were recorded on a Waters XEVO G2QTof (Micro YA263) mass spectrometer.

Solvents like methanol and ethanol (Merck, India) were of reagent grade and dried before the experiment. Deionized water from MilliQ Millipore was used for UV/vis and fluorescence studies. Fluorescein sodium salt, 2-chloromethylpyridine, $Hg(ClO_4)_2{\cdot}3H_2O$ and metal salts such as the perchlorates of Zn^{2+}, Mg^{2+}, Co^{2}, Ni^{2+}, Cu^{2+}, Pb^{2+}, Al^{3+}, Cr^{3+}, Cd^{2+}, Pd^{2+}, Fe^{2+}, Fe^{3+}, Mn^{2+}, Na^+, K^+, Ca^{2+}, and Ag^+ were bought from Sigma-Aldrich and used as received. Sodium salts of anions like SO_4^{2-}, $S_2O_4^{2-}$, SO_3^{2-}, $S_2O_3^{2-}$, PO_4^{3-}, S^{2-}, Cl^-, F^-, Br^-, I^-, $H_2PO_4^-$, CN^-, NO_2^-, CO_3^{2-}, ClO_4^- and N_3^- were of reagent grade and used as received. All other compounds were bought from commercial sources.

Solution preparation for UV-vis/fluorescence studies

For UV-vis and fluorescence experiments, 10 mL 1.0×10^{-3} M stock solution of $\mathbf{H_2L^3}$ (5.91 mg) was made by dissolving the required amount of ligand in DMF–MeOH (1 : 9 v/v). In a similar way, standard solutions of 1.0×10^{-3} M $Hg(ClO_4){\cdot}3H_2O$ and 1.0×10^{-3} M of sodium sulfide (Na_2S) in water were also prepared. Standard solutions of the other cations and anions were made in MeOH/H_2O. 250 mL of 10 mM HEPES buffer in water was prepared and the pH was maintained at 7.2 by using HCl and NaOH. 2.5 mL of this buffer solution was pipetted out into a cuvette to which the required volume (50 μL in T-200) of 1.0×10^{-3} M probe was transferred to achieve 20 μM final concentration for fluorescence titration. At regular intervals Hg^{2+} ions were transferred incrementally beginning from 0 to 230 μM and fluorescence spectra were collected for all solutions. Cuvettes with 1 cm path length were used for absorption and emission studies. Fluorescence experiments were performed using 5 nm × 3 nm slit width.

Preparation of fluorescein hydrazide (L^1)

L^1 was prepared according to a literature method.[58]

Preparation of 2-(pyridin-2-ylmethoxy)-naphthalene-1-carbaldehyde (L^2)

L^2 was synthesized by a modification of a literature method.[43] 2-Hydroxy-napthaldehyde (10 mmol, 1.72 g) and K_2CO_3 (18 mmol, 2.52 g) were added to dry MeCN (50 mL). The mixture was allowed to reflux for 1 h. After that, a catalytic amount of KI (0.10 g) and 2-picolyl chloride (10 mmol, 1.64 g) were added to the reaction mixture. Furthermore, the reaction mixture was refluxed for 8 h and then filtered after cooling the solution to room temperature. The filtrate was concentrated and diluted with water. Then, 1 M HCl solution was added to maintain the pH at 4 and extracted with dichloromethane (DCM; 2 × 30 mL). The pH of the aqueous solution was further adjusted to 8 by adding 4.0 mmol of Na_2CO_3 solution and extracted with DCM (3 × 20 mL). Then the combined organic phase was evaporated to dryness after drying with anhydrous Na_2SO_4 to get a solid residue. Finally, the crude solid product was recrystallized from MeOH/DCM (6 : 4, v/v) to achieve the desired product as an off-white crystalline solid. Yield: 72%. ^{1}H-NMR (in $CDCl_3$): (δ ppm) 11.06 (1H, s, –ArCHO), 9.3 (1H, d, –ArH), 8.64 (1H, d, –ArH), 8.05 (1H, d, –ArH), 7.79 (2H, t, –ArH), 7.63 (1H, d,–ArH), 7.56 (1H, d, –ArH), 7.46 (2H, t, –ArH), 7.35 (1H, t, –ArH) (Fig. S1, ESI†). ESI-MS$^+$: m/z = 264.02 ($C_{17}H_{13}NO_2 + H^+$) (Fig. S2, ESI†).

Preparation of probe H_2L^3

In a 250 mL round-bottom flask, fluorescein hydrazide (0.692 g, 2 mmol) and 2-(pyridin-2-ylmethoxy)-naphthalene-1-carbaldehyde (0.5262 g, 2 mmol) were suspended in 20 mL ethanol. The mixture was refluxed for 6 h with stirring to get a clear solution. Following the reaction, the mixture was allowed to cool to room temperature. The pale yellow precipitate formed was separated by filtration and finally washed with 3 × 10 mL ethanol. 70% yield was obtained. ^{1}H-NMR (DMSO-d_6): δ (ppm) = 9.93 (d, 3H), 8.56 (s, 1H), 8.43 (d, 1H), 8.19 (s, 2H), 7.90 (d, 2H), 7.63 (d, 2H), 7.43 (d, 2H), 7.30 (s, 3H), 7.17 (d, 1H), 6.60 (s, 2H), 6.54 (d, 2H), 6.46 (d, 2H), 5.33 (s, 2H) (Fig. S3, ESI†). ^{13}C-NMR (DMSO-d_6): δ (ppm) = 164.07, 159.08, 156.90, 152.79, 150.69, 149.55, 147.60, 137.52, 134.38, 133.17, 130.81, 130.28, 129.63, 129.36, 128.74, 128.02, 125.92, 124.51, 124.42, 123.60, 123.47, 121.80, 115.67, 114.85, 112.82, 110.71, 102.89, 71.72, 65.96 (Fig. S4, ESI†). FT-IR spectrum: –OH (3123 cm^{-1}), –C═N (1610 cm^{-1}), –ArH (2919 cm^{-1}), –C═O (1647 cm^{-1}) (Fig. S5, ESI†). ESI-MS$^+$: m/z = 592.07 ($C_{37}H_{25}N_3O_5 + H^+$) (Fig. S6, ESI†).

 This journal is © The Royal Society of Chemistry and the Centre National de la Recherche Scientifique 2019

Published on 09 February 2019. Downloaded by Jadavpur University on 12/5/2022 5:01:18 AM.

Preparation of the H_2L^3–Hg^{2+} complex

$Hg(ClO_4)_2$ (0.272 g, 0.6 mmol) was added to a 10 mL MeOH solution of $\mathbf{H_2L^3}$ (0.295 g, 0.5 mmol) and the mixture was stirred for about 30 minutes. It was then filtered and allowed to evaporate slowly at ambient temperature to get a crystalline solid product. ^{1}H-NMR (DMSO-d_6): δ (ppm) = 9.78 (s, 1H), 8.68 (s, 1H), 7.95 (m, 1H), 7.93 (m, 1H), 7.90 (m, 1H), 7.81 (m, 2H), 7.78 (m, 1H), 7.62 (m, 4H), 7.42 (m, 1H), 7.35 (m, 4H), 7.28 (m, 1H), 6.61 (s, 1H), 6.53 (m, 2H), 6.45 (m, 2H), 5.43 (s, 2H) (Fig. S7, ESI†). ^{13}C NMR (DMSO-d_6): δ (ppm) = 164.45, 161.16, 159.22, 155.51, 154.20, 152.21, 151.03, 150.87, 147.84, 147.08, 134.83, 133.48, 131.08, 129.79, 129.52, 128.94, 128.64, 128.22, 126.04, 124.92, 123.78, 118.10, 115.49, 114.84, 113.01, 112.57, 110.11, 103.36, 102.99, 79.58, 79.38, 69.16 (Fig. S8, ESI†). FTIR spectrum: –OH (3261 cm^{-1}), –C═N (1587 cm^{-1}), –C═O (1617 cm^{-1}) (Fig. S9, ESI†). ESI-MS$^+$: m/z = 791.07 ($C_{37}H_{24}N_3O_5$) (Fig. S10, ESI†).

Computational studies

To gain better insight into geometries, electronic structures and optical properties, DFT study is an important tool. The calculation of the ground state electronic structures of both the ligand and its Hg^{2+} complex was performed using the DFT[59] method combined with the conductor like polarizable continuum model (CPCM).[60] For this study Becke's hybrid functional[61] with the Lee–Yang–Parr (LYP) correlation functional[62] was used. The ligand and complex were fully optimized without any symmetry constraints. In this work we chose a 6-31G basis set for the ligand and a LanL2DZ basis set for Hg atoms for the optimization of the ground state. All the calculations were achieved with the Gaussian 09W software package.[63]

Cell culture

Human hepatocellular carcinoma (HepG2) cells (NCCS, Pune, India) were grown in DMEM supplemented with 10% FBS and antibiotics (penicillin-100 μg mL^{-1}; streptomycin-50 μg mL^{-1}). Cells were cultured at 37 °C in 95% air, 5% CO_2 incubator.

Cell cytotoxicity assay

The cytotoxicity for $\mathbf{H_2L^3}$ was evaluated with the help of 3-(4,5-dimethylthiazol-2-yl)-2,5-diphenyltetra-zolium bromide (MTT) cell viability assay. HepG2 cells (1 × 10^5 cells per well) were cultured in a 96-well plate and incubated at 37 °C, and were exposed to varying concentrations of $\mathbf{H_2L^3}$ (1, 5, 10, 20, 30, 40, 50, 60, 70, 80, 90 and 100 μM) for 24 h. After the incubation, 10 μL of MTT solution [5 mg mL^{-1}, dissolved in 1× phosphate-buffered saline (PBS)] was added to each well of a 96-well culture plate, then the cells were incubated at 37 °C for 4 h. Media were decanted from the wells and 100 μL of 0.04 N acidic isopropyl alcohol was added into each well to solubilize intracellular formazan crystals (blue-violet) formed. The absorbance of the solution was measured at 595 nm wavelength (EMax Precision MicroPlate Reader, Molecular Devices, USA). Values were calculated as means ± standard errors of three independent experiments. The cell viability was expressed as the optical density ratio of the treatment to control.

Cell imaging study

HepG2 cells were cultured in a 35 mm × 10 mm culture dish on a coverslip for 24 h at 37 °C. The cells were treated with a 5 μM solution of $\mathbf{H_2L^3}$, prepared by dissolving $\mathbf{H_2L^3}$ in a mixed solvent DMSO : water = 1 : 9 (v/v), and incubated for 1 h at 37 °C. For $\mathbf{Hg^{2+}}$ complex formation study, HepG2 cells were pre-incubated with varying concentrations of $\mathbf{Hg^{2+}}$ (5 μM, 10 μM and 20 μM) for 60 min at 37 °C and washed three times with 1× PBS and then incubated with 5 μM of $\mathbf{H_2L^3}$ for 60 min at 37 °C and washed with 1× PBS two times. For quenching study, HepG2 cells were pre-incubated with 20 μM of $\mathbf{Hg^{2+}}$ for 60 min at 37 °C followed by washing three times with 1× PBS and then incubated with 5 μM of $\mathbf{H_2L^3}$ for 60 min at 37 °C and then further incubated with 5 μM of Na_2S, and subsequently washed three times with 1× PBS. Fluorescence images of HepG2 cells were taken using a fluorescence microscope (Leica DM3000, Germany) with an objective lens of 40× magnification.

Results and discussion

A simple reaction between fluorescein hydrazide (L^1) and 2-(pyridin-2-ylmethoxy)-naphthalene-1-carbaldehyde (L^2) in ethanol leads to the formation of $\mathbf{H_2L^3}$ in quantitative yield (Scheme 1), which was thoroughly characterized by ^{1}H-NMR, ^{13}C-NMR, ESI-MS$^+$, and IR studies. The unique peak at δ = 65.96 ppm in the ^{13}C-NMR spectrum corresponding to **C4** (Fig. S4, ESI†) in $\mathbf{H_2L^3}$ supports that the probe exists in solution predominantly in its fluorescence inactive spiro-lactam form.

UV-vis recognition of Hg^{2+}

The spectrophotometric titration was performed to analyze the interaction of Hg^{2+} (0–70 μM) with $\mathbf{H_2L^3}$ in 10 mM HEPES

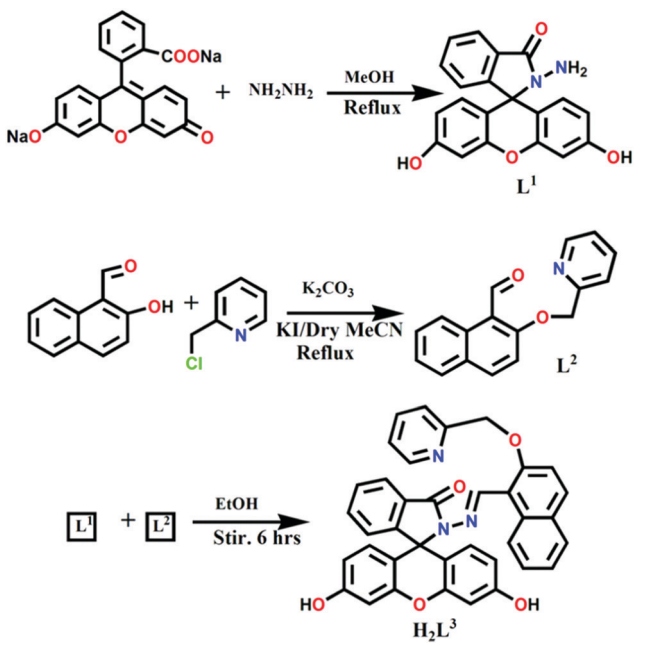

Scheme 1 Synthetic route of chemosensor $\mathbf{H_2L^3}$.

Published on 09 February 2019. Downloaded by Jadavpur University on 12/5/2022 5:01:18 AM.

buffer at pH 7.2. The absorption titration of $\mathbf{H_2L^3}$ as a function of Hg^{2+} concentration was performed at room temperature. Upon addition of Hg^{2+} ions in the range 0–70 μM, the absorption band at 370 nm decreased rapidly and absorption change occurred around 475 nm and the absorption became saturated at about 70 μM Hg^{2+} ions, keeping the concentration of $\mathbf{H_2L^3}$ fixed at 20.0 μM, and we also performed a dilution effect study where we see that the two spectra are almost the same (Fig. S11, ESI†). So, we can say that the absorption change of $\mathbf{H_2L^3}$ occurs due to the dilution effect.

Fluorescence recognition of Hg^{2+}

The emission spectra of $\mathbf{H_2L^3}$ and fluorescence titration with Hg^{2+} were recorded in 10 mM HEPES buffer at pH 7.2. Free $\mathbf{H_2L^3}$ displayed very weak-fluorescence; however, on gradual addition of Hg^{2+} (0–230 μM) to an aqueous solution of $\mathbf{H_2L^3}$ (20.0 μM), a significant enhancement of the fluorescence intensity with a band centered at λ_{em} = 520 nm on excitation at λ_{ex} = 475 nm was displayed (Fig. 1). The specific response of $\mathbf{H_2L^3}$ towards Hg^{2+} was supposed to be based on the opening of the spirolactam ring. Meanwhile, this may be because the reaction of Hg^{2+} with the chelating probe leads to a rigid complex $\mathbf{[Hg(HL^3)]^+}$ and tends to contribute to a chelation enhanced fluorescence (CHEF).[64–66] These results demonstrate that $\mathbf{H_2L^3}$ could serve as an alluring "turn on" chemosensor for detecting toxic Hg^{2+} ions. A plot of FI *vs.* $[Hg^{2+}]$ gives a straight line up to 230 μM where nonlinear eqn (1)[67] becomes $y = a + b \times c \times x$ under the conditions $1 \gg c \times x$ with $n = 1$ and the linear dependence of such a plot gives a slope = $b \times c$, where b = fluorescence maximum (F_{max}) and $c = K_f$ = apparent formation constant. So, slope/F_{max} gives $K_f = (0.43 \pm 0.04) \times 10^4\ M^{-1}$.

$$y = \frac{a + b \times c \times x^n}{1 + c \times x^n} \quad (1)$$

The mole fraction at 0.5 for Hg^{2+} in Job's plots (Fig. S12, ESI†) indicated 1 : 1 binding stoichiometry between $\mathbf{H_2L^3}$ and Hg^{2+}. The bindings were further supported by mass spectrometry. The unique peak assigned at m/z 791.07 (calculated for $\mathbf{[Hg(HL^3)]^+}$ = 791.13) corresponds to 1 : 1 stoichiometry between the probe and Hg^{2+} (Fig. S10, ESI†). The limit of detection (LOD) of Hg^{2+} was calculated by the 3σ method and found to be 1.24 μM (Fig. S13, ESI†). The quantum yield of $\mathbf{H_2L^3}$ (Φ = 0.0132) is enhanced upon binding with the Hg^{2+} ions (Φ = 0.1122) using fluorescein as a standard (0.5 in ethanol) (see the ESI†).

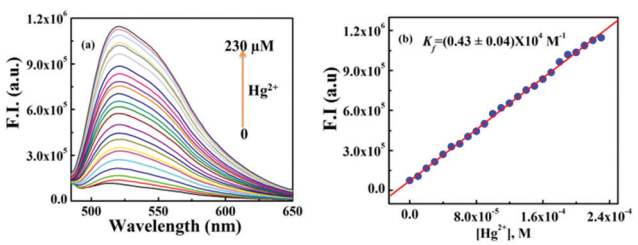

Fig. 1 (a) Fluorescence titration of $\mathbf{H_2L^3}$ (20.0 μM) in 10 mM HEPES buffer at pH 7.2 by the gradual addition of Hg^{2+} with λ_{ex} = 475 nm and λ_{em} = 520 nm. (b) Linear fit plot of FI *vs.* $[Hg^{2+}]$.

Probable mechanism of recognition of Hg^{2+}

The plausible mechanism proposed for the formation of the $\mathbf{[Hg(HL^3)]^+}$ complex by opening of the spiro-lactam ring was established through IR, ^{1}H and ^{13}C-NMR studies. The characteristic stretching frequency at 1610 cm^{-1} in the free $\mathbf{H_2L^3}$ due to (–CH═N) is shifted significantly to 1587 cm^{-1}. This supports the participation of the azomethine nitrogen of $\mathbf{H_2L^3}$ in binding with Hg^{2+}. The band at 1647 cm^{-1} can be assigned to the ν(–C═O) of the cyclic spiro form of fluorescein. This peak moves to a lower frequency at 1617 cm^{-1}, indicating the opening of the spirolactam ring on coordination to Hg^{2+}. The cation recognition mechanism of the probe with Hg^{2+} was also substantiated by ^{1}H-NMR experiments. The ^{1}H-NMR titration was performed independently with $\mathbf{H_2L^3}$ and $\mathbf{[Hg(HL^3)]^+}$ in DMSO-d_6. Upon addition of Hg^{2+}, the imine proton (–CH═N) shifted downfield by δ = 0.18 ppm (8.68 to 8.50 ppm), signifying the coordination of azomethine-N to Hg^{2+}. The two separate phenolic proton signals (–OH) of $\mathbf{H_2L^3}$ then appeared to be one and moved up-field from 9.9 ppm to 9.78 ppm. These results clearly demonstrate the spirolactam ring opening mechanism of the probe and one of the phenolic C–OH's tautomerized to –C═O.[68] Also, the disappearance of the signal at δ = 65.96 ppm from the ^{13}C-NMR spectrum for the sp^3-hybridized tertiary carbon of the spiro-lactam ring of $\mathbf{H_2L^3}$ (labelled 4, Fig. 2) upon addition of Hg^{2+} strongly supports the opening of the spiro-lactam ring and coordination through O atoms.[69] Thus, based on ^{1}H-NMR, ^{13}C-NMR, IR, ESI-MS$^+$ and Job's plot, we proposed a probable mechanism of binding of Hg^{2+} ions to $\mathbf{H_2L^3}$ as shown in Scheme 2.

Selectivity

Selectivity is one of the important parameters to scrutinize the practical applicability of a probe. Thus, competitive reactions of

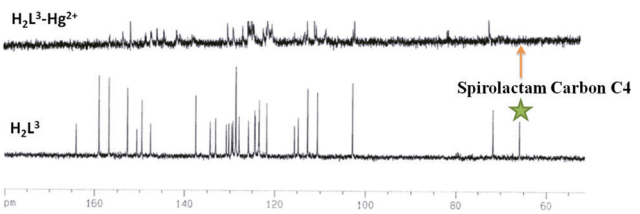

Fig. 2 ^{13}C NMR spectra of $\mathbf{H_2L^3}$ and $\mathbf{H_2L^3{-}Hg^{2+}}$ in DMSO-d_6 recorded on a Bruker 500 MHz spectrometer.

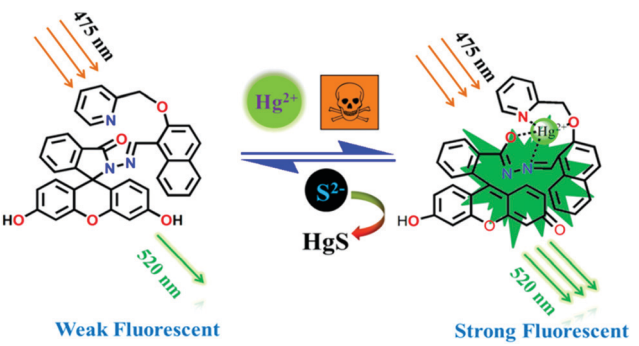

Scheme 2 Proposed mechanism for the recognition of Hg^{2+}.

 This journal is © The Royal Society of Chemistry and the Centre National de la Recherche Scientifique 2019

Published on 09 February 2019. Downloaded by Jadavpur University on 12/5/2022 5:01:18 AM.

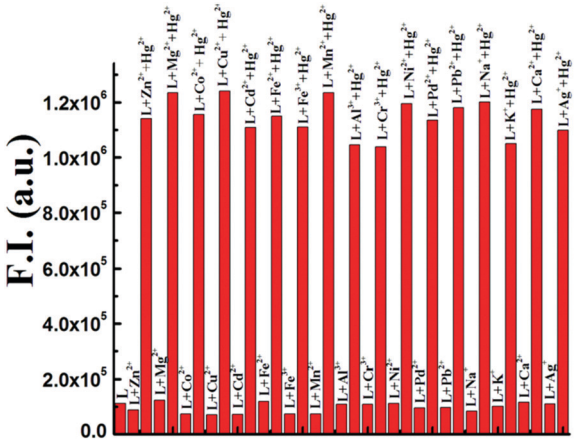

Fig. 3 Competitive fluorescent responses of H_2L^3 to different metal ions in 10 mM HEPES buffer at pH 7.2.

H_2L^3 (20 μM) towards Hg^{2+} ions in the presence of 10 equivalents of various cations like Zn^{2+}, Mg^{2+}, Co^{2+}, Ni^{2+}, Cu^{2+}, Pb^{2+}, Al^{3+}, Cr^{3+}, Cd^{2+}, Pd^{2+}, Fe^{2+} Fe^{3+}, Mn^{2+}, Na^{+}, K^{+}, Ca^{2+}, and Ag^{+} in 10 mM HEPES buffer were carried out. As shown in Fig. 3 and Fig. S14 (ESI†) the competitive cations did not reveal any noticeable interference in the detection of Hg^{2+} ions. So, H_2L^3 serves as a highly sensitive 'naked-eye sensor' for the selective detection of Hg^{2+} in aqueous buffer solution.

Fluorescence spectral responses for S^{2-}

To observe the performance of the $[Hg(HL^3)]^+$ complex in anion sensing, the fluorescence changes of the complex were recorded in the presence of various anions. Fig. 4 displays the changes in the fluorescence emissions of $[Hg(HL^3)]^+$ upon addition of 10 equivalents of a series of anions like SO_4^{2-}, $S_2O_4^{2-}$, SO_3^{2-}, $S_2O_3^{2-}$, PO_4^{3-}, S^{2-}, Cl^-, F^-, Br^-, I^-, $H_2PO_4^-$, CN^-, NO_2^-, CO_3^{2-}, ClO_4^- and N_3^-. It is very exciting to note that only S^{2-} causes a significant fluorescence quenching. This indicates that the $[Hg(HL^3)]^+$ complex can selectively detect S^{2-}. Besides, the detection of S^{2-} was not perturbed by the presence of other sulphur species like SO_4^{2-}, $S_2O_4^{2-}$, SO_3^{2-}, and $S_2O_3^{2-}$.

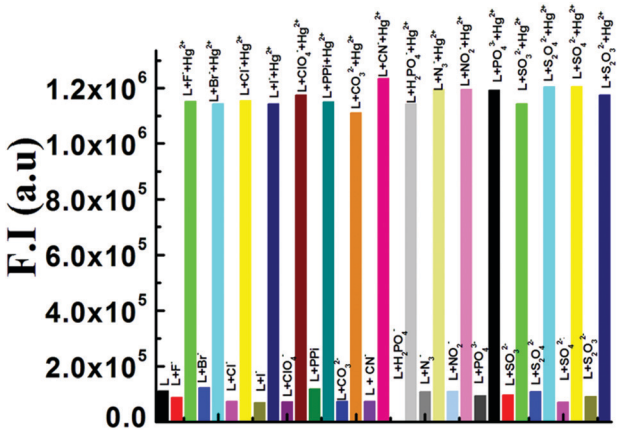

Fig. 4 Competitive test for the fluorescent responses of H_2L^3 to various anions in 10 mM HEPES buffer at pH 7.2.

A competitive experiment was subsequently performed by adding S^{2-} to the $[Hg(HL^3)]^+$ complex containing the other anions (Fig. 4). Before the addition of S^{2-}, there was an almost negligible fluorescence change at 520 nm in the presence of the other anions. The fluorescence emission intensity at 520 nm disappeared completely upon addition of 210 μM of S^{2-} to the $[Hg(HL^3)]^+$ solution. This clearly demonstrates that any anions considered in this study did not interfere with the detection of S^{2-}. Thus the $[Hg(HL^3)]^+$ complex displays high specificity for S^{2-}. A fluorescence titration was carried out to investigate the interaction between $[Hg(HL^3)]^+$ and S^{2-}. As shown in Fig. 5, the fluorescence intensity of $[Hg(HL^3)]^+$ gradually decreased as the concentration of S^{2-} was increased. The LOD of S^{2-} was determined to be 2.35 μM (Fig. S15, ESI†). The mass spectrum of the $[Hg(HL^3)]^+$ complex in the presence of S^{2-} was compared with those of H_2L^3 and the free $[Hg(HL^3)]^+$ complex to determine the interaction between $[Hg(HL^3)]^+$ and S^{2-}. In the mass spectrum the peak at m/z = 592.06 corresponds to $H_2L^3 \approx C_{17}H_{13}NO_2 + H^+$ (Fig. S6, ESI†), indicating the S^{2-} induced displacement of Hg^{2+} from the $[Hg(HL^3)]^+$ complex. This is attributed to the stronger binding force between Hg^{2+} and S^{2-}. These results clearly demonstrate that the $[Hg(HL^3)]^+$ complex could serve as a secondary sensor for S^{2-} *via* a displacement approach (Scheme 2). This proves the reversibility between $[Hg(HL^3)]^+$ and S^{2-}.

Reversibility of H_2L^3 for sensing Hg^{2+}

The reversibility of the chemosensor is an essential aspect for sensory applications. We carried out reversibility experiments by using Na_2S for Hg^{2+} in aqueous solution. Upon addition of 210 μM of S^{2-} into a solution containing 20 μM H_2L^3 and 230 μM Hg^{2+}, a notable decrease of the fluorescence emission intensity at 520 nm was observed (Fig. 6). It can be attributed to the fact that the S^{2-} anion has a strong affinity towards Hg^{2+} and their binding constant may be much higher than that towards H_2L^3. Thus, the addition of S^{2-} causes demetallation of Hg^{2+} from the $[Hg(HL^3)]^+$ complex, releasing free H_2L^3 with the

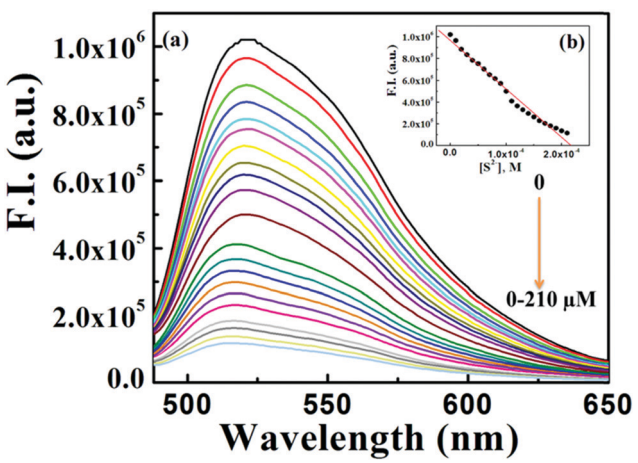

Fig. 5 (a) Fluorescence titration of $[Hg(HL^3)]^+$ by adding S^{2-} in 10 mM HEPES buffer at pH 7.2. (b) Fluorescence intensity at 520 nm was linearly related to the concentration of S^{2-}.

Published on 09 February 2019. Downloaded by Jadavpur University on 12/5/2022 5:01:18 AM.

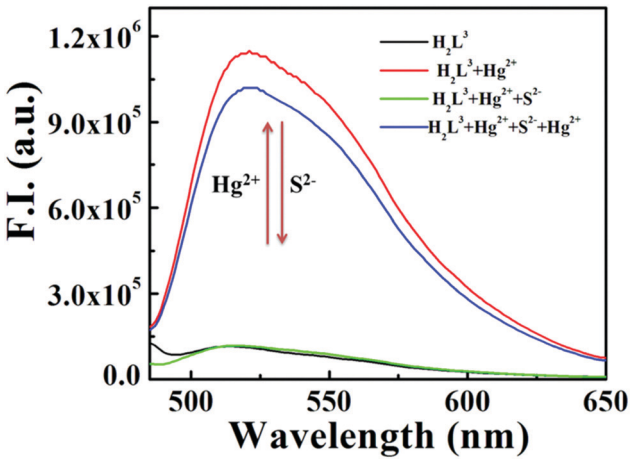

Fig. 6 Reversibility of Hg^{2+} coordination to $\mathbf{H_2L^3}$ by Na_2S. The black curve represents the fluorescence intensity of free $\mathbf{H_2L^3}$, the red line represents the fluorescence enhancement after the addition of 230 μM Hg^{2+}, the green line represents the fluorescence decrease after the addition of 210 μM S^{2-} into a solution of $\mathbf{[Hg^{2+}(HL3)]^+}$ species, and the blue line represents the fluorescence enhancement again after the addition of 230 μM Hg^{2+} into the $[\mathbf{[Hg^{2+}(HL^3)]^+} + \mathbf{S^{2-}}]$ solution.

re-establishment of the spirolactam ring. With further addition of Hg^{2+} in slight excess (230 μM), the fluorescence intensity was revived again. This reversible process is repeated three times with a little loss of sensitivity (Fig. S16, ESI†). This clearly demonstrates that $\mathbf{H_2L^3}$ is a reversible sensor towards Hg^{2+} ions. This restoration capability indicates that $\mathbf{H_2L^3}$ could be re-used with suitable management and $\mathbf{[Hg(HL^3)]^+}$ could be used as a secondary sensor for S^{2-}.

pH dependence

For biological application, the dependence of the fluorescence emission intensity of $\mathbf{H_2L^3}$ on the pH of the reaction solution was investigated in detail. As shown in Fig. 7, the fluorescence intensity of $\mathbf{H_2L^3}$ showed almost no change in the pH range of 2.0–7.0. However, there was a slight enhancement in fluorescence intensity at pH > 7.0. This can be attributed to the deprotonation of the aromatic –OH group[70–73] at high pH. As demonstrated in Fig. 7 upon addition of 230 μM of Hg^{2+}, the fluorescence intensity of $\mathbf{H_2L^3}$ at 520 nm is significantly enhanced at pH = 6.0–9.0, which indicates that the Hg^{2+} ions induce the formation of the ring-opened $\mathbf{[Hg(HL^3)]^+}$ complex. In the present work, 10 mM HEPES buffer solution at pH 7.2 was chosen for potential application throughout the experiment for the detection of Hg^{2+} ions.

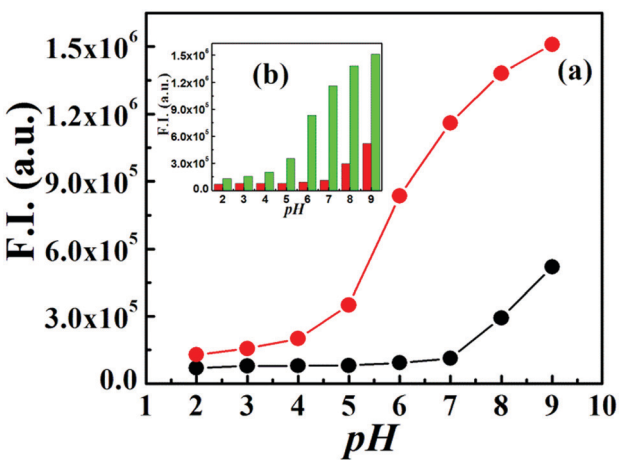

Fig. 7 (a) Fluorescence intensity *vs.* pH plot at 520 nm with $\mathbf{H_2L^3}$ (20 μM; denoted by black circles) and the $\mathbf{[Hg(HL^3)]^+}$ complex (denoted by red circles) and (b) the corresponding histogram plot.

Geometry optimization and electronic structure

The ground state geometry optimization for $\mathbf{H_2L^3}$ and the $\mathbf{[Hg(HL^3)]^+}$ complex was performed using B3-LYP. The global minima of all these species are confirmed by the positive vibrational frequencies. Both $\mathbf{H_2L^3}$ and the $\mathbf{[Hg(HL^3)]^+}$ complex have the C1 point group. The main optimized geometrical parameters of the complex and ligand are listed in Tables 1 and 2 and the optimized structures of $\mathbf{H_2L^3}$ and the $\mathbf{[Hg(HL^3)]^+}$ complex are given in Fig. 8.

The four co-ordinated metal center possesses a distorted tetrahedral geometry around the Hg^{2+} ion. All calculated Hg–O distances fall in the range 2.24–2.53 Å and the Hg–N distance is 2.27 Å. In the case of $\mathbf{H_2L^3}$ in the ground state, the electron densities at the HOMO and LUMO mainly reside on the 1-iminomethyl-naphthalen-2-ol and (2-hydroxy-naphthalen-1-ylmethylene)-hydrazide moieties respectively. The energy difference between the HOMO and LUMO is 3.95 eV in $\mathbf{H_2L^3}$. In the case of $\mathbf{[Hg(HL^3)]^+}$ the HOMO mainly originates from ligand π and π* orbital contributions, while the LUMO mainly

Table 1 Selected optimized geometrical parameters for $\mathbf{H_2L^3}$ in the ground state calculated at the B3LYP level

Bond distance (Å)			
C13–C18	1.24404	N34–C35	1.29994
C13–N3	1.40307	C39–O53	1.39060
N3–N34	1.38507	C57–N66	1.35324
Bond angle (°)			
C54–O53–C39	120.266	N34–N3–C13	128.646
C37–C35–N34	133.768	N3–C13–O2	126.645
C35–N34–N3	123.773		

Table 2 Selected optimized geometrical parameters for the complex in the ground state calculated at the B3LYP level

Bond distance (Å)			
C17–C18	1.49306	O1–Hg70	2.24728
C17–O1	1.33876	N6–Hg70	2.27472
C17–N5	1.40550	N6–C15	1.31663
O56–Hg70	2.53569	N69–Hg70	2.27861
Bond angle (°)			
N69–Hg70–O56	72.184	C17–N5–N6	115.635
O56–Hg70–N6	76.878	O1–Hg70–N69	136.108
N6–Hg70–O1	74.535	N5–N6–C15	113.987

 This journal is © The Royal Society of Chemistry and the Centre National de la Recherche Scientifique 2019

Published on 09 February 2019. Downloaded by Jadavpur University on 12/5/2022 5:01:18 AM.

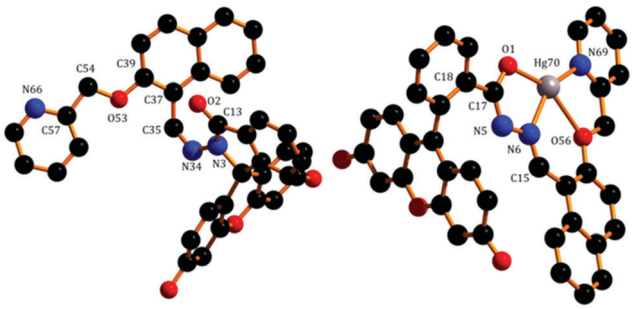

Fig. 8 Optimized geometries of H_2L^3 and the $[Hg^{2+}(HL^3)]^+$ complex under DFT calculation.

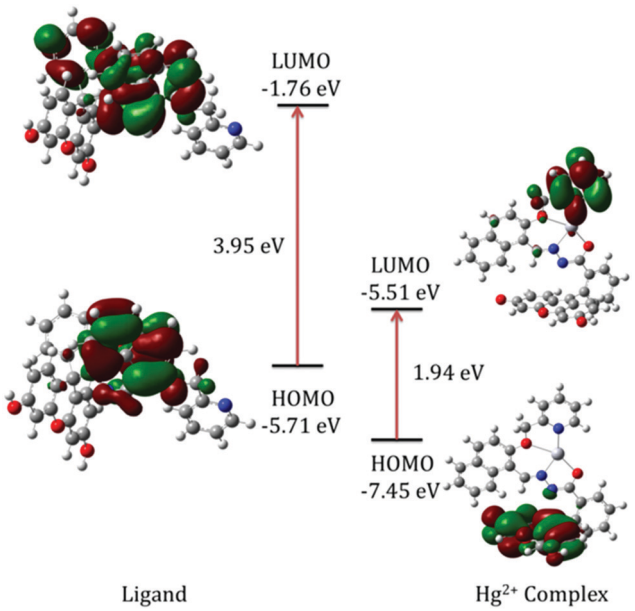

Fig. 9 Frontier molecular orbitals of the Hg^{2+} complex as well as ligand optimized under DFT.

resides on the pyridin-2-yl-methano moiety. The energy difference between the HOMO and LUMO is 1.94 eV (Fig. 9). From this study, it is clear that the energy gap between the highest occupied molecular orbital (HOMO) and the lowest unoccupied molecular orbital (LUMO) are 3.95 and 1.94 eV for the free ligand and its Hg^{2+} complex respectively. As a result, a substantial change in fluorescence intensity is observed.

Design of logic gates

The molecular probe H_2L^3 displays logic gate operation with its spectroscopic properties. We consider the output by consecutive addition of Hg^{2+} and S^{2-} and monitoring their emission. The emission band maxima at 520 nm appeared due to the interaction of H_2L^3 with the analyte Hg^{2+} ion, selected as an output signal (Fig. S17, ESI†). When Hg^{2+} was added to the H_2L^3 solution, the emission intensity at 520 nm again decreased. Thus with the two inputs Hg^{2+} and S^{2-} the sensor H_2L^3 has the capability to exhibit an INHIBIT logic gate function, which has been summarised in the truth table (Fig. S13d, ESI†). Only when Hg^{2+} is present, the output at 520 nm is 1, otherwise the output is 0.

Application in bioimaging

Taking into account the highly specific selective nature of H_2L^3 in the detection of Hg^{2+} ions, it was further checked for its Hg^{2+} sensing ability in living cells. To determine if H_2L^3 has cytotoxic effects, a cell viability assay using **MTT** was done by calculating % cell viability on HepG2 cells (Fig. S18, ESI†). There was no significant reduction in the tetrazolium salt (reflected by a decrease in formazine production) for H_2L^3 up to 10 μM, thus suggesting that below 10 μM ligand concentration, H_2L^3 would be much more effective for the analysis of its complex formation with Hg^{2+} ions *in vitro*. A cell viability higher than 90% was observed for H_2L^3 at 5 μM, after which the viability of the HepG2 cells decreased. Hence, further experiments were carried out with 5 μM of H_2L^3 for treatment.

The probe H_2L^3 exhibited an absence of intracellular fluorescence on HepG2 cells treated with 5 μM of the ligand and incubated for 1 h (Fig. 10). However, a prominent intracellular green fluorescence signal was observed when the HepG2 cells were incubated with 5 μM of Hg^{2+} for 60 min at 37 °C, followed by incubation with 5 μM of H_2L^3. The intracellular fluorescence was found to be prominently localized in the cytoplasmic region, suggesting that H_2L^3 specifically forms a complex with the Hg^{2+} ions transported to the cytoplasm. Keeping the ligand H_2L^3 concentration constant (5 μM), increasing the concentration of Hg^{2+} (5 μM, 10 μM and 20 μM) results in Hg^{2+} ion concentration-dependent enhancement in the intracellular green fluorescence, caused by the formation of a complex with H_2L^3. Again, in the presence of 5 μM of Na_2S, the fluorescence signal decreased significantly, acting as a quencher for the ligand. Hence, the present ligand with low cytotoxicity and biocompatibility for cellular cytoplasmic Hg^{2+} ions can be used for Hg^{2+} ion detection in biological samples.

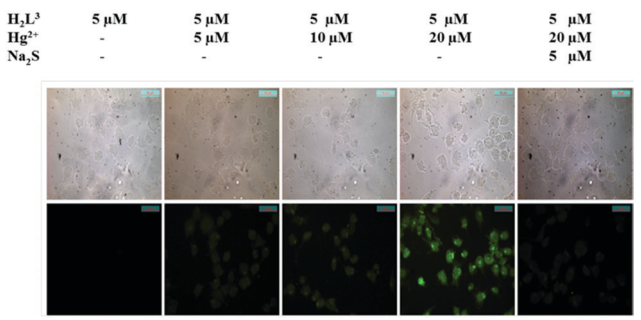

Fig. 10 The fluorescence images of HepG2 cells were captured (40×) after incubation with 5 μM of H_2L^3 for 60 min at 37 °C, followed by washing thrice with 1× PBS, and incubation with 5 μM, 10 μM and 20 μM of Hg^{2+} for 60 min at 37 °C followed by incubation with 5 μM of H_2L^3 for 60 min at 37 °C. The fluorescence images show no fluorescence signal by the fluorophore H_2L^3 (5 μM) in the absence of Hg^{2+} ions, while the fluorescence gradually increases with higher concentration of Hg^{2+} ions; again, the fluorescence emission decreased significantly in the presence of 5 μM of Na_2S, acting as a quencher.

Published on 09 February 2019. Downloaded by Jadavpur University on 12/5/2022 5:01:18 AM.

Conclusion

In summary, we successfully designed and prepared a new fluorescein-based sensor ($\mathbf{H_2L^3}$) with potential N_2O_2 donor atoms, which was found to act as a fluorogenic sensor for selective recognition of Hg^{2+} emission at 520 nm in semi-aqueous medium at pH 7.2 (10 mM HEPES buffer) and 25 °C. The probe was thoroughly characterized by ^{1}H and ^{13}C NMR, IR, and ESI-MS spectroscopy. The fluorescence enhancement was explored in terms of the configuration transformation of the fluorescein from the spirolactam ring form to a ring-opened amide form on binding with Hg^{2+} in a 1 : 1 mole ratio, which was established by Job's method and ESI-MS$^+$ (m/z) studies. The corresponding LOD was evaluated by the 3σ method and found to be 1.24 μM. The sensor demonstrates a reversible change in fluorescence upon successive additions of Hg^{2+} and S^{2-} in $\mathbf{H_2L^3}$ solution with negligible interference from other anions. Moreover, it can be applied for the successful fabrication of molecular 'INHIBIT' logic gates. This work would offer a reference for the development of sensors with sequential recognition of Hg^{2+} and S^{2-}. Table S1 (ESI†) summarises a few aspects of some recently published chemosensors for the Hg^{2+} ion: *e.g.* working medium, biological study, reversibility and quantum yield.[74–83] However, in most cases, no biological study or logic gate operation was investigated, with a few exceptions.[75,76,78] Also most of the studies were done in organic or mixed organo-aqueous media.

Conflicts of interest

There are no conflicts to declare.

Acknowledgements

Financial support from the DST (Ref. No. 809(Sanc)/ST/P/S&T4G-9/2104), West Bengal, and the CSIR (Ref. 01(2896)/17/EMR-II), New Delhi, India, is gratefully acknowledged. H. Mohammad is grateful for a UGC-MANF (2012-13-MANF-MUS-WES-13502), UGC, New Delhi, India. A. S. M. Islam is grateful for a CSIR-SRF, New Delhi, India.

References

1 P. M. Bolger and B. A. Schwetz, Mercury and Health, *N. Engl. J. Med.*, 2002, **347**, 1735–1736.
2 H. H. Harris, I. J. Pickering and G. N. George, The Chemical Form of Mercury in Fish, *Science*, 2003, **301**, 1203.
3 T. W. Clarkson, L. Magos and G. J. Myers, The Toxicology of Mercury – Current Exposures and Clinical Manifestations, *N. Engl. J. Med.*, 2003, **349**, 1731–1737.
4 A. Renzoni, F. Zino and E. Franchi, Mercury Levels along the Food Chain and Risk for Exposed Populations, *Environ. Res.*, 1998, **77**, 68–72.
5 D. B. Gil, M. I. Rodriguez-Cáceres, M. del, C. HurtadoSánchez and A. M. de la Pena, Fluorescent Determination of Hg^{2+} in Water and Fish Samples Using a Chemodosimeter Based in a Rhodamine 6G Derivative and a Portable Fiber-Optic Spectrofluorimeter, *Appl. Spectrosc.*, 2010, **64**, 520–527.
6 O. Malm, Gold Mining as a Source of Mercury Exposure in the Brazilian Amazon, *Environ. Res.*, 1998, **77**, 73–78.
7 E. M. Nolan and S. J. Lippard, Turn-On and Ratiometric Mercury Sensing in Water with a Red-Emitting Probe, *J. Am. Chem. Soc.*, 2007, **129**, 5910–5918.
8 W. F. Fitzgerald, C. H. Lamborg and C. R. Hammerschmidt, Marine Biogeochemical Cycling of Mercury, *Chem. Rev.*, 2007, **107**, 641–662.
9 Z. C. Zhang, D. Wu, X. F. Guo, X. H. Qian, Z. Lu and Q. Xu, Visible Study of Mercuric Ion and Its Conjugate in Living Cells of Mammals and Plants, *Chem. Res. Toxicol.*, 2005, **18**, 1814–1820.
10 D. W. Boening, Ecological effects, transport, and fate of mercury: a general review, *Chemosphere*, 2000, **40**, 1335–1351.
11 J. Gutknecht, Inorganic mercury (Hg^{2+}) transport through lipid bilayer membranes, *J. Membr. Biol.*, 1981, **61**, 61–66.
12 M. Harada, Minamata Disease: Methylmercury Poisoning in Japan Caused by Environmental Pollution, *Crit. Rev. Toxicol.*, 1995, **25**, 1–24.
13 P. B. Tchounwou, W. K. Ayensu, N. Ninashvili and D. Sutton, Review: Environmental exposure to mercury and its toxicopathologic implications for public health, *Environ. Toxicol.*, 2003, **18**, 149–175.
14 USEPA, Regulatory Impact Analysis of the Clean Air Mercury Rule Final Report. PA-452/R-05-003, Research Triangle Park, NC, 2005.
15 J. G. Chen, H. W. Chen, X. Z. Jin and H. T. Chen, Determination of ultra-trace amount methyl-, phenyl- and inorganic mercury in environmental and biological samples by liquid chromatography with inductively coupled plasma mass spectrometry after cloud point extraction preconcentration, *Talanta*, 2009, **77**, 1381–1387.
16 L. Ling, Y. Zhao, J. Du and D. Xiao, An optical sensor for mercuric ion based on immobilization of Rhodamine B derivative in PVC membrane, *Talanta*, 2012, **91**, 65–71.
17 X. Fu, X. Chen, Z. Guo, C. Xie, L. Kong, J. Liu and X. Huang, Stripping voltammetric detection of mercury(II) based on a surface ion imprinting strategy in electropolymerized microporous poly(2-mercaptobenzothiazole) films modified glassy carbon electrode, *Anal. Chim. Acta*, 2011, **685**, 21–28.
18 F. Wang, X. Wei, C. Wang, S. Zhang and B. Ye, Langmuir–Blodgett film of *p-tert*-butylthiacalix[4]arene modified glassy carbon electrode as voltammetric sensor for the determination of Hg(II), *Talanta*, 2010, **80**, 1198–1204.
19 W. Huang, D. Wu, G. Wu and Z. Wang, Dual functional rhodamine-immobilized silica toward sensing and extracting mercury ions in natural water samples, *Dalton Trans.*, 2012, **41**, 2620.
20 S. Jayabal, R. Sathiyamurthi and R. Ramaraj, Selective sensing of Hg^{2+} ions by optical and colorimetric methods using gold nanorods embedded in a functionalized silicate sol–gel matrix, *J. Mater. Chem. A*, 2014, **2**, 8918.
21 A. Panja and K. Ghosh, Selective sensing of Hg^{2+} via sol–gel transformation of a cholesterol-based compound, *Supramol. Chem.*, 2018, **8**, 722–729.

 This journal is © The Royal Society of Chemistry and the Centre National de la Recherche Scientifique 2019

Published on 09 February 2019. Downloaded by Jadavpur University on 12/5/2022 5:01:18 AM.

22 S. Xu, L. Chen, J. Li, Y. Guan and H. Lu, Novel Hg^{2+}-imprinted polymers based on thymine–Hg^{2+}–thymine interaction for highly selective preconcentration of Hg^{2+} in water samples, *J. Hazard. Mater.*, 2012, **237**, 347–354.
23 D. T. Quang and J. S. Kim, Fluoro- and chromogenic chemodosimeters for heavy metal ion detection in solution and biospecimens, *Chem. Rev.*, 2010, **110**, 6280–6301.
24 V. K. Gupta, A. K. Jain, G. Maheshwari, H. Lang and Z. Ishtaiwi, Copper(II)-selective potentiometric sensors based on porphyrins in PVC matrix, *Sens. Actuators, B*, 2006, **117**, 99–106.
25 V. K. Gupta, A. K. Jain and P. Kumar, PVC-based membranes of *N*,*N*-dibenzyl-1,4,10,13-tetraoxa-7,16-diazacyclooctadecane as Pb(II)-selective sensor, *Sens. Actuators, B*, 2006, **120**, 259–266.
26 H. Zheng, X. Q. Zhan, Q. N. Bian and X. J. Zhang, Advances in modifying fluorescein and fluorophores as fluorescent chemosensors, *Chem. Commun.*, 2013, **49**, 429–447.
27 A. K. Jain, V. K. Gupta, L. P. Singh and J. R. Raisoni, A comparative study of Pb^{2+} selective sensors based on derivatized tetrapyrazole and calix[4]arene receptors, *Electrochim. Acta*, 2006, **51**, 2547–2553.
28 V. K. Gupta, L. P. Singh, R. Singh, N. Upadhyay, S. P. Kaur and B. Sethi, A novel copper(II) selective sensor based on dimethyl 4,4′(o-phenylene)bis(3-thioallophanate) in PVC matrix, *J. Mol. Liq.*, 2012, **174**, 11–16.
29 J. H. Song, M. X. Huai, C. C. Wang, Z. H. Xu, Y. F. Zhao and Y. Ye, A new FRET ratiometric fluorescent chemosensor for Hg^{2+} and its application in living EC 109 cells, *Spectrochim. Acta, Part A*, 2015, **139**, 549–554.
30 S. K. Srivastava, V. K. Gupta and S. Jain, Determination of lead using a poly(vinyl chloride)-based crown ether membrane, *Analyst*, 1995, **120**, 495–498.
31 V. K. Gupta, A. K. Jain, S. Agarwal and G. Maheshwari, An iron(III) ion-selective sensor based on a μ-bis(tridentate) ligand, *Talanta*, 2007, **71**, 1964–1968.
32 Z. Xu, C. Zhang, X. Zheng, Z. Li and S. Xu, A highly sensitive and selective optical probe for detection of Hg^{2+} based on a 2,5-bis[2-(benzylthio)aniline]-croconaine, *Optik*, 2018, **175**, 54–62.
33 G. Gangatharan, V. Kumar, M. P. Kesavan, A. Tamilselvi, G. Rajagopal, J. D. Raja, K. Sakthipandi, J. P. Rajesh and G. Sivaraman, A reversible fluorescent chemosensor for the rapid detection of Hg^{2+} in an aqueous solution: Its logic gates behaviour, *Sens. Actuators, B*, 2018, **273**, 305–315.
34 A self-assembled tetrapeptide that acts as a "turn-on" fluorescent sensor for Hg^{2+} ions: K. Tomar, G. Kaur, S. Verma and G. Ramanathan, *Tetrahedron Lett.*, 2018, **59**, 3653–3656.
35 A. Han, X. Liu, G. D. Prestwich and L. Zang, Fluorescent sensor for Hg^{2+} detection in aqueous solution, *Sens. Actuators, B*, 2014, **198**, 274–277.
36 A. A. Soares-Paulino, L. Giroldoa, G. Celantea, C. Lodeiro and A. A. Dos Santosa, Formation of an emissive telluroxide promoted by Hg^{2+} in aqueous environment: A new naked-eye and ratiometric rhodamine dimer fluorescent mercury(II) probe, *Dyes Pigm.*, 2018, **159**, 121–127.
37 A. Sikdar, S. Roy, S. Dasgupta, S. Mukherjee and S. S. Panja, Logic gate-based Rhodamine-methionine conjugate highly sensitive fluorescent probe for Hg^{2+} ion and its application: An experimental and theoretical study, *Sens. Actuators, B*, 2018, **263**, 298–311.
38 Q. Lin, X. M. Jiang, X. Q. Ma, J. Liu, H. Yao, Y. M. Zhang and T. B. Wei, Novel bispillar[5]arene-based AIEgen and its application in mercury(II) detection, *Sens. Actuators, B*, 2018, **272**, 139–145.
39 F. Ge, H. Ye, H. Zhang and B. X. Zhao, A novel ratiometric probe based on rhodamine B and coumarin for selective recognition of Fe(III) in aqueous solution, *Dyes Pigm.*, 2013, **99**, 661–665.
40 Y. Zhou, X. Y. You, Y. Fang, J. Y. Li, K. Liu and C. Yao, A thiophen-thiooxorhodamine conjugate fluorescent probe for detecting mercury in aqueous media and living cells, *Org. Biomol. Chem.*, 2010, **8**, 4819–4822.
41 J. K. Ni, B. Li, L. M. Zhang, H. F. Zhao and H. Jiang, A fluorescence turn-on probe based on rhodamine derivative and its functionalized silica material for Hg^{2+}-selective detection, *Sens. Actuators, B*, 2015, **215**, 174–180.
42 Y. Jiao, L. Zhang and P. Zhou, A rhodamine B-based fluorescent sensor toward highly selective mercury(II) ions detection, *Talanta*, 2016, **15**, 14–19.
43 T. Mistri, R. Alam, M. Dolai, S. K. Mandal, P. Guha, A. R. Khuda-Bukhsh and M. Ali, Rhodamine-Based Chromo-/Fluorogenic Dual Signalling Probe for Selective Recognition of Hg(II) with Potential Applications for INHIBIT Logic Devices and Cell-Imaging Studies Imaging Studies, *Eur. J. Inorg. Chem.*, 2013, 5854–5861.
44 K. Bera, A. K. Das, M. Nag and S. Basak, Development of a Rhodamine–Rhodanine-Based Fluorescent Mercury Sensor and Its Use to Monitor Real-Time Uptake and Distribution of Inorganic Mercury in Live Zebrafish Larvae, *Anal. Chem.*, 2014, **86**, 2740–2746.
45 A. Sikdar, S. Roy, S. Dasgupta, S. Mukherjee and S. S. Panja, Logic gate-based Rhodamine-methionine conjugate highly sensitive fluorescent probe for Hg^{2+} ion and its application: An experimental and theoretical study, *Sens. Actuators, B*, 2018, **263**, 298–311.
46 S. Lee, B. A. Rao and Y. A. Son, Colorimetric and "turn-on" fluorescent determination of Hg^{2+} ions based on a rhodamine–pyridine derivative, *Sens. Actuators, B*, 2014, **196**, 388–397.
47 H. Ding, C. Zheng, B. Li, G. Liu, S. Pu, D. Jia and Y. Zhou, A rhodamine–based sensor for Hg^{2+} and resultant complex as a fluorescence sensor for I^-, *RSC Adv.*, 2016, **6**, 80723–80728.
48 M. Wang, F. Y. Yan, Y. Zou, N. Yang, L. Chen and L. G. Chen, A rhodamine derivative as selective fluorescent and colorimetric chemosensor for mercury(II) in buffer solution, test strips and living cells, *Spectrochim. Acta, Part A*, 2014, **123**, 216–223.
49 Y. Jiao, L. Zhang and P. Zhou, A Rhodamine B-based Fluorescent Sensor toward Highly Selective Mercury(II) Ions Detection, *Talanta*, 2016, **150**, 14–19.
50 M. M. Hong, A. F. Liu, Y. Xu and D. M. Xu, Synthesis and properties of three novel rhodamine-based fluorescent sensors for Hg^{2+}, *Chin. Chem. Lett.*, 2016, **27**, 989–992.

Published on 09 February 2019. Downloaded by Jadavpur University on 12/5/2022 5:01:18 AM.

51 A. Sikdar, S. Roy, K. Haldar, S. Sarkar and S. S. Panja, Rhodamine-based Cu^{2+}-selective fluorosensor: Synthesis, Mechanism, and Application in living cells, *J. Fluoresc.*, 2013, **23**, 495–501.
52 S. Erdemir, O. Kocyigit and S. Malkondu, Detection of Hg^{2+} ion in aqueous media by new fluorometric and colorimetric sensor based on triazole-rhodamine, *J. Photochem. Photobiol., A*, 2015, **309**, 15–21.
53 H. J. Kim, J. E. Park, M. G. Choi, S. Ahn and S. K. Chang, Selective chromogenic and fluorogenic signalling of Hg^{2+} ions using a fluorescein-coumarin conjugate, *Dyes Pigm.*, 2010, **84**, 54–58.
54 X. F. Yang, Y. Li and Q. Bai, A highly selective and sensitive fluorescein-based chemodosimeter for Hg^{2+} ions in aqueous media, *Anal. Chim. Acta*, 2007, **584**, 95–100.
55 Y. Feng, Z. Kuaib, Y. Song, J. Guo, Q. Yanga, Y. Shanb and Y. Li, A novel turn-on thiooxofluorescein-based colorimetric and fluorescent sensor for Hg^{2+} and its application in living cells, *Talanta*, 2017, **170**, 103–110.
56 P. Piyanuch, S. Watpathomsuba, V. S. Lee, H. A. Nienaberc and N. Wanichacheva, Highly sensitive and selective Hg^{2+}-chemosensor based on dithia-cyclic fluorescein for optical and visual-eye detections in aqueous buffer solution, *Sens. Actuators, B*, 2016, **224**, 201–208.
57 X. F. Yang, Y. Li and Q. Bai, A highly selective and sensitive fluorescein-based chemodosimeter for Hg^{2+} ions in aqueous media, *Anal. Chim. Acta*, 2007, **584**, 95–100.
58 X. Bao, Q. Cao, X. Wu, H. Shu, B. Zhou, Y. Geng and J. Zhu, Tetrahedron, design and synthesis of a new selective fluorescent chemical sensor for Cu^{2+} based on a pyrrole moiety and a fluorescein conjugate, *Tetrahedron Lett.*, 2016, **57**, 942–948.
59 R. G. Parr and W. Yang, *Density Functional Theory of Atoms and Molecules*, Oxford University Press, Oxford, 1989.
60 M. Cossi, N. Rega, G. Scalmani and V. Barone, Energies, structures, and electronic properties of molecules in solution with the C-PCM solvation model, *J. Comput. Chem.*, 2003, **24**, 669–681.
61 A. D. Becke, Density-functional thermochemistry. III. The role of exact exchange, *J. Chem. Phys.*, 1993, **98**, 5648–5652.
62 C. Lee, W. Yang and R. G. Parr, Development of the Colle-Salvetti correlation-energy formula into a functional of the electron density, *Phys. Rev. B: Condens. Matter Mater. Phys.*, 1998, **37**, 785–789.
63 M. J. Frisch, G. W. Trucks, H. B. Schlegel, G. E. Scuseria, M. A. Robb, J. R. Cheeseman, G. Scalmani, V. Barone, B. Mennucci, G. A. Petersson, H. Nakatsuji, M. Caricato, X. Li, H. P. Hratchian, A. F. Izmaylov, J. Bloino, G. Zheng, J. L. Sonnenberg, M. Hada, M. Ehara, K. Toyota, R. Fukuda, J. Hasegawa, M. Ishida, T. Nakajima, Y. Honda, O. Kitao, H. Nakai, T. Vreven, J. A. Montgomery Jr., J. E. Peralta, F. Ogliaro, M. Bearpark, J. J. Heyd, E. Brothers, K. N. Kudin, V. N. Staroverov, R. Kobayashi, J. Normand, K. Raghavachari, A. Rendell, J. C. Burant, S. S. Iyengar, J. Tomasi, M. Cossi, N. Rega, J. M. Millam, M. Klene, J. E. Knox, J. B. Cross, V. Bakken, C. Adamo, J. Jaramillo, R. Gomperts, R. E. Stratmann, O. Yazyev, A. J. Austin, R. Cammi, C. Pomelli, J. W. Ochterski, R. L. Martin, K. Morokuma, V. G. Zakrzewski, G. A. Voth, P. Salvador, J. J. Dannenberg, S. Dapprich, A. D. Daniels, Ö. Farkas, J. B. Foresman, J. V. Ortiz, J. Cioslowski and D. J. Fox, *Gaussian 09 (Revision A.1)*, Gaussian, Inc., Wallingford, CT, 2009.
64 E. M. Nolan and S. J. Lippard, Tools and Tactics for the Optical Detection of Mercuric Ion, *Chem. Rev.*, 2008, **108**, 3443–3480.
65 A. Tamayo, B. Pedras, C. Lodeiro, L. Escriche, J. Casabo, L. Capelo, B. Covelo, R. Kiveka and R. Sillanpa, Exploring the Interaction of Mercury(II) by N_2S_2 and NS_3 Anthracene-Containing Macrocyclic Ligands: Photophysical, Analytical, and Structural Studies, *Inorg. Chem.*, 2007, **46**, 7818–7826.
66 Y. Zhang, Y. Yang, J. Hao, C. Yin, F. Huo, J. Chao and D. Liu, Spectroscopic study of the recognition of 2-quinolinone derivative on mercury ion, *Spectrochim. Acta, Part A*, 2014, **132**, 27–31.
67 C. R. Lohani, J. M. Kim, S. Y. Chung, J. Yoon and K. H. Lee, Colorimetric and fluorescent sensing of pyrophosphate in 100% aqueous solution by a system comprised of rhodamine B compound and Al^{3+} complex, *Analyst*, 2010, **135**, 2079–2084.
68 Y. Gao, H. Liu, Q. Liu and W. Wang, A novel colorimetric and OFF–ON fluorescent chemosensor based on fluorescein derivative for the detection of Fe^{3+} in aqueous solution and living cells, *Tetrahedron Lett.*, 2016, **57**, 1852–1855.
69 D. Wang, X. Xiang, X. Yang, X. Wang, Y. Guo, W. Liu and W. Qin, Fluorescein-based chromo-fluorescent probe for zinc in aqueous solution: Spirolactam ring opened or closed, *Sens. Actuators, B*, 2014, **201**, 246–254.
70 V. R. Batistela, J. D. C. Cedran, H. P. M. D. Oliveira, I. S. Scarminio, L. T. Ueno, A. E. D. H. Machado and N. Hioka, Protolytic fluorescein species evaluated using chemometry and DFT studies, *Dyes Pigm.*, 2010, **86**, 15–24.
71 L. N. Bogdanova, N. O. Mchedlov-Petrossyan, N. A. Vodolazkaya and A. V. Lebed, The influence of -cyclodextrin on acid–base and tautomeric equilibrium of fluorescein dyes in aqueous solution, *Carbohydr. Res.*, 2010, **345**, 1882–1890.
72 N. O. Mchedlov-Petrossyana, O. N. Tychina, T. A. Berezhnaya, V. I. Alekseeva and L. P. Savvina, Ionization and tautomerism of oxyxanthene dyes in aqueous butanol, *Dyes Pigm.*, 1999, **43**, 33–46.
73 R. Sjoback, J. Nygren and M. Kubista, Absorption and fluorescence properties of fluorescein, *Spectrochim. Acta, Part A*, 1995, **51**, 7–21.
74 X. F. Yang, Y. Lia and Q. Bai, A highly selective and sensitive fluorescein-based chemodosimeter for Hg^{2+} ions in aqueous media, *Anal. Chim. Acta*, 2007, **584**, 95–100.
75 S. Guanga, J. Tiana, G. Weia, Z. Yanc, H. Pand, J. Fengd and H. Xub, A modified fluorescein derivative with improved water-solubility for turn-on fluorescent determination of Hg^{2+} in aqueous and living cells, *Talanta*, 2017, **170**, 89–96.
76 Y. Fenga, Z. Kuaib, Y. Songa, J. Guoa, Q. Yanga, Y. Shanb and Y. Li, A novel "turn-on" thiooxofluorescein-based colorimetric and fluorescent sensor for Hg^{2+} and its application in living cells, *Talanta*, 2017, **170**, 103–110.

 This journal is © The Royal Society of Chemistry and the Centre National de la Recherche Scientifique 2019

Published on 09 February 2019. Downloaded by Jadavpur University on 12/5/2022 5:01:18 AM.

77 P. Piyanucha, S. Watpathomsuba, V. S. Leeb, H. A. Nienaberc and N. Wanichacheva, Highly sensitive and selective Hg^{2+}-chemosensor based on dithia-cyclic fluorescein for optical and visual-eye detections in aqueous buffer solution, *Sens. Actuators, B*, 2016, **224**, 201–208.

78 K. Tripathi, A. Rai, A. Kumar Yadav, S. Srikrishna, N. Kumari and L. Mishra, Fluorescein hydrazone-based supramolecular architectures, molecular recognition, sequential logic operation and cell imaging, *RSC Adv.*, 2017, **7**, 2264.

79 S. Erdemir and O. Kocyigit, A novel dye based on phenolphthalein-fluorescein as a fluorescent probe for the dual-channel detection of Hg^{2+} and Zn^{2}, *Dyes Pigm.*, 2017, **145**, 72–79.

80 U. Diwan, A. Kumar, V. Kumara, K. K. Upadhyay and P. K. Roychowdhury, A water compatible turn 'on' optical probe for Cu2+ based on a fluorescein–sugar conjugate, *Sens. Actuators, B*, 2014, **1963**, 45–351.

81 N. Wanichacheva, O. Hanmeng, S. Kraithonga and K. Sukrat, Dual optical Hg^{2+}-selective sensing through FRET system of fluorescein and rhodamine B fluorophores, *J. Photochem. Photobiol., A*, 2014, **278**, 75–81.

82 Z. Xie, F. Huo, J. Su, Y. Yang, C. Yin, X. Yan and S. Jin, Sensitive Colorimetric and Fluorescent Detection of Mercury Using Fluorescein Derivations, *Open J. Appl. Biosens.*, 2012, **1**, 44–52.

83 H. J. Kim, J. E. Park, M. G. Choi, S. Ahn and S. K. Chang, Selective chromogenic and fluorogenic signalling of Hg^{2+} ions using a fluorescein-coumarin conjugate, *Dyes Pigm.*, 2010, **84**, 54–58.

Inorganica Chimica Acta 543 (2022) 121165

Contents lists available at ScienceDirect

Inorganica Chimica Acta

journal homepage: www.elsevier.com/locate/ica

Research paper

A fluorescein-2-(Pyridin-2-ylmethoxy) benzaldehyde conjugate for fluorogenic turn-ON recognition of Hg^{2+} in water and living cells with logic gate and memory device applications

Hasan Mohammad [a], Abu Saleh Musha Islam [a,b], Mihir Sasmal [a], Chandraday Prodhan [c], Mahammad Ali [a,*]

[a] Department of Chemistry, Jadavpur University, Kolkata 700 032, India
[b] School of Chemical Sciences, Indian Association for the Cultivation of Science, 2A & 2B Raja S. C. Mullick Road, Kolkata 700032, India
[c] Department of Molecular & Human Genetics Division, CSIR-Indian Institute of Chemical Biology, 4 Raja S.C. Mallick Road, Kolkata 700032, India

ARTICLE INFO

Keywords:
Mercury ion sensing
Spirolactum ring opening
Molecular logic gate
Cell permeable

ABSTRACT

An effective Hg^{2+} specific probe, fluorescein-2-(Pyridin-2-ylmethoxy)-benzaldehyde conjugate (FO_{511}), was designed, synthesized and characterized by various instrumental techniques. The sensing behavior of FO_{511} was investigated by fluorescence technique which clearly established the high selectivity towards Hg^{2+} through OFF–ON fluorescence response in the presence of other metal ions like Zn^{2+}, Mg^{2+}, Co^{2+}, Ni^{2+}, Cu^{2+}, Pb^{2+}, Al^{3+}, Cr^{3+}, Cd^{2+}, Pd^{2+}, Fe^{2+} and Fe^{3+} in aqueous medium (pH 7.2, 10 mM HEPES buffer). The sensing mechanism could be attributed to the Hg^{2+} triggered spirolactam ring opening of the fluorescein moiety and simultaneous formation of a 1:1 FO_{511}–Hg^{2+} complex. The interaction and formation of FO_{511}–Hg^{2+} species was supported by the observations gained from fluorescence titrations, Job's plot, ^{1}H NMR and HRMS, and other spectroscopic studies. For the Hg^{2+} interaction towards FO_{511} the binding constant was evaluated to be $(3.21 \pm 0.05) \times 10^4$ M^{-1} with detection limit 92.7 nM. On addition of S^{2-} to the FO_{511}–Hg^{2+}complex, the fluorescence intensity was totally quenched due to removal of Hg^{2+} from the complex by S^{2-} ion arising out of stronger affinity of Hg^{2+} towards S^{2-} resulting concomitant formation of ring closed non-fluorescent form, FO_{511}. The tentative coordination environment in the FO_{511}–Hg^{2+}complex was established by DFT studies. FO_{511} exhibits low cytotoxicity and cell permeability, which makes it capable for bioimaging applications in living HepG2 cells.

1. Introduction

Mercury is known to be one of the most prevalent toxic metals in the environment. Mercury pollution pervades the globe and threatens to human health and the environment. Hg(0), Hg(II) and organic mercury, CH_3Hg^+ are the prevailing forms of Hg in nature and all of them are highly toxic. A living cell can be exposed to mercury through multiple pathways like, air [1], water [2], cosmetic products [3], and even vaccines [4]. More importantly; Hg (0) and Hg (II) ions present in soil or in waste water are assimilated and converted to methyl mercury, a potent neurotoxin, by the lower aquatic organisms which is subsequently bioaccumulated in the human body through food chain [5–7]. Organomercury can easily cross the cell membrane and the blood–brain barrier impairing nefrological and neurological functions. Therefore, mercury exposure, even at very low concentrations, can cause serious metabolic, motor and cognitive disorders and long term diseases in human beings [8–10]. The extreme toxicity of mercury and its derivatives results from their affinity towards thiol groups in proteins and enzymes that lead to malfunctioning of living cells [7] and eventually to serious health hazards.

Therefore, identification and quantification of mercury in numerous circumstances need efficient detection methods. Among various traditional methods, fluorescence spectroscopy might be the best choice for the detection of Hg^{2+} due to its rapid, sensitive, selective, non-destructive and easy operative features. In addition, it allows on-site and remote detections of mercury in the environmental samples [11–13]. Due to high atomic mass (A) and large spin − orbit coupling constant (ζ) Hg^{2+} mostly acts as a fluorescence quencher [14] and it is very difficult to realize an actual 'OFF–ON' fluorescence probe for Hg^{2+}. Again, an unavoidable background fluorescence signal restricts its

* Corresponding author at: Tel.: +91 33 2457 2035; Fax: +91 33 2414 6223.
E-mail addresses: m_ali2062@yahoo.com, mahammad.ali@jadavpuruniversity.in (M. Ali).

https://doi.org/10.1016/j.ica.2022.121165
Received 20 May 2022; Received in revised form 29 July 2022; Accepted 19 August 2022
Available online 28 August 2022
0020-1693/© 2022 Elsevier B.V. All rights reserved.

application in bio imaging process. Thus, fluorescein-based conjugate supposed to be a suitable choice for building an 'OFF–ON' fluorescent chemosensor exhibiting a special structural feature (spirolactam ring) and excellent photophysical properties of longer wavelengths of absorption and emission with larger absorption coefficient [15–20].

$S^{2-}$is extensively used in the industrial conversion S^{2-} into sulphur and sulphuric acid, in the manufacturing of cosmetics and dyes, in the production of wood pulp etc. [21] that may lead to contamination of water. The other sources of S^{2-} in nature are sulphur-containing amino acids in the meat proteins and microbial reduction of sulphate by anaerobic bacteria. Sulphide can irritate mucous membranes and even causes unconsciousness and respiratory paralysis [22,23]. Once protonated, HS^- or H_2S is even more toxic than sulphide (S^{2-}) itself. Abnormal concentrations of H_2S can cause Down syndrome, Alzheimer's disease, and liver cirrhosis [24]. H_2S can also cause loss of consciousness, permanent brain damage, or even death through asphyxiation [25,26]. So, there is an urgent need to develop a method with high sensitivity and selectivity for detection of sulphide ion in aqueous medium and in biological systems.

In this work, we are disclosing a new fluorescent sensor FO_{511} which selectively binds with Hg^{2+} to form FO_{511}–Hg^{2+} displaying a 'turn-on' fluorescence response through spirolactam ring opening, and subsequently reacts with S^{2-} displaying a 'turn-off' fluorescence response due to dislodging the Hg^{2+} ion from FO_{511}–Hg^{2+} complex selectively over other possible competitive anions leaving behind the ring closed non-fluorescent spirolactam form.

2. Experimental

2.1. Materials and instruments

Infrared spectra (400–4000 cm^{-1}) were recorded in solid state on a Nickolet Magna IR 750 series-II FTIR spectrometer. ^1H NMR spectra were generated in DMSO-d_6 and $CDCl_3$ solutions on a Bruker 300 MHz (AVI, 300) NMR spectrometer. Chemical shifts are expressed in parts per million (ppm, δ) and are referenced to tetramethylsilane ($\delta = 0$) as an internal standard. Signal description: s = singlet, d = doublet, t = triplet, m = multiplet, dd = doublet of doublets, q = quartet. ^{13}C NMR spectra were recorded in DMSO-d_6 with complete proton decoupling. ESI-MS^+ (m/z) studies of the ligand and complex were performed on a Waters' HRMS spectrometer (Model: **XEVO G2QTof**). UV–vis spectra were generated on an Agilent diode-array spectrophotometer (Model, Agilent 8453). Steady-state fluorescence measurements were carried out with a PTI QM-40 spectrofluorimeter. pH values of the reaction solutions were measured with a digital pH meter (Model: Systronics 335, India) in the pH range 2–10 which was prior calibrated using buffers of pH 4, 7 and 10. Fluorescein sodium salt, 2-chloromethylpyridine, $Hg(ClO_4)_2{\cdot}3H_2O$ and metal salts such as perchlorates of Zn^{2+}, Mg^{2+}, Co^2, Ni^{2+}, Cu^{2+}, Pb^{2+}, Al^{3+}, Cr^{3+}, Cd^{2+}, Pd^{2+}, Fe^{2+} Fe^{3+}, Mn^{2+}, Na^+, K^+, Ca^{2+}, and Ag^+ were bought from Sigma–Aldrich and used as received (Caution! Metal perchlorate salts are potentially explosive and should be handled in small quantity with care).Sodium salts of anions like SO_4^{2-}, $S_2O_4^{2-}$ SO_3^{2-}, $S_2O_3^{2-}$, PO_4^{3-}, S^{2-}, Cl^-, F^-, Br^-, I^-, $H_2PO_4^-$, CN^-, NO_2^-, CO_3^{2-}, ClO_4^- and N_3^- were of reagent grade and used as received.

2.2. Solution preparation for UV–Vis/fluorescence studies

For UV–Vis and fluorescence experiments, a 10 mL 1.0×10^{-3} M stock solution of FO_{511} was prepared by dissolving required amount of ligand in DMF-MeOH (1:9 v/v). In a similar way, standard solutions of 1.0×10^{-3} M $Hg(ClO_4)_2{\cdot}3H_2O$ and 1.0×10^{-3} M of sodium sulphide (Na_2S) in water were also prepared freshly at the time of spectroscopic studies. The standard solutions of other cations and anions were made in MeOH/H_2O. A 250 mL of 10 mM HEPES buffer in water was prepared and pH was maintained to 7.2 by using HCl and NaOH keeping ionic strength at 0.1 M with respect to NaCl. 2.5 mL of this buffer solution was pipetted out into a cuvette to which required volume of 1.0×10^{-3} M probe solution was transferred to achieve 10 μM final concentrations for fluorescence titration. In a regular interval of volume Hg^{2+} ions were added incrementally beginning from 0 to 46 μM and fluorescence and UV–Vis spectra were collected for each solution. The cuvettes of 1 cm path length were used for absorption and emission studies. Fluorescence experiments were done using 5 nm × 3 nm slit width.

2.3. Preparation of fluorescein hydrazide (L^1)

L^1 was prepared according to a literature method [27] as described in **Scheme S1** of supplementary information.

2.4. Preparation 2-(Pyridin-2-ylmethoxy)benzaldehyde (L^2):

L^2 was synthesized according to a literature method [28] as outlined in **Scheme S1**.

2.5. Synthesis of the receptor (FO_{511})

A mixture of 2-(Pyridin-2-ylmethoxy)benzaldehyde (0.692 g, 2 mmol)) and Fluorescein Hydrazide (0.424 g, 2 mmol) was dissolved in 20 mL of ethanol in the presence of 4 drops of acetic acid and the resulting solution was stirred under reflux for 6 h at an ambient temperature. The product precipitated from the reaction mixture and was collected by filtration. It was washed with cold ethanol and dried under vacuum to afford a white solid. 70 % yield was obtained. ^1H NMR (DMSO-d6): $\delta = 9.87$ (S, 2H), 8.91 (s, 1H), 8.59 (d, 1H), 7.96(m, 2H), 7.61 (m, 3H), 7.42 (m, 1H), 7.27 (d, 2H), 7.05 (s, 2H), 6.94 (m, 1H), 6.55 (d, 2H), 6.48 (s, 1H), 6.44 (s, 1H), 6.41 (s, 2H), 5.10 (s, 2H), (**Fig. S1**). **FT-**IR spectrum:–OH (3143 cm^{-1}), -C═N (1657 cm^{-1}), -C═O (1647 Cm^{-1}) (**Fig. S2**). ESI-MS^+: $m/z = 542.32$ (**$C_{33}H_{23}N_3O_5 + H^+$**) (**Fig. S3**).

2.6. Synthesis of the FO_{511}–Hg^{2+} complex

To a methanolic solution (5 mL) of the ligand (0.424 g, 0.27 mmol), a methanolic solution of $Hg(ClO_4)_2{\cdot}3H_2O$ (0.272 g, 0.6 mmol) was added. The resulting mixture was stirred for 1 h. The solvent was removed under vacuum and the whole mass was washed with ether several times to afford the complex as orange solid. ^1H NMR (DMSO-d_6): $\delta = 9.24$ (S, 1H), 8.92 (m, 1H), 8.35 (s, 1H), 7.88 (m, 2H), 7.57 (m, 2H), 7.35 (m, 2H), 7.09 (m, 2H), 6.60 (m, 10*H*), 5.43 (d, 2H), (**Fig. S4**). FTIR spectrum:–OH (3381 cm^{-1}), -C═N (1546 cm^{-1}), -C═O (1601 Cm^{-1}) (**Fig. S5**). ESI-MS^+: $m/z = 840.24$ (**$C_{37}H_{22}N_3O_5Hg_1ClO_4$**) (**Fig. S6**).

2.7. Computational studies

All calculations relating to optimization of geometries of FO_{511} and FO_{511}-Hg^{2+} were performed with the Gaussian 09 program [29] with the help of the density functional theory (DFT) at the B3LYP [30] level. The calculations were supported by the Gauss View visualization program. All elements except Hg were assigned the 6-31G basis set. For the Hg atom the LanL2DZ basis with effective core potentials was employed. Vibrational frequency calculations were performed to ascertain that the optimized geometries correspond to local minima as reflected by positive eigenvalues.

2.8. Cell culture

Human hepatocellular liver carcinoma (HepG2) cell lines (NCCS, Pune, India), were grown in DMEM supplemented with 10 % FBS and antibiotics (penicillin-100 μg/ml; streptomycin-50 μg/ml). Cells were cultured at 37 °C in 95 % air, 5 % CO_2 incubator.

2.9. Cell cytotoxicity assay

Cytotoxic effects of FO_{511} on living cells were assessed employing 3-(4,5-dimethylthiazol-2-yl)-2,5-diphenyltetrazolium bromide (MTT) by cell viability assay method. HepG2 cells (3 × 104 cells/well) were cultured in a 96-well plate and incubated at 37 °C followed by exposure to varying concentrations of FO_{511} (1, 5, 10, 20, 40, 50, 60, 70, 80, 90 and 100 μM) for 24 h. After the incubation, 10 μL of MTT solution [5 mg/ml, dissolved in 1X phosphate-buffered saline (PBS)] was added to each well of a 96-well culture plate, and then incubated at 37 °C for 4 h. Media were decanted from wells and 100 μL of 0.04 N acidic isopropyl alcohol was added into each well to solubilize intracellular formazan crystals (blue-violet) formed and absorbance of each solution was measured at 595 nm on EMax Precision MicroPlate Reader (Molecular Devices, USA). Values were calculated as mean ± standard errors of three independent experiments. The cell viability was expressed as the optical density ratio of the treatment to control.

2.10. Cell imaging study

HepG2 Cells (1×10^3) were cultured in 35 × 10 mm culture dish on coverslip for 24 h at 37 °C. The cells were treated with 10 μM solutions FO_{511}, prepared by dissolving FO_{511} in the mixed solvent DMSO: water = 1:9 (v/v) and incubated for 1 h at 37 °C. To study the complex formation ability with Hg^{2+} ions, HepG2 cells were pre-incubated with 10 μM and 20 μM of Hg^{2+} for 60 min at 37 °C. Then it was washed three times with 1X PBS and subsequently incubated with 10 μM of FO_{511} for 60 min at 37 °C. Fluorescence images of HepG2 cells were taken by a fluorescence microscope (Leica DM3000, Germany) with an objective lens of 40X magnification.

3. Result and discussion

As demonstrated in **Scheme S1**, the probe FO_{511} was readily prepared from the acetic acid mediated condensation reaction between 2-(Pyridin-2-ylmethoxy)-benzaldehyde (**L**^{1}) and equimolecular amount of Fluorescein hydrazide in ethanol for 6 h under reflux. The pure product was achieved as an off-white solid in 80 % yield. Then, it was thoroughly characterized using ^{1}H NMR, ESI-MS$^+$ and FT-IR spectral analysis (**Fig. S1–S3**). In the IR spectrum, the appearance of the characteristic peak of imine (-C═N) at 1657 Cm^{-1} clearly suggests the formation of the Schiff base.

3.1. Photophysical characteristics of FO_{511}

The UV–Vis spectrum of the probe FO_{511} was recorded in 10 mM HEPES buffer at pH 7.2. On addition of Hg^{2+} the absorption band at 370 nm showed a gradual red shift with concomitant increase in absorption at around 475 nm without developing a well-defined absorption peak. The dilution effects on spectra were also studied where it was observed that the two spectra are almost same (**Fig. S7**). So, we can say that the absorption change of FO_{511} is occurred due to dilution effect [31].

The fluorescence titration of the probe FO_{511} was executed in pure aqueous buffer at pH 7.2 using 10 mM HEPES (2-[4-(2-hydroxyethyl)-1-piperazinyl]ethane sulfonic acid). As delineated in Fig. 1**a**, free probe FO_{511} itself is very weakly fluorescent due to the Spiro cyclic structure. However, upon addition of increasing concentrations of Hg^{2+} (0–46 μM) to a 10.0 μM solution of FO_{511}, an intense new fluorescence emission band at 511 nm was noticed. It displayed a strong green fluorescence with an approximately ~44-fold enhancement in the fluorescence intensity. This enhancement was attributed to Hg^{2+} promoted spirolactam ring opening [18] of FO_{511}.

Thus, the reaction of Hg^{2+} with a chelating agent FO_{511} induces spirolactam ring opening along with rigidity in the resulting molecule that leads to a large enhancement of fluorescence intensity (CHEF effect) [7,32,33]. The detection of Hg^{2+} was not perturbed by the presence of Zn^{2+}, Mg^{2+}, Co^{2+}, Ni^{2+}, Cu^{2+}, Pb^{2+}, Al^{3+}, Cr^{3+}, Cd^{2+}, Pd^{2+}, Fe^{2+}, Fe^{3+} (**Fig. S8**) and Ag^+ (**Fig. S9**). However, other competitive metal ions like Zn^{2+}, Mg^{2+}, Co^{2+}, Ni^{2+}, Cu^{2+}, Pb^{2+}, Al^{3+}, Cr^{3+}, Cd^{2+}, Pd^{2+}, Fe^{2+} and Fe^{3+} have hardly any response towards enhancement of emission of the probe (**Fig. S10**). This establishes the fact that FO_{511} binds selectively with Hg^{2+} in the presence of a variety of interfering metal ions present in environmental and biological settings. Furthermore, for the biological application, the effect of pH on the fluorescence response of probe FO_{511} upon binding with Hg^{2+} was also scrutinized at varying pH values from 2.0 to 10.0 by fluorescence titration. As depicted in Fig. 2, the fluorescence intensity of FO_{511} is stable in the range pH 2–7 without obvious fluorescence responses. When the pH is greater than 7, the deprotonation of the aromatic hydroxyl group (–OH) [34-37] leads to slight fluorescence enhancement at alkaline conditions. However, upon addition of 46 μM Hg^{2+}, there is a gradual increase in fluorescence intensity on increase in pH of the medium from 4.0 to 10.0, especially from 7.0 to 10.0, which suggests that Hg^{2+} promotes the formation of ring-opened FO_{511}–Hg^{2+} complex. Hence, considering the above observations we set pH 7.2 as the experimental condition, which also mimics physiological environment, to detect Hg^{2+} ions.

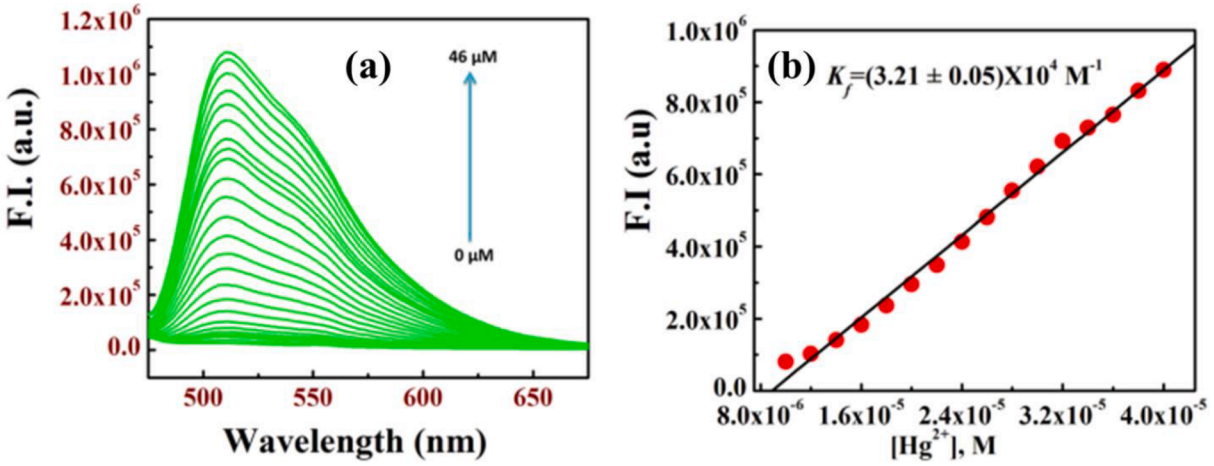

Fig. 1. (a) Fluorescence titration of **FO_{511}** (10.0 μM) in 10 mM HEPES buffer at pH 7.2 by addition of increasing concentration of Hg^{2+} (0–46 μM) with λ_{ex} = 475 nm and λ_{em} = 511 nm. (b) linear fit plot of FI vs [Hg^{2+}].

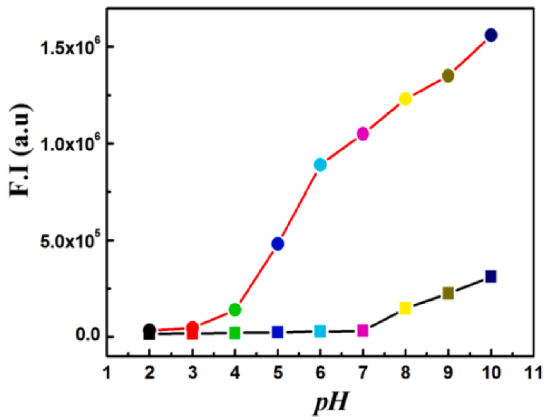

Fig. 2. Fluorescence intensity vs pH plot at 511 nm with 10 μM (demonstrated by black line) of FO_{511} and FO_{511}-Hg^{2+} complex (denoted by red line).

3.2. Determination of binding constant and stoichiometry of the reaction

The binding constant was evaluated by plotting FI versus [Hg^{2+}] that gives an excellent linear curve, which was solved by adopting the equation $y = (a + b \times c \times x^n)/(1 + c \times x^n)$ [38], where a = FI of free probe, b = maximum fluorescence in the presence of excess Hg^{2+} (F_{max}), c = K_f, formation constant with the assumption that $1 \gg c \times x^n$ with n = 1. So, slope of the curve is b × c and slope/F_{max} gives $K_f = (3.21 \pm 0.05) \times 10^4\ M^{-1}$ (where b = 1.07894 × 10^6) (Fig. 1**b**). The Job's plot displayed a 1:1 stoichiometry between the probe FO_{511} and Hg^{2+} (**Fig. S11**). Furthermore, ESI-MS^+ were used to confirm the 1:1 coordination mode between FO_{511} and Hg^{2+}. Without Hg^{2+}, the *m/z* 542.32 peak corresponds to $(FO_{511} + H)^+$. When, Hg^{2+} was introduced into a solution of **FO_{511}**, a peak appeared at *m/z* 840.24 was assigned to the complex (FO_{511}–Hg^{2+} - H^+), and this agreed with the calculated value of 840.3 for the 1:1 complex. (Fig. 3).

3.3. Limit of detection

The 3σ method was adopted to determine the limit of detection (LOD) of Hg^{2+} and S^{2-}. It was evaluated to be 92.7 nM (**Fig. S12**) for Hg^{2+} and 0.231 μM (**Fig. S13**) for S^{2-}. It clearly suggests that FO_{511} is an efficient probe for monitoring traces of Hg^{2+} and S^{2-} ions. The present probe has better detection limit as compared to earlier reported probes [39,40] The quantum yields of FO_{511} and FO_{511}-Hg^{2+} complex were also determined to be 0.0041 and 0.1435, respectively using fluorescein as a standard (0.5 in ethanol). The quantum yield of FO_{511} is increased upon binding with the Hg^{2+} ion. However, some of the fluorescent probe reported earlier could not enhance the quantum yield on binding of Hg^{2+} ions [41]. These results suggested that the probe FO_{511} is highly sensitive towards Hg^{2+} ions.

3.4. S^{2-} induced displacement of Hg^{2+} and S^{2-} sensing

From the above experiment, we can conclude that FO_{511} specifically binds with Hg^{2+} to form FO_{511}–Hg^{2+} complex with a remarkable enhancement in fluorescence intensity. As Hg^{2+} can bind with S^{2-} to form a stable species HgS, we conjectured that the FO_{511}–Hg^{2+} ensemble can serve as a candidate for a turn-off fluorescent sensor for S^{2-}. To support this idea, the fluorescence spectra of the FO_{511}–Hg^{2+} ensemble, (prepared in solution by adding 10 μM FO_{511} and 46 μM Hg^{2+}) and were studied in the presence of 5 equivalents of different anions such as SO_4^{2-}, $S_2O_4^{2-}$, SO_3^{2-}, $S_2O_3^{2-}$, PO_4^{3-}, Cl^-, F^-, Br^-, I^-, $H_2PO_4^-$, CN^-, NO_2^-, CO_3^{2-}, ClO_4^- and N_3^- which did not induce any significant change in emission intensity (**Fig. S14**). However, it is very interesting to note that upon addition of 70 μM S^{2-} to the FO_{511}–Hg^{2+} solution only S^{2-} causes a significant fluorescence quenching at 511 nm (Fig. 4). Besides, the detection of S^{2-} was not perturbed by the presence of other sulphur species like SO_4^{2-}, $S_2O_4^{2-}$, SO_3^{2-}, $S_2O_3^{2-}$. It is considered that the decrease in fluorescence intensity is due to the formation of HgS thereby releasing FO_{511} in its spirolactam form indicating the fact that Hg^{2+} has a stronger affinity towards Hg^{2+} compared to that of FO_{511}.

3.5. Binding Mechanism:

The proposed mechanistic pathway of the formation of FO_{511}–Hg^{2+} complex via opening of spirolactam ring was investigated through IR and ^1H NMR studies. IR studies revealed that the characteristic stretching frequency for the 'C═O' in amide group of the fluorescein moiety at 1657 cm^{-1} was shifted to lower wave number of 1601 cm^{-1} in the presence of 1.5 equivalent of Hg^{2+}. The larger shift towards lower

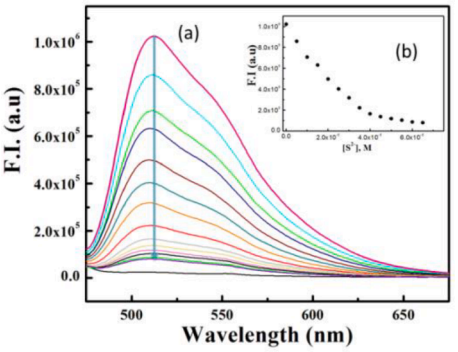

Fig. 4. (a) Fluorescence titration of FO_{511}-Hg^{2+} by adding S^{2-} (70 μM) in 10 mM HEPES buffer at pH 7.2 (b) Fluorescence intensity at 511 nm vs concentration of S^{2-}.

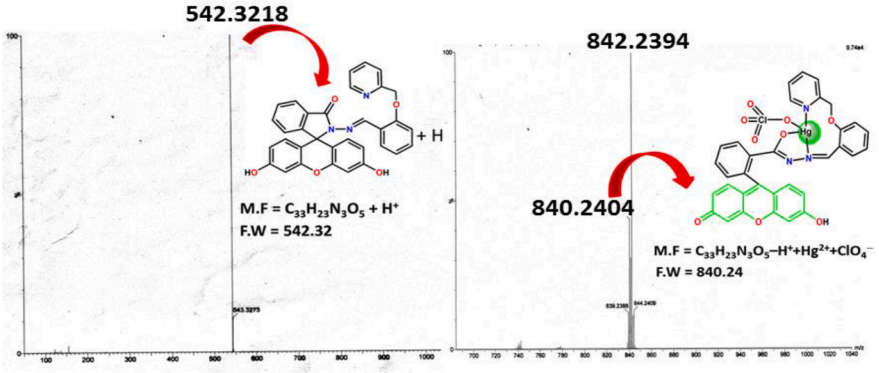

Fig. 3. HRMS spectrum of **FO_{511}** and the **FO_{511} - Hg^{2+}** complex.

wave number signifies a higher polarization of the C═O bond upon efficient binding with Hg^{2+} ion (**Fig. S5**). Also, in ^{1}H NMR, the imine proton (–CH = N) showed downfield shift by $\delta = 0.24$ ppm (8.59 to 8.35 ppm) in the presence of 1.5 equiv. Hg^{2+} of ions signifying the coordination of azomethine-N to Hg^{2+} (**Fig. S4**). It was confirmed by HRMS analysis and the result was displayed in Fig. 3. Without Hg^{2+}, the *m/z* 542.32 peak corresponded to $[FO_{511} + H]^+$. When Hg^{2+} was introduced to a solution of FO_{511}, a peak appeared at *m/z* 840.23 can be assigned to the complex $[FO_{511} - Hg^{2+} - H]^+$ (**Fig. S6**). Thus, based on ^{1}H NMR, IR, ESI-MS$^+$, Job's plot and HRMS studies, we proposed a probable mechanism of binding of Hg^{2+} ions to FO_{511} as shown in (scheme 1).

3.6. Reversibility

Reversibility and regeneration are other important factors for the development of successful devices for sensing of analytes for practical applications. The reversibility of the binding process between FO_{511} and Hg^{2+} was established when the introduction of 70 μM of S^{2-} into a solution containing FO_{511} (10 μM) and Hg^{2+} (46 μM) resulted in quenching of emission intensity at 511 nm (Fig. 5). Due to strong affinity of S^{2-} for the Hg^{2+} ions, demetallation of FO_{511}–Hg^{2+} complex occurred causing the fluorescence quenching. Then further addition of Hg^{2+} (80 μM) ions under the same condition, immediately revived the fluorescence. Therefore, this study renders the probe as a reversible sensor for the selective recognition of Hg^{2+} ions in pure aqueous medium under physiological conditions.

3.7. Geometry optimization and electronic structure

Both probe (**FO_{511}**) and the complex (**FO_{511}–Hg^{2+}**) have the *C1* point group. The main optimized geometrical parameters of the complex and ligand are listed in **Tables S1 and S2** and the optimized structures of probe (FO_{511}) and the complex (FO_{511}–Hg^{2+}) are given in Fig. 6**a**. In the ground state of **FO_{511}** the HOMO and LUMO electron densities mainly spreaded over the formic acid (2-methoxy-benzylidene)-hydrazide and 2-Methyleneamino-2,3-dihydro-isoindol-1-one moieties respectively with a HOMO - LUMO energy gap of 4.24 eV. In the case of FO_{511}–Hg^{2+} the HOMO mainly has ligand π and π* orbital contributions, while the LUMO resides mainly on the Mercuric perchlorate part with a HOMO – LUMO energy gap of 1.03 eV (Fig. 6**b**). As a result, a substantial change in fluorescence intensity is observed on moving from free ligand to its Hg^{2+} complex.

3.8. Molecular logic operation

It has been observed that FO_{511} itself is in fluorescence OFF state which on coordination with Hg^{2+} forms FO_{511}–Hg^{2+} complex, resulting in the fluorescence "**ON**" state; while on further addition of S^{2-} to FO_{511}–Hg^{2+} complex restoration of fluorescence 'OFF' state occurs. Based on this principle, we can make a correlation by taking two inputs,

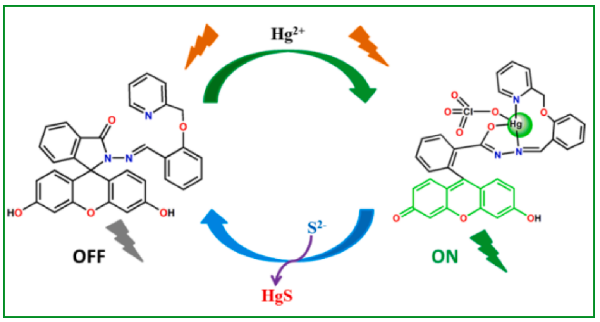

Scheme 1. A proposed binding mechanism between the receptor **FO_{511}** and Hg^{2+}.

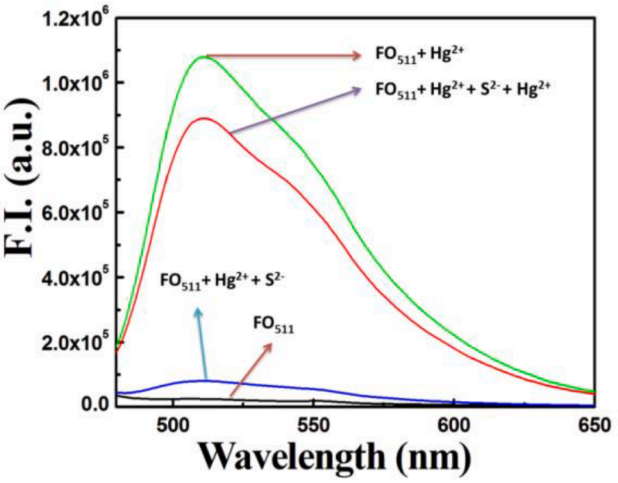

Fig. 5. Reversibility checking of Hg^{2+} coordination to **FO_{511}** and subsequent displacement by Na_2S. The black curve represents the fluorescence intensity of free FO_{511}; the green line represents the fluorescence enhancement after the addition of 46 μM Hg^{2+}, the blue line represents the fluorescence decrease after the addition of 70 μM S^{2-} into the solution of **FO_{511}–Hg^{2+}** species and the red line represents the fluorescence enhancement again after the addition of 80 μM Hg^{2+} into the [**FO_{511}–Hg^{2+}** + S^{2-}] solution.

namely input 1 (Hg^{2+}) and input 2 (S^{2-}), along with fluorescence intensity changes of the probe FO_{511} at 520 nm as the outputs. For the input 1, output is assigned as 1 (ON state) while for input 1 and then input 2 the output is 0 (OFF state). The four possible input combinations are possible as (0, 0), (1, 0), (0, 1) and (1, 1), as shown in the truth table (Fig. 7**a**). Again, with no input, or with S^{2-} input alone, the output was 0. With Hg^{2+} input alone the output signal was 1. Therefore, monitoring the fluorescence at 520 nm, upon addition of Hg^{2+} and S^{2-} and their combined mixture satisfies an INHIBIT logic gate function (Fig. 7**b**).

3.9. Cell imaging studies

Considering the selective binding property of FO_{511} with Hg^{2+} ion, it tempted us to check its sensing ability of Hg^{2+} in living cells. Before doing this, we checked the cytotoxicity of FO_{511} on living cells using MTT assay on HepG2 cells (**Fig. S15**.). It is interesting to note that at 10 μM of FO_{511} ~ 80 % cell viability could be achieved; as evidenced from a decrease in formazan production by FO_{511} up to 10 μM, thus suggesting that below 10 μM concentration FO_{511} would be much more effective for *in vitro* tracking of Hg^{2+} ion. Hence, further experiments were carried out with 10 μM of FO_{511}.

When excited at 465 nm, the ligand FO_{511} exhibited absence of intracellular fluorescence on HepG2 cells. However, on treatment with 10 μM of FO_{511} for 1 h (Fig. 8) followed by incubation with 10 μM of Hg^{2+} for 1 h at 37 °C HepG2 cells showed a prominent green intracellular fluorescence, predominantly localized in the cytoplasmic region. Keeping the ligand FO_{511} concentration constant at 10 μM, and increasing concentration of Hg^{2+} ions (from 10 μM to 20 μM) a concentration-dependent enhancement in the intracellular green fluorescence is prevalent. Again, upon incubation with 20 μM of Hg^{2+} towards 10 μM FO_{511} for 1 h followed by washing and then incubation with 10 μM S^{2-} exhibited a tremendous reduction in the intracellular fluorescence. Hence the present ligand with low cytotoxicity can be used as a potential *in vitro* selective tracker of Hg^{2+}.

4. Conclusions

A simple fluorescein-based reversible chemosensor FO_{511} has been developed which selectively and sensitively recognises Hg^{2+} over other competing metal ions in 100 % aqueous medium at pH 7.2 (10 mM

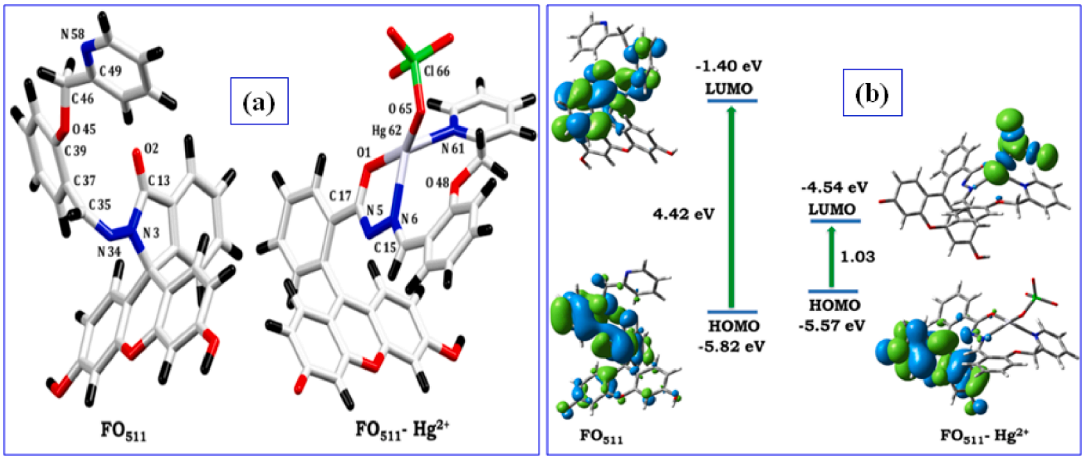

Fig. 6. (a) Optimized geometries of probe (**FO_{511}**) and the complex (**FO_{511}–Hg^{2+}**) in DFT calculation. (b) Frontier molecular orbital of **FO_{511}** as well as **FO_{511}–Hg^{2+}** complex optimized under DFT.

Input		output
In 1 (Hg^{2+})	In 2 (S^{2-})	Out (at 511 nm)
0	0	0
1	0	1
0	1	0
1	1	0

(a)

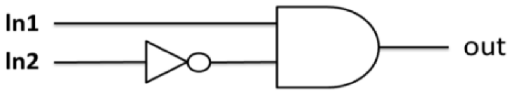

(b)

Fig. 7. (a) Truth table of the logic gate. (b) a general representation of an INHIBIT logic gate.

HEPES buffer), temperature 25 °C with 44-fold fluorescence enhancement due to spirolactam ring opening upon coordination with Hg^{2+}. A 1:1 mol binding ratio is evidenced from Job's method and ESI-MS^{+} (*m/z*) studies. The corresponding LOD was found to be 92.7 nM. Theoretical calculations established the metal–ligand binding through optimizing their structures. The cell imaging and MTT assay experiments further demonstrated the cell permeability and negligible cytotoxicity making the probe suitable for the assessment of Hg^{2+} in biological systems. Thus, FO_{511} meets all the requirements to be an excellent fluorescent probe for wide applications in the field of bio-labelling, bio sensing, imaging and so on. Table S3 has been prepared to compare a few aspects e.g. working medium, limit of detection, biological study, reversibility and quantum yield of some recently published chemosensors for the Hg^{2+} ion [42–47]. In most cases, biological studies were not performed. Also most of the studies were done in mixed organo-aqueous or organic medium.

CRediT authorship contribution statement

Hasan Mohammad: Investigation, Methodology, Writing – original draft. **Abu Saleh Musha Islam:** Software, Validation. **Mihir Sasmal:** Investigation, Methodology. **Chandraday Prodhan:** Validation. **Mahammad Ali:** Conceptualization, Formal analysis, Funding acquisition, Investigation, Methodology, Project administration, Resources, Supervision, Visualization, Writing – review & editing.

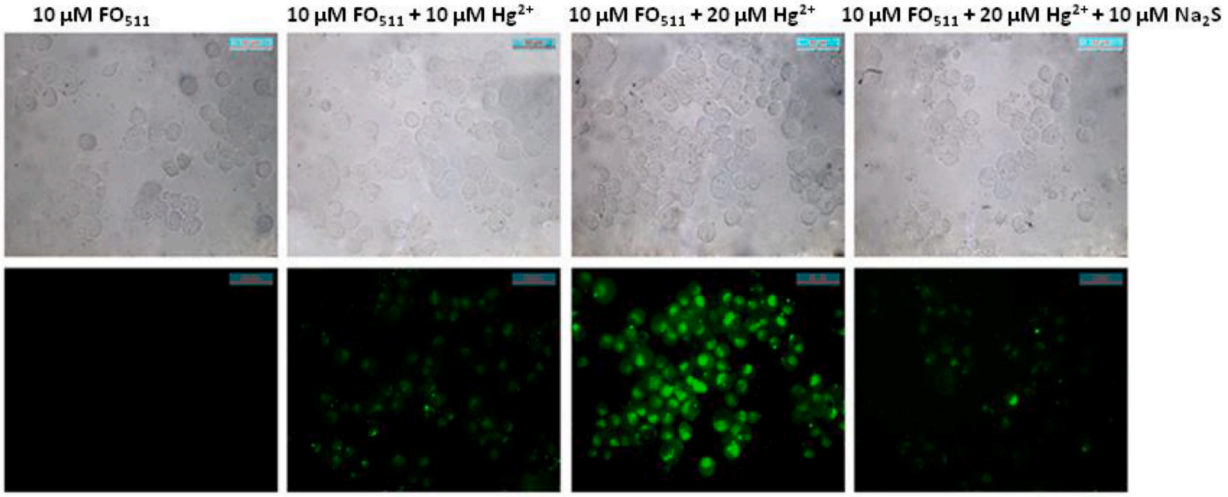

Fig. 8. The fluorescence images of HepG2 cells were captured (40X) after incubation with 10 μM of **FO_{511}** for 1 h at 37 °C followed by washing thrice with 1X PBS. Incubation separately with 10 μM and 20 μM of Hg^{2+} for 1 h at 37 °C and then washing with 1X PBS followed by incubation with 10 μM of **FO_{511}** for 1 h at 37 °C. Again, the fluorescence emission reduced significantly in presence of 10 μM of Na_2S, acting as a quencher.

Declaration of Competing Interest

The authors declare that they have no known competing financial interests or personal relationships that could have appeared to influence the work reported in this paper.

Data availability

Data will be made available on request.

Acknowledgements

Financial supports from the DST (Ref. No. 809(Sanc.)/ST/P/S&T4G-9/2104), West Bengal and the CSIR (Ref. 01(2896)/17/EMR-II), New Delhi, India are gratefully acknowledged. HM is grateful for UGC-MANF Fellowship (2012-13-MANF-MUS-WES-13502), UGC, New Delhi, India, ASMI acknowledges the Science and Engineering Research Board (SERB) for a National Postdoctoral Fellowship (NPDF).

Appendix A. Supplementary data

Supplementary data to this article can be found online at https://doi.org/10.1016/j.ica.2022.121165.

References

[1] S.A. Counter, L.H. Buchanan, Toxicol. Appl. Pharmacol. 198 (2004) 209–230.
[2] H. Kariyanna, G.S. Sitaram, J. Appl. Geochem. 9 (2007) 142–149.
[3] I. Al-Saleh, I. Al-Doush, J. Toxicol. Environ. Health 51 (1997) 123–130.
[4] E.K. Silbergeld, Am. J. Public Health 98 (2008) 1350.
[5] H.H. Harris, I.J. Pickering, G.N. George, Science 301 (2003) 1203.
[6] S. Yoon, A.E. Albers, A.P. Wong, C.J. Chang, J. Am. Chem. Soc. 127 (2005) 16030.
[7] E.M. Nolan, S.J. Lippard, Chem. Rev. 108 (2008) 3443.
[8] H.H. Harris, I.J. Pickering, G.N. George, Science 303 (2004) 764.
[9] S.K. Arya, S. Bhansali, Chem. Rev. 111 (2011) 6783.
[10] A.K. Manna, J. Mondal, R. Chandra, K. Rout, G.K. Patra, J. Photochem. Photobiol., A 356 (2018) 477–488.
[11] N. Wanichacheva, M. Siriprumpoonthum, A. Kamkaew, K. Grudpan, Tetrahedron Lett. 50 (2009) 1783–1786.
[12] W. Liu, J. Chen, L. Xu, J. Wu, H. Xu, H. Zhang, P. Wang, Spectrochim. Acta Part A Mol. Biomol. Spectrosc. 85 (2012) 38–42.
[13] X. Hu, X. Zhang, G. He, C. He, C. Duan, Tetrahedron 67 (2011) 1091–1095.
[14] J.F. Zhang, J.S. Kim, Anal. Sci. 25 (2009) 1271–1281.
[15] A. Ajaya ghosh, P. Carol, S. Sreejith, J. Am. Chem. Soc. 127 (2005) 14962.
[16] J.W. Lee, H.S. Jung, P.S. Kwon, J.W. Kim, R.A. Bartsch, Y. Kim, S. Kim, J.S. Kim, Org. Lett. 10 (2008) 3801.
[17] L. Xue, Q. Liu, H. Jiang, Org. Lett. 11 (2009) 3454.
[18] M. Leermakers, W. Baeyens, P. Quevauviller, M. Horvat, Trends *Anal. Chem.* 24 (2005) 383.
[19] C.C. Huang, H.T. Chang, Anal. Chem. 78 (2006) 8332.
[20] S. Cai, Y. Lu, S. He, F. Wei, L. Zhao, X. Zeng, Chem. Commun. 49 (2013) 822.
[21] Hydrogen Sulfide; World Health Organization: Geneva, 1981(Environmental Health Criteria, No. 19).
[22] R. E. Gosselin, R. P. Smith, H. C. Hodge, Hydrogen Sulfide. In Clinical Toxicology of Commercial Products, Williams and Wilkins: Baltimore, MD, 1984; pp. III-198−III-202.
[23] S.A. Patwardhan, S.M. Abhyankar, Colourage 35 (1988) 15–18.
[24] R. Wang, F. Yu, L. Chen, H. Chen, L. Wang, W. Zhang, Chem. Commun. 48 (2012) 11757.
[25] P. A. Patnaik, Wiley: New York, 2007.
[26] A.K. Manna, J. Mondal, R. Chandra, K. Rout, G.K. Patra, Anal. Methods 10 (20) (2018) 2317–2326.
[27] X. Bao, Q. Cao, X. Wu, H. Shu, B. Zhou, Y. Geng, J. Zhu, Tetrahedron, Tetrahedron Lett. 57 (2016) 942–948.
[28] A.S.M. Islam, R. Bhowmick, H. Mohammad, A. Katarkar, K. Chaudhuri, M. Ali, New J. Chem. 40 (2016) 4710.
[29] M. J. Frisch, G. W. Trucks, H. B. Schlegel, G. E. Scuseria, M. A. Robb, J. R. Cheeseman, G. Scalmani, V. Barone, B. Mennucci, G. A. Petersson, H. Nakatsuji, M. Caricato, X. Li, H. P. Hratchian, A. F. Izmaylov, J. Bloino, G. Zheng, J. L. Sonnenberg, M. Hada, M. Ehara, K. Toyota, R. Fukuda, J. Hasegawa, M. Ishida, T. Nakajima, Y. Honda, O. Kitao, H. Nakai, T. Vreven, J. A. Montgomery Jr., J. E. Peralta, F. Ogliaro, M. Bearpark, J. J. Heyd, E. Brothers, K. N. Kudin, V. N. Staroverov, R. Kobayashi, J. Normand, K. Raghavachari, A. Rendell, J. C. Burant, S. S. Iyengar, J. Tomasi, M. Cossi, N. Rega, J. M. Millam, M. Klene, J. E. Knox, J. B. Cross, V. Bakken, C. Adamo, J. Jaramillo, R. Gomperts, R. E. Stratmann, O. Yazyev, A. J. Austin, R. Cammi, C. Pomelli, J. W. Ochterski, R. L. Martin, K. Morokuma, V. G. Zakrzewski, G. A. Voth, P. Salvador, J. J. Dannenberg, S. Dapprich, A. D. Daniels, Ö. Farkas, J. B. Foresman, J. V. Ortiz, J. Cioslowski and D. J. Fox, Gaussian 09 (Revision A.1), Gaussian, Inc., Wallingford, CT, 2009.
[30] (a) M. Cossi, N. Rega, G. Scalmani and V. Barone, Energies, structures, and electronic properties of molecules in solution with the C-PCM solvation model, *J. Comput. Chem.*, 2003, 24, 669–681 Cross Ref CAS PubMed. (b) A. D. Becke, Density-functional thermochemistry. III. The role of exact exchange, J. Chem. Phys., 1993, 98, 5648–5652 Cross Ref CAS. (c) C. Lee, W. Yang and R. G. Parr, Development of the Colle-Salvetti correlation-energy formula into a functional of the electron density, Phys. Rev. B: *Condens. Matter Mater. Phys.*, 1998, **37,** 785–789.
[31] H. Mohammad, A.S.M. Islam, R. Bhowmick, C. Prodhan, M. Ali, New J. Chem. 43 (2019) 4710.
[32] A. Tamayo, B. Pedras, C. Lodeiro, L. Escriche, J. Casabo, L. Capelo, B. Covelo, R. Kiveka, R. Sillanpa, Exploring the Interaction of Mercury (II) by N_2S_2 and NS_3 Anthracene-Containing Macrocyclic Ligands: Photophysical, Analytical, and Structural Studies, Inorg. Chem. 46 (2007) 7818–7826.
[33] Y. Zhang, Y. Yang, J. Hao, C. Yin, F. Huo, J. Chao, D. Liu, Spectroscopic study of the recognition of 2-quinolinone derivative on mercury ion, Spectrochim. Acta A 132 (2014) 27–31.
[34] V.R. Batistela, J.D.C. Cedran, H.P.M.D. Oliveira, I.S. Scarminio, L.T. Ueno, A.E.D. H. Machado, N. Hioka, Dyes Pigm. 86 (2010) 15–24.
[35] L.N. Bogdanova, N.O. Mchedlov-Petrossyan, N.A. Vodolazkaya, A.V. Lebed, Carbohydr. Res. 345 (2010) 1882–1890.
[36] N.O. Mchedlov-Petrossyana, O.N. Tychina, T.A. Berezhnaya, V.I. Alekseeva, L. P. Savvina, Dyes Pigm. 43 (1999) 33–46.
[37] R. Sjoback, J. Nygren, M. Kubista, Spectrochim. Acta A 51 (1995) 7–21.
[38] C.R. Lohani, J.M. Kim, S.Y. Chung, J. Yoon, K.H. Lee, Analyst 135 (2010) 2079–2084.
[39] Y. Yang, F. Huo, C. Yin, Y. Chu, J. Chao, Y. Zhang, J. Zhang, S. Li, H. Lv, A. Zheng, D. Liu, Sens. Actuators, B 177 (2013) 1189.
[40] K. Tripathi, A. Rai, A.K. Yadav, S. Srikrishna, N. Kumari, L. Mishra, RSC Adv. 7 (2017) 2264.
[41] E.M. Nolan, M.E. Racine, S.J. Lippard, Inorg. Chem. 45 (2006) 2742.
[42] L.i. Huanga, Y. Suna, G. Zhaoa, L. Wang, X. Menga, J. Zhoua, H. Duan, J. Mol. Struct. 1255 (2022), 132427.
[43] D. Liu, Y. Wang, R. Wang, B. Wang, H. Chang, J. Chen, G. Yang, H. He, Inorg. Chem. Commun. 89 (2018) 46–50.
[44] Y. Fenga, Z. Kuaib, Y. Songa, J. Guoa, Q. Yanga, Y. Shanb, Y. Li, A novel "turn-on" thiooxofluorescein-based colorimetric and fluorescent sensor for Hg^{2+} and its application in living cells, Talanta 170 (2017) 103–110.
[45] P. Piyanucha, S. Watpathomsuba, V.S. Leeb, H.A. Nienaberc, N. Wanichacheva, Highly sensitive and selective Hg^{2+}-chemosensor based ondithia-cyclic fluorescein for optical and visual-eye detectionsin aqueous buffer solution, Sens. Actuators B: Chem. 224 (2016) 201–208.
[46] K. Tripathi, A. Rai, A. Kumar Yadav, S. Srikrishna, N. Kumari, L. Mishra, Fluorescein hydrazone-based supramolecular architectures, molecular recognition, sequential logic operation and cell imaging, RSC Adv. 7 (2017) 2264.
[47] S. Erdemir, O. Kocyigit, A novel dye based on phenolphthalein-fluorescein as a fluorescent probe for the dual-channel detection of Hg^{2+} and Zn^{2+}, Dyes Pigm. 145 (2017) 72–79.

ARTICLE

A Fluorescein-2-Hydroxy-3-hydroxymethyl-5-methyl-benzaldehyde conjugate as a highly selective and sensitive chemosensor for Hg^{2+} ions with cell imaging possibility

Received 00th January 20xx,
Accepted 00th January 20xx

DOI: 10.1039/x0xx00000x

Hasan Mohammad[a], Mihir Sasmal[a], Chandraday Prodhan[b], and Mahammad Ali[a,*]

The design and synthesis of an effective Hg^{2+}- specific probe **HL^3** based on Fluorescein-2-Hydroxy-3-hydroxymethyl-5-methyl-benzaldehyde conjugate. The sensing performance of **HL^3** was investigated by fluorescence spectroscopy. The probe displayed excellent sensitivity and selectivity towards Hg^{2+} over other tested metal ions in CH_3OH : H_2O 7:3 medium (pH 7.2, 10 mM HEPES), which could be ascribed to the Hg^{2+} induced ring opening of the spirolactam of the flourescein moiety. The 1:1 binding of **HL^3** to Hg^{2+} was recognized by Job's method and confirmed by ESI-MS$^-$ (m/z) studies and the Lod value was calculated and found to be 0.46 µM. The **HL^3** also shows bio-compatibility and low cytotoxicity and is suitable for fluorescence cell imaging of Hg^{2+} ions in live HepG2 cells.

Introduction

Heavy metal pollution has identified one of the global environmental pollution problems of concern [1]. Due to exhaust emissions, mining, sewage irrigation and the excessive use of heavy metal products, the content of heavy metal ion has surpassed the normal range. This can damage to human health and also can harm to environmental quality [2–5].

Mercury is one of the most hazardous and prevalent global pollutant.[6] The long atmospheric residence time of Hg(0) vapor and its oxidation to soluble inorganic Hg^{2+} provides a pathway for contaminating vast amounts of water and soil. [7]

In the marine system, both elemental mercury (Hg) and ionic (Hg^{2+}) can be converted into methyl mercury by bacteria, which then will be absorbed into biological membranes and entered into human food chain [8–11]. Then, human as the final consumer who will accumulate more mercury, which can lead to the dysfunction of cells and consequently causing many health problems in the brain, kidney, central nervous, mitosis and endocrine system, even at a low concentration of Hg^{2+} [12,13]. Due to the perniciousness of mercury, Hg^{2+} ions contamination have been severely affected the environment and human health, developing of rapid and sensitive analytical methods are critical for monitoring the level of Hg^{2+} in the environment and biological systems [14,15].

Nowdays, many detection methods have been applied such as atomic absorption spectroscopy , inductively coupled plasma mass spectrometry and electrochemical analysis [16–19]. However, most of the conventional methods are expensive and time-consuming, as they need sophisticated experimental apparatus and tediously long sample preparation steps. In contrast, due to less expensive, easy handing, rapid response and more importantly excellent sensitivity and selectivity, the fluorescent sensors are getting more and more attention in the field of heavy metal detection [20–28]. Various

[a.] *Department of Chemistry Jadavpur University, Kolkata 700 032, India.*
[b.] *Department of Molecular & Human Genetics Division, CSIR-Indian Institute of Chemical Biology, 4 Raja S.C. Mallick Road, Kolkata -700032, India.*

† Electronic Supplementary Information (ESI) available: [details of any supplementary information available should be included here]. See DOI: 10.1039/x0xx00000x

fluorophores such as coumarin [29], pyrene [30], 1,8-naphthalimide [31], xanthenes [32], cyanine [33] and BODIPY [34] are used over the past few years . For detection of Hg^{2+}, most of the sensors are based on rhodamine compounds [35–37]. Among the various fluorophores, fluorescein is common fluorophore having some excellent spectroscopic properties such as , emission wavelength , long absorption , high fluorescence quantum yield, easy operation and fast response, good biocompatibility and low toxicity [38]. However, fluorescein-based probes have received comparatively little attention [39,40]. Herein, we presented and synthesized a chemosensor, name **HL^3**. The chemosensor **HL^3** exhibited significant fluorescence enhancements to Hg^{2+} ions with particular sensitivity
and selectivity. In addition, cellular imaging experiment showed that **HL^3** could be used as a fluorescent sensor for reliably detecting Hg^{2+} in living cells.

Experimental Section:

Materials and Instruments: Fluorescein Sodium and metal salts such as perchlorates of Na^+, K^+, Ca^{2+}, Fe^{2+}, Co^{2+}, Ni^{2+}, Zn^{2+}, Pb^{2+}, Cd^{2+}, Hg^{2+} and Cu^{2+} and anions such as SO_4^{2-}, NO_3^-, PO_4^{3-}, S^{2-}, Cl^-, F^-, Br^-, OAc-, H_2AsO_4-, N_3^-, ClO4-, PPi, $S_2O_4^{2-}$, HCO_3^-, SCN^-, CO_3^{2-}, $P_2O_7^{4-}$ and NO_2^- were purchased from Sigma–Aldrich and used as received. All solvents used for the synthetic purposes were of reagent grade (Merck) unless otherwise mentioned. For spectroscopic (UV/Vis and fluorescence) studies HPLC-grade MeCN and deionized water from MiliQMillipore were used.

UV/Vis absorption spectra were recorded on an Agilent 8453 diode array spectrophotometer. Steady-state fluorescence studies were carried out with a PTI (QM-40) spectrofluorimeter. NMR spectra were recorded on a Bruker spectrometer at 300 MHz. The ESI-MS+ spectra were recorded on a Waters XEVO G2QTof mass spectrometer.

Preparation of Fluorescein Hydrazide (L^1): Fluorescein Hydrazide was prepared according to a literature method. [41]

Preparation of 2-Hydroxy-3-hydroxymethyl-5-methyl-benzaldehyde(L^2): 2-Hydroxy-3-hydroxymethyl-5-methyl-benzaldehyde was prepared according to a literature method[42].

Preparation of (HL^3): In a 250 mL RB Fluorescein Hydrazide (0.692g, 2 mmol) and 2-Hydroxy-3-hydroxymethyl-5-methyl-benzaldehyde (0.332g, 2 mmol) were suspended in 20 mL ethanol. The mixture was refluxed for 6 hr with stirring to form a clear solution. Following the reaction, the mixture was allowed to cool to room temperature. The pale yellow precipitated that formed was separated by filtration and washed with 3x 10 mL ethanol. 70% yield was obtained.

Analysis: 1H NMR (DMSO-d_6): δ = 10.527(s, 1 H), 10.0316 (s, 2 H), 8.929 (s, 1 H), 7.962 (d, 1 H), 7.65 (m, 2 H), 7.189(s, 1 H), 7.133(d, 2 H), 6.930 (s, 1 H), 6.687 (d, 2 H), 6.572(m, 4 H), 5.06 (t, 1 H), 4.417 (d, 2 H), 2.118(s, 3 H) ppm (**Fig.S1**). IR: $\tilde{\nu}$ = 1613 cm^{-1} (–C=N), -OH (3188 cm^{-1}), -C=O (1667 Cm^{-1}) (**Fig.S2**), ESI-MS^+ : m/z= 495.1458 (**$C_{29}H_{22}N_2O_6 + H^+$**) (**Fig.S3**).

Preparation of complex HL^3-Hg^{2+}: $Hg(ClO4)_2$ (0.272 g, 0.6 mmol)was added to a 10 mL MeOH solution of **HL^3** (0.255g, 0.5 mmol) and the mixture was stirred for about 30 minutes. It was then filtered and allowed to evaporate slowly at ambient temperature to get crystalline solid product.

Analysis : ^{1}H NMR (DMSO-d_6): δ = 10.215 (s, 1 H), 10.000 (s, 1 H), 8.824 (s, 1 H), 7.927 (d, 1 H), 7.50 (m, 3 H), 7.27 (s, 1 H), 7.103 (d, 2 H), 6.746 (s, 1 H), 6.642 (m, 2 H), 6.467 (m, 4 H), 4.566 (t, 1 H), 4.511 (s, 2 H), 2.082 (s, 3 H) ppm (**Fig.S4**). IR: $\tilde{\nu}$ = 1578 cm^{-1} (–C=N), -OH (3372 cm^{-1}), -C=O (1613 Cm^{-1}) (**Fig.S5**), ESI-MS^- : *m/z*= 793.0594 (**$C_{29}H_{22}ClHgN_2O_{10}$**) (**Fig.S6**).

Solution Preparation for fluorescence studies

For fluorescence studies, a stock solution 1.0 x 10^{-3} M of **HL^3** was prepared by dissolving required amount of ligand in 9 ml MeOH and finally the volume was adjusted to 10 ml by de-ionized water. In a similar way, 1.0 x 10-3 M stock solution of Hg^{2+} was prepared in MeOH. A 250 mL 10 mM HEPES buffer solution in 7:3 MeOH: H_2O (v/v) was prepared and pH was adjusted to 7.2 by using HCl and NaOH. 2.5 ml of this buffer solution was pipetted out into a cuvette to which

This journal is © The Royal Society of Chemistry 20xx

required volume of 1.0 x 10^{-3} M probe was added to achieve 20 µM final concentrations for fluorescence titration, respectively. In a regular interval of volume of Hg^{2+} ions were added incrementally and fluorescence spectra were recorded for each solution. The cuvettes of 1 cm path length were used for absorption and emission studies. Fluorescence measurements were performed using 3 nm x3 nm slit width.

Cell culture

Human hepatocellular liver carcinoma cells (HepG2) cell line (NCCS, Pune, India), were grown in DMEM supplemented with 10% FBS and antibiotics (penicillin-100 µg/ml; streptomycin-50 µg/ml). Cells were cultured at 37ºC in 95% air, 5% CO_2 incubator.

Cell Cytotoxicity Assay

Cytotoxicity for ligand **HL^3** was evaluated with the help of 3-(4,5-dimethylthiazol-2-yl)-2,5-diphenyltetra-zolium bromide (MTT) cell viability assay. HepG2 cells (1 × 105 cells/well) were cultured in a 96-well plate at incubated at 37°C, and were exposed to varying concentrations of **HL^3** (1, 5, 10, 20, 30, 40, 50, 60, 70, 80, 90 and 100 µM) for 24 hours. After the incubation, 10 µl of MTT solution 5 mg/ml, dissolved in 1X phosphate-buffered saline (PBS)] was added to each well of a 96-well culture plate, and then incubated at 370C for 4 hours. Media were decanted from wells and 100 µL of 0.04 N acidic isopropyl alcohol was added into each well to solubilize the intracellular formazan crystals (blue-violet) formed. Absorbance of the solution was measured at 595 nm wavelength (EMax Precision MicroPlate Reader, Molecular Devices, USA). Values were calculated as mean ± standard errors of three independent experiments. The cell viability was expressed as the optical density ratio of the treatment to control.

Cell Imaging Study

HepG2 Cells were cultured in 35 x 10 mm culture dish on coverslip for 24h at 37◦C. The cells were treated with 5µm solutions of **HL^3**, prepared by dissolving **HL^3** to the mixed solvent DMSO: water = 1:9 (v/v) and incubated for 1 hour at 370C. For Hg2+ complex formation study, HepG2 cells were pre incubated with varying concentrations of Hg^{2+} (5 µM, 10 µM and 20 µM) for 60 min at 37 ^{0}C followed by incubation with 5µM of **HL^3**for 60 min at 370C, and subsequent washing for three times with 1X PBS. Fluorescence images of HepG2 cells were taken by a fluorescence microscope (Leica DM3000, Germany) with an objective lens of 40X magnification.

Results and Discussion

A Schiff base condensation between L^1 and L^2 in methanol (Scheme 1) under refluxing conditions affords **HL^3**, which was thoroughly characterized by ^{1}H-NMR, IR and ESI-MS$^+$ spectroscopy. The spectral data were in agreement with the desired structures.

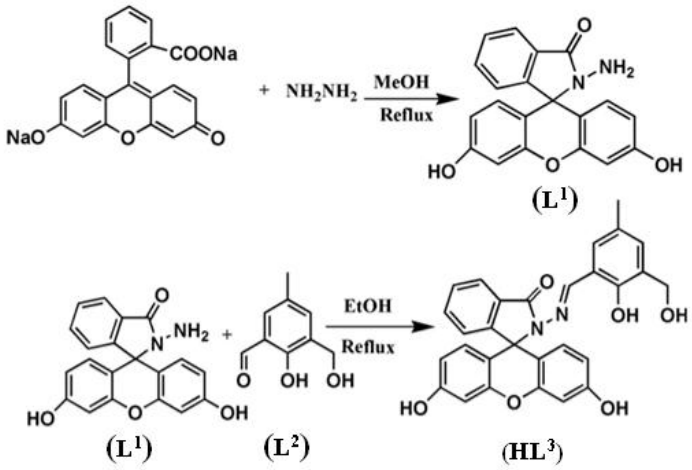

Scheme1. Synthetic path to **HL^3**

Fluorescence Studies:

We executed fluorescence titration to examine the interaction between **HL^3** and Hg^{2+} in methanol and 10 mM HEPES buffer at pH 7.2. (H_2O:CH_3OH = 3:7). The solution of free **HL^3** displayed very weak fluorescence in visible region at around 519 nm. However, on increasing addition of 100 µM Hg^{2+}, the same solution exhibited notable enhancement of the fluorescence intensity with band centered at λ_{em} = 519 nm, on excitation at λ_{ex} = 443 nm. (**Fig.1**) This attributed due to the opening of the spirolactam ring.

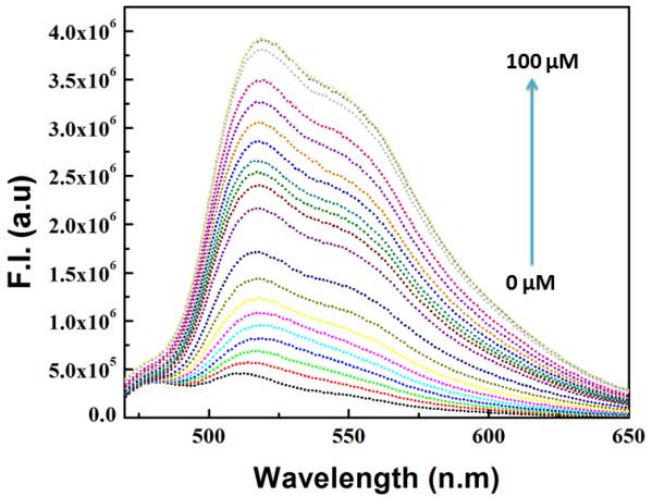

Fig.1 Fluorescence titration of **HL**^{3} (20.0 µM) in HEPES buffer at pH 7.2, λ_{em} = 519 nm on excitation at λ_{ex} = 443 nm.

A Benesi-Hildebrand plot (eqn(1)) of $[F_{max}-F_0]/(F-F_0)$ vs $1/[Hg^{2+}]$ gives a straight line with a slope K_d= (1.18± 0.01)X 10^{-4}). A K_d value of (1.18 ± 0.01)X 10^{-4}) suggests a moderately binding of **HL**^{3} towards Hg^{2+} (**Fig.2**). The 1 : 1 stoichiometry of the Hg^{2+} complex with **HL**^{3} was determined by Job's method. (**Fig.S7)**

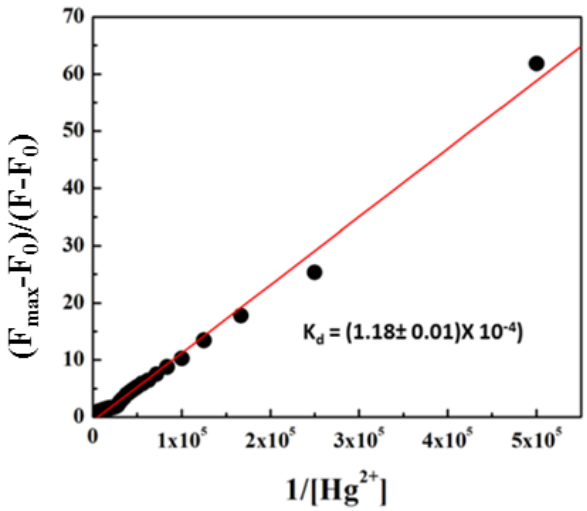

Fig.2 Benesi–Hildebrand plot of F.I (at 519 nm) vs $[Hg^{2+}]$ for the corresponding emission titration.

The detection of Hg^{2+} was not affected by the presence of biologically abundant metal ions like Na^+, K^+, Ca^{2+} and Mg^{2+}. Likewise, under identical reaction conditions no significant color or spectral change was observed for transition-metal ions, namely Cr^{3+}, Mn^{2+}, Fe^{2+}, Fe^{3+}, Co^{2+}, Cu^{2+}, Ni^{2+} and Zn^{2+}, and heavy-metal ions, like $Cd^{2+}$and Pb^{2+} (**Fig.3**)and also anions like SO_4^{2-}, NO_3^-, PO_4^{3-}, S^{2-}, Cl^-, F^-, Br^-, OAc^-, H_2AsO^{4-}, N_3^-, ClO_4^-, PPi, $S_2O_4^{2-}$, HCO_3^-, SCN^-, CO_3^{2-}, $P_2O_7^{4-}$ and NO_2^- (**Fig.S8**).

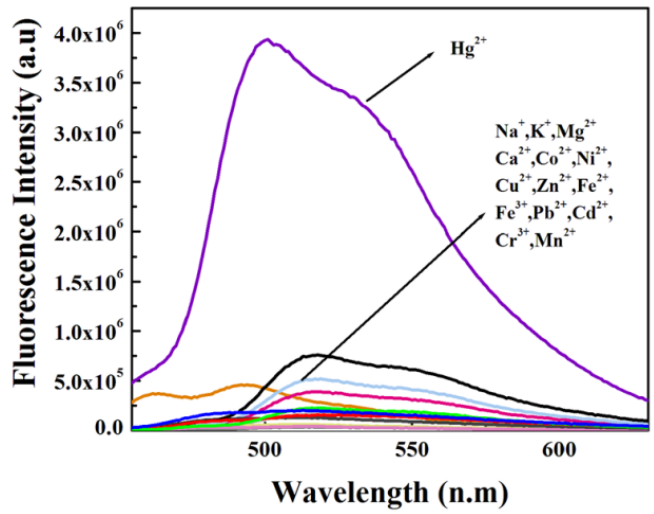

Fig.3. Fluorescence spectra of HL^{30} (20.0 µM) in the presence of different cations (100 µM) at pH 7.2 with $H_2O:CH_3OH$ = 3:7(v/v), λ_{em} = 519 nm on excitation at λ_{ex} = 443 nm.

Mechanism of ring opening

The characteristic stretching frequency of the –C=O bond of the flourescein moiety at 1667cm^{-1} is shifted to a lower wave number (1613 cm^{-1}) with the addition of of Hg^{2+} (**Fig.S5**) indicating a strong polarization of the –C=O bond upon efficient binding to the Hg^{2+} ion and also the stretching frequency of the (-CH=N) bond at 1613 cm^{-1} is significantly shifted to a lower wave number (1588 cm^{-1}). This supports the participation of azomethine nitrogen of **HL**^{3} in bonding with Hg^{2+}. To further explore the complexation between **HL**^{3} with Hg^{2+}, ^{1}H NMR experiment was done (**Fig.S3)** in DMSO-d_6.The two separate phenolic proton (b proton) signals (-OH) of **HL**^{3} now appeared to be one. These results clearly validate the spirolactam ring opening mechanism of the probe and one of the phenolic C–OH tautomerized to –C=O[43]. we proposed a probable mechanism of binding of Hg^{2+} ions to HL^{30} as shown in (**Scheme 4.2**).

This journal is © The Royal Society of Chemistry 20xx

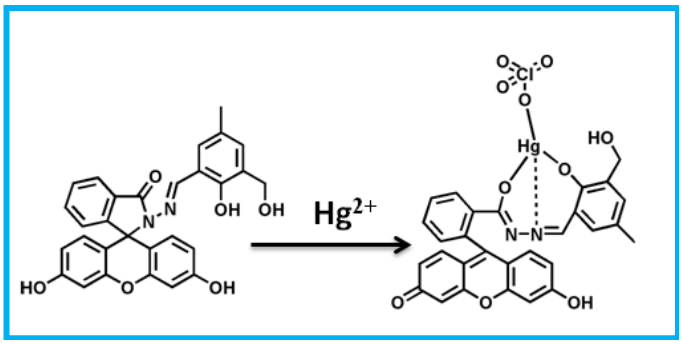

Scheme 4.2 Proposed mechanism for the recognition of Hg^{2+}.

pH Stability Check: The pH-titration was performed to investigate the practical applicability of **HL**^{3}. The effect of pH on the fluorescence response of probe **HL**^{3} to Hg^{2+} ions was examined in a series of solution with different pH values, ranging from 2.0 to 10.0. In the absence of Hg^{2+} , it reveals no obvious fluorescence emission of **HL**^{3} between pH 2.0 to 10.0, indicating that the spirolactam form of **HL**^{3} was the dominant conformation and the sensor was stable in a wide range of pH. However in presence of Hg^{2+}, the fluorescence intensity was enhanced under different pH values from 6.0 to 8.0, especially from 7.0 to 8.0, which suggested that the Hg^{2+} ions induced the formation of the ring-opened **HL**^{3}-**Hg**$^{2+}$complex(**Fig.4**).Therefore, considering that the physiological environment is slightly alkaline, so we chose pH 7.2 as it becomes fluorescent between the pH 6.5-8 suggesting a convenient application of this probe under physiological conditions.

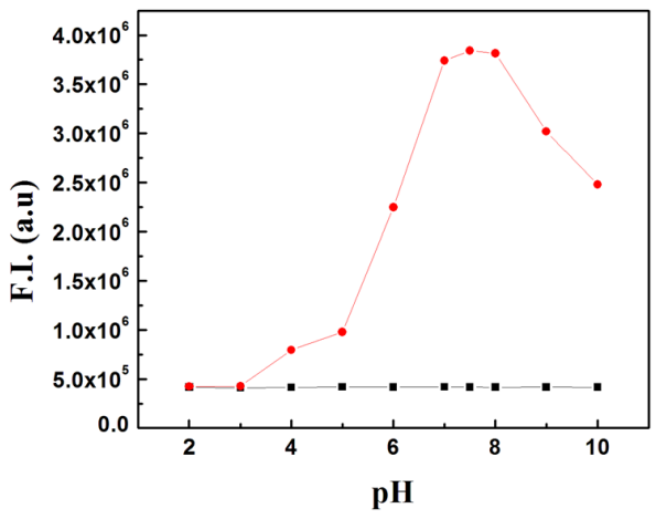

Fig.4 pH dependence of the FIs of the free ligand **HL**^{3} (black) and the[**HL**^{3}-**Hg**$^{2+}$**]** complex (red) in the HEPES buffer medium with λ_{em} = 519 nm on excitation at λ_{ex} = 443 nm.

Determination of LOD: The 3σ method was adopted to determine the limit of detection (LOD) of Hg^{2+} and was found to be as low as 0.46 μM (**Fig.5**) which indicates that **HL**^{3} is an ideal chemosensor for Hg^{2+} ion.

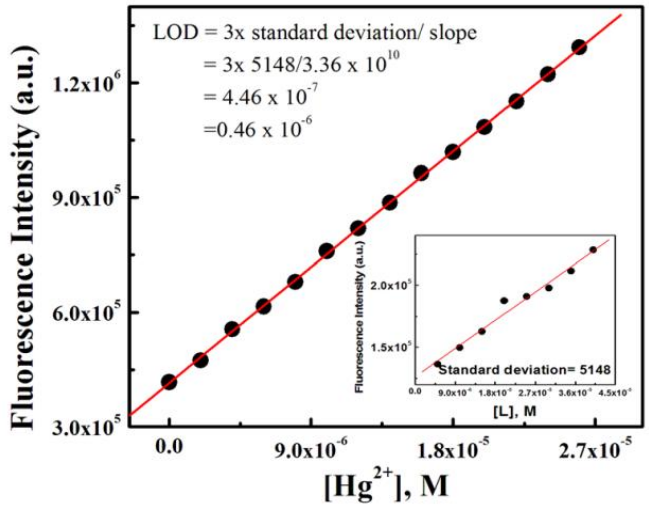

Fig. 5 LOD of Hg^{2+}

Cell imaging studies

Taking into account the highly specific selective nature of **HL**^{3} in the detection of Hg^{2+} ions, it has been further checked for its Hg^{2+} sensing ability in living cells. To determine if **HL**^{3} has cytotoxic effects, a cell viability assay using MTT was done with calculating % cell viability on HepG2 cells (**Fig.S8)**. There was no significant reduction in the tetrazolium salt (reflected by a decrease in formazan production) for **HL**^{3} up to 10 μM, thus suggesting that bellow 10μM ligand concentration for **HL**^{3} would be much more effective for the analysis of its complex formation with Hg^{2+} ions in vitro. A cell viability higher than 90% was observed for **HL**^{3} at 5 μM, after which the viability of the HepG2 cells decreased. Hence, further experiments were carried out with 5 μM of **HL**^{3} for treatment.

The ligand **HL**^{3} exhibited absence of intracellular fluorescence on HepG2 cells treated with 5μM of the ligand and incubated for 1 hour (**Fig.6**), however, prominent intracellular green fluorescence signal was observed cells when the HepG2 cells were incubated with 5 μM of Hg^{2+} for 60 min at 370C, followed by incubation with 5 μM of **HL**^{3}. The intracellular fluorescence was found to be prominently localized in

Please do not adjust margins

the cytoplasmic region, suggesting that **HL**^{3} is specifically making complex with the Hg^{2+} ions transported to the cytoplasm. Keeping the ligand **HL**^{3} concentration constant (5μM), and increasing concentration Hg^{2+} (from 5 μM, 10 μM and 20 μM) shows Hg^{2+} ion concentration-dependent enhancement in the intracellular blue fluorescence, caused by formation of complex with **HL**^{3}. Intense intracellular fluorescence was observed due to complex formation between Hg^{2+} and the ligands **HL**^{3} nearly at 20 μM of Hg^{2+}.Hence the present ligand with low cytotoxicity and biocompatible for cellular cytoplasmic Hg^{2+} ion detection, can be used for Hg^{2+} ion detection in biological samples.

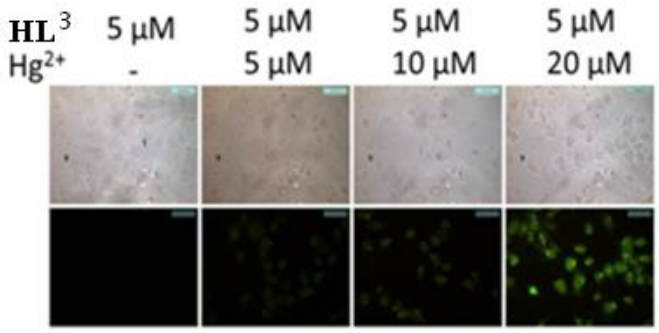

Fig 6. The fluorescence images of HepG2 cells were capture (40X) after incubation with 5μM of **HL**^{3} for 60 min at 37 °C, followed by washing thrice with 1X PBS, and incubation with 5 μM, 10 μM and 20 μM of Hg^{2+} for 60 min at 37°C followed by incubation with 5μM of **HL**^{3} for 60 min at 37 °C . The fluorescence images show no fluorescence signal by the fluorophore **HL**^{3} (5 μM) in absence of Hg^{2+} ion, while the fluorescence gradually increases with higher concentration of Hg^{2+} ion.

Conclusion: a novel fluorescein derivative (**HL**^{3}) was synthesized successfully by a simple two-step methods and characterized. Their ring-opening reaction mechanisms were proposed and the **HL**^{3} bound with Hg^{2+} in a 1:1 stoichiometric ratio. Moreover, **HL**^{3} possesses a good selectivity and sensitivity towards Hg^{2+} over other common competitive alkali, alkaline earth and transition metal ions. Experimental results indicated that **HL**^{3} was a good candidate and had a potential application for rapid, selective and sensitive detection Hg^{2+}in methanol-aqueous media.The MTT assay revealed that **HL**^{3} exhibits low cytotoxicity toward living HepG2 cells.

Conflicts of interest

There are no conflicts to declare.

Acknowledgements

Financial supports from the DST (Ref. No. 809(Sanc)/ST/P/S&T4G-9/2104), West Bengal and the CSIR (Ref. 01(2896)/17/EMR-II), New Delhi, India are gratefully acknowledged. H.Mohammad is grateful for UGC-MANF Fellowship (2012-13-MANF-MUS-WES-13502), UGC, New Delhi, India.

References

1 T.W. Clarkson, L. Magos, G.J. Myers, *N. Engl. J. Med,.* 2003, **349,** 1731–1737.

2 J. Gutknecht, *J. Membr. Biol.,* 1981, **61,** 61–66.

3 S.K. Ko, Y.K. Yang, J. Tae, I. Shin, *J. Am. Chem. Soc.,* 2006, **128,** 14150–14155.

4 Y.P. Zhu, T.Y. Ma, T.Z. Ren, Z.Y. Yuan, *ACS Appl. Mater. Interfaces,* 2014, ***6,*** 16344–16351.

5 Z. Yang, L. Hao, B. Yin, M. She, M. Obst, A. Kappler, et al., *Org. Lett.,* 2013, **15,** 4334–4337.

6 U.S. EPA, Regulatory Impact Analysis of the Clean Air Mercury Rule: EPA-452/R-05-003, 2005.

7 Boening, D. W., *Chemosphere,* 2000, **40,** 1335-1351.

8 P. Piyanuch, S. Watpathomsuba, V.S. Lee, H.A. Nienaberc, N. Wanichacheva, *Sens. Actuators B*

Chem., 2016, **22,** 4201–208.

9 H.H. Harris, I.J.Pickering, G.N. George, *Science,* 2003 **301,** 1203.

10 M. Harada, *Crit. Rev. Toxicol.,* 1995, **25,** 1–24.

11 H. Khani, M.K. Rpfouei, P. Arab, V.K. Gupta, Z. Vafaei, *J. Hazard. Mater.,* 2010, **183,** 402–409.

12 E.M. Nolan, S.J. Lippard, *Chem. Rev.,* 2008, **108,** 3443–3480.

13 Z.X. Han, B.S. Zhu, T.L. Wua, Q.Q. Yang, Y.L. Xue, Z. Zhang, X.Y. Wu, A Chin. *Chem. Lett.,* 2014, **25,** 73–76.

14 H.N. Kim, M.H. Lee, H.J. Kim, J.S. Kim, *Chem. Soc.*

This journal is © The Royal Society of Chemistry 20xx

Please do not adjust margins

Rev., 2008, **37,** 1465–1472.

15 M. Yuan, Y. Li, J. Li, C. Li, X. Liu, J. Lv, J. Xu, H. Liu, W. Su, D. Zhu, *Org. Lett.,* 2007, **92,** 313–2316.

16 N.H. Bings, A. Bogaerts, A.C. Broekaert, *Anal. Chem.,* 2006, **78,** 3917.

17 O.T. Butler, W.R. Cairns, J.M. Cook, C.M. Davidson, *J. Anal. At. Spectrom.,* 2012, **27,** 187.

18 F. Xuan, X.T. Luo, I.M. Hsing, *Anal. Chem.,* 2013,

85, 4586.

19 V.K. Gupta, S. Jain, U. Khurana, **Electroanalysis,** 1997, 9478–480.

20 D.T. Quang, J.S. Kim, *Chem. Rev.,* 2010, **110,** 6280–6301.

21 V.K. Gupta, A.K. Jain, G. Maheshwari, Heinrich Lang, Z. Ishtaiwi, *Sens. Actuators B: Chem.,* 2006, **117,** 99–106.

22 V.K. Gupta, A.K. Jain, P. Kumar, PVC-based membranes Sens. Actuators B: Chem. 2006, **120,** 259–266.

23 H. Zheng, X.Q. Zhan, Q.N. Bian, X.J. Zhang *Chem. Commun.,* 2013, **49,** 429–447.

24 A.K. Jain, V.K. Gupta, L.P. Singh, J.R. Raisoni, *Electrochim. Acta.,* 2006, **51,** 2547–2553.

25 V.K. Gupta, L.P. Singh, R. Singh, N. Upadhyay, S.P. Kaur, B. Sethi, *J. Mol. Liq.,* 2012, **174,** 11–16.

26 J.H. Song, M.X. Huai, C.C. Wang, Z.H. Xu, Y.F. Zhao, Y. Ye, *Spectrochim. Acta,* 2015, **139,** 549–554.

27 S.K. Srivastava, V.K. Gupta, S. Jain, *Analyst,* 1995, **120,** 495–498.

28 V.K. Gupta, A.K. Jain, S. Agarwal, G. Maheshwari, *Talanta,* 2007, **71,** 1964–1968.

29 L. He, Q. Xu, Y. Liu, H. Wei, Y. Tang, W. Lin, *Appl. Mater. Interfaces,* 2015, **7,** 12809.

30 B. Tang, Y. Yang, G. Wang, Z. Yao, L. Zhang, H.C. Wu, *Org. Biomol. Chem.,* 2015, **13,** 8708.

31 J.C. Spiteri, J.S. Schembri, D.C. Magr, *New J. Chem.,* 2015, **39,** 3349.

32 N. Kumar, V. Bhalla, M. Kumar, *Analyst,* 2014, **139,** 543.

33 M.V. Kuperman, S.V. Chernii, M.Y. Losytskyy, D.V. Kryvorotenko,N.O. Derevyanko, Y.L. Slominskii, V.B. Kovalska, S.M. Yarmoluk, *Anal. Biochem.,* 2015, **484,** 9–17.

34 S. Wang, H. Liu, J. Mack, J. Tian, B. Zou, H. Lu, Z. Li, J. Jiang, Z. Shen, *Chem. Commun.,* 2015, 13389.

35 Y. Zhou, X.Y. You, Y. Fang, J.Y. Li, K. Liu, C. Yao, *Org. Biomol., Chem.,* 2010, **8,** 4819–4822.

36 J.K. Ni, B. Li, L.M. Zhang, H.F. Zhao, H. Jiang, *Actuators B: Chem ,* 2015, **215,** 174–180.

37 Y. Jiao, L. Zhang, P. Zhou, *Talanta,* 2016, **15,** 14–19.

38 F. Ge, H. Ye, H. Zhang, B.X. Zhao, *Dyes Pigm.,* 2013, **99,** 661–665.

39 H.J. Kim, J.E. Park, M.G. Choi, S. Ahn, S.K. Chang, *Dyes Pigm.,* 2010, **84,** 54–58.

40 X.F. Yang, Y. Li, Q. Bai, *Anal. Chim. Acta,* 2007, **584,** 95–100.

41 X. Bao, Q. Cao, X. Wu, H. Shu , B. Zhou , Y. Geng , J. Zhu, *Tetrahedron Lett.*, 2016, **57,** 942-948.

42 G. C. Sun, Z. H. He, Z. J. Li, X. D. Yuan, Z. J. Yang, G. Xi. Wang, L. F.Wang and C.R. Liu, *Molecules*, 2001, ***6,*** 1001-1005.

43 Y. Gao, H. Liu, Q. Liu, W. Wang, A novel colorimetric and OFF–ON fluorescent chemosensor based on fluorescein derivative for the detection of Fe^{3+} in aqueous solution and living cells, *Tetrahedron Lett.*, 2016, **57,** 1852-1855.